High Performance Epoxy-Layered Silicate Nanocomposites

A Thesis submitted for the degree of Doctor of Philosophy

Lars-Ole Becker

(Dipl.-Ing.)

School of Physics & Materials Engineering
Monash University
Melbourne
Australia

February 2003

Executive Summary

A recent development to improve and diversify polymers is through the incorporation of highly dispersed layered silicate fillers into the polymer matrix. The silicate materials are relatively inexpensive and, being orders of magnitude smaller than conventional fillers (approximately 1 nm in thickness with aspect ratios up to 1000) they offer the ability to dramatically improve the composite properties.

The overall aim of the project is to investigate the effect of epoxyphilic rendered layered silicates on high functionality epoxy resins (processing conditions, mechanical properties and the structure/property correlation). Most work done to date has been focusing on epoxy systems with low glass transition temperatures using the bifunctional diglycidyl ether of bisphenol A (DGEBA) resin, and little has been reported about layered silicate nanocomposites based on more rigid, highly crosslinked high performance resin systems as considered in this project.

In addition to the studies on processing conditions and mechanical properties outlined above, ingress of moisture as well as thermal stability is also investigated in this work. Both are prime concerns in environmental damage to epoxy and composite structures.

In a further step, the ability to supplementary toughen epoxy resin carbon-fibre composites through incorporation of layered silicates into the polymer matrix is investigated. This is intended to reduce the main failure mechanism such as delamination, which occurs upon low energy impact in composites. Although it is assumed that small-sized particles have great potential for supplemental reinforcement of fibre-composites, little is known about the use of layered silicates as such supplementary tougheners.

The initial studies on the processing conditions of epoxy organically modified layered silicate (OLS) nanocomposites in this work show that the rate of reaction and therefore the time to gelation and vitrification of the polymer

network are significantly decreased through the filler addition. It is concluded that the compatibilizer, the acidic octadecyl ammonium ions, have a catalytic effect on both, epoxy homopolymerization as well as the epoxy/amine cure.

Studies on the effect of cure temperature on nanocomposite morphology show that the balance between extragallery and intergallery polymerization, which determines the separation of the silicate layers, can be improved with increased cure temperatures. The bifunctional DGEBA resin gave better exfoliation than the resins of higher functionalities. The higher cure temperatures were found to improve clay delamination and both toughness and modulus in most cases. The balance between amine cure and etherification and the effect on crosslink density as manipulated through the cure temperature may have a major impact on mechanical properties along with the changes in organoclay dispersion.

Overall, the great advantage of epoxy-clay nanocomposites lies in the fact that relevant properties to many high performance applications can be improved at relatively low levels of filler concentration, and hence small effects on processability. This work has shown that modulus and toughness can be simultaneously improved, while the equilibrium water uptake is reduced. All of these features can be achieved with only minimal effect upon the glass transition temperature, thermal stability and viscosity before cure.

Preliminary investigations into applying this technology in advanced composites showed significant promise, as seen by an improvement in composite fracture toughness with increasing layered silicate concentration. Further work is recommended to further evaluate the potential of layered silicates as supplementary reinforcing agents.

Table of Contents

Declaration of Originality

This PhD research program has been conducted under the principal supervision of Dr. George P. Simon, School of Physics and Materials Engineering, Monash University, Melbourne.

I hereby declare that this thesis contains no material which has been accepted for the award of any other degree in any other university, institute or college and to the best of my knowledge and belief, contains no material previously published or written by any other person or group of people, except where due reference is made in the text.

Melbourne, February 2003

Ole Becker

Acknowledgments

First and foremost I would like to acknowledge my principal supervisor Dr. George Simon, whose knowledge and enthusiasm has been a tremendous source of guidance and inspiration through this thesis. Similar appreciation goes to my co-supervisors Dr. Russell Varley and Dr. Yi-Bing Cheng for their assistance and helpful discussions.

Furthermore, the support of the School of Physics and Materials Engineering staff is gratefully acknowledged: special appreciation goes to Allan Holland and his team from the SPME workshop for technical support.

Peter Halley, Nara Altmann, Peter Sopade and Romain Bourdonnay from the University of Queensland are acknowledged for their assistance with rheological measurements and helpful discussions; Henry Sautereau, Jannick Duchet, Jean Francois Gerard, Loic Le Pluart from the Institute National des Sciences Appliquées de Lyon are also acknowledged for helpful discussions and assistance with in-situ XRD measurements. Graham Tranter (Leica Microsystems Pty Ltd), Gunta Jaudzems and Graham Winkelmann (Monash University), as well as Lee Brockhurst (University of Woolongong) are acknowledged for their introduction and assistance with the ultra microtome and transmission electron microscope.

Furthermore, I would like to acknowledge the financial support through the Dr.-Jürgen-Ulderup-Foundation, the German Merit Foundation (Studienstiftung des deutschen Volkes), the German Academic Exchange Service (DAAD), Monash Graduate School and the Australian Research Council.

My appreciation also goes to my close friends and student fellows for making the whole experience most enjoyable.

Finally, I would like to thank my family, Ursula, Manfred, Marc, Sophie, Helga and Peter and my partner Tracey – thank you for all the encouragement, patience and tremendous support.

List of Publications

The following list of publications has arisen from this PhD thesis and related work:

1. Papers Published in Refereed Journals:

(1) Ole Becker, Yi-Bing Cheng, Russell J. Varley, George P. Simon, Layered Silicate Nanocomposites based on Various High-Functionality Epoxy Resins: The Influence of Cure Temperature on Morphology, Mechanical Properties and Free Volume, *Macromolecules* in press

(2) Ole Becker, George Simon, Russell Varley, Yi-Bing Cheng, Jonathan Hodgkin, Thermal and Mechanical Characterisation of intercalated Epoxy Nanocomposites, *International Journal of Materials and Product Technology* **18**, 2-20 (2003)

(3) D. Ratna, R. Varley, O. Becker, R. Krishnamurthy, G.P. Simon, Nanocomposites Based on a Combination of Epoxy Resin, Hyperbranched Epoxy and a Layered Silicate, submitted for publication to *Polymer*

(4) Ole Becker, Romain Bourdonnay, Peter J. Halley, George P. Simon, Layered Silicate Nanocomposites based on Various High-Functionality Epoxy Resins: Part II - The influence of an Organoclay on the Rheological Behaviour of epoxy Prepolymers, submitted for publication to *Polymer Engineering & Science*

(5) Ole Becker, George P. Simon, Russell J. Varley, Peter J. Halley, Layered Silicate Nanocomposites based on Various High-Functionality Epoxy Resins: The Influence of an Organoclay on Resin Cure, *Polymer Engineering & Science* in press

(6) Ole Becker, Russell J. Varley, George P. Simon, Morphology, Thermal Relaxations and Mechanical Properties of Layered Silicate Nanocomposites based upon High-Functionality Epoxy Resins, *Polymer* **43**, 4365-4373 (2002)

(7) Ruth Lelarge, Ole Becker, George P. Simon, Thomas Rieckmann, Ternary Systems of Epoxy Resin, Layered Silicate and Liquid Rubber, submitted for publication to *Polymer*

(8) Ole Becker, Russell J. Varley, George P. Simon, Water Uptake and Thermal Stability of High Performance Epoxy Layered Silicate Nanocomposites, in preparation for submission to *European Polymer Journal*

(9) Ole Becker, George P. Simon, Thermosetting Layered Silicate Nanocomposites - A Review, in preparation for submission to *Progress in Polymer Science*

2. Papers Presented at Conferences:

(1) G.P. Simon, R. LeLarge, D. Ratna, O. Becker, Y.-B. Cheng, Ternary Epoxy Resin - Clay - Rubber Nanocomposites, Polymeric Nanomaterials - 2002 Biennial Symposium, November 17-20, 2002, Rohnert Park, California, USA

(2) Ole Becker, Russell J. Varley, George P. Simon, High Performance Epoxy Layered Silicate Nanocomposites: An Overview, Materials Week 2002, 29. September - 2. October 2002, Munich, Germany

(3) Ole Becker, George P. Simon, Russell J. Varley, Epoxy-Clay Nanocomposites for High Performance Applications, 25th Australasian Polymer Symposium, February 10-13. 2002 Armidale, NSW, Australia

(4) Ole Becker, George P. Simon, Russell Varley, Layered Silicate Nanocomposites of High-Functionality Epoxy Resins: Processing Conditions and Mechanical Properties, Europolymer Conference, 27.05 – 01.07.2001 Gargnano, Italy

(5) Ole Becker, George P. Simon, Russell Varley, Nara Altmann, Peter Halley, Rheology and Mechanical Properties of Epoxy Nanocomposites, 24th Australasian Polymer Symposium, February 4-8. 2001 Beechworth, Victoria, Australia

(6) O. Becker, G. Simon, R. Varley, J. Hodgkin, Y.B. Cheng, An Introduction into Epoxy Based Montmorillonite Nanocomposites, ACUN-2 Conference - Composites in the Transportation Industry, 14-18 February 2000 UNSW, Sydney, Australia

Invited Conference Lectures:

(7) Ole Becker, Russell J. Varley, George P. Simon, Opportunities for high performance epoxy layered silicate nanocomposites, Nanocomposites 2002, 23-25. September 2002, San Diego, California, USA

Abbreviations

Å	Angstrom
A	ampere
AFM	atomic force microscopy
BDMA	benzyldimethylamine
BTFA	boron trifluoride monoethylamine
CEC	cation exchange capacities
CTBN	carboxy terminated butadiene nitrile rubber
3DCM	3,3'-dimethylmethylenedi (cyclohexylamine)
DDS	4,4'-diaminodiphenyl sulfone
DETDA	diethyltoluene diamine
DGEBA	diglycidyl ether of bisphenol A
DSC	differential scanning calorimetry
DMTA	dynamic mechanical thermal analysis
G	giga
HDPE	high density polyethylene
J	joule
K	kilo
V	volt
m	milli
M	mega
MCDEA	4,4'-methylene-bis(3-chloro 2,6-diethylaniline)
min	minutes
μm	micrometer
mPDA	meta-phenylenediamine
nm	nanometer
NMA	nadic methyl anhydride
OLS	organically modified layered silicate
Pa	pascal
PACM	bisparaamino-cyclohexylmethane
PALS	positron annihilation lifetime spectroscopy
rpm	revolutions per minute
T_g	glass transition temperature
$T_{g\infty}$	ultimate glass transition temperature
TGA	thermo gravimetric analysis
TGAP	triglycidyl p-amino phenol
TGDDM	tetraglycedyl diamino diphenylmethane
TMA	thermomechanic analysis
TTT	time-temperature-transformation
WAXS	wide angle X-ray scattering
XRD	X-ray diffraction

Introduction

A recent approach to improve polymer materials is through the incorporation of layered silicates into the polymer matrix. Being only 1 nm thick and usually between 200 - 500 nm in diameter, these mica type fillers have shown some dramatic improvement in polymer material performance. The development of these novel nanocomposite materials offers promising opportunities to improve and diversify industrially applied polymers.

The fundamental principle behind nanocomposite formation is that the polymer or its monomers are able to move into and, in case of monomers, react within the interlayer galleries of the layered silicate. Only if the nature and polarity of the gallery is similar to that of the polymer or the monomer, the molecule will slide into the gallery, a process known as intercalation, in which the clay layers are pushed slightly apart. If the individual layers are pushed fully apart by the incoming material, a true (exfoliation) nanocomposite will result, with the individual layers dispersed throughout the matrix. To enable swelling or intercalation and exfoliation of the layered silicate, the inorganic interlayer cations are usually exchanged by organophilic ions. Layered silicate based polymeric nanocomposites exhibit attractive properties, such as increased modulus (and toughness in some cases), barrier and flame retardant properties, decreased water and solvent uptake, as well as improved optical and electrical properties, all at fairly low silicate concentrations compared to traditional fillers. It is the simultaneous improvement in a number of properties that makes the nanocomposite strategy particularly attractive.

To date, the use of layered silicates in epoxy resin systems has been limited. Nonetheless, the work reported has shown excellent potential - primarily an increased modulus due to exfoliated silicate platelets. One common feature of most work to date is that predominantly bifunctional, widely used diglycidyl ether of bisphenol A (DGEBA) cured with aliphatic hardeners has been used. This is due to the fact that highly flexible resins with low glass transitions were reported to give larger improvements, compared to more highly crosslinked epoxy

systems. However, for highly crosslinked epoxy resins, even small improvements can have a great benefit in comparison to higher concentrations of commonly used fillers, since these resin systems are more difficult to improve.

Although DGEBA based resin systems are widely used, aerospace materials and other high performance applications require epoxies of higher functionality due to the required higher modulus and glass transition temperature. As well as the commonly used DGEBA resin, this project will focus on two resins of higher functionalities, the trifunctional triglycidyl *p*-amino phenol (TGAP) and the tetrafunctional tetraglycidyl diaminodiphenylmethane (TGDDM). The curing agent used is the aromatic diethyltoluene diamine (DETDA), which is also widely used in high performance resin systems.

Based on the resins mentioned above, nanocomposites of different clay concentrations have been produced. The processing conditions and curing kinetics of these materials were investigated as well as the structure, mechanical properties and thermal stability of the cured material.

In most resin applications, the polymer is combined with another phase, such as fibres (carbon, graphite, glass or Kevlar), which are chopped, long and aligned or woven in various ways. Fibre reinforcement produces materials that usually exhibit high tensile strength in the fibre direction and strong matrix rigidity due to the high crosslink density of the resin. However, low ductility of these materials leads to problems in terms of low impact velocity strength and delamination resistance, since the out-of-plane strength of these materials is low. The materials often show low damage tolerance in the translaminar direction so that even relatively low impacts can cause serious internal damage such as delamination. This kind of damage is difficult to identify since it often occurs sub-surface and consequently can go undetected and lead to premature failure. Selected nanocomposite systems, as developed in the first part of this work, will be used to supplementary reinforce or "z-directional toughen" epoxy-fibre composites.

Chapter 1
Literature Review

This literature review presents an introduction into the components used for the synthesis of epoxy nanocomposites as investigated in this thesis. A review on cure kinetics and reaction mechanism of epoxy resins will also be presented. This is followed by a discussion of the opportunities that nanocomposites present and the work reported to date for the different classes of polymers (elastomeric, thermoplastic and thermosetting materials). A key aim of this project is to investigate the mechanical properties of epoxy nanocomposites as a function of their processing conditions. Other issues addressed in this review include the areas of organosilicate dispersion, environmental stability (thermal stability and water uptake) of epoxy layered silicate nanocomposites, which are also studied in this work. Carbon fibre reinforced composites will be toughened through the incorporation of layered silicates in the polymer matrix. Therefore, a summary of toughening techniques and mechanisms will also be presented.

1.1   Epoxy Resins

The term 'epoxy resin' refers to both the prepolymer and the cured resin/hardener system. The former is a low molecular weight oligomer that contains one or more epoxy groups per molecule. More than one unit per molecule is required if the resultant material is to be crosslinked. The characteristic group, a three-membered ring known as the epoxy, epoxide, oxirane, glycidyl or ethoxyline group is highly strained and therefore very reactive. The chemical structure of the epoxy group is illustrated in Figure 1.1. Curing agents or hardeners, respectively, have three or more reactive groups and thus enable the material to crosslink in a three-dimensional fashion.

$$H_2C \overset{\textstyle\diagup}{—} \overset{\textstyle\diagdown}{CH} —$$
$$O$$
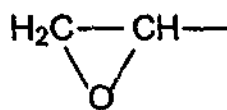
Figure 1.1: Chemical structure of the epoxy group.

Whilst the main hardeners have been primary amines, acid anhydrides, phenol-formaldehyde and amino formaldehyde, there is now an even wider range of hardeners available to suit many different applications [1]. Development in the resin industry has led to the introduction of polyfunctional amines, polybasic carboxylic acids, mercaptans and inorganic chemicals as hardeners for epoxy resins.

Epoxy resins gained particular commercial significance after Pierre Castan (Switzerland) and Sylvian Greenlee (United States) independently synthesized the first bisphenol-A epichlorohydrin based resin material in the late 1930s [2]. Since then, the use of epoxy resins has steadily increased. The wide variety of epoxy resin applications includes various coating applications, electrical, automotive, marine, aerospace and civil infrastructure as well as tool fabrication and pipes and vessels in the chemical industry. Due to its low density, around 1300 kg/m^3, epoxy resins are widely used in the transportation industry, usually in the form of fibre-reinforced composites. These materials also tend to have low shrinkage during cure and resultant high modulus.

1.1.1 Reaction Chemistry of Epoxy Resins

Two fundamental reactions occur during the epoxy resin/amine cure process [3]: the initial conversion reaction (I), where the two different functional groups react and form a linear or branched material, and the crosslinking, where macromolecules couple into a three-dimensional network (II). There are also a number of side-reactions that can occur. The most common side reaction is the etherification (III), where a hydroxyl group reacts with an epoxide group,

forming an ether linkage and a further hydroxyl group. The amine addition and etherification reactions are shown in Figure 1.2.
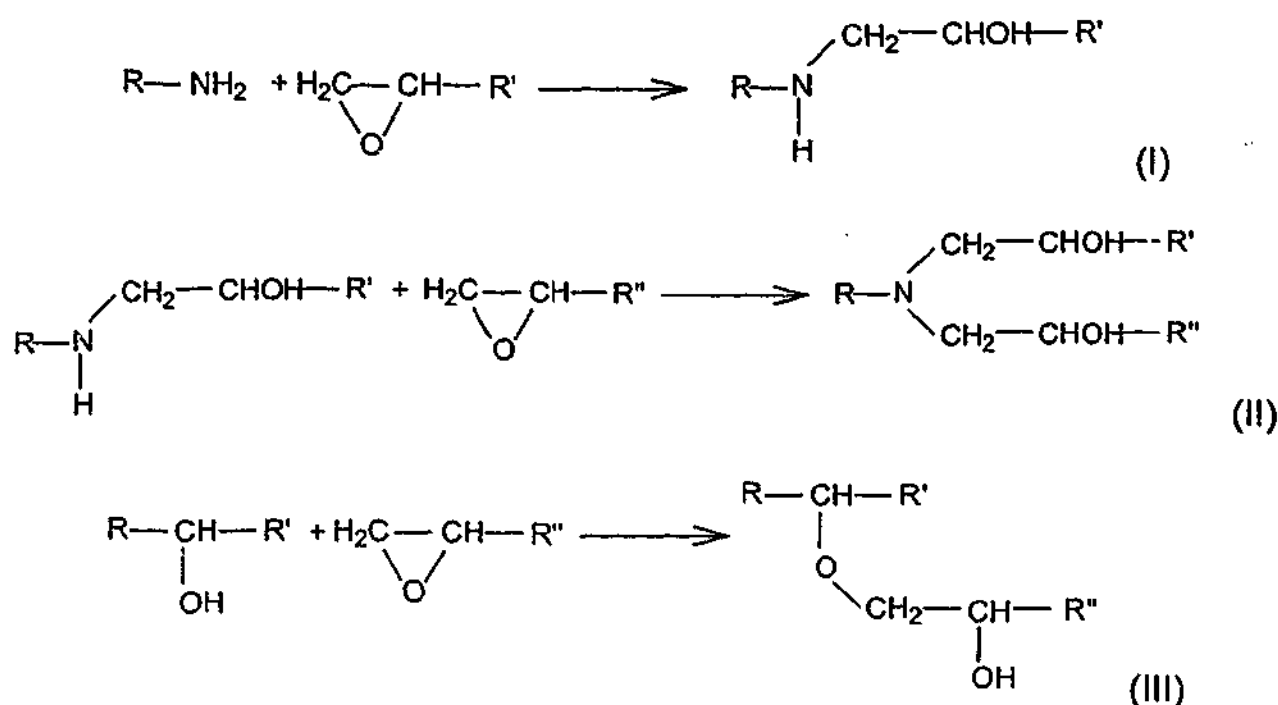
Figure 1.2: The three possible main reactions during cure of an epoxy resin with an amine - (I) primary amine-epoxy addition, (II) secondary amine-epoxy addition, (III) etherification [3].

The initial reaction takes place through addition of the primary amine with an epoxide group, forming a hydroxyl group and a secondary amine. This reaction largely continues until the primary amine groups are exhausted and a highly branched polymer is formed. Following that, the newly formed secondary amines react with epoxy groups producing a highly crosslinked network through tertiary amine moieties. The extent to which etherification takes place during cure, depends on the structure and chemistry of the resin and the hardener as well as the cure conditions [4]. Varley et al. [5] monitored the concentrations of primary and secondary amines and the hydroxyl production as an indication of side reactions of DDS-cured TGAP during cure using near infrared spectroscopy. In this work, it was shown that before gelation, predominantly reactions between the primary amine and epoxy groups occur, with most crosslinking occurring after gelation through the reaction of secondary amines

with epoxy groups. It was also shown that the steric hindrance and spatial separation at increased conversion enables the side reactions to compete with the secondary amine addition.

During cure, the epoxy group reacts either with itself or with the curing agent, forming a macromolecule. When the branched structures extend throughout the whole sample, the gel point is reached. At this characteristic point, the crosslinked resin will not dissolve in a suitable solvent of the parent resin although a soluble (sol) fraction may still dissolve. Further cure is required to increase the degree of crosslinking and to finally produce a structural material with a mechanical modulus of a vitrified or glassy solid material. This point, when the glass transition temperature of the growing network reaches the cure temperature, is known as vitrification.

1.1.2 Cure Behaviour and Monitoring Cure Kinetics

A useful tool to express the different stages of an epoxy/amine cure process is the time-temperature-transformation (TTT) cure diagram, which was first introduced by Gillham [6]. The phase diagram enables the physical state of the polymer to be determined at any particular time during isothermal cure. A generalised TTT diagram as shown in Figure 1.3 illustrates the various phase transitions, which are possible during the cure process. For example, the resin will not vitrify during isothermal cure if the curing temperature is above the ultimate glass transition temperature, $T_{g\infty}$ (but rather eventually chars).
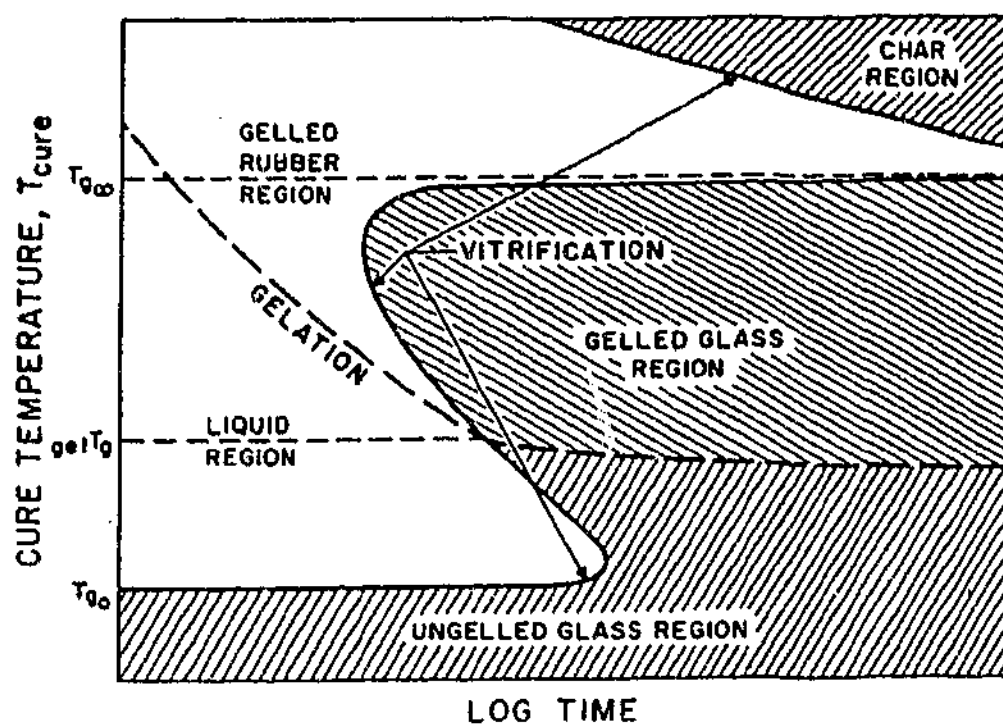
Figure 1.3: Generalized Time-Temperature-Transformation (TTT) phase diagram [7].

1.2   *Toughening of Epoxy Resins and Composites*

Although the high functionality of epoxy resins leads to a high crosslink density and thus the required matrix rigidity, toughness in these materials can often be problematic. Toughening of thermosets has thus been widely studied. Usually, the toughening strategy involves modification of the matrix with a second phase. In this section, the commonly used techniques of thermoset toughening and the toughening mechanisms will be discussed. Furthermore, a brief outline of 'supplementary' or 'z-directional' toughening of epoxy/fibre composites will be presented.

1.2.1   Rubber Toughening of Epoxy Resins

Elastomeric modification is probably the most common way to toughen epoxy resin systems. Of all categories of rubbers studied, (reactive butadiene-acrylonitrile rubbers, polysiloxanes, fluoroelastomers and acrylate elastomers)

carboxy terminated butadiene nitrile rubbers (CTBNs) have possibly shown the greatest benefits [1]. The major drawback in rubber toughened epoxy resins is that some of the beneficial resin properties, such as high glass transition temperature, thermal expansion, yield strength and modulus are sacrificed through the incorporation of the rubber. Table 1.1 illustrates how an increase in toughness through rubber incorporation decreases the tensile strength and modulus of the resin system [8].

Table 1.1: Change of mechanical properties of a rubber toughened epoxy system as a function of rubber concentration [8].

Rubber [%]	Tensile strength [MPa]	Tensile Modulus [GPa]	Toughness [kJ]
0	6.92	276.1	1.40
3	6.08	318.0	4.57
6	5.19	290.0	3.31
9	4.75	234.7	2.94
12	4.10	210.3	3.00

In rubber toughening, it is particularly important that the rubber/resin blend develops a two-phase morphology during the crosslinking reaction where the rubber particles are dispersed in and (preferably) bonded to the resin matrix. The amount of rubber used is usually limited to a concentration of 10 - 15 % to ensure that the rubber is the dispersed phase. Higher rubber concentrations can lead to phase inversion, which would result in a dramatic loss of strength and stiffness of the material. For the same reason, the cure profile must be adjusted to optimise the overall morphology, and resulting material performance. Any soluble rubber remaining in the matrix plasticises the polymer, decreasing the glass transition temperature.

1.2.2 Thermoplastic Toughening of Epoxy Resins

Although the first attempts of epoxy resin toughening through thermoplastic addition showed only modest enhancement in toughness [9], these studies created much interest in the field, which resulted in the exploration of many factors of thermoplastic toughening of epoxy systems and significant improvements. The main areas explored were the toughening effect of reactive endgroups, morphology, matrix ductility as well as backbone and molecular weight of the thermoplastic on the epoxy system. Since thermoplastic toughening of epoxies is not part of this project, the relevance of the aforementioned aspects will only be summarized briefly [10]:

Reactive endgroups - although there is no complete agreement in the literature, the use of reactively-terminated endgroups appears necessary.

Morphology - phase inverted or co-continuous morphologies leads to an optimum toughness (which is not the case in rubber-toughened systems).

Matrix ductility - thermoplastic additives have been found to toughen highly crosslinked resin/amine systems more effectively than low crosslink density resins.

Thermoplastic backbone - good thermal stability is required. The thermoplastic should be soluble in the unreacted resin but must phase separate during cure in order to form a binary system.

Molecular weight - the blend toughness rises with increasing molecular weight of the toughening thermoplastic, due to the linear polymers mechanical properties.

1.2.3 Toughening Mechanisms

The actual mechanism by which the enhancement of toughness occurs due to inclusion of a phase separated structure has been widely discussed. The toughening model independently developed by Kinloch et al. [11] and Pearson

and Yee [12] is based on localized cavitation, plastic deformation and plastic shear yielding in the matrix. This is now known to be in best agreement with recent experimental data [1]. This model theorizes that the crack growth resistance in a rubber-toughened resin arises from the large energy-dissipating deformations, which occur in the vicinity of the crack tip. The proposed deformation process is the localized cavitation in the rubber particles or the interfaces respectively, caused by the dilatation near the crack tip, as well as the shear yielding in the resin matrix. In the modified epoxy system, shear yielding plays a much more important role for the energy dissipation compared to the unmodified system. This is due to the interaction between the stress fields ahead of the crack tip and the toughening phase as well as crack blunting and bridging.

In thermoplastic-toughened, highly crosslinked epoxies, however, these two mechanisms are not as likely to occur. According to Pearson and Yee [13], the toughening mechanisms in these systems are crack bridging, crack pinning, crack path deflection or particle induced shear banding. The various discussed toughening mechanisms are illustrated in Figure 1.4.
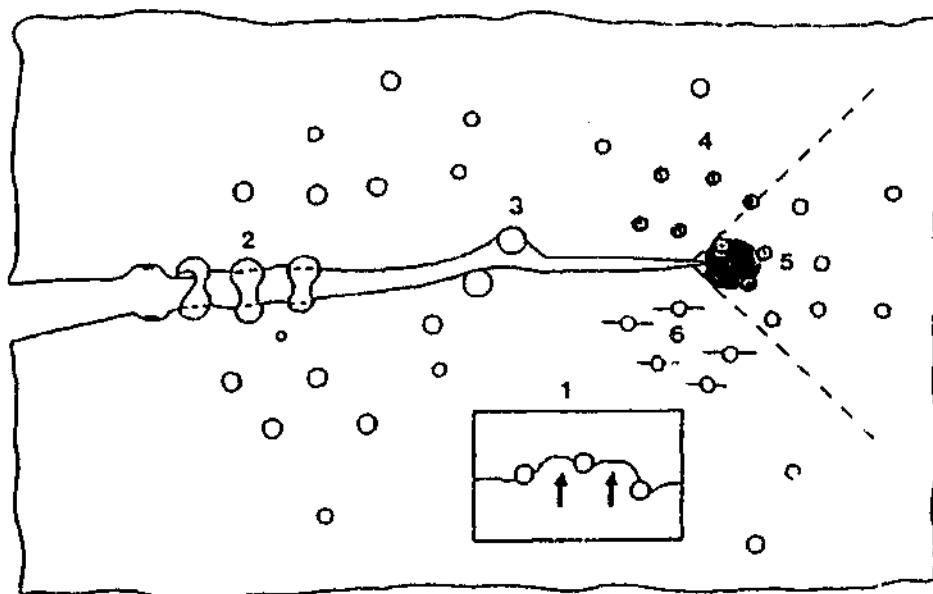
Figure 1.4: Schematic of different toughening mechanisms - 1) crack pinning, 2) particle bridging, 3) crack path deflection, 4) particle yielding, 5) particle yielding induced shear banding, 6) microcracking, adapted from Pearson and Yee [13].

1.2.4 Z-Directional Toughening of Fibre Reinforced Composites

In high performance composites, be they unidirectional or woven, the fibre phase such as carbon, graphite or glass induces high modulus and strength, however these composite systems usually show low ductility. This can lead to problems in terms of reduced impact strength at low velocities and delamination resistance since their out-of-plane strength is poor [14]. Such damage can be sub-surface and remain undetected, yet reduce material performance. Whilst improving matrix toughness can alleviate this to some degree, such strategies are not able to toughen composites as effectively. Therefore much work has been done with regards to the composite phase itself, often related to fibre/matrix properties. A more recent research direction has involved improvements made in the laminates through more three dimensional (3D) structures [15, 16] since 2D structures primarily offer good properties only in the plane of the laminate. 3D laminates are found to encourage fibre debonding and micro-cracking, as well as resisting crack growth between layers. 3D composites can involve processes such as weaving, knitting and stitching but this requires special techniques, which may be problematic or labour intensive (such as resin transfer moulding) to introduce the resin.

A more attractive way of producing effective, 3D laminates and reducing impact weakness and delamination is a strategy known as "z-directional" toughening or "supplementary reinforcement" in which short fibres are introduced in the z-direction (perpendicular to the laminates) [17]. Early work by Garcia et al. [18] and Yamashita [19] demonstrated this effect, predicting the need for fibres somewhat less than a micron in diameter. They used SiC whiskers of 0.1 - 0.5 μm in diameter. Low concentrations of this filler led to improved edge delamination, although in-plane properties were decreased. Jang and co-workers [20] have reported work where whiskers of various types were incorporated into fibre composites but had less improvement than expected due to clumping of fibres. In addition, the required concentrations led to increased viscosity and difficulty in handling and degassing materials, thus producing remnant voids. Nonetheless, Jang and other groups such as that of Hu [21] showed that using short fibres such as Kevlar could lead to improved properties

by mechanisms such as crack bridging - provided dispersion was good. It will be indicated in this work that the proposed use of intercalated or ordered exfoliate silicate-layered nanoparticles in such systems can prove optimal, along with other benefits.

1.3   *Layered Silicates - Crystallography and Modification*

Layered silicates belong to the structural group of swelling phyllosilicates minerals also known as 2:1 phyllosilicates or smectites. Often, these minerals are simply referred to as clays, with the term 'clay' by definition strictly referring to mineral sediments of particles with a dimension of less than 2 μm [22]. The individual layered silicate is usually referred to by its mineral name (for example, montmorillonite) or its rock name (bentonite) [22]. Montmorillonite is the name of the rarely found neat silicate mineral and principal component of the more widely found bentonite rocks, which contain fine dispersed, quartz and other impurities [23]. Along with montmorillonite, the more commonly used smectites are hectorite and saponite [24]. The main characteristic property of these layered minerals is their high aspect ratio and the ability to swell i.e. to absorb water and other organic molecules, leading to an increase in the interlayer distance.

Smectites consist of periodic stacks of approximately 1 nm thick layers. Stacks of these layers form tactoids with a thickness usually between 0.1 and 1 μm [25]. The crystal lattice of the silicate platelets consists of two tetrahedral silica sheets that are fused at the tip to a central octahedral sheet of alumina or magnesia [23]. Through sharing common oxygen atoms, as illustrated in Figure 1.5, chains are formed. Isomorphous replacement of central anions of lower valences in the tetrahedral or octahedral sheet results in a negative charge of the silicate surface. Common substitutions are Si^{4+} for Al^{3+} in the tetrahedral lattice and Al^{3+} for Mg^{2+} in the octahedral sheet [22]. The negative charge at the platelet surface is counterbalanced by alkali or alkaline earth cations between the layers, the interlayer or gallery.

O   oxygen
⊖   hydroxyl
●   aluminium and magnesium
O and ●   silicon
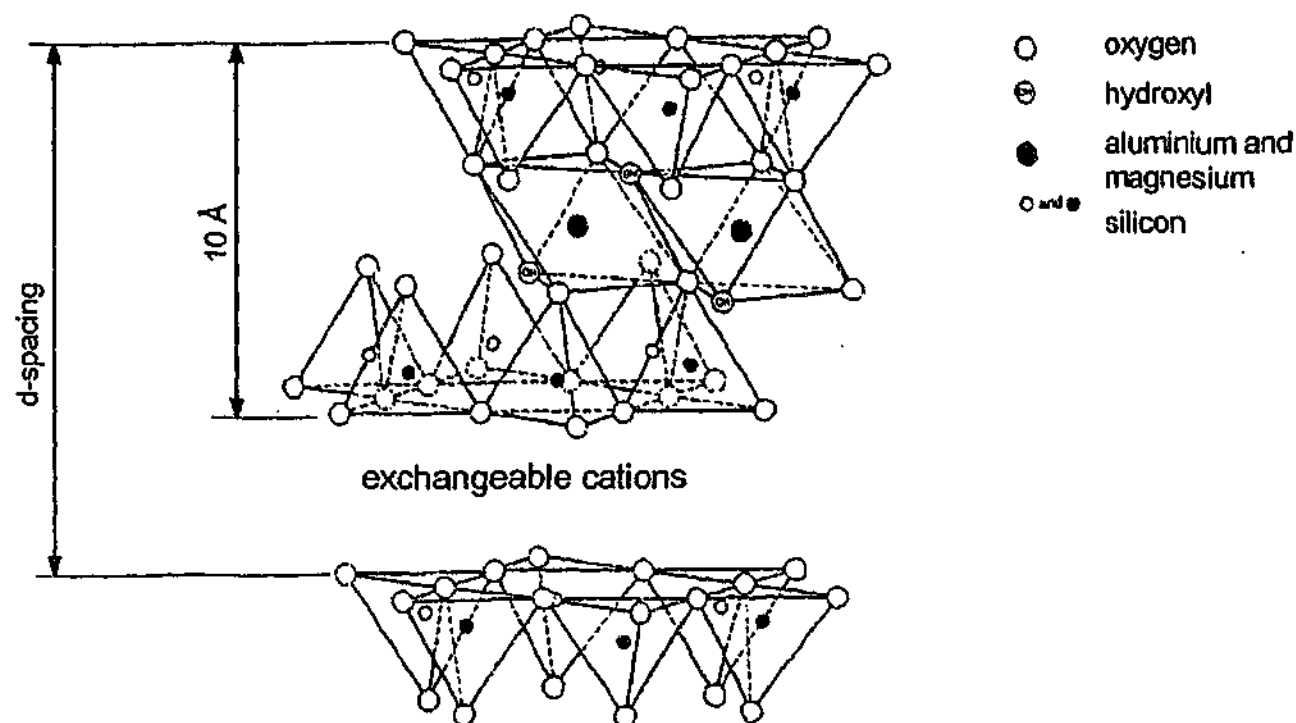
Figure 1.5: Model structure of layered silicates (Montmorillonite, adapted from Kornmann [26]).

The amount and the site of the isomorphous substitution determine the surface charge density and hence significantly influence the surface and colloidal properties of the layered silicate [27]. The charge per unit cell is thus a significant parameter to classify phyllosilicates. The intermediate value for the charge per unit cell of smectites [28] ($x \approx 0.25 - 0.6$) compared to talc ($x \approx 0$) or mica ($x \approx 1 - 2$) enables cation exchange and gallery swelling for this group of phyllosilicates and hence makes them suitable for epoxy nanocomposite formation [25]. The negative surface charge determines the cation exchange capacity, CEC [meq/100 g], which is the key for the organic surface modification. The untreated smectite has a high affinity to water and is hence not suitable for the absorption of most organic substances. However, the low van-der-Waals forces between stacks allow the intercalation and exchange of small molecules and ions, respectively, into the galleries. In order to render the hydrophilic clay organophilic, the inorganic ions in the gallery can be exchanged by the cations of organic salts. Whilst the absorption of organic materials through cation exchange in montmorillonite has been the subject of studies for

some years [27, 29], more recent papers give detailed information on how the layered silicate can be rendered epoxyphilic [30, 31]. Figure 1.6 illustrates how the exchanged alkyl amine ions increase the layer spacing from less than 1 nm to 1.2 - 2.5 nm depending on the chemistry and length of the exchanged ions as well as the charge density of the silicate.
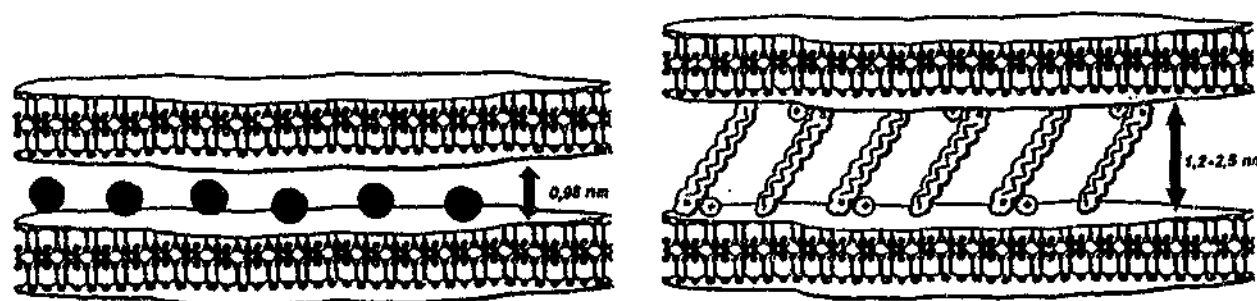
Figure 1.6: Unmodified layered silicate (left) and layered silicate with interlayer exchanged alkyl amine ions (right) [32].

1.4   Intercalation and Exfoliation of Nanocomposites

Although layered silicates have been used as polymer fillers for a long time [22, 33,34] it is only since the pioneering work of Toyota researchers [35-37], that intercalated and exfoliated clays have gained commercial importance in the polymer industry, along with a dramatic increase in research effort. Almost 15 years ago, researchers of Toyota company [38] polymerised ε-caprolactame in the interlayer gallery of an alkyl ammonium modified clay, thereby forming a true nanocomposite. The new materials showed dramatically improved mechanical properties, as well as improved thermal resistance. At a concentration of less than 5 % layered silicate, the strength increased more than 50 %, the modulus increased more than 100 % and the heat distortion temperature increased by 80 °C compared to the pristine material. Additional advantages that have been reported for polymer nanocomposite materials are increased moisture and solvent barrier properties [39, 40], improved dimensional [41] and thermal stability [24] and better flame-retardation [42-44], all at fairly low concentrations of layered silicate.

The fundamental principle behind nanocomposite formation is that the monomer or polymer is able to move into and (in case of a monomer) react within the interlayer galleries. Polymer nanocomposite formation can be divided into three different groups: in-situ polymerisation, intercalation of the polymer from solution, and melt intercalation of the polymer. Regardless of the method of formation, an increase in the d-spacing between the silicate layers occurs, swelling the interlayer galleries. As a result, the composite may have an intercalated or exfoliated morphology. In the intercalated state, the silicate consists of a well-dispersed layered structure with polymer chains inserted into the clay galleries. Resins of well dispersed, intercalated silicate platelets are known as 'tactoids'. In the exfoliated or delaminated state, the silicate platelets are fully separated and thus the reinforcement is of 1 nm thickness and approximately 200 - 500 nm in diameter, randomly dispersed in the polymer matrix. However, recent discussions have shown that these terms describe idealized structures only and additional descriptions such as 'ordered, disordered and partially exfoliated' have been suggested to further specify the nanocomposite morphology [45]. If there is no swelling (intercalation or exfoliation), the layered silicates act simply as a conventional filler material (dispersed on a micrometer scale) with particles of the order of 5 – 15 μm. The structure of the final composite material thus depends on various factors, such as the nature of the clay interlayer ion and the polymer, as well as reaction conditions, such as reaction temperature and mixing conditions in case of an in-situ polymerised nanocomposite. Figure 1.7 illustrates the three idealised possible structures of a layered silicate composite.
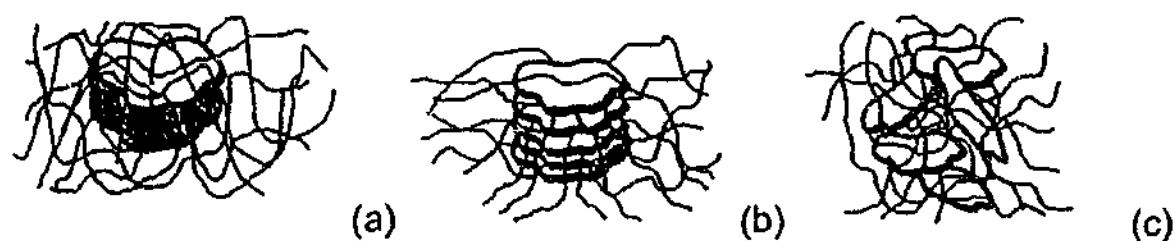
Figure 1.7: Schematic illustration of different possible structures of layered silicate polymer composite: (a) microcomposite (b) intercalated nanocomposite (c) exfoliated nanocomposite [31].

The first technique used to synthesize polymer nanocomposites was the in-situ polymerization of polyamide-6. According to this method, the organoclay is firstly swollen in the liquid monomer to enable polymer formation in the interlayer galleries as well as outside. The polymerization of thermoplastics can be initiated by heat, radiation or addition of a curing agent. For thermosets such as epoxy resins a curing agent is usually added to start the polymerization. A key issue in the in-situ polymerization is to be able to control the reaction occurring within the layer galleries, since slower cure kinetics in the intra gallery regions impedes exfoliation.

The second technique is to form nanocomposites via solution, where a solvent is used to swell the organoclay. The polymer is dissolved in the same solvent, and then added to the swollen clay. In the next step, the solvent is removed under vacuum while the clay platelets reassemble, sandwiching the polymer. For example, high density polyethylene (HDPE) [46] and polyimide [35] nanocomposites have been produced using this method.

The third method, the melt intercalation of polymers, was first extensively investigated by Giannelis, Vaia and co-workers [47-50]. In this method, the organoclay is mixed with the polymer in the molten state. If the silicate surfaces are sufficiently modified for the chosen thermoplastic, the polymer can intercalate into the galleries and form a nanocomposite without the need of a solvent. Due to its high potential for industrial applications this process has gained great importance. Amongst others, polyamide-6 [51] and styrene [52] nanocomposites have been successfully produced from melt intercalation. A few polymers such as polyethylene oxide [53] are readily able to intercalate both with and without surface modification of the clay.

1.5   *Elastomeric Nanocomposites*

Only a few studies have been reported in the area of intercalated and exfoliated rubber/clay nanocomposites. Kojima et al. [54] investigated the gas permeability of a highly dispersed ion exchanged montmorillonite nitrile rubber. It was found

that the permeability of water vapour and hydrogen were reduced by approximately one third compared to the pristine nitrile rubber, due to the tortuosity of the diffusion path caused by the clay platelets. A different study has shown a significant reduction of the oxygen permeability of rubber-clay nanocomposites, with a patent for use in tire inner-liners and inner-tubes [55]. Recently, Wang, Zang and co-workers [56, 57] synthesized and characterized styrene-butadiene rubber (SBR)-layered silicate nanocomposites by both latex and solution methods. The characterization of the final material has shown a well-dispersed intercalated system of 4 - 10 nm thick layer bundles. Compared with the solution method, the latex method led to better mechanical properties [57]. Mechanical properties of the rubber nanocomposites equalled that of the commonly used rubber fillers such as carbon black. Some properties, such as hardness, tear strength and tensile strength even exceeded the properties of carbon black reinforced rubber.

1.6 Thermoplastic Nanocomposites

Most work on polymer - layered silicate nanocomposites to date has been reported in the field of intercalation and exfoliation of thermoplastics. The development and commercialisation of nylon-6 nanocomposites by Toyota Company has been mentioned. This was followed by work involved polyamid-12 nanocomposites, for example the work by Reichert et al. [58], which reported an increase in modulus from 1620 to 2600 MPa at a clay loading of only 2 % without the usual loss in toughness. Further work using polyamides as well as the following development of nanocomposites in polypropylene, polystyrene and others has also shown promising results and has recently been summarized [24, 59, 60].

1.7   *Thermosetting Nanocomposites*

This review contains a detailed summary of the synthesis and properties of thermosetting layered silicate nanocomposites. Aspects such as the effect of processing conditions on cure chemistry, morphology and final material properties are discussed. The majority of the work reported to date in the field of thermosetting nanocomposites is based on epoxy resins, mostly using the diglycidyl ether of bisphenol A (DGEBA) resin. However, this review also includes work reported on other thermosetting systems.

1.7.1 Factors Influencing the Dispersion of Layered Silicates

Several reports have discussed the mechanism of organoclay exfoliation during the in-situ polymerization of epoxy resins. Early work by Lan et al. [61] pointed out the important role of the balance between intergallery and extragallery reaction rate as well as the accessibility of the resin and hardener monomers to the clay galleries on the exfoliation process. The common process for epoxy nanocomposite synthesis is to pre-intercalate the organoclay with the epoxy resin before cure. It is reported that the penetrating monomers swell the silicate layers until a thermodynamic equilibrium is reached between the polar resin molecules or resin/hardener blend and the high surface energy of the silicate layers [61, 62]. The pre-intercalation is likely limited to a certain d-spacing increase, although little literature exists on this. The mixing method before cure [63] or the use of solvents as processing aids [63, 64] were found to have little impact on the structure of the final nanocomposite. Further, increases in the distance between organoclay platelets requires the driving force of the resin/hardener cure reaction or homopolymerization to overcome the attractive electric forces between the negative charge of the silicate layers and the counterbalancing cations in the galleries [61]. Decreasing polarity during reaction of the resin in the galleries displaces the equilibrium and allows further monomers to diffuse into and react within the silicate galleries.

Chen et al. [65] have divided the interlayer expansion mechanism into three stages, which are basically the initial interlayer expansion due to resin and hardener monomers intercalating the silicate galleries and the interlayer expansion state where the interlayer spacing steadily increases due to intergallery polymerization. The final stage of interlayer expansion is characterized by a decreasing interlayer expansion rate. In some cases even a slight decrease in interlayer spacing could be observed before coming to rest, due to restrictions through extragallery polymerization (gelation).

Lü et al. [63] have formulated a thermodynamic approach of the exfoliation process. In this approach it is assumed that the exothermal curing heat of the intergallery epoxy resin, ΔH_1, must be higher than the endothermic heat to overcome the attractive forces between the silicate layers, ΔH_2 or in brief: $\Delta H_1 > \Delta H_2$.

In comparison to the formation of thermoplastic nanocomposites the transformation from the liquid reactive resin to the crosslinking solid strictly limits the exfoliation process of thermosetting nanocomposites to a small processing window. It was found that significant changes in the interlayer distance occur at the early stage of cure, before gelation restricts the mobility of the clay platelets [66]. The following aspects were reported to influence the balance between intergallery and extragallery reaction, and hence the formation of epoxy nanocomposites:

The Nature of the Silicate and the Interlayer Exchanged Ion

Two fundamental aspects of the organoclay determine the formation of epoxy nanocomposites from in-situ polymerization: the ability of the interlayer exchanged ion to act as a compatibilizer and render the layered silicate 'epoxyphilic' and the catalysing effect of the exchanged ion on the polymerization reaction in the galleries [25].

The charge density of the smectite determines the amount of ions in the interlayer galleries that can be exchanged and therefore the amount of epoxy

monomer that can be preloaded in the galleries of the modified organoclay. Lan and coworkers [61] investigated the effect of various smectites with cation exchange capacities (CEC) varying from 67 mmol equivalent/100 g (meq/100 g) for hectorite to 200 meq/100 g for vermiculite. It was reported that silicates such as montmorillonite and hectorite with intermediate layer charge densities are found to be well suited for the required layered silicate modification. Generally, layered silicates with a low charge density are more easily accessible for intragallery polymerization than high charge density clays with a higher population of gallery onium ions. Thus, the low charge density layered silicates provide higher degrees of layer exfoliation. Kornmann et al. [62] reported similar results for two different montmorillonite clays, with a CEC of 94 and 140 meq/100 g. After modifying the layer surfaces of the clay with an octadecylamine ion, TEM images of the correlating DGEBA/Jeffamine D-230 nanocomposites have shown regular stacks of 9 nm for the high CEC and 11 nm for the low CEC montmorillonite. The difference in organoclay layer separation was assumed to be due to the population density of alkylamine ions in the galleries and hence the space available for the epoxy resin. It was theorized that the layered silicate with the lower CEC contains less alkylamine ions, which leaves more space for the DGEBA molecules and allows homopolymerization to occur to a larger extent compared to the layered silicate with the higher CEC.

The nature of the interlayer exchanged ion also significantly determines the compatibility of the layered silicate with the epoxy resin, as well as the inter-gallery reaction rate. Pinnavaia and coworkers performed several studies using different types of organically modified layered silicates [61, 67-72]. Before the intergallery reaction can be initiated the clay tactoids must be preloaded with the epoxy monomer. The population density of the gallery onium ions and the basal spacing of the smectite determine the initial accessibility of the epoxy and hardener monomers to the clay galleries. It was shown [61] for a series of alkylammonium ion, $CH_3(CH_2)_{n-1}NH_3^+$, exchanged montmorillonite with n = 4, 8, 10, 12, 16 and 18 that the length of the alkylammonium ion greatly affects the clay expansion before cure. The degree of exfoliation during cure was also

found to depend on the amount of pre-intercalated resin in the clay galleries. An alkylamine cation chain length larger than eight methylene groups is necessary for nanocomposite formation. In more recent work by Zilg et al. [73] it was reported that the alkyl chain length for an organically modified fluorhectorite had to exceed six C-units to promote intercalation or exfoliation respectively. A chain length higher than eight C-units however did not further improve the exfoliation process.

Wang and Pinnavaia [74] found for a series of primary to quaternary octadecyl onium ion modified clays as shown in Figure 1.8 that the primary and secondary amines exfoliated in a DGEBA/meta-phenylenediamine (mPDA) system whilst the tertiary and quaternary ion-modified clays remained in an intercalated formation. This effect has been ascribed to the higher acidity and hence the stronger Bronsted-acid catalytic effect of the primary and secondary onium ions on the intergallery reaction. Since the tertiary and quaternary ions are less acidic, intercalation of the curing agent is less favourable, varying the gallery expansion of these nanocomposites, which is determined by the initial loading of resin and curing agent in the gallery.

$$CH_3(CH_2)_{17} - NH_3^+ \quad (1) \qquad CH_3(CH_2)_{17} - NH_2^+ - CH_3 \quad (2)$$

$$CH_3(CH_2)_{17} - \underset{\underset{CH_3}{|}}{NH^+} - CH_3 \quad (3) \qquad CH_3(CH_2)_{17} - \underset{\underset{CH_3}{|}}{\overset{\overset{CH_3}{|}}{N^+}} - CH_3 \quad (4)$$
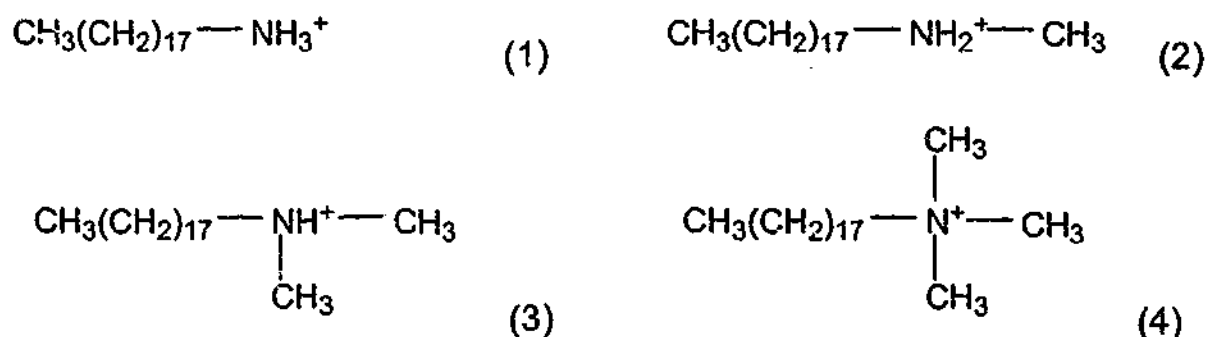
Figure 1.8: Examples of primary (1), secondary (2), tertiary (3) and quaternary (4) octadecy amine ions – the more acidic ions (1), (2) favour exfoliation [74].

Results are in good agreement with more recent work reported by Zilg et al. [31]. In their work, nanocomposite formation based upon various layered silicate modification has shown that ion exchange with protonated primary amines, such as 1-aminodedecane ions, gave larger interlayer distances in the

nanocomposite than those based on quaternary amine modification (for example *N,N,N*-trimethyldodecylamine ions).

Generally, long, primary linear chain alkyl ammonium ions such as $CH_3(CH_2)_{15}NH_3^+$ have proven to be appropriate substances for the synthesis of exfoliated systems and have been the most widely used in epoxy layered silicate nanocomposite systems to date.

Curing agent

Although the silicate interlayer exchanged ions have been widely studied with respect to control of intercalation or exfoliation of the nanocomposite system, the choice of a suitable curing agent is also reported to be a significant factor determining delamination of the thermosetting nanocomposite system. Recent research by Jiankun et al. [63] has shown, for example, that low viscosity curing agents can intercalate more easily into the clay galleries than highly viscous curing agents, thus favouring the interlayer reaction and therefore exfoliation.

Kornmann et al. [75] investigated the correlation of diffusion rate and reactivity of an epoxy system and the consequent degree of exfoliation. In this work it was shown that the molecular mobility and reactivity of the curing agent are important factors affecting the balance between intergallery and extragallery reaction. For the three different curing agents investigated, Jeffamine 230, 3,3'-dimethylmethylenedi (cyclohexylamine) (3DCM) and bisparaamino-cyclohexylmethane (PACM), it was found that the Jeffamine 230 gave better exfoliation of a DGEBA/octadecylammonium montmorillonite system than the cycloaliphatic polyamines 3DCM and PACM.

Messersmith and Giannelis [76] investigated the influence of three different curing agents (nadic methyl anhydride (NMA), benzyldimethylamine (BDMA) and boron trifluoride monoethylamine (BTFA)) on the formation of a DGEBA based nanocomposite. The montmorillonite silicate used in this study was modified with a quaternary bis (2-hydroxyethyl) methyl tallow alkyl ammonium ion, rather than the commonly used primary alkyl ammonium ions. For this

particular modified clay it was found that bifunctional primary and secondary amines resulted in immediate clouding of the resin and little or no increase in layer separation. It was assumed that this behaviour could be ascribed to bridging of the silicate layers through the bifunctional amine, preventing further layer expansion. However, primary and secondary amines did work well for exfoliation of the alkyl ammonium ion exchanged clays.

Cure Conditions

The effect of the cure temperature on nanocomposite formation has been the subject of several studies. In various cases [75, 77, 78] it was found that higher cure temperatures gave better exfoliation of the organosilicate. The improved exfoliation was mainly ascribed to the higher molecular mobility and diffusion rate of the resin and hardener into the clay galleries, leading to an improved balance between intergallery and extragallery reaction rate. Recent in-situ small angle XRD studies on a synchrotron by Tolle and Anderson [78] showed for a *m*-phenylenediamine cured octadecylammonium montmorillonite/DGEBA nanocomposite that increased cure temperatures exfoliated the organoclay in a shorter period of time and increased the basal spacing in the final morphology. Lan et al. [79] also reported improved exfoliation when the moulds were preheated to the cure temperature, before filling the nanocomposite premix into the moulds. However, there appears no general agreement in the literature about the effect of cure temperature on exfoliation of layered silicate in the epoxy matrix. Whilst the exfoliation process of some epoxy systems was found to be independent of the cure temperature [63, 77], Lan et al. [61] even reported an optimum temperature interval which has shown better organoclay delamination than higher or lower cure temperatures. Figure 1.9 shows XRD traces of *m*-phenylenediamine cured DGEBA/$CH_3(CH_2)_{15}NH_3^+$-montmorillonite nanocomposites cured at different temperatures. In this work it was theorized that too low cure temperatures may lead to slow intercalation rates. In these instances, the extragallery polymerization will dominate, leading to intercalated rather than exfoliated nanocomposite structures. Furthermore, too high cure temperatures also favour extragallery polymerization. Therefore, depending on

the nature of the resin and curing agent, cure cycles should balance the intra-
and extragallery polymerization rates. It was stated [61, 69, 80] that cure should
preferably involve exfoliation at lower temperatures with a subsequent cure at
elevated temperatures; faster cure too early in the reaction may lead to
encapsulated tactoids.
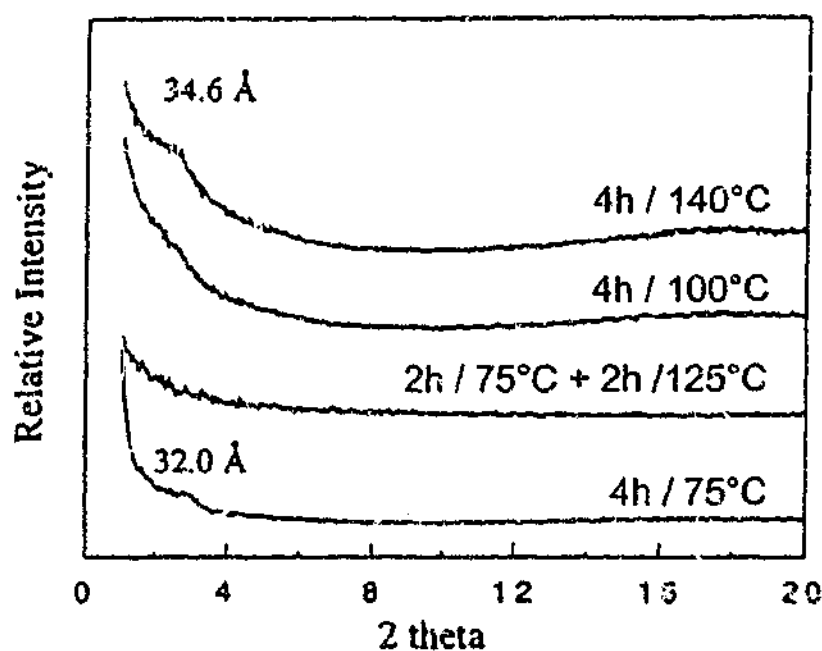
Figure 1.9: X-ray traces of epoxy nanocomposites - intermediate cure
temperatures show best exfoliation (the cure cycles are indicated above the
traces) [61].

Other Strategies

A number of other strategies to manipulate epoxy nanocomposite formation
have been discussed in the literature. Chin et al. [81] investigated the influence
of the stoichiometric resin/hardener ratio on exfoliation of a mPDA/DGEBA/
octadecylammonium montmorillonite using in situ small-angle X-ray scattering.
In that work it was found that resin cure with under-stoichiometric amounts of
mPDA up to the homopolymerization of DGEBA with no hardener (as earlier
reported by Lan et al. [69]) led to the formation of exfoliated nanocomposites
with lower amine concentrations giving better exfoliation. The extragallery
reaction was dominant at stoichiometric resin/hardener ratios and above,

leading to increased rates of extragallery reaction and therefore only intercalated nanocomposite structures.

The use of a low-boiling solvent such as acetone to enhance the processability and hence the structure of the final nanocomposite has been investigated by Brown et al. [64]. Whilst their work showed that the preloading of the layered silicate with the resin could be processed at significantly lower temperatures due to the decreased viscosity compared to the neat systems, no change in the curing reaction, morphology or mechanical properties could be observed. More recently, Salahuddin et al. [82] synthesized highly filled epoxy organoclay nanocomposite films of up to 70 % montmorillonite using acetone as a processing aid. The low boiling solvent was necessary to enable mixing of the clay with the resin/hardener blend. The final material was a transparent film with the clay platelets being parallel arranged with d-spacings of 30 and 70 Å.

Triantafillidis et al. [83, 84] recently investigated a new approach of epoxy layered silicate nanocomposites with reduced organic modifier. In their work, the layered silicate was treated with diprotonated forms polyoxypropylene diamines of the type α,ω-[NH$_3$CHCH$_3$CH$_2$(OCH$_2$CHCH$_3$)$_x$NH$_3$]$^{2+}$ (with x=2.6, 5.6, and 33.1). The silicate modifier played the triple role of surface modifier, polymerization catalyst and curing agent. Along with improved mechanical properties this strategy greatly reduced the plasticising effect of the modifier that can often be found with mono-amine modified layered silicates.

1.7.2 Cure Properties

Knowledge about the curing behaviour, especially about the thermal transitions such as gelation and vitrification during cure of the epoxy system, is of vital importance to optimise processing conditions and therefore the final properties of the crosslinked polymer [85-88]. To date, the effect of unmodified [89] and organically-modified layered silicates [64, 66, 69, 90] on epoxy cure kinetics has mainly been investigated by differential scanning calorimetry (DSC). Bajaj et al. [89] investigated the effect of unmodified mica on the curing behaviour of a

4,4'diaminodiphenylmethane cured diglycidyl ether of bisphenol A resin. It was found that mica accelerates the curing reaction substantially. In their work it was assumed that the hydroxyl-groups on the mica surface act as hydrogen bond contributors that accelerate the crosslinking reaction through participation in the glycidyl-ring opening process as shown in Figure 1.10.
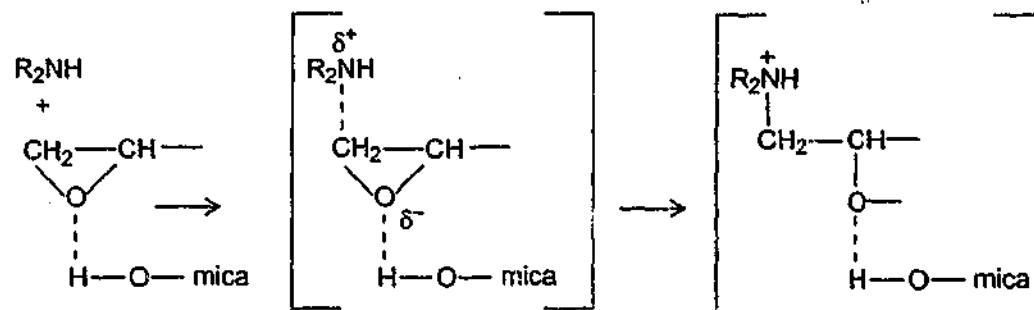
Figure 1.10: Catalytic effect of unmodified mica on epoxy cure as proposed by Bajaj et al. [89].

Lan et al. [69] found that acidic onium ions catalyse self-polymerisation of DGEBA at increased temperatures as judged by the DSC technique. A mechanism for the homopolymerization in the organoclay galleries was proposed, as shown in Figure 1.11. Protons are formed through dissociation of the primary alkyl ammonium cations attacking the glycidyl-ring, therefore catalysing the homopolymerization.

Brown et al. [64] investigated the influence of two different organoclays on the homopolymerization of neat DGEBA and on the reaction of a Jeffamine 2000 cured DGEBA using DSC. In their work it was found that both the epoxy homopolymerization and the amine-cured reaction were mildly catalysed through the presence of a dimethyl ditallow ammonium montmorillonite (Rheox B34) where the organoclay showed only a slight increase in the interlayer distance during cure. More significant catalytic effects were observed for a bis(2-hydroxy-ethyl)methyl tallow ammonium montmorillonite (S30A, Southern Clay Products) where the organoclay exfoliated during the resin/hardener cure reaction.
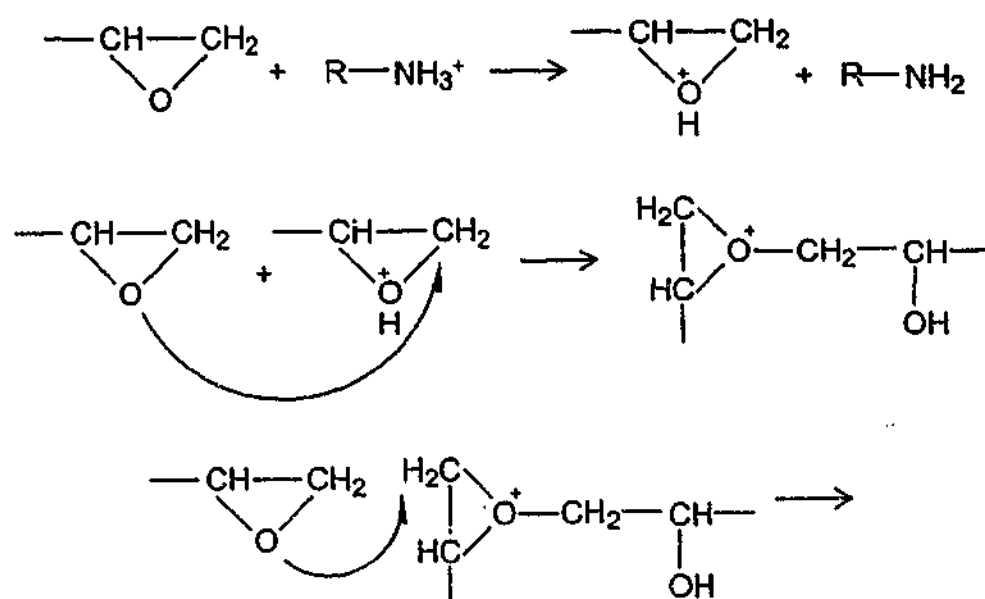
Figure 1.11: Catalytic effect of the organoclay on epoxy homopolymerization as proposed by Lan et al. [69].

Ke et al. [66] reported decreasing gelation times with increasing organoclay concentration for a N,N-dimethylbenzylamine (DMBA) cured DGEBA containing 0 - 7 % organoclay using a device where the resin is stirred on a heated plate until the resin can be pulled into continuous fibres. Further reaction kinetics studies on a Jeffamine 230 cured DGEBA system using an octadecyl alkylammonium modified montmorillonite were reported by Butzloff et al. [90]. In this work the kinetics of layered silicate/epoxy resin and layered silicate/hardener/epoxy resin was investigated using DSC. For the two-part mixture a significant decrease in enthalpy was reported for OLS concentrations above 5 %. Interestingly, the three-part mixture showed a maximum in activation energy at 2.5 % organoclay concentration. A composition dependence on exfoliation is also reported with mixtures of intercalated and exfoliated layered silicates occurring at concentrations above 2.5 %.

1.7.3 Glass Transition Temperature

The effect of the organoclay on the α-relaxation or glass transition temperature (T_g) has been the subject of various studies. A commonly used method is to

determine the T_g of a material from the temperature location of the tan δ peak in dynamic mechanical thermal analysis (DMTA) traces. In a number of cases a constant or slightly increased T_g has been reported with increasing organoclay addition [64, 71, 76, 91]. A tan δ peak broadening and increase in the T_g has been related to restricted segmental motions near the interface between the organic and inorganic phase [76]. Kelly et al [91] investigated DGEBA-layered silicate nanocomposites cured with Epon "R" V-40 (Henkel), a condensation product of polyamines with dimer acids and fatty acids, and found an increase in the glass transition temperature when the organoclay was initially swollen with the curing agent rather than the epoxide. It was concluded that initial swelling of the layered silicate in the curing agent leads to better epoxy absorption.

Others found a reduction in the glass transition temperature with increasing organosilicate content. Kornmann et al. [77] reported a steady decrease in T_g for highly crosslinked high glass transition temperature resin systems. The complexity of the cure reaction and possible side reactions involved made it difficult to determine the governing factor causing the reduction in T_g. The organoclay may catalyse epoxy etherification and unreacted entrapped resin, hardener or compatibilizer molecules may act as a plasticiser. In addition the high cure temperatures required for these resin systems may degrade the layered silicate surface modifier, which are nominally stable to about 200 – 250 °C.

Chen et al. [65] found a decreased T_g for an hexahydro-4-methylphtalic anhydride cured epoxy (3,4-Epoxycyclohexylmethyl-3,4-epoxycyclohexane) layered silicate nanocomposite. The layered silicate was rendered organophilic through bis-2-hydroxyethyl methyl tallow ammonium cations. The decrease in T_g was proposed to be due to the formation of an interphase consisting of the epoxy resin, which is plasticised by the surfactant chains.

1.7.4 Mechanical Properties

It was reported [70] that flexible resin systems with a low glass transition temperature generally show better improvements in mechanical properties upon forming nanocomposites in comparison with those systems that exhibit higher glass transitions. A summary of improvement in mechanical properties of epoxy nanocomposites in both the rubbery and the glassy state is reported in the following.

Flexural-, Tensile- and Compressive Properties

In the early work by Messersmith and Giannelis [76] on epoxy systems, a nadic methyl anhydride (NMA) cured DGEBA-based nanocomposite containing 4 vol % silicate showed an increase in the glassy modulus by 58 % and a much greater increase of some 450 % in the rubbery region. Pinnavaia and coworkers [61, 68, 70, 74, 92] investigated a number of intercalated and exfoliated rubbery and glassy epoxy nanocomposites. A series of nanocomposites based on DGEBA, Jeffamine 2000 and a range of homoionic $CH_3(CH_2)_{n-1}NH_3^+$ montmorillonites with n = 8, 12, 18, showed a steady increase in both tensile strength and modulus with increasing carbon number, as well as increasing organoclay concentration. More than a 10-fold increase in strength and modulus was achieved through addition of 15 % of the $CH_3(CH_2)_{17}NH_3^+$ modified montmorillonite. The order of reinforcement was found to be dependant on the extent of exfoliation. Figure 1.12 illustrates the tensile properties of a series of epoxy-magadiite nanocomposites with different degrees of exfoliation [25]. It is assumed that the alignment of platelet particles under strain contributes to the high improvement in the rubbery state. This alignment enables the platelets to function or act like long fibres in a fibre reinforced composite [70]. Rather modest improvements in strength and modulus were reported for glassy *m*-phenylenediamine DGEBA nanocomposites [61].

Generally, the modulus is the primary mechanical property that is improved through the inclusion of exfoliated layered silicates. The degree of improvement can be ascribed to the high aspect ratio of the exfoliated platelets. It is assumed

[31, 70] that the reinforcement provided through exfoliation is due to shear deformation and stress transfer in the platelet particles.
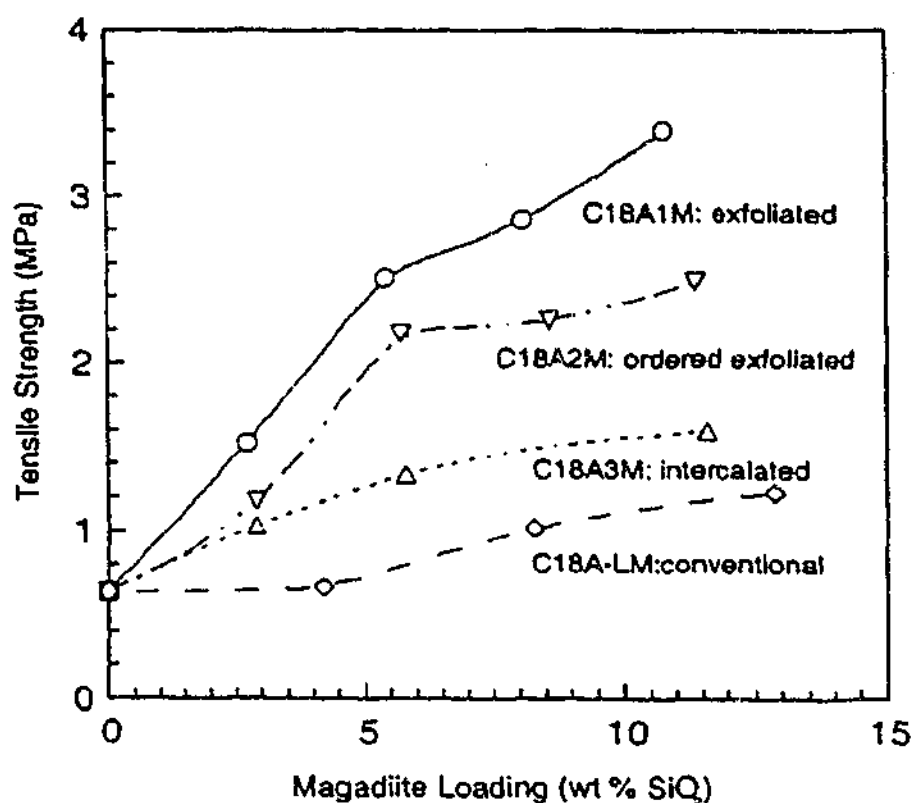
Figure 1.12: Tensile strength of DGEBA/Jeffamine 2000/magadiite nanocomposites with different degrees of organoclay layer separation [25].

Zilg et al. [31, 73] characterized the modulus and tensile strength of various hexahydrophthalic anhydride cured DGEBA nanocomposites based on different smectites and different layered silicate modifications. All systems investigated in this work exhibited an increase in Young's modulus, and in several cases along with a decrease in tensile strength and elongation at break. It was assumed that the loss in tensile strength might be related to an inhomogeneous network density due to different cure rates of the intergallery and extragallery reaction. This may lead to internal stresses in the material, which reduces the resistance against mechanical strains. Kornmann et al. [77] found improvement in toughness and stiffness, along with a slightly decreased tensile strength and

elongation at break for a series of glassy, highly crosslinked (TGDDM/DDS) nanocomposites.

Massam and Pinnavaia [71] investigated the compressive properties of intercalated and exfoliated glassy epoxy nanocomposites. In their work it was found that exfoliated systems gave significant improvements in compressive strength and modulus with increasing layered silicate concentration in the investigated range of 0 - 10 %. In contrast, the intercalated nanocomposite systems were ineffective in improving reinforcement under compression. Different levels of improvement were reported for various exfoliated systems. The variation in improvement was related to differences in interfacial interactions, for example, due to different aspect ratios and layer charge densities.

Zerda and Lesser [93] investigated the behaviour of intercalated glassy epoxy nanocomposites under compression. Their work also showed that compressive strength and modulus of the intercalated epoxy nanocomposite systems did not change noticeably. However, the yielding mechanism was found to be a different one in the nanocomposite compared to the unfilled epoxy system. Whilst the unfilled system exhibited a gross yield behaviour with no apparent void formation, the nanocomposite yielded in shear as evidenced by scattering of visible light by voids in the layered silicate aggregates.

Fracture Properties

Whilst many papers focus on the improvement of flexural properties of nanocomposites, less work has been reported regarding the fracture behaviour of these materials. However, the work presented to date has shown that the layered silicate nanocomposite strategy is able to simultaneously improve fracture toughness and stiffness, although it is often believed that improvement in one property sacrifices the other. A study by Zilg et al. [31] showed that a well dispersed intercalated epoxy nanocomposite primarily improved the toughness, whereas the completely exfoliated stage reinforced the stiffness of the material.

A range of hexahydrophthalic anhydride cured DGEBA resin nanocomposite systems based on various compatibilized layered silicates showed an increase in modulus and toughness with increasing silicate content. It was noted that conventional fillers or exfoliated nanocomposites usually improve stiffness without an increase in toughness or even sacrificing toughness. It is well known [93] that toughening occurs within a specific size range of the reinforcement. Whilst the fully dispersed individual silicate platelets are too thin to provide toughening, the lateral micron-sized structure of intercalated layered silicate tactoids is likely able to provide this toughening mainly through a crack bridging mechanism and an increased fracture surface area.

Improved fracture toughness was also reported for other intercalated or partially exfoliated epoxy nanocomposite systems [73, 77]. Zerda and Lesser [93, 94] investigated the fracture behaviour of intercalated DGEBA/Jeffamine D230 nanocomposites. The material investigated showed a modest increase in modulus along with a significant decrease in ultimate stress and strain at break. The fracture behaviour of these materials as represented by the stress intensity factor, K_{IC}, showed significant improvements at layered silicate concentrations of 3.5 % and above. The increase in fracture toughness was ascribed to a decrease in (tactoid) inter-particle distance. SEM images of the fracture surfaces showed a more tortuous path of crack propagation around areas of high silicate concentration in the nanocomposite, compared to the neat system. The fracture surfaces of nanocomposites were very rough and showed a significantly higher surface area compared to the smooth fracture surface of neat epoxy resins. The creation of additional surface areas on crack propagation was thus assumed to be the primary factor for the toughening effect.

1.7.5 Environmental Stability and other Properties

Dimensional Stability

Massam et al. [71] investigated the thermal expansion coefficient, α, of a series of polyoxyalkylene amine cured DGEMA layered silicate nanocomposites by means of thermomechanical analysis (TMA). Measurements in the range of 40 - 120 °C showed reduced expansion coefficients for both the rubbery and the glassy state. A decrease in the expansion coefficient by 27 % was reported for the 5 % nanocomposite in the glassy state. A constantly decreasing expansion coefficient with increasing layered silicate concentration was found in the rubbery state with an organoclay loading of 15 % showing a 20 % reduction in α.

Water Uptake and Solvent Resistance

A thorough study by Massam et al. [25, 71] investigated the resistance of glassy DGEBA based nanocomposites towards organic solvents and water. The absorption of methanol, ethanol and propanol was faster in the neat epoxy system compared to the nanocomposite. Furthermore, the mechanical properties of the neat resin systems were more affected by the absorbed solvent. In water however, only the rate of absorption was reduced, with little change in the equilibrium water uptake. It was further observed that the barrier to solvent uptake was more significant in the exfoliated composite compared to the conventional or intercalated layered silicate composite.

Shah et al. [95] recently reported a study on moisture uptake of vinyl ester based layered silicate nanocomposites. Although the moisture diffusivity was decreased upon addition of the organoclay, the equilibrium moisture uptake was found to increase with the amount of layered silicate added. The increased equilibrium water uptake was ascribed to the natural hydrophilic behaviour of the clay, which is still existent to some extent in the surface treated state. It was theorized that the total exposed surface area of the clay particles is indicative of

the amount of water absorbed. Higher concentrations of layered silicate may lead to aggregates or tactoids of layered silicate with less exposed surface area, leading to a negative deviation from the linear relationship between equilibrium water absorbed and organoclay concentration. Furthermore, it was reported that the diffusion coefficient did not differ significantly between two different clay modifications, which gave different dispersion or separation of the layered silicate. The decreased diffusivity was generally ascribed to the restricted motion of polymer chains that are tethered to the clay particles.

Thermal Stability and Flammability

Thermogravimetric analysis (TGA) is the most commonly used method to investigate thermal stability, which is also an important property for the flammability performance of a material [42-44]. Lee and Jang [96] reported improved thermal stability for intercalated epoxy nanocomposite synthesised by emulsion polymerization of unmodified layered silicate, as indicated by a shift in the onset of thermal decomposition (in a nitrogen atmosphere) towards higher temperatures. Wang and Pinnavaia [74] compared TGA measurements (under a nitrogen atmosphere) of intercalated and exfoliated organically modified magadiite based nanocomposites. Whilst the intercalated epoxy nanocomposite showed a low temperature weight loss indicative of the thermal decomposition of the clay modifier, the exfoliated nanocomposite did not show such a low onset temperature for weight loss. It was assumed that the interlayer exchanged ions were incorporated into the polymer network. In this work, it was stated that the thermal stability of the polymer was not sacrificed through the incorporation of organosilicate. However, a direct comparison between TGA traces of the nanocomposite and the neat polymer was not presented in this work.

The flammability of nanocomposites has been the subject of various studies by Gilman and coworkers [44, 97, 98] Flammability properties are most often investigated using the cone calorimeter, a method where the fire relevant properties such as heat release rate (HRR) and the carbon monoxide yield

during combustion of a material are measured. Table 1.2 shows the results of combustion of different thermosets obtained from cone calorimetry [44]. It can be seen that the peak and average release rate, as well as mass loss rates, were all significantly improved through the organoclay addition. Furthermore, no increase in heat of combustion, specific extinction area (soot) or CO yields was observed.

Table 1.2: Cone calorimeter data for modified bisphenol A vinyl ester (Mod-Bis-A Vinyl Ester), bisphenol A novolac vinyl ester (Bis-/Novolac Vinyl Ester) and methylenedianiline (MDA) and benzyldimethylamine (BDMA) cured epoxy resins and their intercalated nanocomposites (*) containing 6% dimethyl dioctadecyl ammonium-exchanged montmorillonite. Heat flux = 35kW/m², HRR = heat release rate, MLR = mass loss rate, H_c = heat of combustion, [44].

Sample	Residue Yield [%]	Peak HRR [kW/m²] (Δ%)	Mean HRR [kW/m²] (Δ%)	Mean MLR [g/s m²] (Δ%)	Mean H_c [MJ/kg]	Mean CO yield [kg/kg]
Mod-Bis-A Vinyl Ester	0	879	598	26	23	0.06
Mod-Bis-A Vinyl Ester*	8	656 (25%)	365 (39%)	18 (30%)	20	0.06
Bis-/Novolac Vinyl Ester	2	977	628	29	21	0.06
Bis-/Novolac Vinyl Ester*	9	596 (39%)	352 (44%)	18 (39%)	20	0.06
DGEBA/MDA	11	1296	767	36	26	0.07
DGEBA/MDA*	19	773 (40%)	540 (29%)	24 (33%)	26	0.06
DGEBA/BDMA	3	1336	775	34	28	0.06
DGEBA/BDMA*	10	769 (42%)	509 (35%)	21 (38%)	30	0.06

The mechanism of improved flame retardation is not yet fully understood and there is no general agreement which structure (intercalated or exfoliated) gives the best flammability properties [44]. It was found that the reduced mass loss

rate occurred only when the sample surface was partially covered with char. It is believed that the nanocomposite structure in the char acts as an insulator for heat and mass transfer. TEM images of the char of different nanocomposite systems (thermoplastics and thermosets) showed that the interlayer spacing of the char was constant (1.3 nm), independent of the chemical structure of the polymer nanocomposite. The nanocomposite strategy for flame retardation offers a number of benefits, such as improved flammability along with improved mechanical properties, whilst being more environmentally friendly compared to most of the commonly used flame retardation additives, all at relatively low concentrations and costs. It is believed that the additional use of layered silicates for improved flammability performance may allow the removal of significant portion of the conventionally used flame retardant [97], although it is likely that layered silicates on their own cannot be used for this purpose.

Optical Properties

Layered silicate nanocomposites are often found to exhibit good transparency. Wang et al. [92] compared the optical properties of organically modified magadiite and smectite based epoxy nanocomposites of a 1 mm thick sample with a concentration of 10 % layered silicate. Both systems showed good optical properties. A better transparency of the magadiite nanocomposite, however, was related to either better exfoliation or the fact that the refraction index may better match that of the organic matrix. Comparison of intercalated and exfoliated epoxy nanocomposites of up to 20 % organoclay concentration by Brown et al. [64] showed good transparency for all exfoliated systems as well as for low concentrations of intercalated layered silicates. Recent work by Salahuddin at al. [82] showed that films of highly filled epoxy nanocomposites (up to 70 % layered silicate) have shown good transparency due to the molecular level of the dispersion.

Chapter 2
Materials and Experimental Methods

This chapter introduces the different materials used for the synthesis of epoxy layered silicate nanocomposites. An illustration and discussion of the nanocomposite synthesis process is also presented. Furthermore, the different analytical techniques applied in this work are outlined this chapter.

2.1 Materials

2.1.1 Epoxy Resins and Hardener

The synthesis of epoxy layered silicate nanocomposites in this study is based on three different epoxy resins of different structures and functionalities. In addition to the widely applied diglycidyl ether of bisphenol A (DGEBA), two resin systems of higher functionality are used in this work.

The DGEBA (DER 331) is a Dow epoxy resin with a molecular weight of 380 g/mol or an equivalent of 5.3 mmol epoxide per gram resin respectively. The structure of this resin is shown in Figure 2.1. DGEBA is a clear, colourless resin, which is viscous at room temperature.
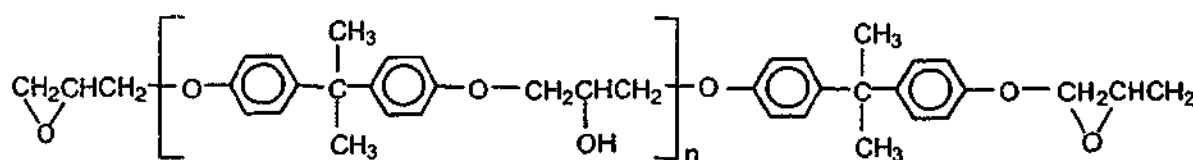
Figure 2.1: Structure of diglycidyl ether of bisphenol A (DGEBA).

The high functionality resins used in this study are triglycidyl *p*-amino phenol (TGAP) and tetraglycidyl diaminodiphenylmethane (TGDDM). Both resins are commonly used in aerospace and other high performance applications.

The TGAP, Araldite MY 510 (Figure 2.2), is supplied by Ciba Speciality Chemicals. TGAP is a light yellow, clear liquid of low viscosity at room temperature with a molecular weight of 277 g/mol and an epoxy equivalent of 9.4 mmol epoxide per gram resin according to the materials data sheet.
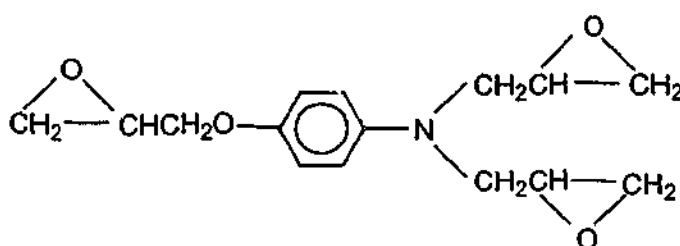
Figure 2.2: Structure of triglycidyl p-amino phenol (TGAP).

The tetrafunctional TGDDM, Araldite MY 720 (Figure 2.3), is also supplied by Ciba Speciality Chemicals. TGDDM is a clear, yellow material of very high viscosity with a molecular weight of 422 g/mol and 8.0 mmol epoxide per gram resin according to the materials data sheet.
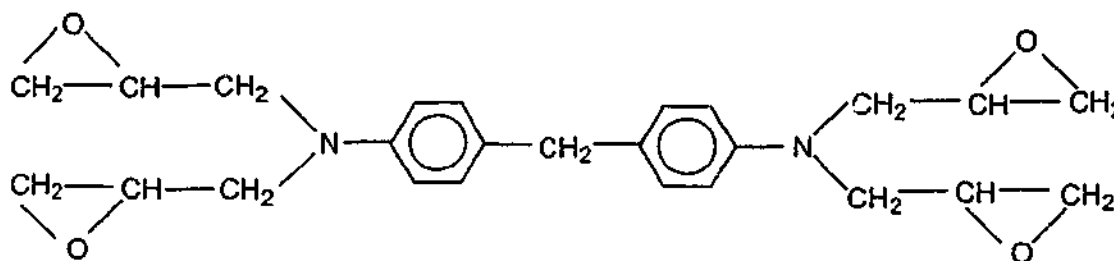
Figure 2.3: Structure of tetraglycidyl diaminodiphenylmethane (TGDDM).

The curing agent, Ethacure 100, of Albemarle Corporation is a mixture of the two diethyltoluene diamine (DETDA) isomers as shown in Figure 2.4. The blend

consists of 74 - 80 % 2,4 isomer and 18 - 24 % 2,6 isomer according to the materials data sheet. DETDA is an aromatic amine, which cures at high temperatures. Aromatic amines are commonly used in high performance epoxy systems with high glass transition temperatures. The aromatic ring gives the epoxy system increased mechanical, thermal, chemical and electrical properties compared to aliphatic amines [99]. DETDA is a dark brownish liquid of low viscosity at room temperature.
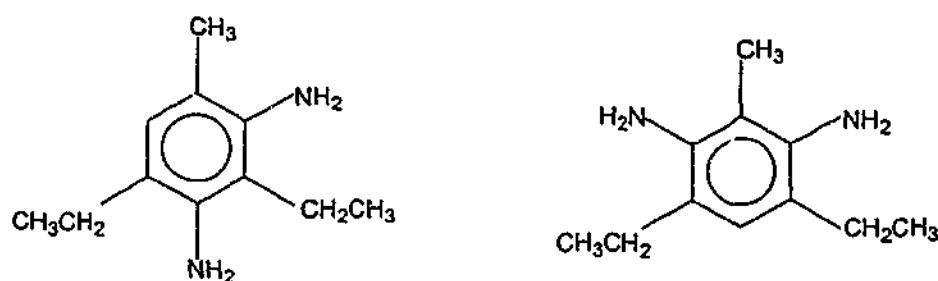
Figure 2.4: The two DETDA isomers: 3,5-Diethyltoluene-2,4-diamine (left) and 3,5-Diethyltoluene-2,6-diamine (right).

Prior to use, the hardener and the resins were heated up to 50 °C for 2 h under vacuum to remove moisture. Both resins and hardener were used without further purification.

2.1.2 Layered Silicate

The organoclay used in this work is a commercially available organically modified smectite by Nanocor Inc. (USA), Nanomer I.30E. The naturally occurring inorganic layered silicate is a bentonite, which belongs to the 2:1 phyllosilicate family. The interlayer ions have been exchanged with octadecylamine ions, $CH_3(CH_2)_{17}NH_3^+$ (a primary organo-ion). The organic content of the whole filler weight is 25 - 30 % as determined by TGA. The initial d-spacing of the silicate platelets is 23 Å.

2.1.3 Calcium Carbonate

The material used for comparison of the influence of the filler on epoxy resin viscosity was a stearic acid surface treated calcium carbonate, Omyacarb 1T, by Omya Southern PTY Ltd. (Australia). According to the materials data sheet, this material has a surface area of 5.5 m^2/g and an average particle diameter of 1.7 μm.

2.1.4 Unidirectional Carbon Fibre

Unidirectional carbon fibre for the synthesis of carbon fibre nanocomposites was obtained from Advanced Composites (Australia). According to the materials specifications, the bonded unidirectional fabric, type FFC200U0300BS, has a density of 1.8 g/cm^3, a tensile strength of 4800 MPa, a tensile modulus of 240 GPa and an elongation at break of 2.0 %. The linear density of the fibre is 800 tex (g/km fibre).

2.2   *Synthesis of Epoxy-Nanocomposites*

All initial materials were dried at 50 °C under vacuum for 2 h prior to sample preparation. The layered silicate was dispersed in the resin at approximately 80 °C using a PTFE anchor stirrer at 500 revolutions per minute (rpm). After stirring for 45 minutes the DETDA was added and mixed under vacuum at 60 °C. An epoxide to amine molar ratio of 1:0.9 was chosen for each resin system to ensure an excess of epoxide groups, as unreacted amine groups present after cure reduce the overall properties of the final material [100]. Curing was performed using a number of different temperature profiles, as illustrated in Table 2.1.

The cure cycles will be further referred to by their initial cure temperature as shown in the 'Sample Identification' column. The in-situ polymerization process

is most commonly used for thermoset nanocomposite formation. Figure 2.5 shows a schematic of the process as applied in this work.

Table 2.1: Different cure profiles of epoxy nanocomposites synthesis.

Sample Identification	Step 1	Step 2	Step 3	Step 4
80 °C	80 °C for 12 h	130 °C for 1 h	160 °C for 12 h	200 °C for 2 h
100 °C	100 °C for 2 h	130 °C for 1 h	160 °C for 12 h	200 °C for 2 h
120 °C	120 °C for 2 h	130 °C for 1 h	160 °C for 12 h	200 °C for 2 h
140 °C	140 °C for 2 h	--	160 °C for 12 h	200 °C for 2 h
160 °C	--	--	160 °C for 12 h	200 °C for 2 h

Initially, the layered silicate is swollen by epoxy monomer. As outlined in section 1.7.1, this step is determined by the nature of the resin, the smectite and its modification and is limited to a certain extent of gallery extension by a thermodynamic equilibrium. Further layer separation occurs when cure reaction is initiated through the addition of the amine and application of heat in the oven.
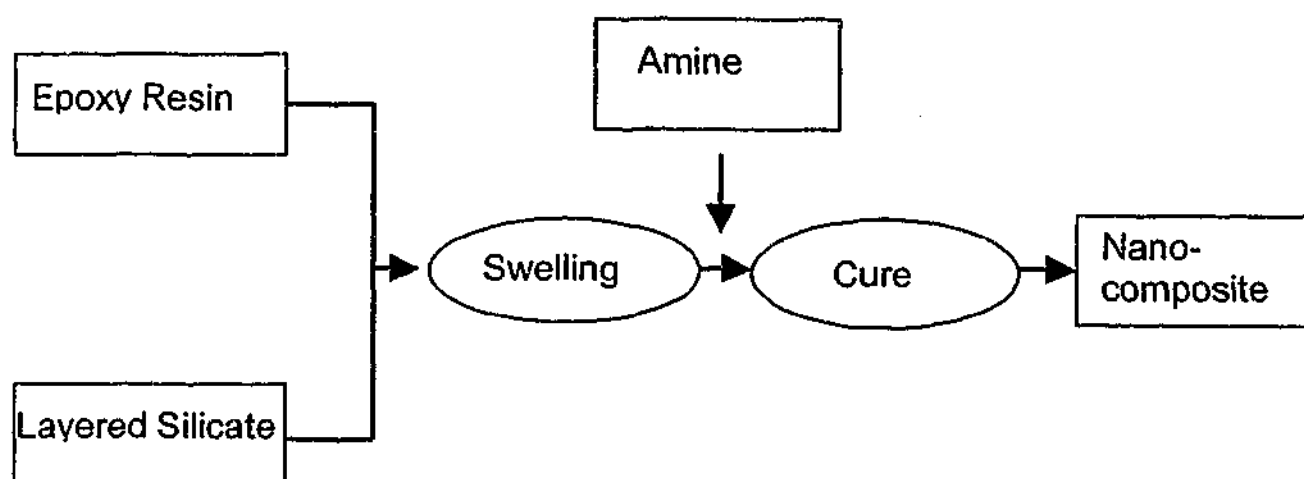

Figure 2.5: Flowchart of the nanocomposite synthesis.

2.3   *Preparation of Epoxy Carbon Fibre Nanocomposites*

In a further step, the epoxy-organoclay premix was combined with unidirectional carbon-fibre into composites. An aluminium mould was built for the prepreg synthesis, in which the resin system is applied to a fibre cloth. The mould consists of a ground and top plate which sandwich a 5 mm thick frame with a square hole of 200 x 200 mm^2. The sandwiching plates were covered with a PTFE foil to allow the removal of the composite material after cure. The fibre cloth was cut to size and carefully painted with a ratio of 1.09 g of nanocomposite premix per gram of cloth. In order to allow even distribution without damaging the fibre cloth, the nanocomposite premix was heated to about 70 °C to decrease its viscosity prior to painting. The prepregs were then aligned in the mould and stacked to a 28-ply laminate. A piece of 13 μm thick and 88 mm broad polyimide foil (Upilex$^®$ by UBE Industries LTD, Japan) was placed in the mid-thickness of the fibre plies as a crack initiator for the mode I fracture toughness test. The resin and fibre loaded mould was then placed in a hot press, heated up to 160 °C within 10 minutes and isothermally cured for 12 hours. Initially, a pressure of 7 bar was applied which was further increased to 40 bar at gelation. The time to gelation was determined from prior chemorheological experiments (see section 3.3). Prepregs were postcured for 2 h at 200 °C in an oven without any further pressure applied. A 25 mm wide strip was cut off from each edge and the remaining material used for further materials tests.

2.4   *Viscosity and Cure Monitoring Studies*

2.4.1 Dynamic Rheology

Dynamic rheology was used to determine the influence of the layered silicate on the flow behaviour of the resin before cure. Measurements were taken from blends of the resin with the layered silicate only, i.e. in the swollen state without any hardener, as represented by the first oval in Figure 2.5. These

measurements were of particular interest since layered silicates are often used as rheological additives. Hence, significant changes in flow behaviour may be expected due to the presence of the filler. Knowledge about the effect of the layered silicate on rheological behaviour prior to cure reaction is important to adjust processing conditions if required, and thus optimise the properties of the final material. It has been reported [101, 102] that the addition of particles to a liquid system not only changes the magnitude of viscosity but can also induce deviation from Newtonian flow behaviour, such as shear thinning or shear thickening.

Rheological properties are usually characterised by the relationship between stress and strain. Stress represents the force exerted on the material, the shear rate is the response to that stress. The ratio of stress and shear rate is given as

$$\eta = \frac{\tau}{\dot{\gamma}} \qquad \textit{Equation 1}$$

where τ is the shear stress, $\dot{\gamma}$ is the shear rate and η is the dynamic viscosity. A commonly used representation is the plot of viscosity as a function of shear rate.

Viscosity measurements of the resin containing 0 – 10 % of the modified layered silicate were performed on a Rheometric ARES using parallel plates of 50 mm. Samples of about 1 mm thickness were placed between the plates, which were preheated to the required temperature. Initial strain sweeps were performed to confirm that measurements were taken within the viscoelastic region (Figure 2.6). Frequency sweeps were run at 40, 60 and 80 °C using a low and a high strain value from the viscoelastic region. The frequencies covered were 1 - 200 rad/min.
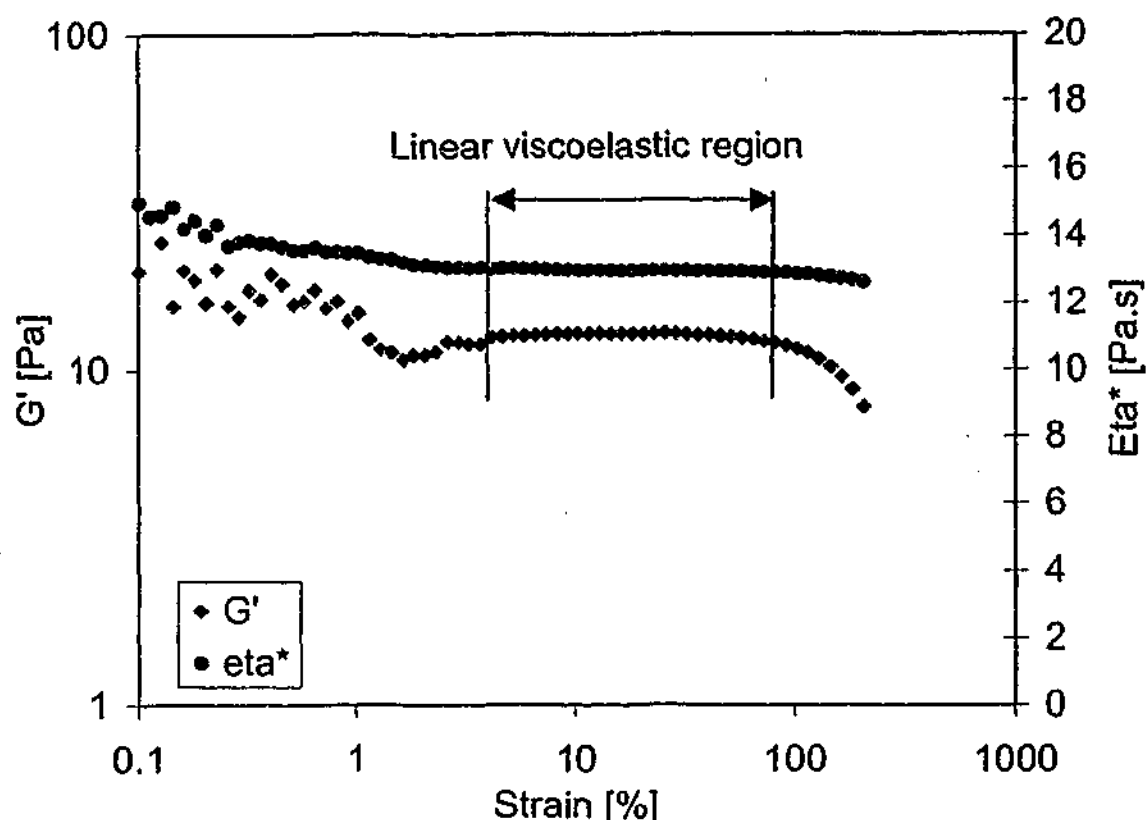
Figure 2.6: Dynamic strain sweep (TGDDM, 2.5 % OLS, 60°C) to determine linear viscoelastic region.

2.4.2 Chemorheology

Knowledge about the time and temperature dependence of the thermal transitions such as gelation and vitrification of a crosslinking network, is of major importance to adjust processing conditions and therefore to optimise the properties of the final material. The layered silicates may impose changes in the rate of network formation or the degree of conversion at which a transition occurs. Some of these effects have been discussed previously in section 1.7.2. Chemorheology is used in this work to determine and understand the role of the organically modified layered silicate on the network formation. Rheological measurements during cure can provide information on the crosslinking process. It is commonly accepted that dynamic mechanical measurements allow direct determination of the instant at which the polymer network reaches gelation. Several rheological techniques for the measurement of the gel point were classified and investigated by Halley et al. [87]. Since the epoxy/amine systems

studied in this project had an under-stoichiometrical balance between the hardener and the resin, the gel point was determined from the point where the loss tangent is independent of frequency [87]. Figure 2.7 shows a typical cross over in tan δ related to the gelation point as determined from chemorheological measurement.
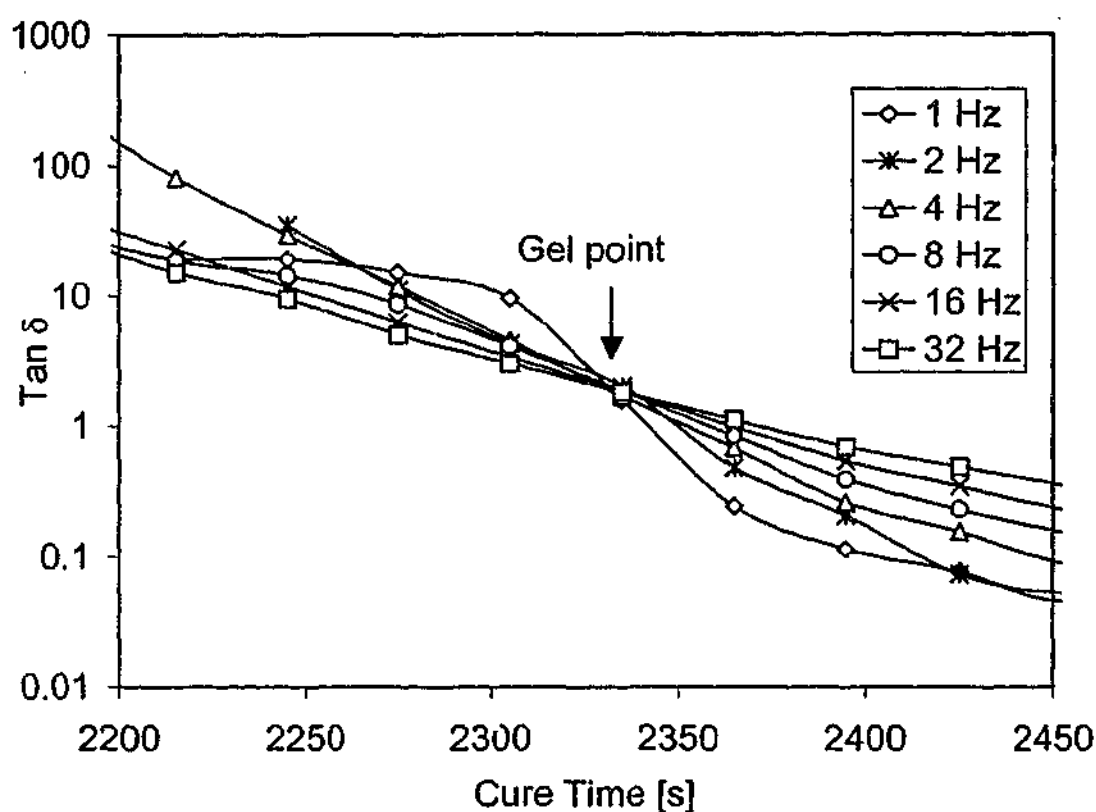
Figure 2.7: Determination of the gelation point from the cross over in tan δ of rheological measurements during isothermal cure.

Chemorheological measurements were performed on a Rheometric RDS 2 to determine gelation times of the curing systems. Experiments were conducted using parallel plates of 25 mm diameter. Samples of 0.7 to 1.4 mm thickness were placed between the plates at 50 °C and brought to cure temperature at 20 °C / min. The complex modulus was measured through the heating process and during isothermal cure at 140, 160 and 180 °C using a multi-wave technique, which allows data collection at several frequencies simultaneously. Measurements were taken at 1, 2, 4, 8, 16 and 32 Hz and 10 % strain.

2.4.3 Flexural Braid Test

The flexural braid test allows the determination of the gelation and vitrification times of the crosslinking network from viscoelastic measurements of the resin premix supported by an inert braid during cure. Gelation and vitrification can be determined from isothermal cure traces as previously discussed by Gillham [6]. Typical DMTA traces of an isothermal scan (of DGEBA/DETDA/10 % OLS cured at 120°C) are illustrated in Figure 2.8. Two successive peaks can be observed in the tan δ traces. Although the precise meaning of the first has been the subject of discussion [6, 103] it is usually associated with gelation [104, 105], whilst the second peak is related to vitrification of the resin system [6, 103, 104]. As well as the two peaks in tan δ , a steep increase in the modulus can be observed. The rapid increase in modulus is followed by a plateau, which indicates that no further reaction takes place at the given isothermal temperature [106].

The aim of the series of experiments was to confirm gelation times as determined from chemorheological measurements. Furthermore, vitrification times were determined using this technique. Experiments were carried out on a Polymer Laboratories dynamic mechanical thermal analyser (DMTA) fitted with a Mark II power head. The uncured liquid nanocomposite premix was painted onto the glass fibre tape for support. Samples of the supported resin were cut to 45 mm lengths and clamped in the dual cantilever mode, using a frame with a 5 mm free length as illustrated in Figure 2.9. The strain amplitude was set at 4µm, while the oscillating frequency of the drive shaft was 1, 3 and 10 Hz. The temperature was ramped up at a rate of 25 °C/minute to 10 °C below the desired temperature, after which the temperature increased at 10 °C/min until the desired temperature was reached.
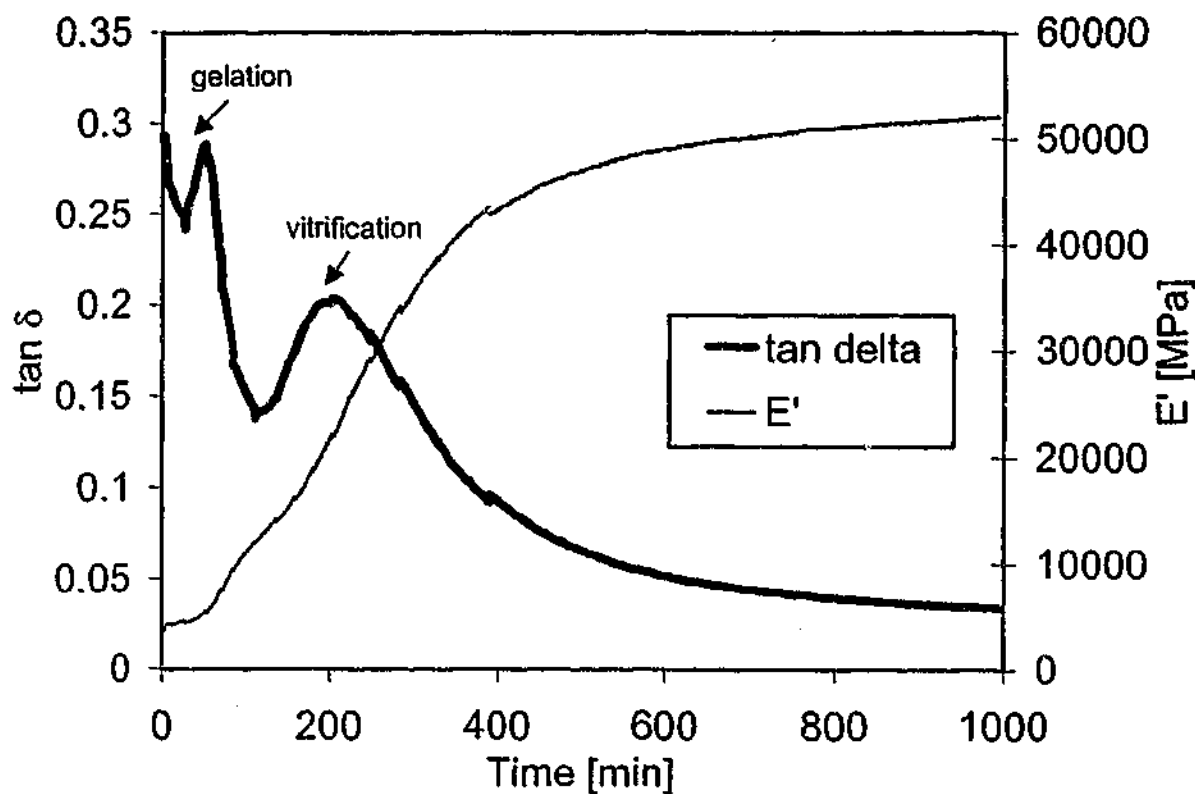
Figure 2.8: Typical DMTA thermogram of an epoxy/amine isothermal cure.

Samples were then isothermally cured to completion, as evidenced by no further changes in storage modulus at the chosen temperature. Following this, the sample was quenched down to room temperature and a dynamic temperature rescan from 50 - 300 °C at a rate of 2 °C/min was performed. The isothermal cure temperatures ranged from 100 - 180 °C, in steps of 20 °C.
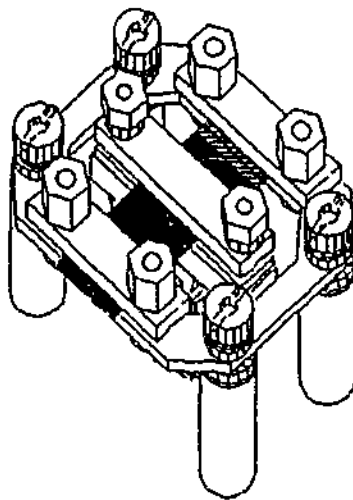
Figure 2.9: Frame assembly of the DMTA showing a sample clamped in the dual cantilever mode for the flexural braid test [107].

Figure 2.10 shows an example of a dynamic temperature DMTA rescan after isothermal cure. The tan δ trace shows two distinct peaks with corresponding changes in the modulus spectra. The two transitions are related to two different T_gs. The glass transition at the lower temperature is referred to as the $^\alpha T_g$, which is the actual T_g and which is often found to be 10 - 30 °C above the cure temperature. The second transition is the ultimate glass transition, $^u T_g$, and is a result of further cure at increased temperatures ($T > ^\alpha T_g$) during the dynamic temperature scan.
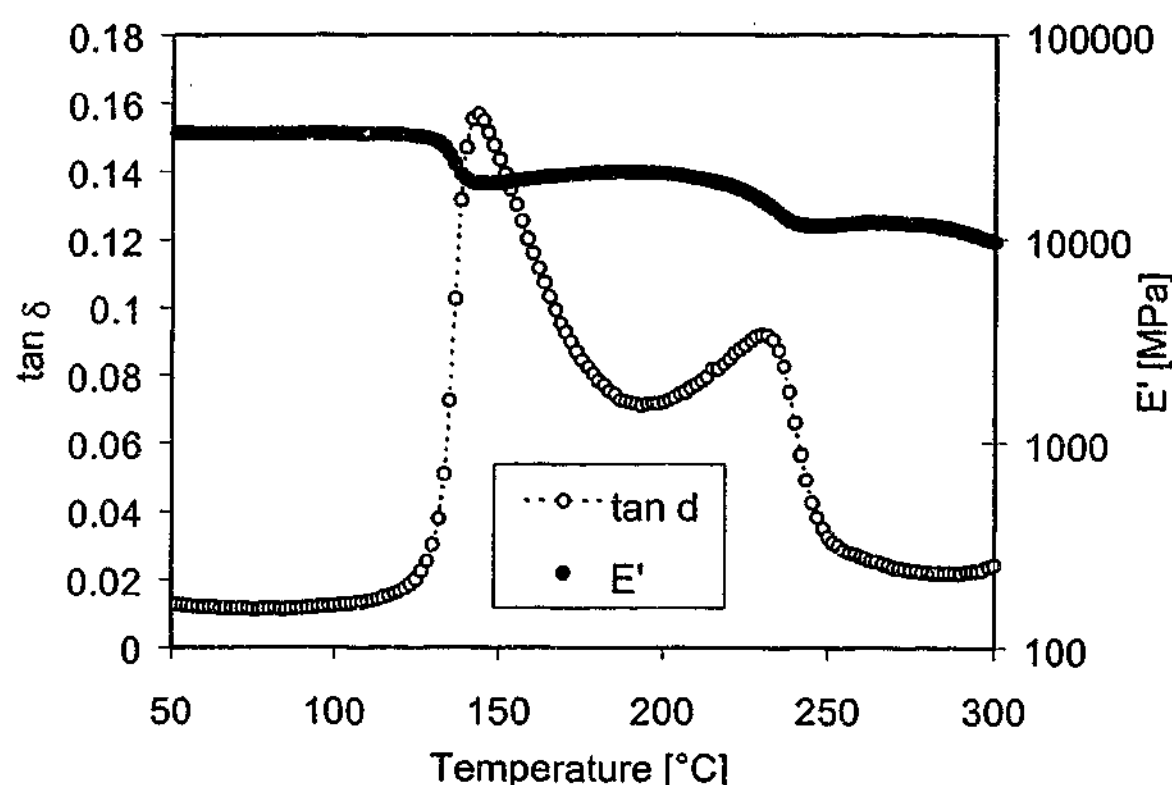
Figure 2.10: Typical thermogram of a DMTA temperature rescan after isothermal cure.

2.4.4 Differential Scanning Calorimetry

Differential scanning calorimetry (DSC) is a commonly used method to monitor the curing reaction of epoxy resins. The utility of DSC is its ability to measure the changes in the heat content during a transition or reaction of a sample with respect to temperature or time. A sample is treated with a programmed temperature profile (isothermal or dynamic temperature scan) and the absorbed

or released energy is measured by comparison with the energy balance of an empty reference cell. Since epoxy curing reactions are exothermic (with a heat output of approximately 105 kJ/mol epoxy groups [108]) the energy release can be used to monitor the conversion.

DSC measurements were carried out using a Perkin Elmer DSC-7. Data analysis was performed using Pyris software. Prior to measurements, the DSC was calibrated with an indium and a zinc standard. The uncured resin samples of 5-8 mg were sealed in aluminium crucibles and heated from 50 °C to 300 °C at a scanning rate of 10 °C/min under a nitrogen atmosphere. Figure 2.11 shows a typical DSC thermogram of a dynamic temperature measurement of an epoxy/amine cure reaction. The trace exhibits a single large exothermic peak associated with the epoxy amine polymerization. Assuming that the heat evolved during cure is directly related to the disappearance of epoxy groups, the area underneath the peak may be related to the fractional conversion. For dynamic temperature measurements the fractional conversion, α, can be calculated as follows:

$$\alpha = 1 - \frac{\Delta H_{residual}}{\Delta H_{total}} \qquad \textit{Equation 2}$$

where $\Delta H_{residual}$ is the residual heat output determined from a dynamic (re)scan after a sample has been exposed to a certain amount of cure, and ΔH_{total} is the total heat output of the complete cure reaction. This equation was used to determine the degree of conversion at significant stages of cure, such as at gelation.
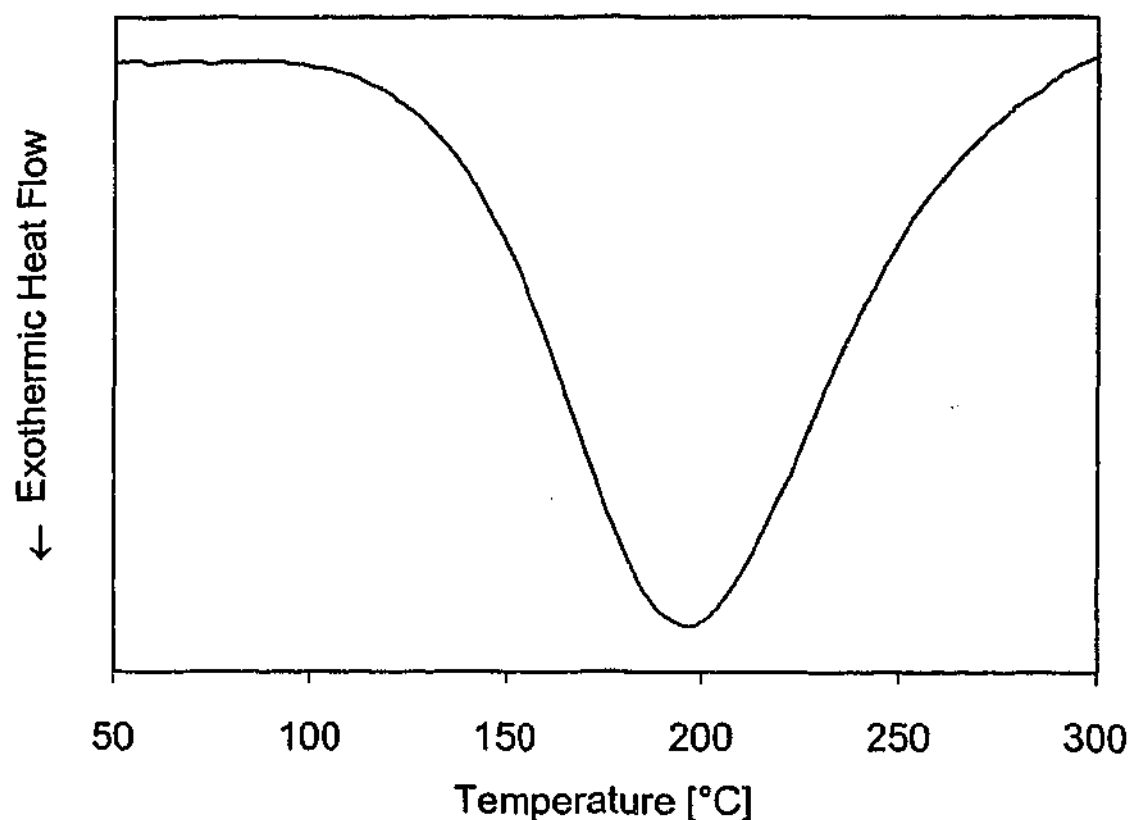
Figure 2.11: Typical DSC thermogram of an epoxy/amine temperature scan.

2.5   *Structural Analysis*

2.5.1 X-Ray Diffraction (XRD)

The utility of wide angle x-ray diffraction, XRD, or WAXS (wide angle x-ray scattering), is commonly used to determine the distance between silicate layers in the pristine smectite or in the polymer-intercalated state respectively. A repeated distance between layers, the d-spacing, can be determined through the diffraction from two scattering planes, i.e. two consecutive clay layers as illustrated in Figure 2.12. The distance or d-spacing between two layer surfaces is marked as d. The two layers intercept with the x-rays of the wavelength λ at the incident angle 2θ. A constructive interference occurs when the Bragg Law is fulfilled:

$$n \cdot \lambda = 2 \cdot d \cdot \sin \theta \qquad\qquad \text{Equation 3}$$

The integer n refers to the diffraction such that if d_{001} is 1 nm, then d_{002} is approximately 0.5 nm. Therefore, with a known incident angle and wavelength the layer distance can be calculated from equation 3. Figure 2.13 illustrates typical WAXS traces of an intercalated nanocomposite system and the pristine clay. Both, the neat clay and the nanocomposite system show a peak at $2\theta = 19.5°$. This peak represents the (110) reflection of the montmorillonite [109]. The (hk0) plane characterizes the atomic arrangement in the plane that is parallel to the z-axis. This peak is therefore independent of the distance between silicate platelets and its location can be used as a reference.
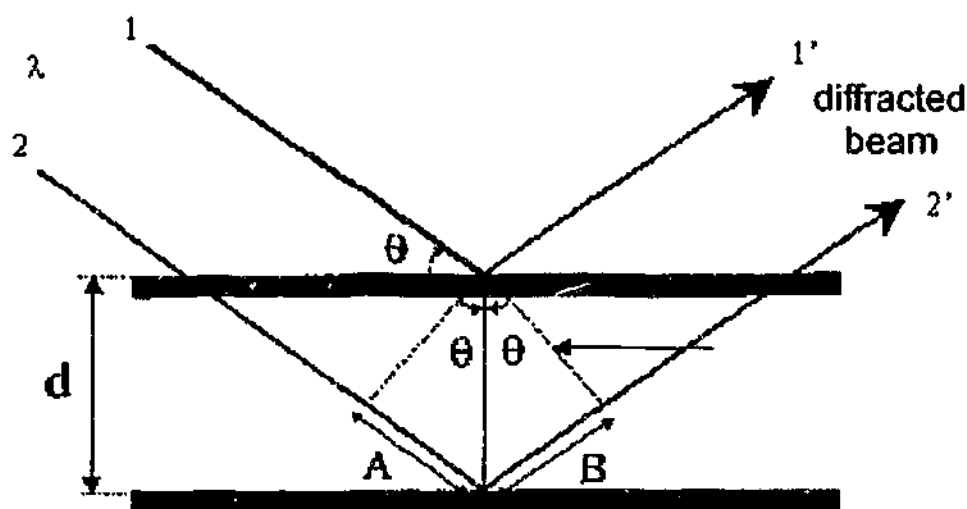
Figure 2.12: Principle of X-ray diffraction adapted from Kornmann [26].

Wide angle x-ray diffraction (XRD) analysis were performed using a Rigaku Geigerflex generator with a wide angle goniometer. An acceleration voltage of 40 KV and a current of 22.5 mA was applied using Ni filtered Cu-K-α radiation. The sample surfaces were polished prior to measurement. The radiation wavelength was $\lambda = 1.540598$ Å.
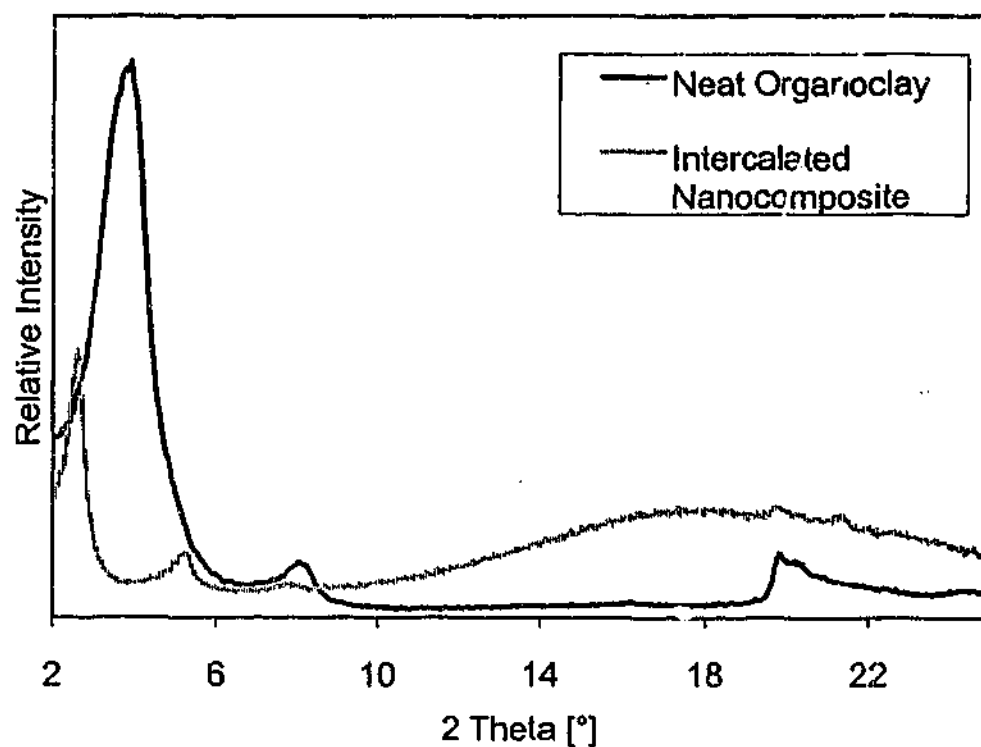
Figure 2.13: WAXS traces of pristine organoclay (Nanomer I.30E) and an intercalated epoxy nanocomposite.

2.5.2 Optical and Atomic Force Microscopy

Two different microscopy techniques with different resolutions and magnifications were used to investigate the bulk surface and the microstructure of the nanocomposites.

Electronically recorded optical micrographs were obtained using a Leica DMRM optical microscope in the reflection mode.

Atomic force microscopy (AFM) images were recorded from thin sections using a Digital Instruments Nanoscope IIIa scanning probe microscope in the phase contrast mode.

2.5.3 Dynamic Mechanical Thermal Analysis

The effect of the layered silicate on the glass transition temperature and the β-relaxation of the cured nanocomposites were determined using dynamic

mechanical thermal analyses (DMTA). The ability of a material to store energy is generally expressed as the dynamic storage modulus, represented as E'. The loss modulus, E", measures the viscous behaviour, i.e. the ability of the material to dissipate heat energy. The ratio of lost energy to energy stored is defined as the loss tangent, tan δ. The value of tan δ maxima is widely used to characterize the relaxation due to its sensitivity to changes in the polymer network structure and internal molecular motions. Most polymers also exhibit at least one relaxation in the glassy state (β-relaxation) in addition to the primary α-relaxation.

A Rheometric Scientific DMTA IV was used to determine the α- and β-relaxation temperature from the loss tangent of the nanocomposites. The cured samples were clamped in a medium frame using a small centre clamp in the dual cantilever mode. Measurements were performed in two steps (to avoid high tension in the specimen due to thermal expansion) from -100 °C to 50 °C and from 50 to 300 °C at 2 °C/min and frequencies of 1, 3 and 10 Hz. Liquid nitrogen was used as a cooling agent for the subambient measurements. The data was analysed using RSI Orchestrator software.

2.5.4 Scanning/Transmission Electron Microscopy (SEM/TEM)

Transmission electron microscopy (TEM) was applied to further correlate the morphologies with the XRD experiments. This was necessary since the utility of XRD is limited to a certain resolution. The XRD used in this work was unable to detect regular stacking that exceeded a d-space of approximately 8 nm (80 Å). A large distribution of d-spacings at low clay concentrations could also cause the absence of the (001) reflection. TEM was especially useful, therefore, to confirm if the XRD results with no scattering are truly exfoliated or if the silicate platelets are only highly intercalated and still show some level of ordered, parallel structure.

Transmission electron microscope samples were cut using a Porter-Blum MT-2B ultramicrotome with a DiaTech (Knoxville) diamond knife. Cuts were made at

an angle of 6 degrees and a cutting velocity of about 0.1 mm/sec. Samples were collected on hexagonal 300 mesh copper grids. Micrographs were then obtained using a Philips CM20 transmission electron microscope operating at 200 kV in bright field mode.

Scanning electron microscopy was used to investigate fracture surfaces of the nanocomposites as well as the fibre reinforced nanocomposite systems to understand the failure mechanism of the material. Samples were glued to a supporting aluminium plate using conductive carbon. The specimen were then coated with an ultra-thin layer of gold prior to examination to ensure the required conductivity. The materials were examined using a Philips XL30 field emission scanning electron microscope (SEM).

2.5.5 Near Infrared Spectroscopy

Fourier transformed near infrared spectroscopy was utilized to determine the amount of residual epoxy groups after cure. Samples of 1.5 mm thickness were analysed in 16 successive scans. The degree of cure was determined by measuring the area under the 4530 cm^{-1} epoxy overtone [110]. The area under the epoxy overtone in a separate uncured prepolymer blend allowed quantification of the degree of cure. Measurements of liquid unreacted prepolymer blends were taken from samples sandwiched in a silicone gasket between thin glass plates.

FTIR analysis was performed on a Perkin Elmer Spectrum GX FT-IR System. Samples of 1.5 mm thickness were scanned in a wave number range of 8000 – 4000 cm^{-1}.

2.6   *Nanocomposite Characterization*

2.6.1 Three Point Bending Test

Three point bending tests were carried out to determine the elastic modulus of the different materials. The test procedure followed the ASTM D 790 M-93 standard [111]. An Instron 4486 was used to apply the load at a cross head speed of 1.0 mm/min and the force was recorded with a 1 kN load cell. The elasticity modulus in bending, E, was calculated from the gradient in the load vs. displacement curve:

$$E = \frac{F}{\delta} \cdot \frac{l^3}{4bd^3} \qquad \text{\textit{Equation 4}}$$

where l is the supported length (40 mm), b is the width and d the depth of the specimen and F/δ is the gradient of the load displacement curve.

2.6.2 Fracture Toughness Test

The fracture toughness of the cured nanocomposites was determined using the compact tension method according to ASTM D 5045 - 96 [112]. Measurements were taken on an Instron 4486 universal tester. Specimens were pre-cracked prior to testing by inserting a razor blade into the machined notch and impacting with a hammer. After placing the specimen in a jig, the samples were tested at a cross head speed of 1.3 mm/min. The exact crack length was determined after fracture using an optical microscope fitted with a ruler. The stress intensity factor, K_{IC}, was calculated from the correlation:

$$K_{IC} = \frac{P \cdot Y}{B \cdot \sqrt{W}} \qquad \text{\textit{Equation 5}}$$

where P is the maximum load [N], B is the sample thickness, W the sample width and Y is defined by the correlation of the crack length (a) to thickness (W) ratio:

$$Y = f(R) = \frac{(2+R)(0.886 + 4.64\,R - 13.32\,R^2 + 14.72\,R^3 - 5.6\,R^4)}{(1-R)^{\frac{3}{2}}} \qquad \textit{Equation 6}$$

with R = a / W. A minimum of five samples was used to determine the K_{IC} for each material.

2.6.3 Free Volume Properties

Positron annihilation lifetime spectroscopy (PALS) was applied to determine free volume properties of the cured nanocomposites. A detailed background on the theory and technique of PALS can be found elsewhere [113-115]. Briefly, the antiparticle of an electron, the positron, is used to investigate the free volume between polymer chains. The 'birth' of the positron can be detected by the release of a γ-ray of characteristic energy, which occurs approximately 3ps after positron emission when the ^{22}Na decays to ^{22}Ne. Once inside the polymer material, the positron forms one of two possible types of positroniums, an *ortho*-positronium or a *para*-positronium, obtained by pairing with an electron abstracted from the polymer environment. The decay spectra are obtained by the 'death' event of the positron, *para*-positron or *ortho*-positron species. The lifetimes of the various species and their intensity can be determined through appropriate curve fitting. The lifetime of *ortho*-positronium (τ_3) and intensity (I_3) has been found to be indicative of the free volume in the polymer system since this is where the relevant species become localized, form and decay. τ_3 is related to the size of the free volume sites, the intensity I_3 is related to their probability of formation and their number concentration. Since τ_3 is related to

the radius, $\tau_3^3 \cdot l_3$ is used in this work as an indication of the total free volume fraction.

The PALS unit used was an automated EG&G Ortec fast-fast coincidence system with a ^{22}Na radioactive source and a resolution of 270 ps measured on ^{60}Co. A 1 mm diameter spot source of ^{22}Na was obtained by dropping a ^{22}NaCl solution onto thin titanium foils, with a resultant activity of 40 µCi. Experiments were run in a thermally stable environment at 22°C. No source correction was required, as confirmed by the testing of highly annealed and polished aluminium, which results in the well known, single decay process. Each spectrum consists of 30,000 peak counts, and the data was fitted using the PFPOSFIT program [116].

2.6.4 Density Measurements

Density measurements were performed on a helium-based gas displacement pycnometer, type Micromeritics AccuPyc 1330. The principal of this measuring method is that a sample, which is added to a closed cell of a constant temperature and a certain pressure, will cause an increase in pressure corresponding to its displaced volume. The volume can be calculated with the basic equation:

$$p \cdot V = constant \qquad\qquad Equation\ 7$$

where p is the pressure and V is the volume. At a given sample weight, the density can be calculated by dividing the sample mass by the determined sample volume.

Prior to density measurements the nanocomposite systems were grinded to avoid errors caused by voids and entrapped bubbles in the cured polymer. The pycnometer was calibrated with factory calibrated stainless steel balls of known volume. Each sample was measured ten times and the standard deviation calculated.

2.6.5 Determination of Water Uptake

The water uptake properties of a series of nanocomposites were measured gravimetrically on analytical weighing scales. Prior to testing, three replicates of each sample with the dimension $2 \times 10 \times 40$ mm^3 were dried in a vacuum oven for two days to remove any residual moisture. Each sample was then weighed and stored at 80 °C in test tubes filled with distilled water. The sample weight was determined at certain time intervals over a period of 3600 hours, the sample surface dried with a tissue before weighing.

2.6.6 Thermogravimetric Analysis

The utility of thermogravimetric analysis (TGA) is to measure changes in weight of a material with respect to temperature. The sample material is usually (dynamically or isothermally) scanned according to a defined temperature program and under the constant flow of an inert or oxidising gas.

Measurements were conducted using a Mettler Toledo TGA/SDTA 851^e. Samples of 10 - 15 mg were placed into small, ceramic crucibles and heated from 50 - 800 °C at a heating rate of 5 °C per minute under a nitrogen atmosphere. A thermogram of the organically modified smectite is shown in Figure 2.14.
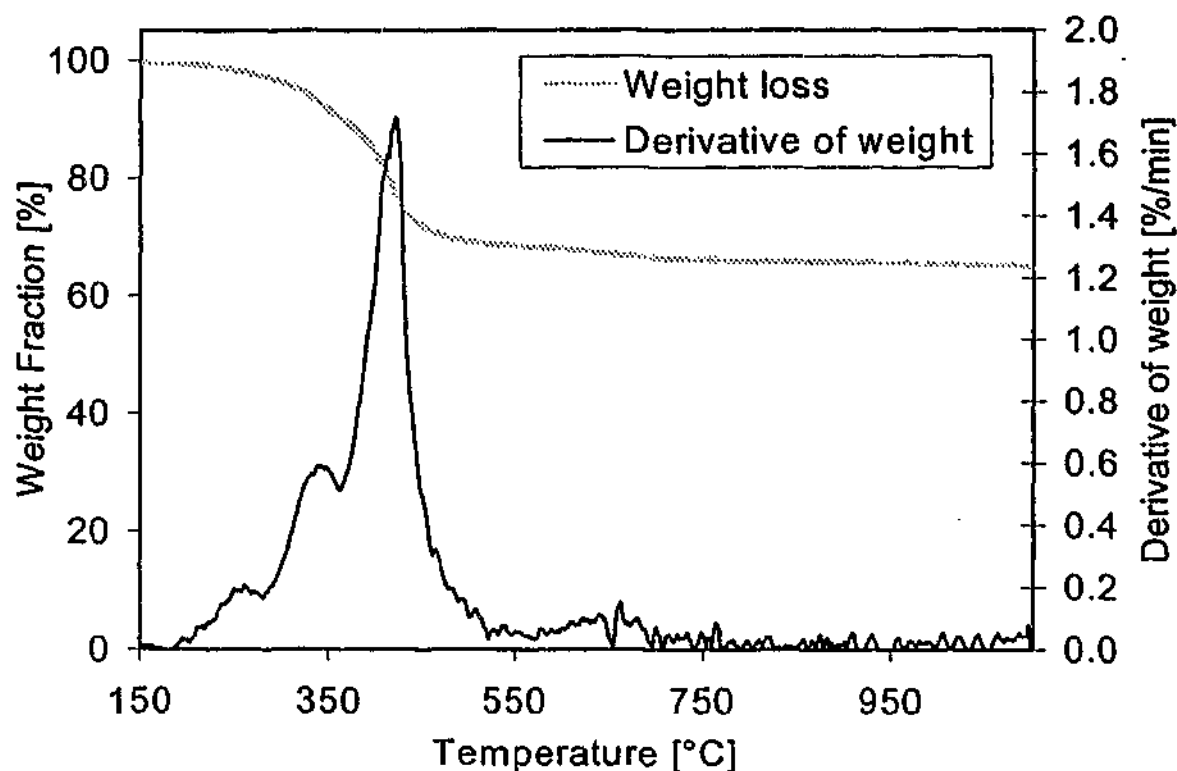
Figure 2.14: Thermogram of the organically rendered layered silicate, Nanocor I.30E.

2.7   Epoxy Carbon Fibre Nanocomposites Characterization

2.7.1   Fibre Content

The fibre content in the cured epoxy fibre nanocomposites was determined according to ASTM D 3171-76 [117]. Three specimens of 0.3 - 0.5 g were cut from each material. The sample weight was determined using analytical weighing scales. The specimens were then placed in 125 ml round bottom flasks and covered with 30 mL of concentrated nitric acid (70 %). Each flask was fitted with a reflux condenser and placed in an oil bath at 75 °C. After 5 hours, the contents of each flask was poured into a sintered glass filter under vacuum and washed three times with distilled water and once with acetone. The carbon fibre was then removed from the filter and dried on a tared petri-dish at 100 °C. After drying, the sample weight was determined using analytical scales. The fibre weight percent (% f_{wt}) and the fibre volume percent (% f_V) was then calculated according to Equation 8 and Equation 9, respectively:

$$\% \, f_{wt} = \left(\frac{W}{w}\right) \cdot 100 \qquad \text{Equation 8}$$

$$\% \, f_{v} = \left[\frac{(W/F)}{(w/c)}\right] \cdot 100 \qquad \text{Equation 9}$$

with W being the weight of fibre in the composite, w the initial specimen weight, F the fibre density and c the composite density.

2.7.2 Mode I Fracture Toughness

The Mode I test method for interlaminar fracture toughness of unidirectional fibre-reinforced polymer matrix composites (ASTM D5528-94a [118]) was used to investigate the supplementary reinforcing effect of layered silicates on the fibre composite. Opening forces are applied to a unidirectional laminated composite specimen, which contains a non-adhesive delamination initiator in the mid-plane as illustrated in Figure 2.15. Specimens were cut into samples of 25 mm width and 150 mm length with a 63 mm long crack starter film. To load the sample, aluminium tabs were glued to the end of the specimen that contains the crack initiator film. One side of the specimen was coated with liquid paper to assist monitoring of the crack growth. The ends of the double cantilever beam specimen were opened with an Instron universal tester at a crosshead speed of 1mm/min, while the load and delamination length was recorded.

Load/displacement curves were produced for each sample. The mode I interlaminar fracture toughness, G_{IC}, is calculated from this data using a modified beam theory as shown in Equation 10:

(a) with piano hinges   (b) with loading blocks
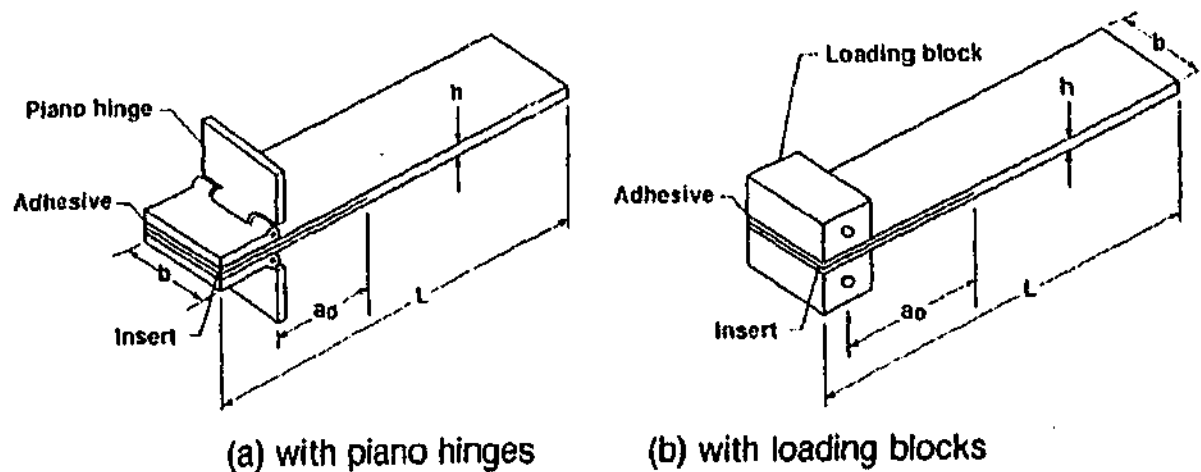
Figure 2.15: Mode I specimen for interlaminar fracture toughness testing of unidirectional fibre composites [118].

$$G_{IC} = \frac{3P\delta}{2b(a+|\Delta|)} \qquad \text{Equation 10}$$

where P is the applied load, δ the load point deflection, b the specimen width, a the delamination length and $|\Delta|$ an experimentally determined correction factor considering rotation at the delamination front. The correction factor is determined to be the x-axis intercept of a plot of the cube root of compliance, $C = \delta / P$, as a function of crack length, a. Figure 2.16 shows an example of a load/displacement curve and the correlating resistance curve (G_{IC} vs. crack length a). The value of $G_{IC\text{-init}}$ is defined as the first (initial) deviation from linearity on the load/displacement curve. Another commonly quoted value in mode I fracture toughness is $G_{IC\text{-prop}}$, which is defined as the value of G_{IC} during steady crack propagation, corresponding to the plateau in the resistance curve and the maximum load.
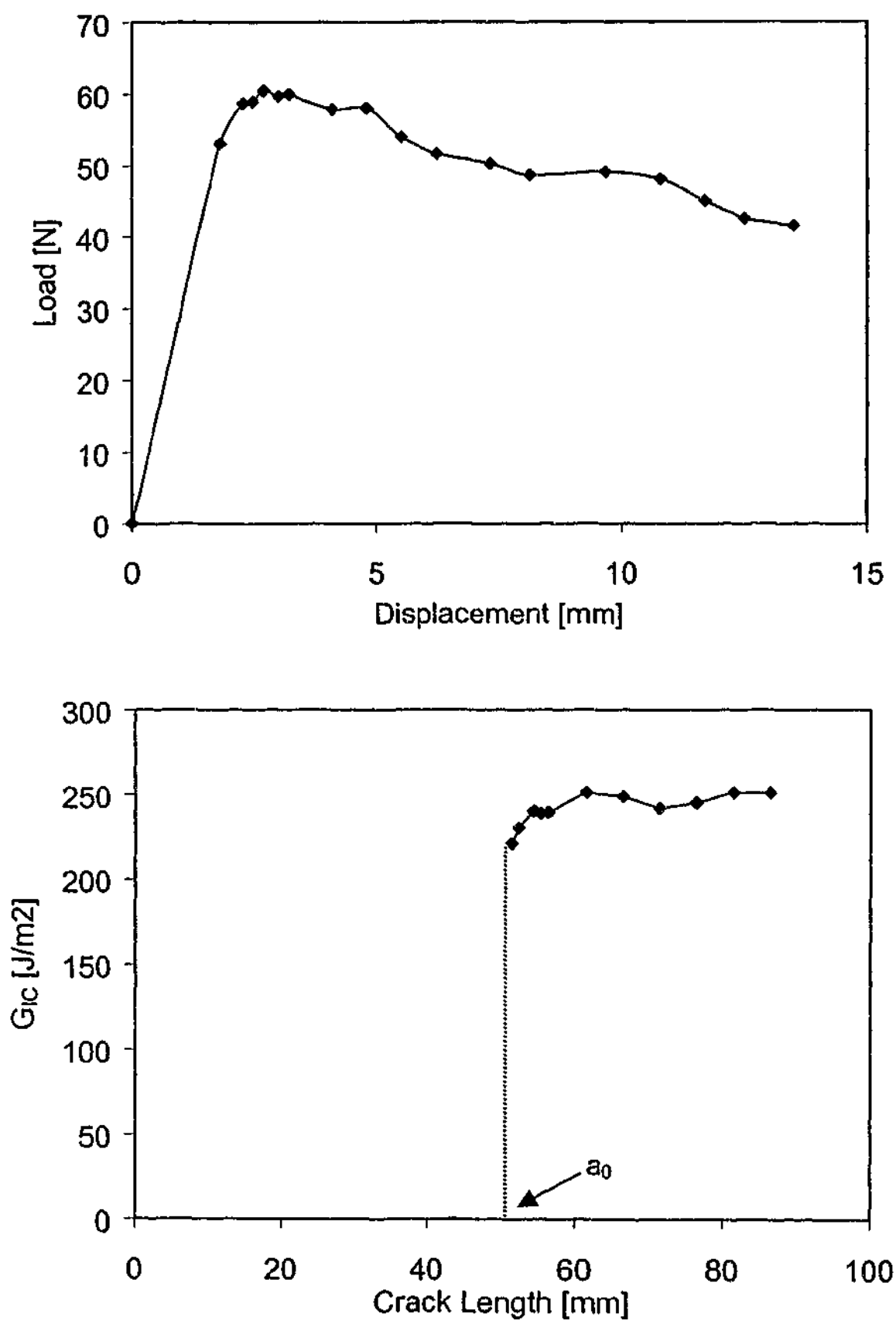
Figure 2.16: Construction of a resistance curve (bottom) from a load
displacement curve (top), for a DGEBA carbon fibre nanocomposite containing
2.5 % layered silicate.

2.7.3 Interlaminar Shear Strength

The interlaminar shear strength was determined according to ASTM D 2344 – 84 [119]. Samples of 5x10x32 mm³ were cut with the longest dimension being the carbon fibre direction. The test specimen was then centred perpendicular to two fixed cylindrical axis and a load applied from the top with a crosshead movement of 3 mm/min until failure occurred. The apparent shear strength, S_H, was calculated from the following equation:

$$S_H = 0.75 \frac{P_B}{b \cdot d} \qquad \text{\textit{Equation 11}}$$

with P_B being the load at failure, b the width of the specimen and d the thickness of the specimen.

2.7.4 Error Analysis

A minimum of five specimens per sample was used in any of the mechanical properties testing techniques. Values represented in the results tables show the average value and the correlating standard deviation (Std. Dev.) as calculated from

$$\text{Std. Dev.} = \sqrt{\frac{n \sum x^2 - \left(\sum x \right)^2}{n(n-1)}} \qquad \text{\textit{Equation 12}}$$

with n being the number of measurements and x the individual value.

Chapter 3
Viscosity and Cure Monitoring Studies

This chapter discusses the influence of the organically layered silicate on the epoxy resin viscosity and the epoxy/amine curing kinetics as determined by rheological, thermal and infrared analysis. Any possible catalytic influence of the organically modified clay on the resin/hardener cure or epoxy homopolymerization is of importance in order to optimise the resin/hardener ratio and the curing profile. Cure conditions have to be controlled to ensure full cure of the resin and to avoid trapped hardener molecules in the polymer matrix. Unreacted amine groups present after cure may be deleterious to the overall properties of the final material [100].

Rheology and gelation and vitrification studies were carried out to determine processing conditions for both the pristine epoxy nanocomposite and the fibre-reinforced nanocomposites. It is well known that accurate determination of the gel point is essential for the understanding and control of any thermoset process [87]. In fibre composite synthesis, for example, the gel point gives an indication of what time in the cure cycle the pressure should be applied for final prepreg shaping.

3.1   Rheology of Resin/Layered Silicate Blends

Rheological measurements of the different resins containing 0 - 10 % layered silicate were conducted to investigate how the resin viscosity changes with organoclay concentration. No hardener was added to avoid cure during experiments. For comparison, measurements were made of resins mixed with 5 % of a micron-sized surface treated calcium carbonate filler. Isothermal

dynamic strain sweeps were performed for epoxy alone, and with organoclay to ensure that subsequent measurements were taken within the viscoelastic region. The linear viscoelastic region was determined from the linear correlation of viscosity as a function of strain. Figure 3.1 and Figure 3.2 show typical dynamic strain sweeps to determine the area of linear viscoelastic response and the correlating dynamic frequency sweeps. In addition, steady shear measurements were taken to compare Power law and Herschel-Bulkley data fits of steady and dynamic measurements, and to determine if the Cox-Merz rule [120] can be applied to the different layered silicate containing systems.

In general, it was found that tests above 40 °C showed very low torque readings at low frequencies, whilst at higher organoclay concentrations, a more highly non-linear viscoelastic response was observed. To ensure reproducibility of subsequent isothermal dynamic frequency scans, two different strains within the linear viscoelastic region (at 10 % and 50 % strain) were selected for testing.
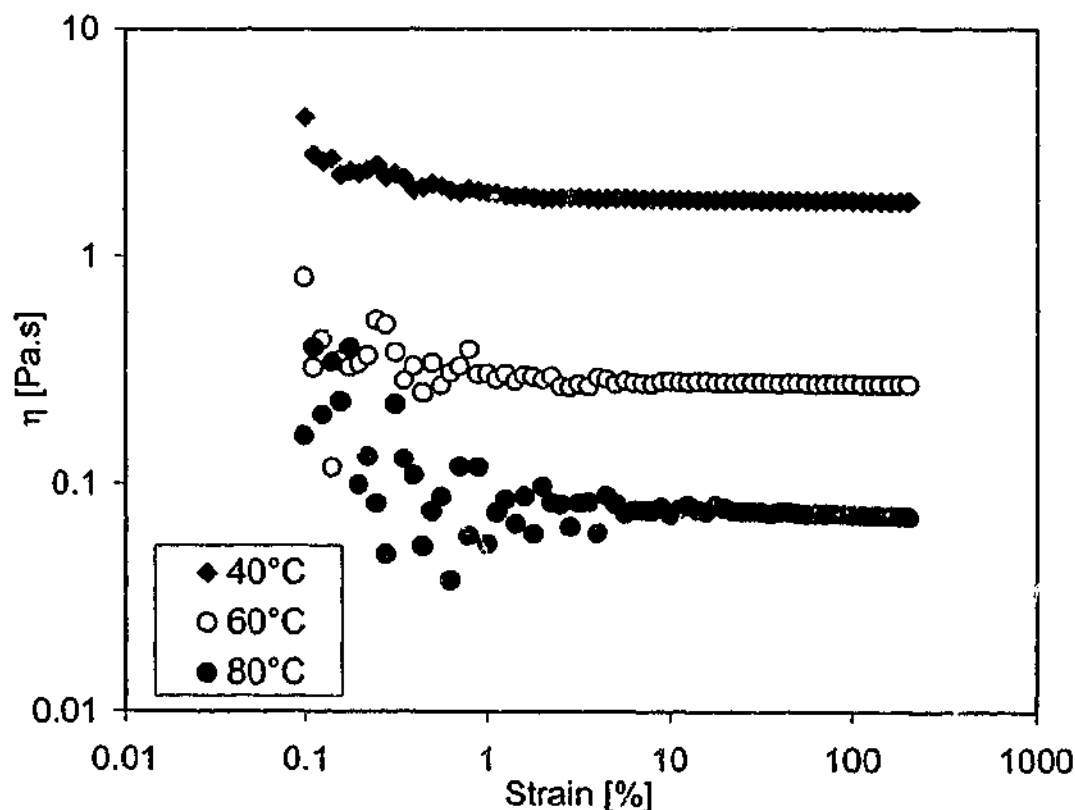
Figure 3.1: Dynamic strain sweeps of DGEBA 5 % OLS to determine the viscoelastic region.
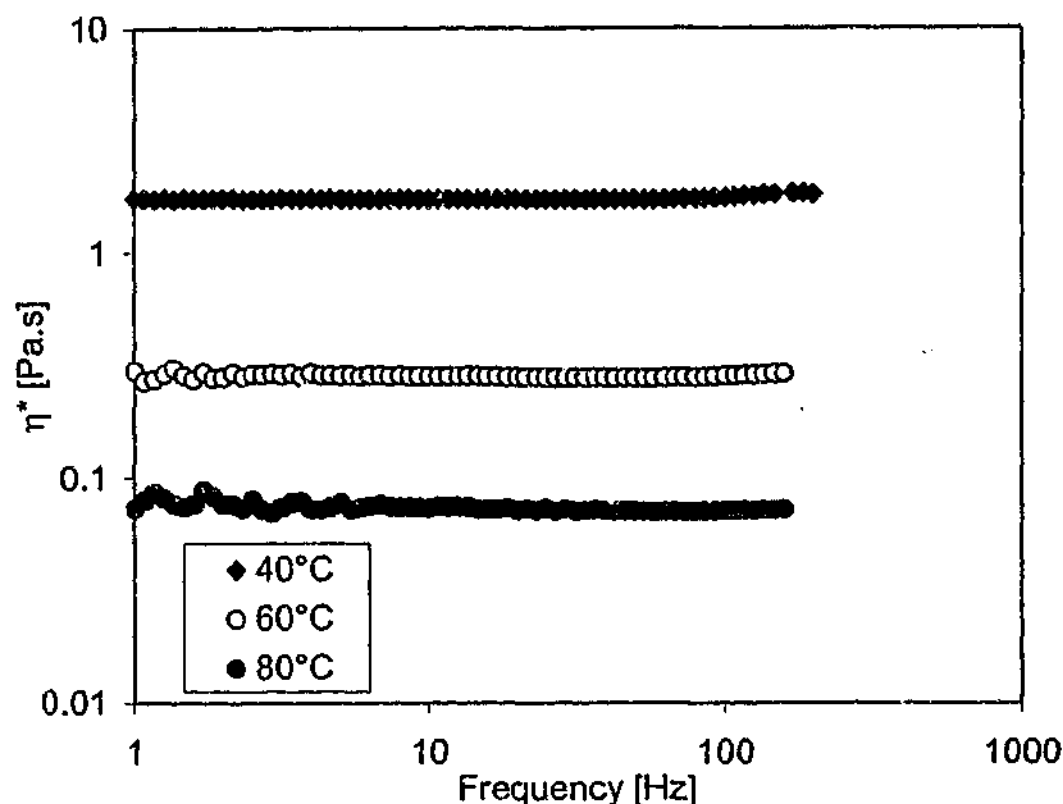
Figure 3.2: Dynamic frequency sweeps of DGEBA 5 % OLS in the viscoelastic region at 10 % strain.

Figure 3.3 to Figure 3.5 show overlaid dynamic and steady shear measurements of the different resin systems containing 0 - 10 % OLS at 40°C. Good correlation between dynamic and steady viscosity measurements can be observed at lower OLS concentrations. However, at layered silicate concentrations of 7.5 % and above results from the two different experiments deviate slightly. A general trend which method yields higher values cannot be observed. For example, dynamic measurements of the TGAP system containing 7.5 % OLS show higher viscosity values compared to steady shear measurements, while values at 10 % show the opposite behaviour. It is possible that there exists structure in these more highly loaded samples, and that imposition of steady shear breaks down and/or builds up this structure, depending on the shear rate. However, it should be noted that the variation between the two measurements is still very low. Further, it can be seen that increased organoclay concentrations lead to an increasing trend of shear thinning behaviour.
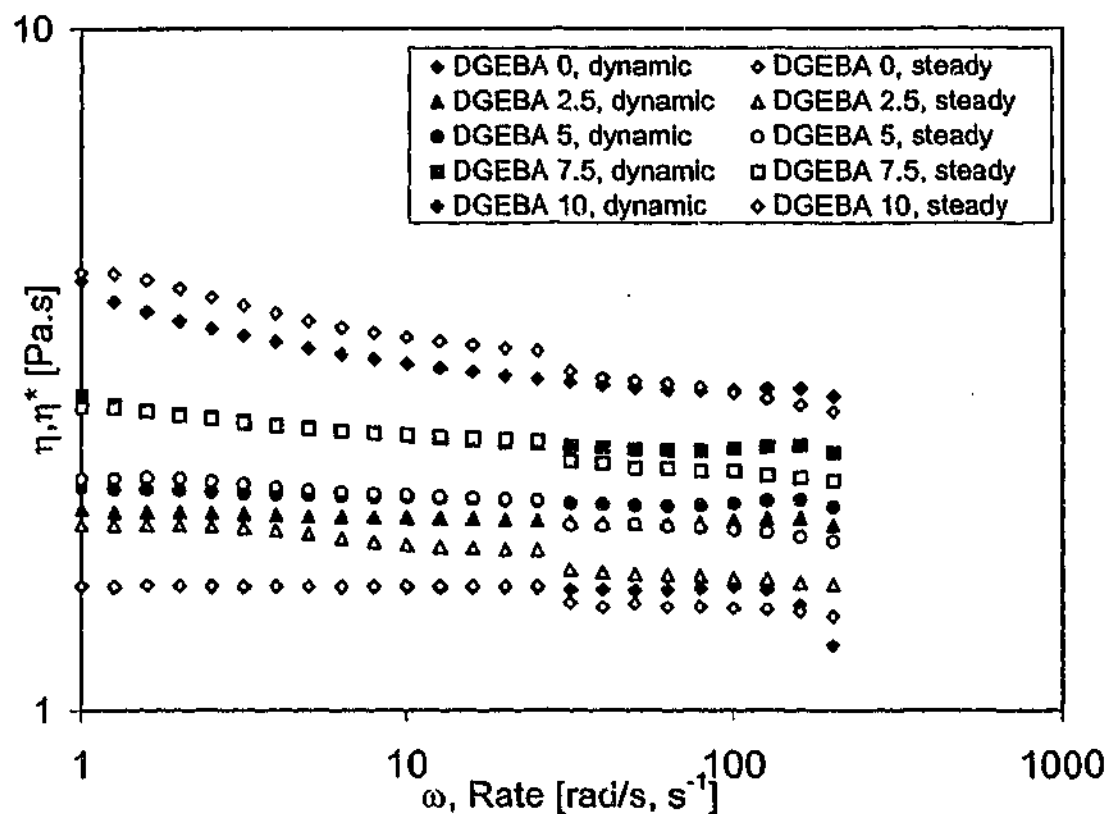
Figure 3.3: Comparison of dynamic (d) and steady (s) viscosities as a function of shear rate of a series of DGEBA/layered silicate blends at 40°C.
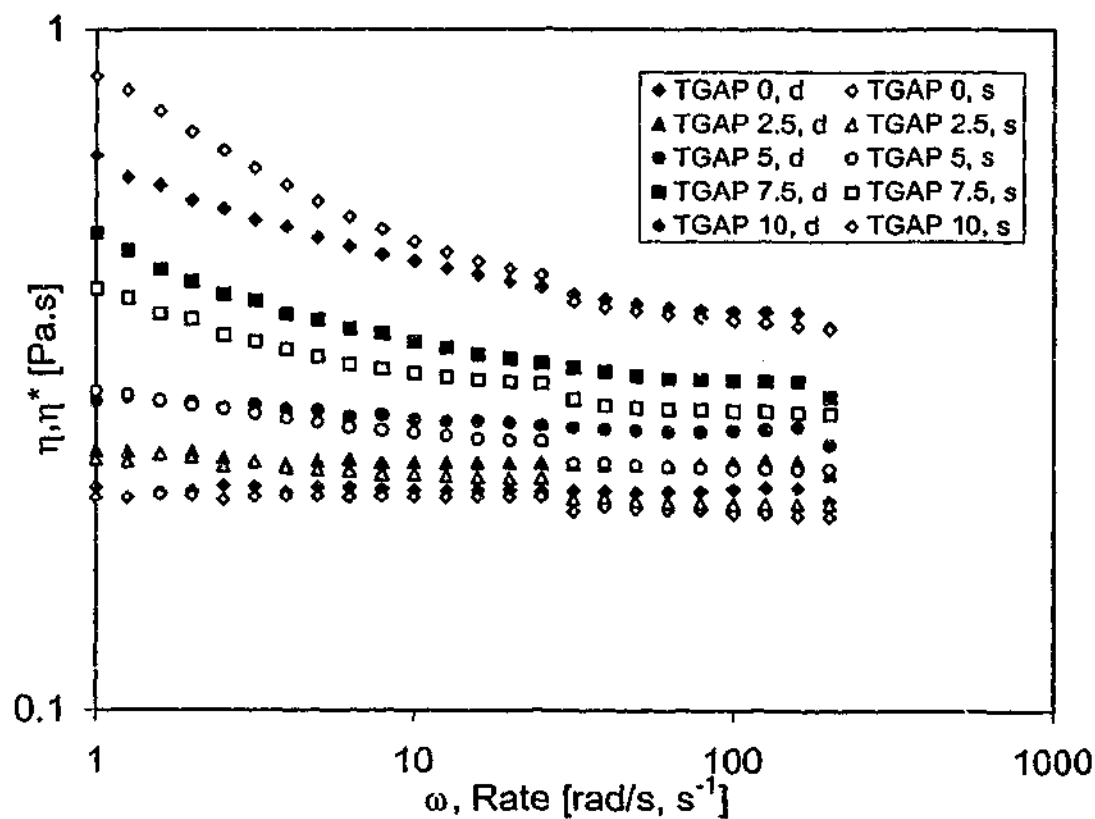
Figure 3.4: Comparison of dynamic (d) and steady (s) viscosities as a function of shear rate of a series of TGAP/layered silicate blends at 40°C.
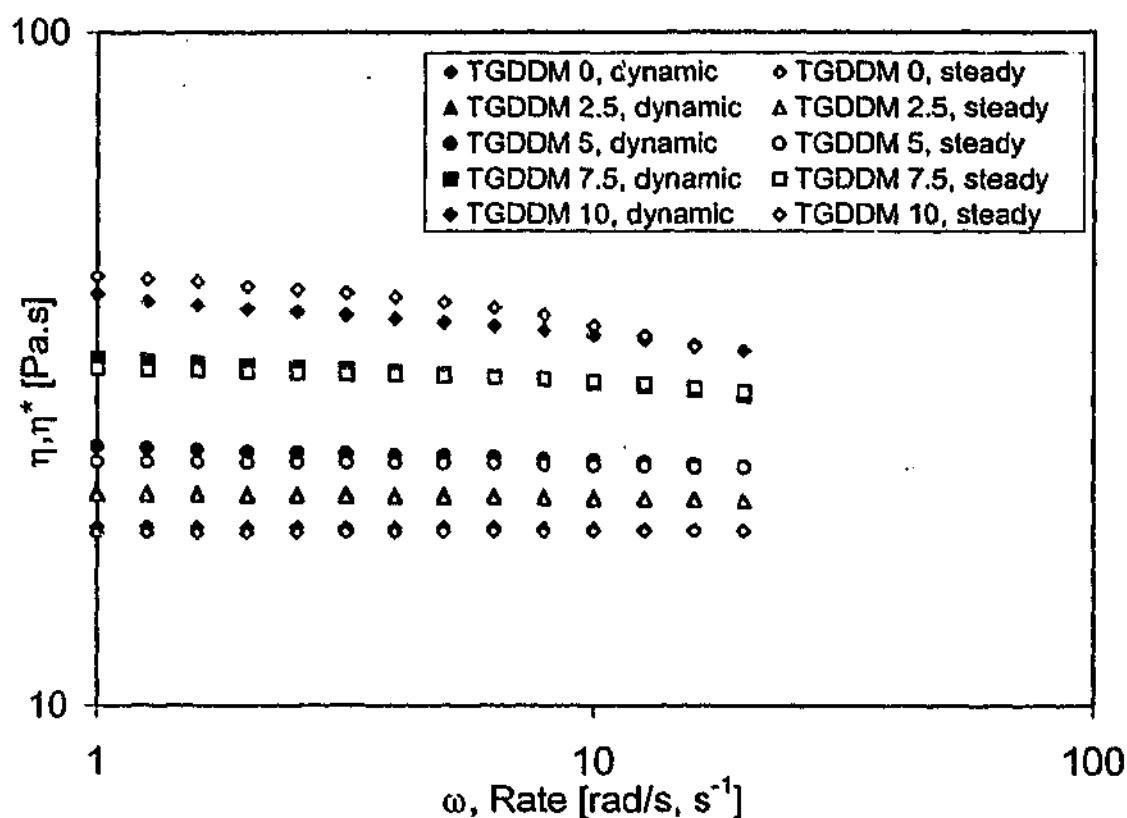
Figure 3.5: Comparison of dynamic (d) and steady (s) viscosities as a function of shear rate of a series of TGDDM/layered silicate blends at 40°C.

In order to determine any deviation from Newtonian flow behaviour and any yield stress, correlating parameters were determined. A series of experiments conducted at 40 °C, which gave the most stable linear viscoelastic response were fitted to a viscosity model (Power Law) and a yield stress model (Herschel-Buckley) [121] to determine any deviation of the epoxy/layered silicate blends from Newtonian behaviour and the existence of a yield stress.

The Power Law model allows prediction of shear thinning or shear thickening behaviour of non-Newtonian fluids. This model is often mathematically described for dynamic and steady measurements as:

$$G'' = C_1 \cdot \omega^{C_2} \qquad \qquad \textit{Equation 13}$$

$$\tau = C_1 \cdot \gamma^{C_2} \qquad \qquad \textit{Equation 14}$$

where G" is the loss modulus, ω the shear rate or oscillatory frequency, C_1 the pre-exponential factor and C_2 the flow behaviour index or Power Law index. τ represents the shear stress and γ the shear rate.

The shear data of fluids with a yield stress is commonly represented by the Herschel-Buckley model [121], which is basically a modification of the Power-law correlation, with an additional yield stress parameter, C_1, and can be represented as:

$$G'' = C_1 + C_2 \cdot \omega^{C_3} \quad \textit{Equation 15}$$

$$\tau = C_1 + C_2 \cdot \gamma^{C_3} \quad \textit{Equation 16}$$

Clay dispersions have often shown a reversible thixotropic behaviour in coatings and other applications, having an initial resistance to flow, which becomes reduced through alignment when shear forces are applied [122-127]. Recent work [127] has shown an interesting correlation between polymer nanocomposite rheology and (anisometric, non-Brownian) liquid crystalline polymer rheology; where shear rate regions of type I-yield stress (low rates), type II-tumbling domains (medium rates) and type III- flow alignment (high rates) are seen in both systems.

This work showed that with increasing organoclay concentrations and increasing temperatures the viscoelastic response of the resin organoclay blend indicated shear thinning behaviour. Shear thinning could be well observed at high organoclay concentrations of 10 % and 12.5 %. Figure 3.6 shows the Power Law parameter, C_2, as determined from loss modulus versus frequency fittings. In all instances, the data measured and the fit are in good agreement with a regression coefficient of 0.998 or above. C_2 values as determined from τ versus shear rate plots follow a similar trend. Figure 3.4 shows that for a series of TGAP/layered silicate blends at 40 °C, increased organoclay concentrations lead to an increasing trend of shear thinning behaviour. However, as illustrated by the low Power Law parameters, the deviation from Newtonian flow behaviour is still fairly low for all systems.
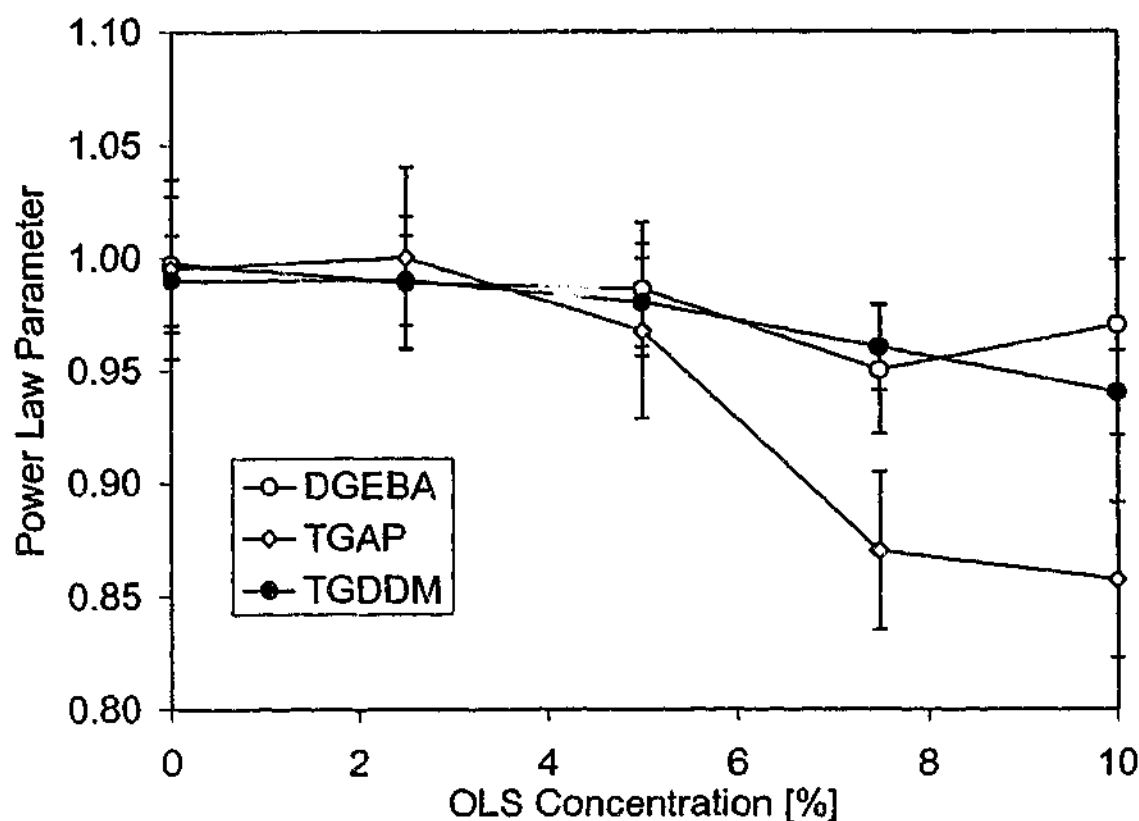
Figure 3.6: Power Law Parameter, C_2, as determined of Power Law fits of G"
vs. ω of different epoxy resin/layered silicate blends at 40 °C.

The yield stress parameter, C_1, as determined from Herschel-Buckley fits of τ"
versus shear rate data is shown in Figure 3.7. It can be seen that for the
DGEBA and TGAP resin systems the C_1 values were close to zero at all layered
silicate concentrations. Only the high-viscous TGDDM resin shows a slight
indication of existing shear thinning at increased layered silicate concentrations
(above 7.5 %).

In order to compare changes of the magnitude of viscosity due to the layered
silicate with those of a commonly used micron-sized filler, viscosities at a given
frequency of 1 rad/s (further referred to as $\eta_{(1rad/s)}$) were compared. Dynamic
shear tests were chosen (over steady shear tests) to minimize disruption or
change to any network formation. Comparative measurements were carried out
with the different resin systems containing 5 % of a surface treated calcium
carbonate.
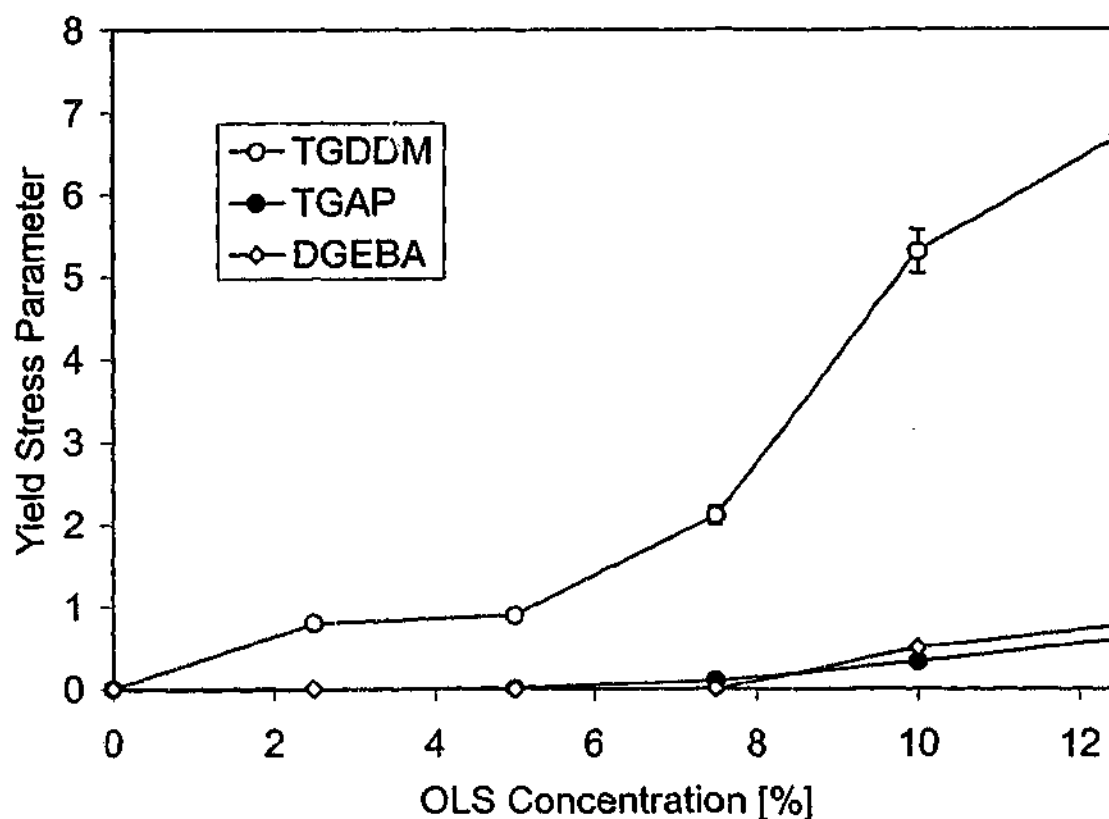
Figure 3.7: Yield Stress Parameter, C_1, as determined from Herschel-Buckley fits for different epoxy resin/layered silicate blends at 40 °C.

Figure 3.8 and Figure 3.9 illustrate the dependence of viscosity on temperature and organoclay concentration for TGAP and TGDDM, respectively. Values for DGEBA organoclay blends follow the same trend, with viscosities ranging from 0.04 Pa·s (0% clay, 80°C) to 2.17 Pa· s (10% clay, 40°C). A summary of all viscosity values is shown in Table 3.1. It was found that the $CaCO_3$-filler containing resins did not vary significantly from viscosity values of the layered silicate resin blends. The $\eta_{(1rad/s)}$ values of $CaCO_3$ mixed systems were only slightly lower than those of the organoclay-resin blend. This could indicate that the layered silicate is still acting as a micron sized filler, since a much higher viscosity would be expected if the platelets had split up into individual layers during mixing with the epoxy resin. For all systems, a steady increase in $\eta_{(1rad/s)}$ was observed with increasing organoclay concentrations, with the increase in viscosity being more significant at low temperatures and higher organoclay loadings.
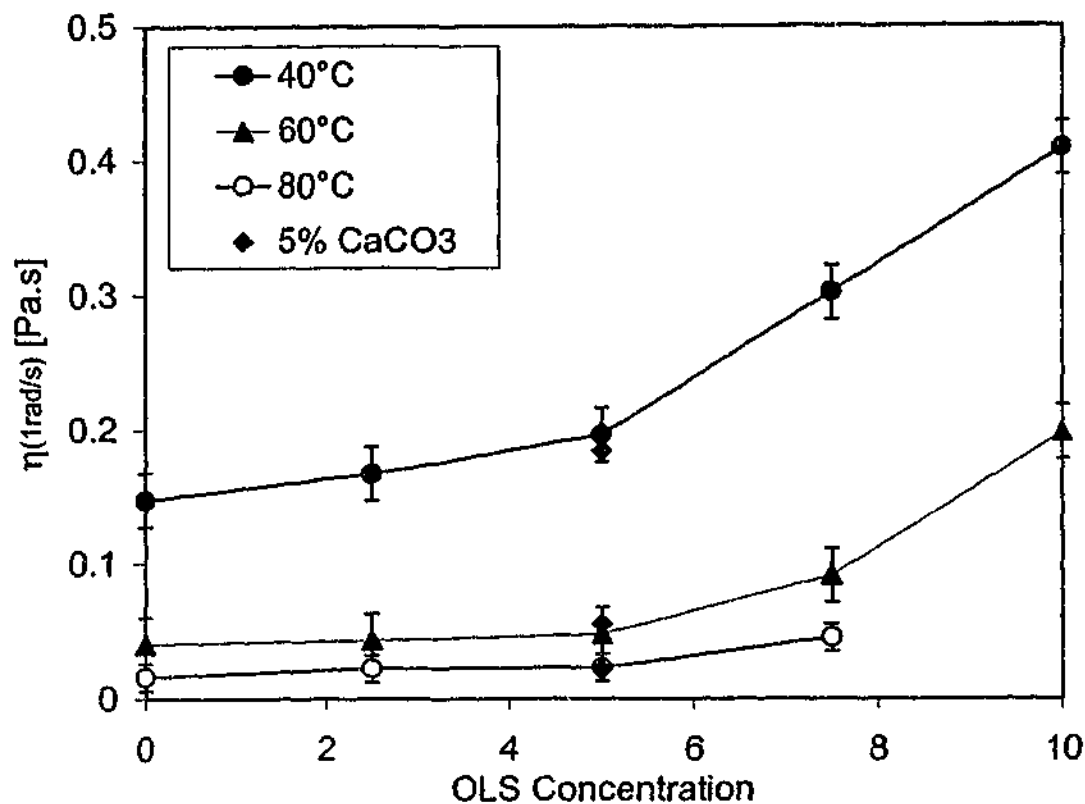
Figure 3.8: Viscosity of TGAP at a frequency of 1 rad/s as a function of organoclay concentration and temperature.
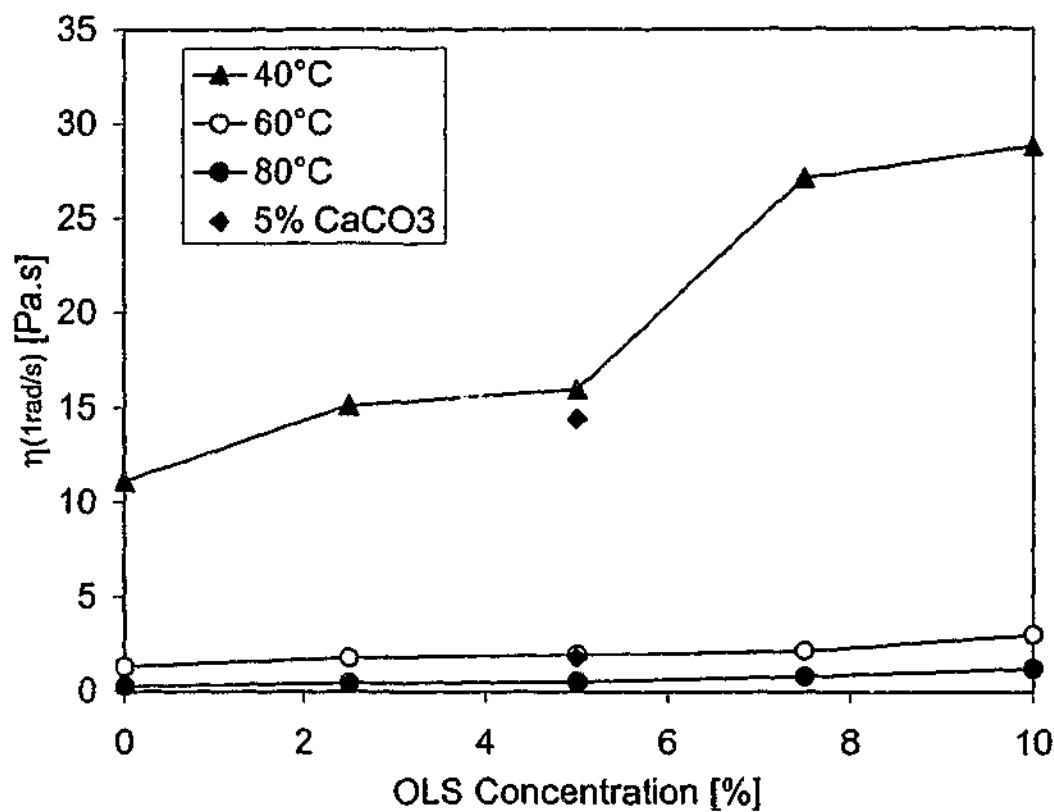
Figure 3.9: Viscosity of TGDDM at a frequency of 1 rad/s as a function of organoclay concentration and temperature.

The activation energy of flow (E_a) was determined from the slope of plots of the logarithm of the viscosity versus the reciprocal thermodynamic temperature, based on the Arrhenius relationship:

$$\eta = A \cdot e^{\left[\frac{E_a}{RT}\right]} \qquad \textit{Equation 17}$$

where η is the viscosity (compared here at a constant $\omega = 1$ rad/s), A is a pre-exponential factor, R is the gas constant and T is the absolute temperature.

Figure 3.10 shows a typical series of Arrhenius plots for the TGAP series. Results for all activation energies are shown in Table 3.1. It can be seen that the nature of the epoxy resin is of major importance for the activation energy of flow. The E_a-flow values increase with increasing bulkiness, and decreasing mobility, of the resin molecule. TGAP monomer, whose structure contains only one benzene ring, has the lowest activation energy around 47 ± 2 kJ/mol, whereas the more bulky, larger TGDDM molecule with two aromatic units and four glycidyl moieties has an activation energy of approximately 84 ± 4 kJ/mol. Bifunctional DGEBA showed an intermediate E_a of 70 ± 4 kJ/mol.

The activation energy of flow of the different resin systems is not affected by the addition of up to 10 % organoclay. The modest variation observed between different clay loadings in these resin systems falls within the error of the method. Results are in good agreement with work reported by Krishnamoorti and Giannelis [124], who reported that the activation energy of flow of thermoplastic poly(ε-caprolactone) (PCL) did not change due to the addition of 1 - 10 % layered silicate.

The average distance between silicate platelets, the d-spacing, of the different resins containing 7.5 % organoclay was determined using wide angle x-ray diffraction to understand the organoclay formation in the viscosity samples.

Table 3.1: Viscosity values of various epoxy systems containing 0 - 10 % OLS or 5 % CaCO₃ at an angular frequency of 1 rad/s.

Resin	OLS content [%]	η at 40°C [Pa·s]	η at 60°C [Pa·s]	η at 80°C [Pa·s]	E_a-Flow [kJ/(kmol K)]
DGEBA	0	0.748	0.172	0.029	74.6
DGEBA	2.5	1.489	0.218	0.069	70.8
DGEBA	5	1.745	0.301	0.073	73.1
DGEBA	7.5	2.036	0.404	0.144	61.1
DGEBA	10	2.258	0.341	--*	--*
DGEBA	5 % CaCO₃	1.24a	0.199	0.062	69.0
TGAP	0	0.147	0.040	0.016	45.5
TGAP	2.5	0.167	0.043	0.021	47.9
TGAP	5	0.169	0.048	0.023	49.9
TGAP	7.5	0.302	0.091	0.045	43.8
TGAP	10	0.409	0.198	--*	--*
TGAP	5 % CaCO₃	0.184	0.055	0.021	49.9
TGDDM	0	11.129	1.298	0.278	84.9
TGDDM	2.5	15.123	1.768	0.432	81.9
TGDDM	5	15.935	1.936	0.518	78.9
TGDDM	7.5	27.059	2.151	0.808	89.9
TGDDM	10	28.800	3.010	1.220	--*
TGDDM·	5 % CaCO₃	14.400	1.760	0.450	80.0
TGAP-TGDDM	0	0.82	0.18	0.057	61.3
TGAP-TGDDM	2.5	1.08	0.22	0.065	64.6
TGAP-TGDDM	5	1.334	0.257	0.09	62.1
TGAP-TGDDM	7.5	1.5	0.463	0.12	57.9
TGAP-TGDDM	10	2.27	0.463	--*	--*
TGAP-TGDDM	5 % CaCO₃	1.08	0.215	0.066	64.3

* samples did not allow determination of reproducible data.
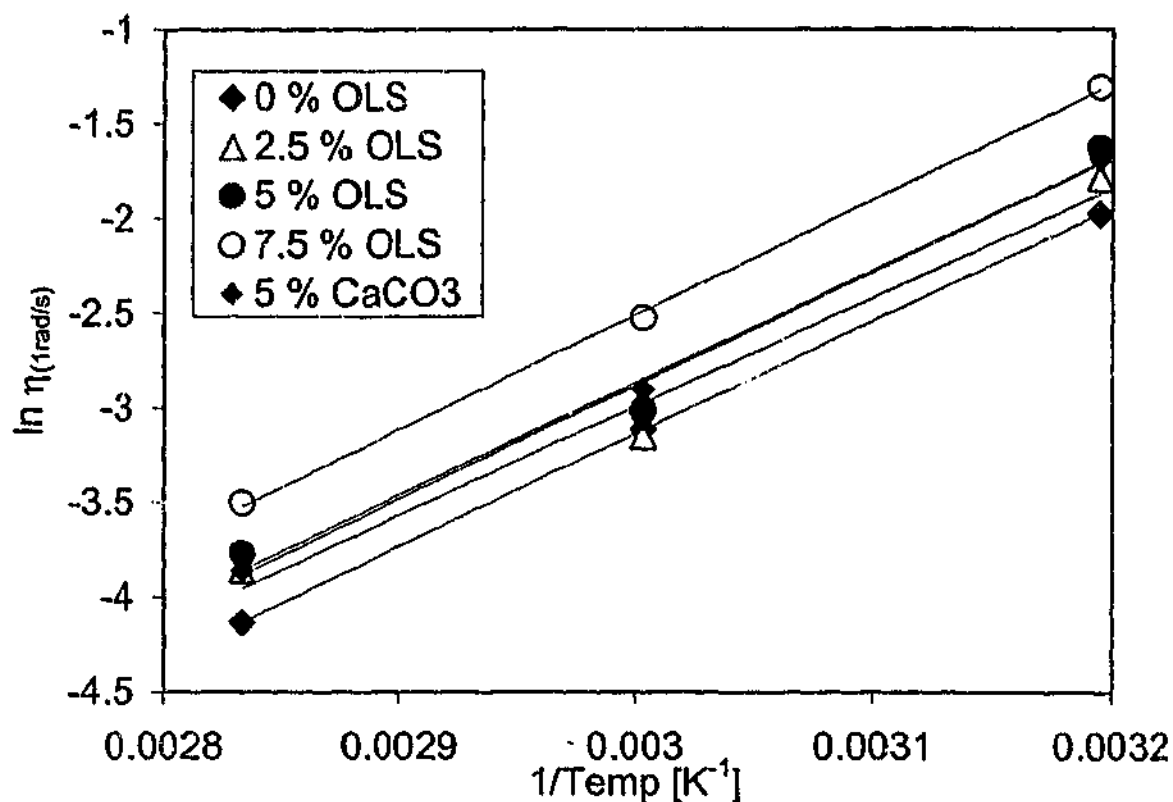
Figure 3.10: Arrhenius plot (relationship between viscosity and reciprocal temperature) of a layered silicate-containing TGAP resin as a function of concentration at an angular frequency of 1 rad/s.

It was found that the interlayer distance increased from initially 23 Å of the dry organoclay to 39.0 ± 0.5 Å for any of the three monomer resin organoclay blends. This amount of increase in d-space due to swelling in the clay is in good agreement with the values reported by Chin et al. [81]. The interlayer d-space in the swollen state correlates with a thermodynamic equilibrium [75] between the resin polarity and the polarity or surface energy of the organoclay and only changes further when much higher temperatures are applied and the epoxy resin molecules undergo an etherification reaction. Therefore, any measurement of the resin organoclay systems alone is assumed to consist of a blend of epoxy resin and swollen organoclay tactoids that remain in the stacks of swollen parallel stacked platelets with a lateral micron sized structure as shown in Figure 3.11.
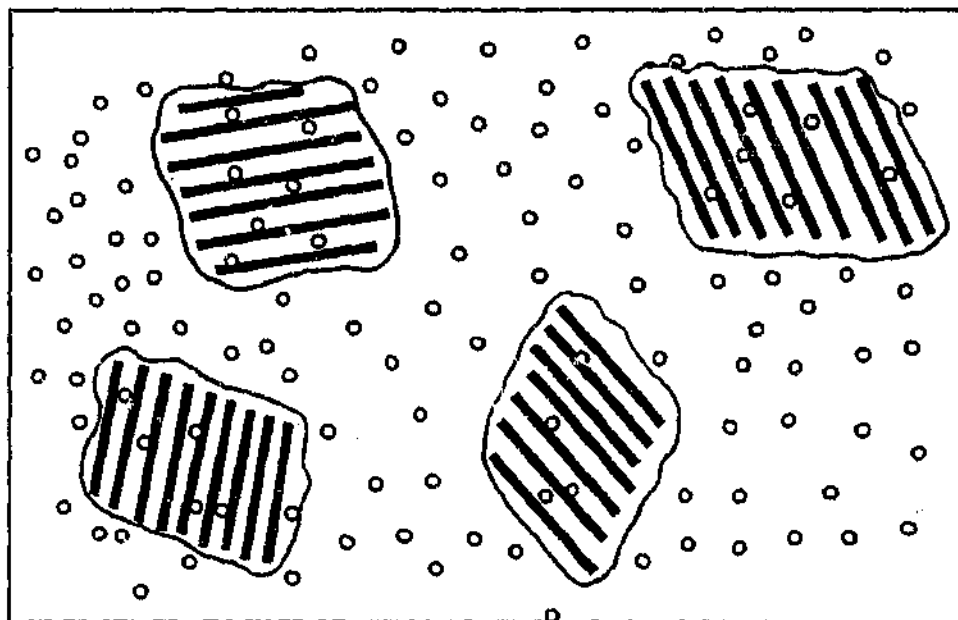
Figure 3.11: Model of the organoclay structure as it exists during viscosity measurements. The black bars represent layered silicate platelets, the small circles represent the resin monomers and the thin black line around stacks of black bars the interface between fluid and tactoids.

3.2   Differential Scanning Calorimetry

Initially, differential scanning calorimetry (DSC) was applied to investigate the effect' of the organoclay on epoxy homopolymerization. Temperature scans of the resins mixed with 0 - 10 % of the organoclay only (no hardener added) were carried out at a heating rate of 10 °C/minute. Single sharp peaks were obtained for all different resin systems. Figure 3.12 to Figure 3.14 illustrate the influence of the clay on the reaction rate of the epoxy self-polymerization of DGEBA, TGAP and TGDDM. Peak temperatures of the homopolymerization reaction are summarized as a function of organoclay concentration in Figure 3.15. The modified clay dramatically influences the DGEBA self-polymerization. The addition of 2.5 % layered silicate decreased the reaction peak temperature by almost 150 °C. Any further addition of clay only decreases the reaction peak temperature slightly. A catalytic effect of a similar alkyl amine ion modified montmorillonite on DGEBA self-polymerization has been reported previously by Lan et al. [69] and Butzloff et al. [90]. In the work by Lan et al. [69] it was possible to clearly distinguish between two different peaks related to an intra-gallery and an extra-gallery polymerization reaction at a scanning rate of

2 °C/min. In contrast, results reported by Butzloff et al. [90] for DSC measurements performed at the same scanning rate as well as our work at a faster scanning rate of 10 °C/min did only show single reaction peaks. It was theorized by Butzloff et al. that the single peak traces may be related to a better organoclay dispersion, depending on the mixing process prior to DSC measurements. A mechanism for the epoxy polymerization in acidic smectite layered silicate clay galleries has been proposed as discussed in section 1.7.2 in the literature review. According to this model, the alkylamine ion generates protons through dissociation, these protons causing further acid-catalysed, ring-opening reaction.

The resins of higher functionalities, TGAP and TGDDM show a much smaller monotonic decrease in the reaction peak temperature by only 3 - 6 °C with each additional 2.5 % of organoclay. This weaker effect is in good agreement with the fact that the resin systems of higher functionalities are more difficult to exfoliate, as will be presented later in this work. The ability of the interlayer exchanged ion to catalyse homopolymerization or resin hardener cure respectively, is of major importance for the exfoliation process.

Figure 3.12: DSC traces of the self-polymerization of DGEBA containing 0 - 10 % organically modified layered silicate (OLS).

Figure 3.13: DSC traces of the homopolymerization of TGAP containing 0 - 10 % organically modified layered silicate (OLS).

Figure 3.14: DSC traces of the homopolymerization of TGDDM containing 0 - 10 % organically modified layered silicate (OLS).
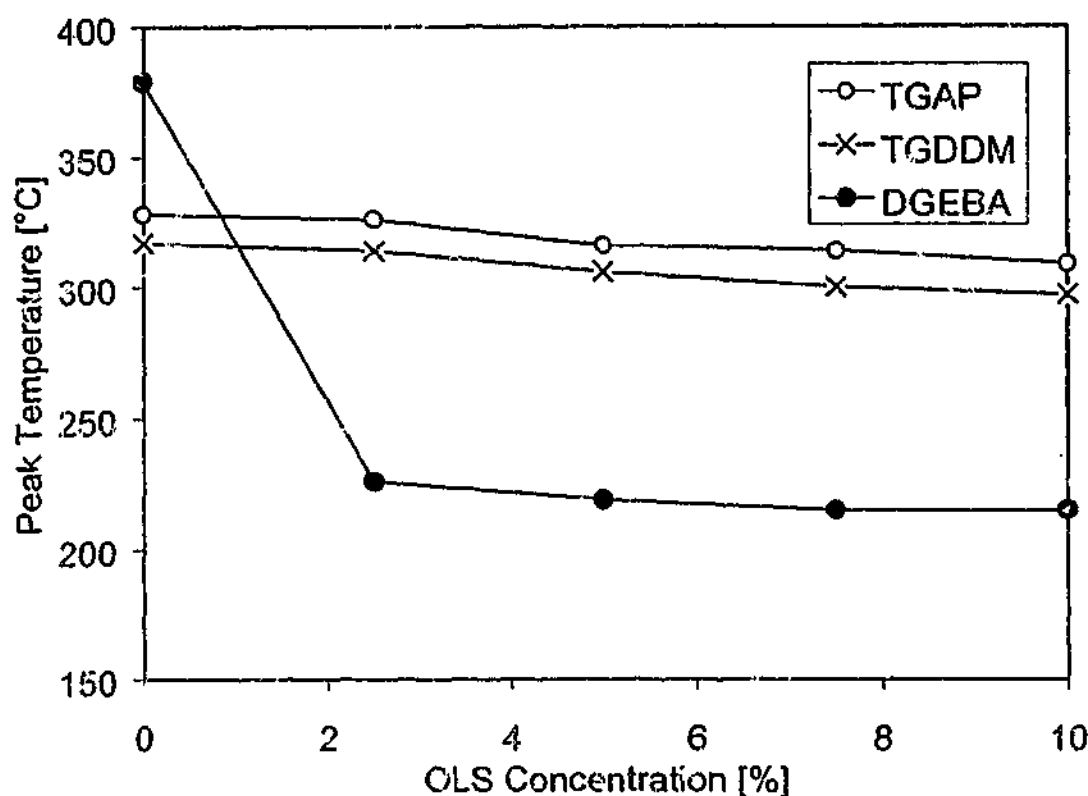
Figure 3.15: Influence of the organoclay on epoxy homopolymerization in the absence of a hardener - reaction peak temperatures determined from DSC temperature scans at a heating rate of 10 °C/minute.

Subsequently, DSC was applied to investigate the cure kinetics of the epoxy/amine/organoclay blends. As illustrated in Figure 3.16 for the DGEBA based-systems, more than one (overlapping) peak can be found. It is likely that these peaks are related to different curing reactions. A catalysed reaction in the layered silicate galleries would likely occur at lower temperatures. This reaction increases with increasing clay concentration, as indicated by the strengthening shoulder in the DSC traces. The second, higher temperature peak is likely due to the curing reaction outside the organoclay galleries and is assumed to refer to the non-catalysed resin/hardener reaction outside the layered silicate galleries. At higher temperatures, organoclay-induced homopolymerization of the DGEBA might occur. The TGAP and TGDDM based resin/organoclay/hardener systems show a single broad reaction peak, with a shoulder towards higher temperatures as shown in Figure 3.17 and Figure 3.18 respectively. For the TGDDM systems the cure reaction peak decreases with

increasing clay concentration from 214 °C for the neat system to 183 °C for the blend containing 10 % organoclay. Since the TGDDM self-polymerization occurs at temperatures above 300 °C, it can be assumed that the exothermic peaks are mainly related to the resin/hardener cure reaction only. A catalytic effect of the $CH_3(CH_2)_{17}NH_3^+$ - ion on the amine cure reaction has been reported previously [63, 70], where the amine ion has a Bronstedt-acid catalysing effect on the cure reaction. Similar to homopolymerization, the DGEBA/DETDA cure appears to be more affected by the catalysing effect of the organoclay than the tri-functional TGAP or the tetra-functional TGDDM resins.
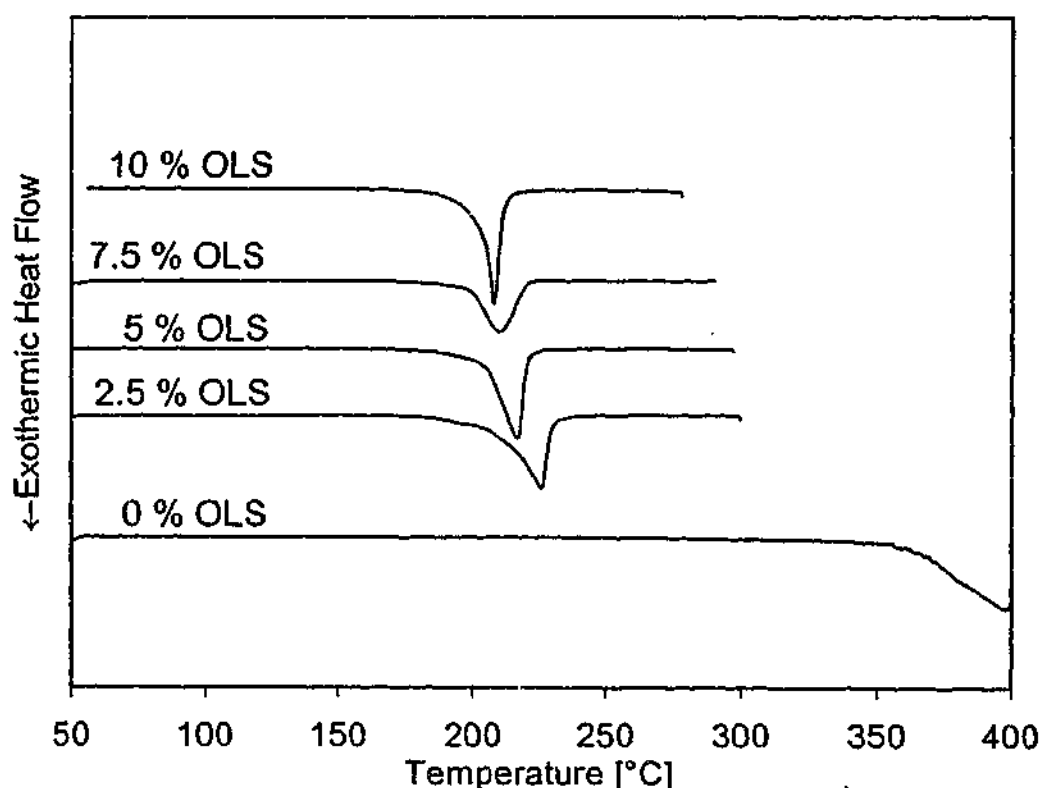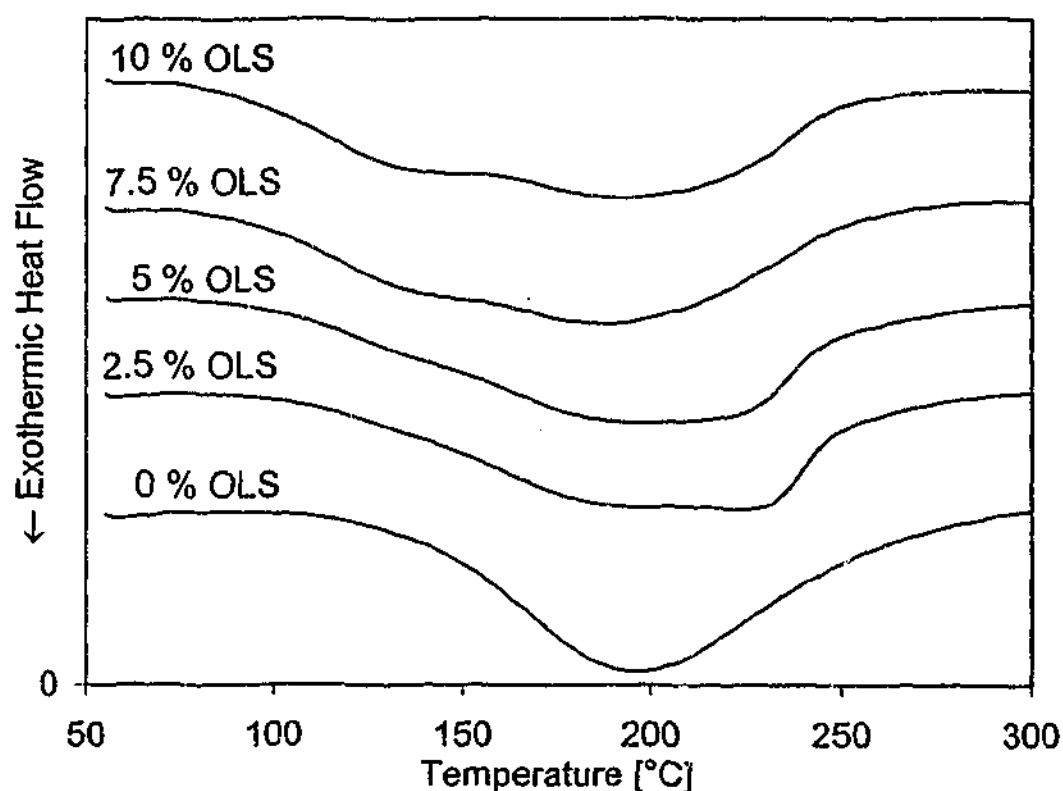

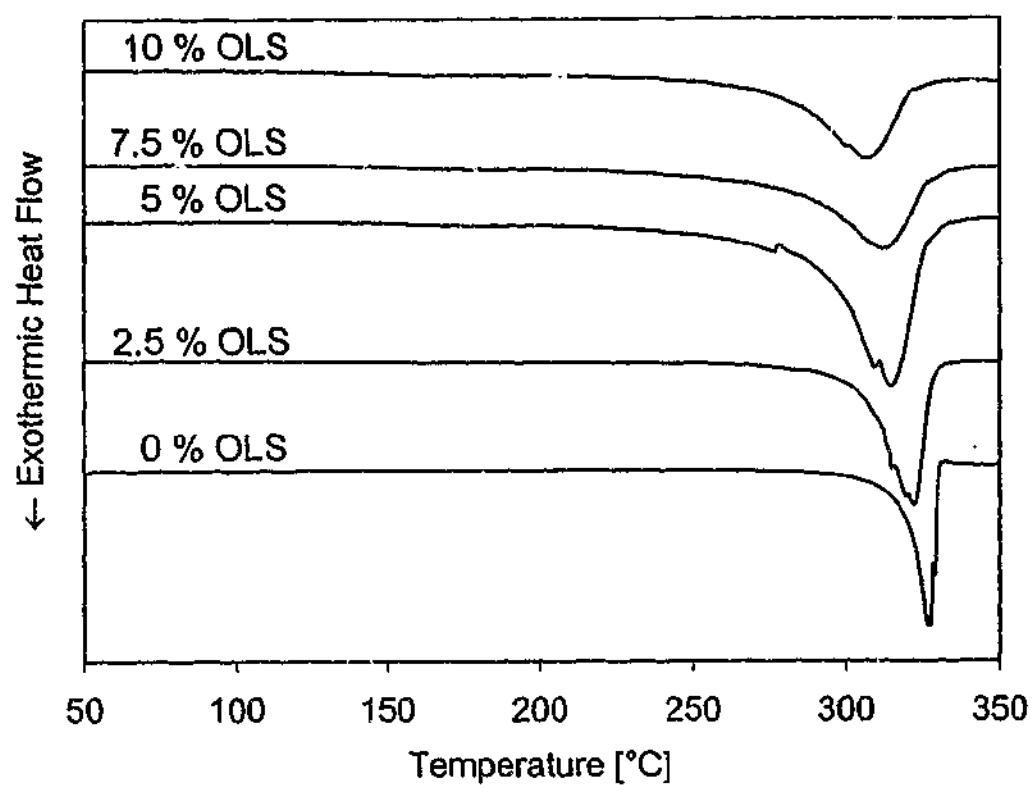Figure 3.16: DSC traces of the DGEBA/OLS/DETDA cure reaction containing 0 - 10 % organically modified layered silicate (OLS).
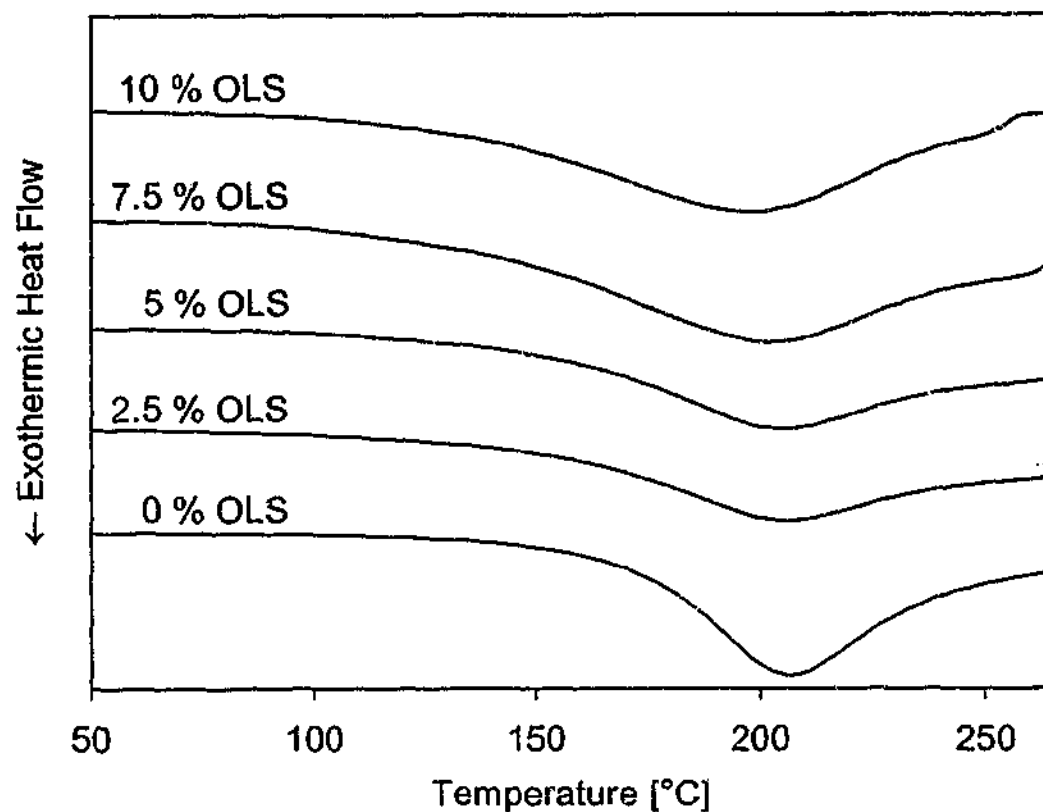
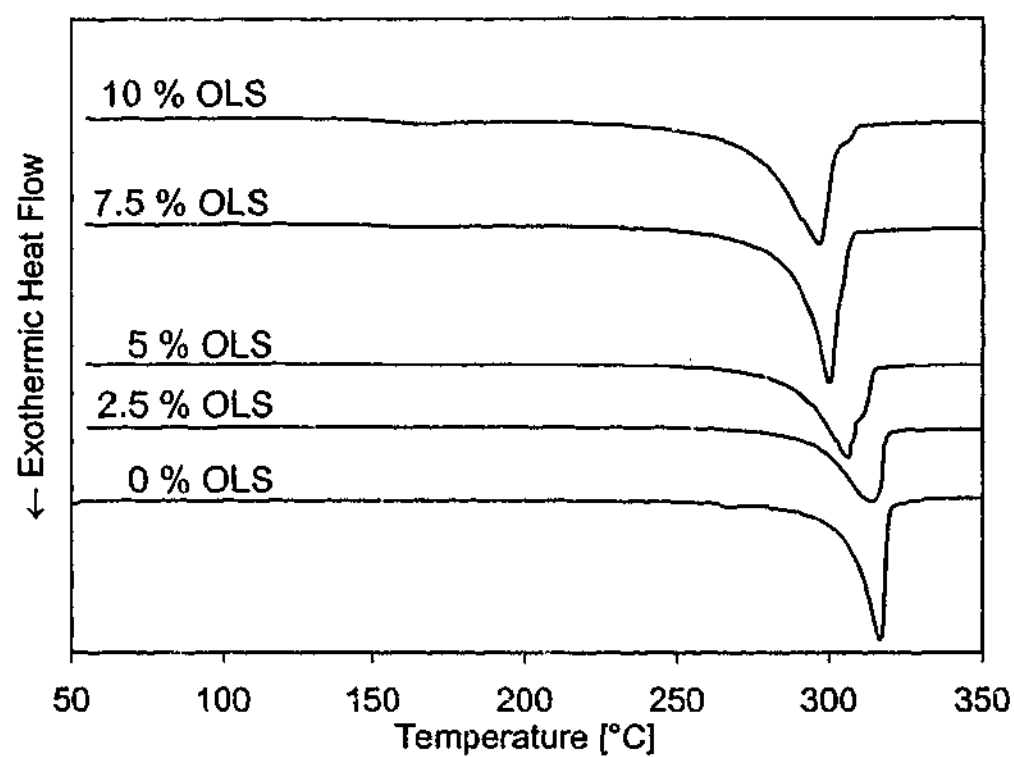Figure 3.17: DSC traces of TGAP/OLS/DETDA cure containing 0 - 10 % organically modified layered silicate (OLS).
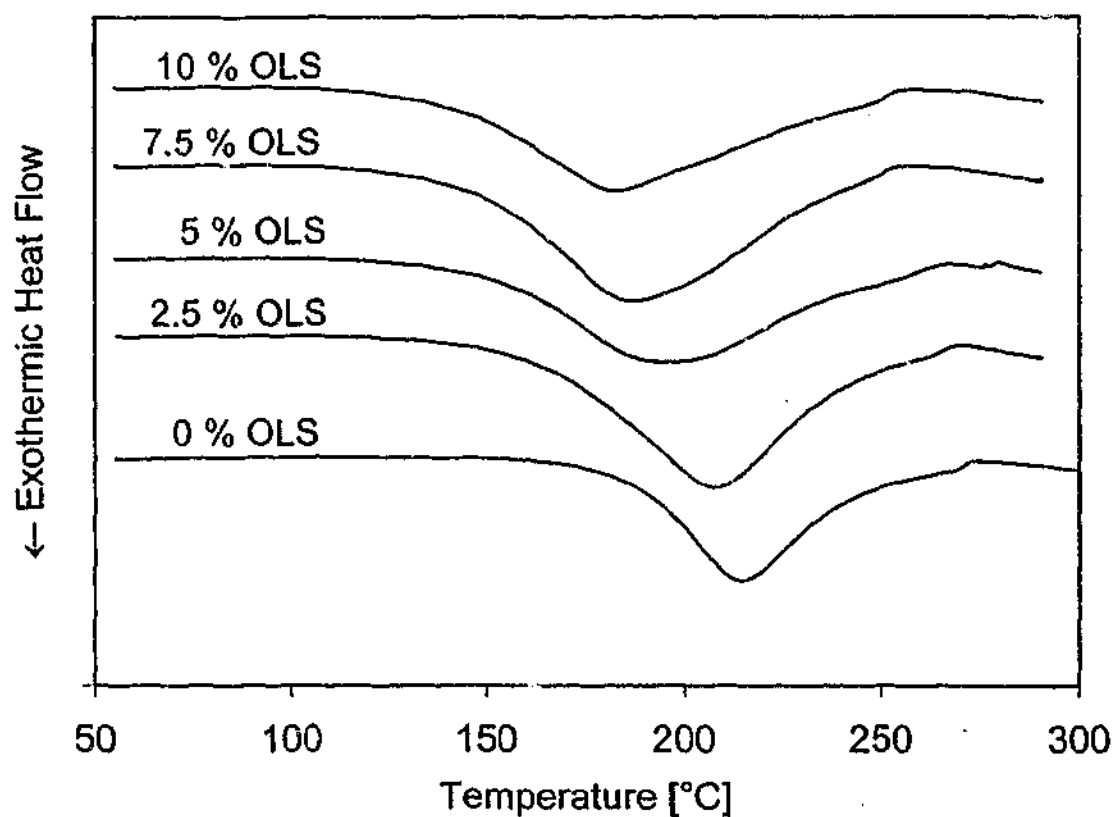
Figure 3.18: DSC traces of TGDDM/OLS/DETDA cure containing 0 - 10 % organically modified layered silicate (OLS).

3.3   Chemorheology

The influence of the organoclay on the gelation time of the three different resins was investigated by dynamic rheology. The gelation time of all systems was taken from the crossover in tan δ, as commonly used in curing characterization of non-stoichiometrically balanced systems [87, 128]. For comparison, the gel time was also determined from the rise in G', due to the rapid increase in elasticity with gelation, often found to occur at similar times as the crossover in tan δ   [128]. For each measurement two tangents were drawn before and after the inflection point in G'. The gelation time was taken from the intersection of these two tangents as illustrated in Figure 3.19.
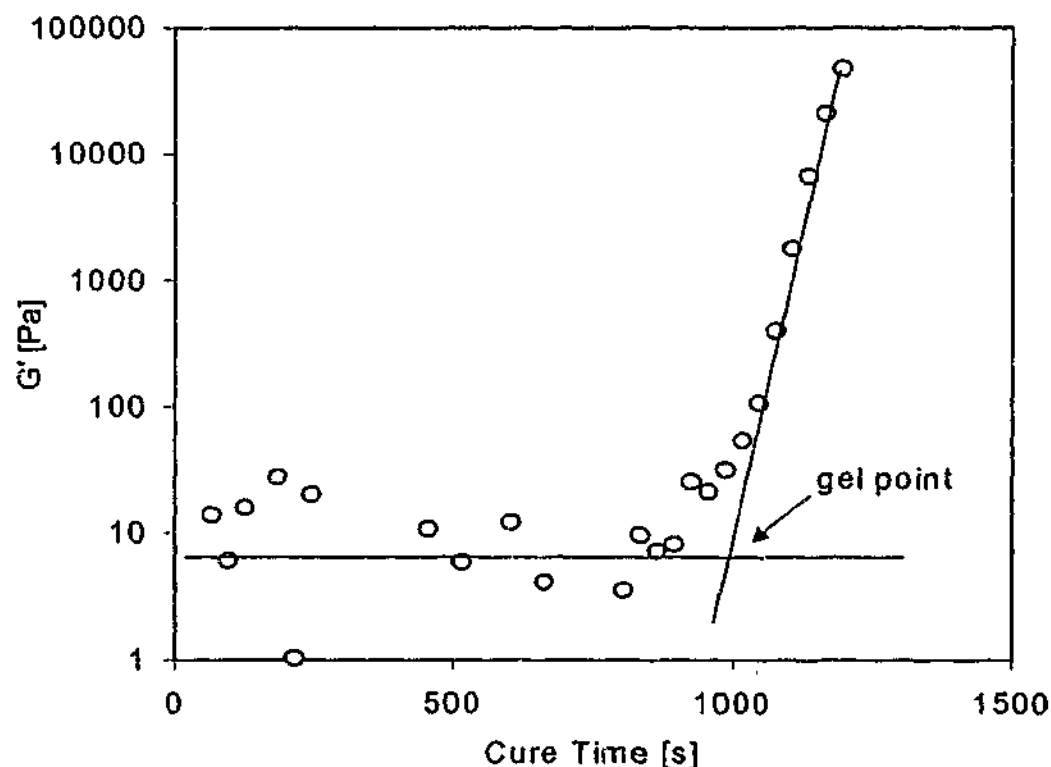
Figure 3.19: Intersection method to determine the gelation time from the rise in G' (here for DGEBA/DETDA/7.5 % organoclay cured at 160 °C, 32 Hz).

There are two main ways in which to conduct the chemorheological experiment in the rheometer. The resin sample can either be loaded between the parallel plates and ramped up to the isothermal cure temperature [128, 129], or the resin can be inserted between the two parallel plates, already at cure

temperature [130]. In either case an error is involved. The first method involves the same error for each measurement, i.e. the time till target temperature is reached. The latter method involves an error due to the required time to load the resin between the parallel plates and heat it up to target temperature. This error can vary significantly between measurements and therefore reduce comparability between results. To allow easier comparison between results of different systems in this work, the resin samples were inserted between the two parallel plates at 50 °C and heated up to the target temperature at 20 °C/minute.

The crossover in tan δ at gelation can be explained by the fact that tan δ decreases with increasing frequency in the liquid state whereas in the rubbery state the resin systems behaves like an elastic solid, with tan δ increasing with increasing frequency. Hence the tan δ traces of each single frequency cross over at the transition from the liquid to the rubbery state. Traces generally followed this trend as shown in Figure 3.20 for the TGAP nanocomposite containing 7.5 % organoclay, cured at 140 °C. However, if the data at the crossover is viewed in a more expanded manner some measurements show a range of crossovers or single frequencies that do not precisely cross (Figure 3.21) This phenomenon occurred even in the unfilled resin systems and can therefore not only be related to the influence of the organoclay (it should be noted that most chemorheological papers do not show data to this level of magnification). By comparison, the gelation time was also determined from the point where G' rises. Results of the apparent crossover region in tan δ and from the rise in G' are shown in Table 3.2 and Table 3.3. Both sets of values are in good agreement. The gelation times determined from the rise in G' traces at 2 Hz compare best with the gel times as determined from tan δ. The gelation times determined from the increase in G' at higher frequencies were slightly lower than those at 2 Hz. Interestingly, with increasing, cure temperature, the values of the two different methods appear to match better. At a cure temperature of 180 °C, some of the gelation times determined from the rise in G' for the TGAP system show slightly higher values than the other method.
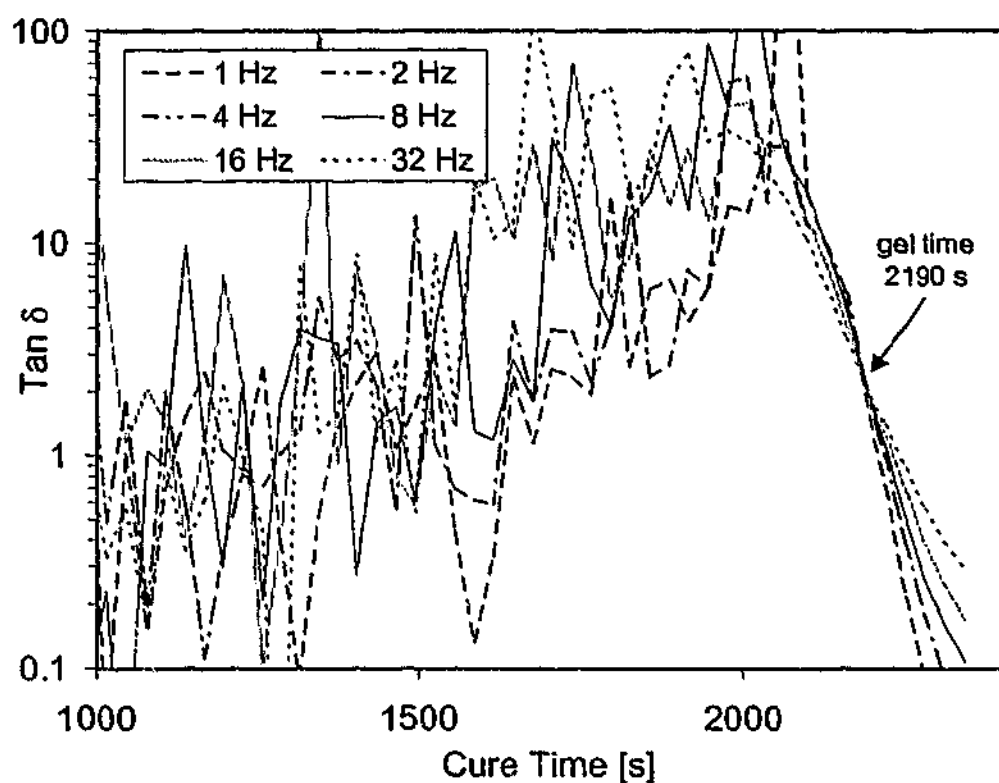
Figure 3.20: Typical tan δ data obtained from parallel plate rheology of TGDDM/DETDA/5 % organoclay at 160 °C.
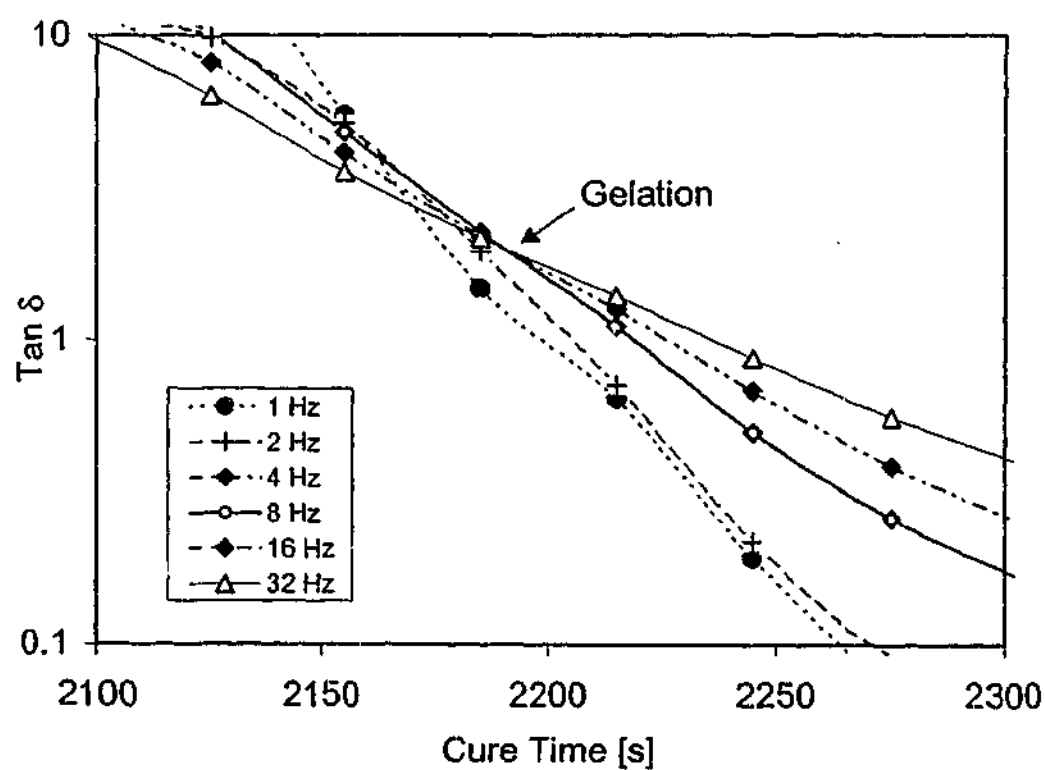
Figure 3.21: Tan δ traces of a TGAP/DETDA blend containing 7.5 % OLS, cured at 140 °C.

Assuming that gelation is a point of constant conversion, the overall activation energy (E_a) of gelation may be determined from Arrhenius plots of the reciprocal thermodynamic temperature versus gelation time according to equation 18.

$$t_{gel} = A \cdot e^{\left[\frac{E_a}{RT}\right]} \qquad \textit{Equation 18}$$

where t_{gel} is the gelation time, A is the pre-exponential factor, R is the gas constant and T is the temperature in Kelvin. The activation energies for the neat systems were found to be 61.3 kJ/mol for DGEBA, 63.4 kJ/mol for TGAP and 76.0 for the TGDDM based system. Whilst DGEBA and TGAP show very similar values, the activation energy of the TGDDM based system is significantly higher. Barral et al. [131] recently determined the activation energy for a relatively similar 4,4'-diaminodiphenylsulphone (DDS) cured TGDDM system. Results as obtained from T_g versus time shift factors and gelation times are 76.2 kJ/mol and 61.0 kJ/mol, respectively.

A general trend of decreasing activation energy with increasing clay concentration can be observed for DGEBA and TGDDM. The TGAP based system initially shows decreased activation energy with organoclay addition followed by an increase in E_a with further organoclay addition. It is very clear, however, that the samples with no clay content all show significantly higher activation energies in comparison to those containing different concentration of clay. Due to the catalytic effect of the clay, less energy is required for gelation to occur in the filled systems compared to the unfilled epoxy resins.

As will be shown later, major changes in the interlayer distance of the organoclay occur at the beginning of cure. Two different aspects have to be considered when investigating the gelation of a layered silicate filled epoxy system during cure: firstly, the formation of a physical gel due to a network of exfoliated platelets that are connected through electrostatic forces and secondly the chemical gelation due to the formation of a crosslinked polymer network.

Table 3.2: Gelation times of various epoxy systems containing 0 - 10 % OLS determined from chemorhological measurements (crossover in tan δ).

Resin / Hardener	OLS content [%]	gel. at 140 °C [sec]	gel. at 160 °C [sec]	gel. at 180 °C [sec]	Overall Ea – [kJ / mol]*
DGEBA / DETDA	0	2650	1540	1050	61.3
DGEBA / DETDA	2.5	2520	1400	950	57.4
DGEBA / DETDA	5	2350	1350	930	55.9
DGEBA / DETDA	7.5	2010	1110	850	55.9
DGEBA / DETDA	10	1950	1170	810	58.4
TGAP / DETDA	0	2960	1680	1110	63.4
TGAP / DETDA	2.5	2430	1500	1040	49.3
TGAP / DETDA	5	2340	1260	960	53.4
TGAP / DETDA	7.5	2190	1250	850	59.7
TGAP / DETDA	10	2030	1090	790	62.6
TGDDM / DETDA	0	3160	1630	1080	76.0
TGDDM / DETDA	2.5	2580	1460	890	63.3
TGDDM / DETDA	5	2290	1260	850	61.8
TGDDM / DETDA	7.5	1930	1080	840	57.9
TGDDM / DETDA	10	1780	960	720	58.7
TGAP-TGDDM / DETDA	0	2780	1430	980	70.5
TGAP-TGDDM / DETDA	2.5	2390	1350	900	59.1
TGAP-TGDDM / DETDA	5	2160	1260	850	59.1
TGAP-TGDDM / DETDA	7.5	2060	1190	840	57.9
TGAP-TGDDM / DETDA	10	2010	1230	820	58.7

Table 3.3: Gelation times of various epoxy systems containing 0 - 10 % OLS as determined from the rise in G'.

OLS [%]		gel. at 140 °C		[s]	gel. at 160 °C		[s]	gel. at 180 °C		[s]
Resin / Hardener		2 Hz	8 Hz	32 Hz	2 Hz	8 Hz	32 Hz	2 Hz	8 Hz	32 Hz
DGEBA / DETDA	0	2540	2450	2465	1560	1555	1520	980	980	990
DGEBA / DETDA	2.5	2350	2250	2180	1410	1390	1350	880	875	840
DGEBA / DETDA	5	2090	1980	1920	1280	1270	1200	930	910	855
DGEBA / DETDA	7.5	1840	1700	1590	1060	1010	965	810	800	775
DGEBA / DETDA	10	1730	1680	1500	1080	1040	975	750	740	700
TGAP / DETDA	0	2900	2910	2870	1650	1640	1630	1040	1050	1040
TGAP / DETDA	2.5	2350	2310	2260	1480	1460	1425	970	970	960
TGAP / DETDA	5	2235	2165	2090	1230	1220	1190	815	810	810
TGAP / DETDA	7.5	2100	2020	1950	1020	1070	1050	875	865	865
TGAP / DETDA	10	1980	1900	1790	1020	1020	1010	915	910	900
TGDDM / DETDA	0	3080	3100	3050	1620	1630	1600	1025	1050	1025
TGDDM / DETDA	2.5	2450	2385	2325	1380	1350	1350	920	875	850
TGDDM / DETDA	5	2190	2060	1990	1200	1185	1150	840	820	810
TGDDM / DETDA	7.5	1750	1680	1620	1005	975	975	810	790	790
TGDDM / DETDA	10	1580	1520	1460	910	890	875	640	660	625

Even at low concentrations layered silicates are able to significantly affect the viscosity of a fluid [64, 123, 125, 132, 133] and the formation of a physical gel may occur although polymer conversion is low. However, this effect did not interfere with our experiments. The rise in G' or the crossover in tan δ respectively were found to occur significantly after major changes in the interlaminar spacing could be observed. The experimental parameters were chosen to yield accurate force signals at gelation and thus the increase in viscosity due to the silicate layer intercalation or delamination, respectively, was not dramatic enough to be detectable in the measurements before gelation due to crosslinking reactions.

In all systems, a decreasing gelation time was found with increasing layered silicate concentration, as well as increasing reaction temperature. The decreased gelation time with increased organoclay concentration is likely due to two reasons. Firstly, the rate of reaction is increased due to a catalytic effect of the clay (if the conversion at gelation stays the same) or secondly, the cure reaction or the conversion at gelation has decreased due to the presence of the clay particles (if the rate of reaction is unaffected). In order to determine if the conversion at gelation changes due to the presence of clay particles, the degree of conversion of each resin containing hardener and 7.5 % organoclay were compared with those of the unfilled systems. Samples of a thickness similar to that used for rheological measurements were cured at 140 °C till gelation (as judged by previous rheology experiments) in an oven, using the appropriate gelation times determined through dynamic rheology tests. The total heat of reaction and the heat of reaction till gelation were determined from DSC measurements of the neat and gelled systems, respectively. The conversion at gelation was determined from the following equation:

$$C_{gel} = \frac{\int_{0}^{\infty} H(t)\,dt - \int_{tgel}^{\infty} H(t)\,dt}{\int_{0}^{\infty} H(t)\,dt} = \frac{H(t_{gel})}{H(t_{\infty})} \qquad \text{Equation 19}$$

where C_{gel} is the degree of conversion at gelation and $H(t)$ is the heat of reaction at the time t.

Similar degrees of conversion were found for the neat and the clay containing system in each case, the variation was within the range of the estimated error of 3%. Values found for the conversion at gelation varied from 0.75 for DGEBA and 0.67 for TGAP to 0.59 for the TGDDM based systems. The values determined have been compared with the theoretical values, as calculated from Flory's classical theory of gelation [134-136]:

$$C_{gel}^{F} = \frac{1}{[r(f-1)(g-1)]^{0.5}} \qquad Equation\ 20$$

where C_{gel}^{f} is the conversion at the gel point, r is the stoichiometric ratio and f and g are the functionalities of the resin and the hardener respectively.

It was found that the degree of conversion at gelation was significantly higher than the theoretical values determined from the Flory equation. Recently, Bonnaud et al. [136] have compared the conversion at gelation of a 4,4'-methylene-bis(3-chloro 2,6-diethylaniline) (MCDEA) cured TGAP and DGEBA system respectively. Whilst their result for the DGEBA system was in good agreement with the theoretical data obtained from Flory's theory, a discrepancy between theoretical and experimental results of 0.2 was reported for the TGAP based system. The large difference was ascribed to the different reactivities of the epoxy groups in TGAP, which exist due to different structures and substitution effects, as well as possible side reactions such as internal cyclisations. The fact that all samples in our case showed a higher degree of conversion can also be explained by the different conditions of heat transfer involved with the method. Gelation times as taken from the rheology experiments were used, and the process simulated in an oven. Whilst the sample size was the same in both experiments, the different environments are

still likely to allow different heat transfer and exothermic energies, leading to a higher degree of reaction.

However, comparison between different systems cured under the same conditions allows one to assess the effect of the clay on the rate of reaction. Although the organoclay-containing systems have a smaller reaction time until gelation, it was found for the DGEBA and TGDDM systems, that these blends in fact show a slightly higher degree of conversion at gelation than the neat systems. TGAP shows similar values for the degree of conversion at gelation for both the neat and nanocomposite system. Results for the degree of conversion at gelation vary slightly between the filled and the unfilled systems. Considering the error involved with this method, the degree of conversion appears not to vary greatly due to the added filler. Therefore, results show clearly that the reduced gelation time for organoclay reinforced resin systems can be ascribed to a higher rate of reaction. The increased rate of reaction can be related to different catalytic effects of the interlayer exchanged ion, as well as the hydroxy groups of the silicate. Since the hydroxy groups are less accessible to the resin than the amine molecules, their catalytic effect is probably of lesser importance.

3.4   Flexural Braid Analysis

Isothermal DMTA scans were run on the different resin blends painted on inert glass fibre braid to monitor changes in the viscoelastic behaviour during cure. A typical isothermal dynamic mechanical spectrum is shown in the introduction (Figure 2.8) for the DGEBA/DETDA/10 % organoclay system cured at 120 °C. Two successive peaks can be observed in the tan δ traces. Although the first one has been the subject of discussion [6, 103], it is most often associated with gelation [104, 105]. The second peak occurs due to the vitrification of the resin system [6, 103, 104]. As well as the two peaks in tan δ a steep increase in the modulus can be observed. The rapid increase in modulus is followed by a plateau, indicating that little further reaction takes place at a given isothermal

temperature [106]. Results for the gelation times are summarized in Table 3.4. As for the results obtained from rheology measurements, a steady decrease in gelation time can be observed with increasing organoclay concentration. This effect is particularly significant at low cure temperatures. The initial addition of organoclay reduces the gel times dramatically, whereas any further addition only slightly reduces the time to gelation further. The TGAP and TGDDM resins follow a similar trend. TGDDM experiments show less well defined peaks compared to the other materials. In particular, the 2.5 % TGDDM sample showed very poor defined traces, for the measurement at 140 °C no values to peak positions were assigned.

Whilst the general effect of the organoclay on gelation is the same, in both methods the actual results for gelation times are not equivalent. However, it is well known that the gelation data obtained from different techniques are not usually precisely the same [137, 138].

Dynamic temperature rescans of the cured braid specimens were undertaken at the end of each isothermal run to determine the final glass transition temperature after isothermal cure. As illustrated in Figure 3.22 for TGDDM containing 10 % organoclay, the resin systems of higher functionalities and higher final glass transition temperatures had two peaks in most of the rescans. This is due to the fact that the resins have been isothermally cured well below their ultimate glass transition temperature $(T_{g\infty})$. The two peaks arise from different T_gs corresponding to the developing network during measurements. The first peak relates to the (actual) glass transition temperature of the partially cured resin. This peak is usually found 10 - 30 °C above the cure temperature. There are different explanations for this discrepancy between T_g and the cure temperature, these being: that the cure reaction continues during the temperature scan leading to an increase in the first peak location, and that the exotherm of cure can locally drive the temperature during cure above the bulk isothermal temperature and allow the reaction to proceed further. The peak at higher temperature is a result of further cure during the DMTA rescan and corresponds to the ultimate glass transition temperature. Figure 3.22 also illustrates how the peak location changes with increasing frequency. It is

obvious that the ability of the molecular chains to move is more limited at higher frequencies thus it appears glassier, with a higher T_g. Hagen and Salmén [139] emphasized the importance of frequency and heating rate when comparing T_g values determined by dynamic mechanical analysis.
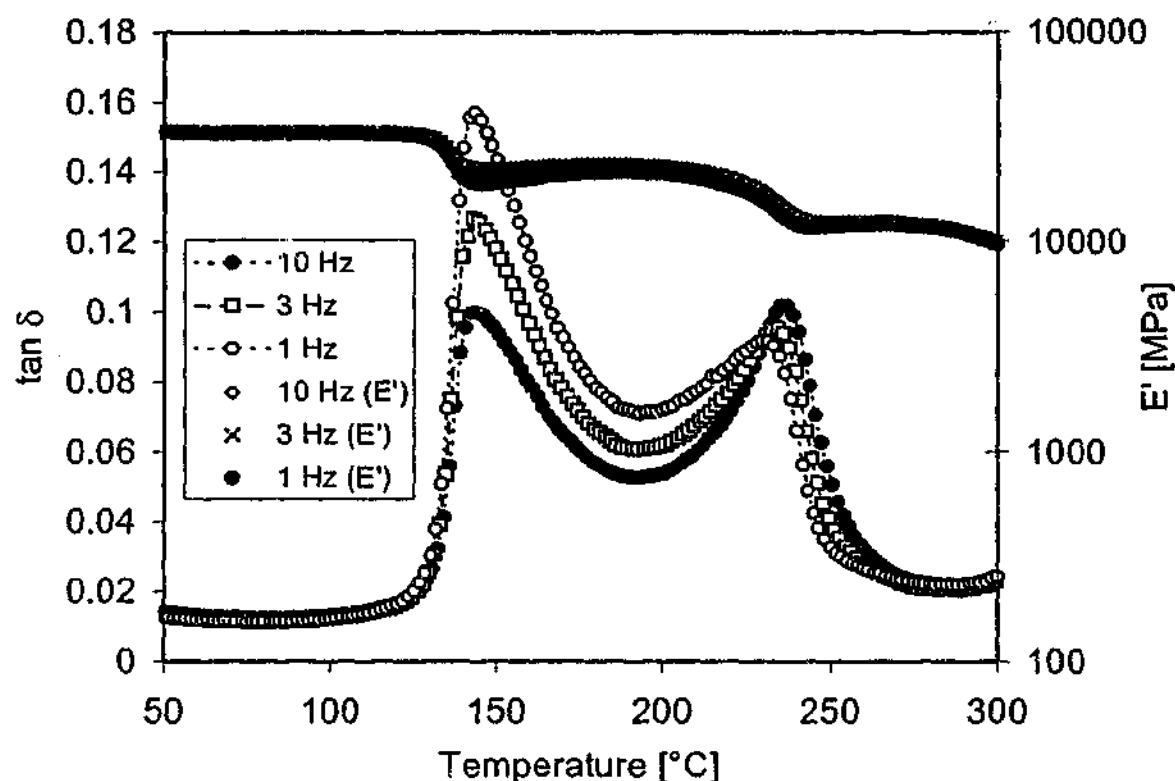
Figure 3.22: Dynamic temperature DMTA scan of isothermally cured TGDDM/DETDA/10 % organoclay at 100 °C.

Whilst the DGEBA based system shows significantly increased T_gs with organoclay addition (as illustrated in Figure 3.23), the TGAP and TGDDM-based systems show only a general trend of slightly increased glass transition temperatures. At first glance, this contradicts the fact that the ultimate glass transition temperatures of organoclay-filled epoxy resins were found to decrease significantly with increasing clay concentration as will be shown later. However, the fact that the T_g of the materials cured below $T_{g\infty}$ show increasing glass transition temperatures with increasing organoclay concentration can be explained by the higher rate of reaction.

Table 3.4: Gelation times of various epoxy systems containing 0 - 10 % OLS as determined from DMTA measurements (10 Hz).

Resin / Hardener	OLS content [%]	gel. at 100 °C [s]	gel. at 120 °C [s]	gel. at 140 °C [s]	gel. at 160 °C [s]	gel. at 180 °C [s]
DGEBA / DETDA	0	18450	9492	3246	2934	1314
DGEBA / DETDA	2.5	6306	3690	2562	1902	1230
DGEBA / DETDA	5	4770	3420	1794	1308	1044
DGEBA / DETDA	7.5	4284	2634	1296	714	510
DGEBA / DETDA	10	5190	2526	1320	966	654
TGAP / DETDA	0	14790	6324	4440	3246	2298
TGAP / DETDA	2.5	9648	4525	2604	1788	1104
TGAP / DETDA	5	8754	3480	1980	930	762
TGAP / DETDA	7.5	7242	3660	1644	642	552
TGAP / DETDA	10	7920	3318	1662	918	816
TGDDM / DETDA	0	11431	4344	2088	1230	1002
TGDDM / DETDA	2.5	7020	3054	*	1158	750
TGDDM / DETDA	5	6474	2994	1422	936	690
TGDDM / DETDA	7.5	5346	2430	1056	630	630
TGDDM / DETDA	10	5247	2316	1140	882	660

* no peak assigned

Since the resins systems are not fully cured and - as outlined above - the organoclay accelerates the resin conversion, the crosslink density can be expected to increase with increasing filler content. Thus, the points are at varying degrees of cure, with the systems of higher clay content being more cured over the same length of time due to the catalysed reaction as outlined above, thus showing a higher T_g. As with the results found by DSC, the DGEBA based system is more affected by the organoclay addition than the nanocomposite systems based upon reins of higher functionalities, likely due to better intercalation.
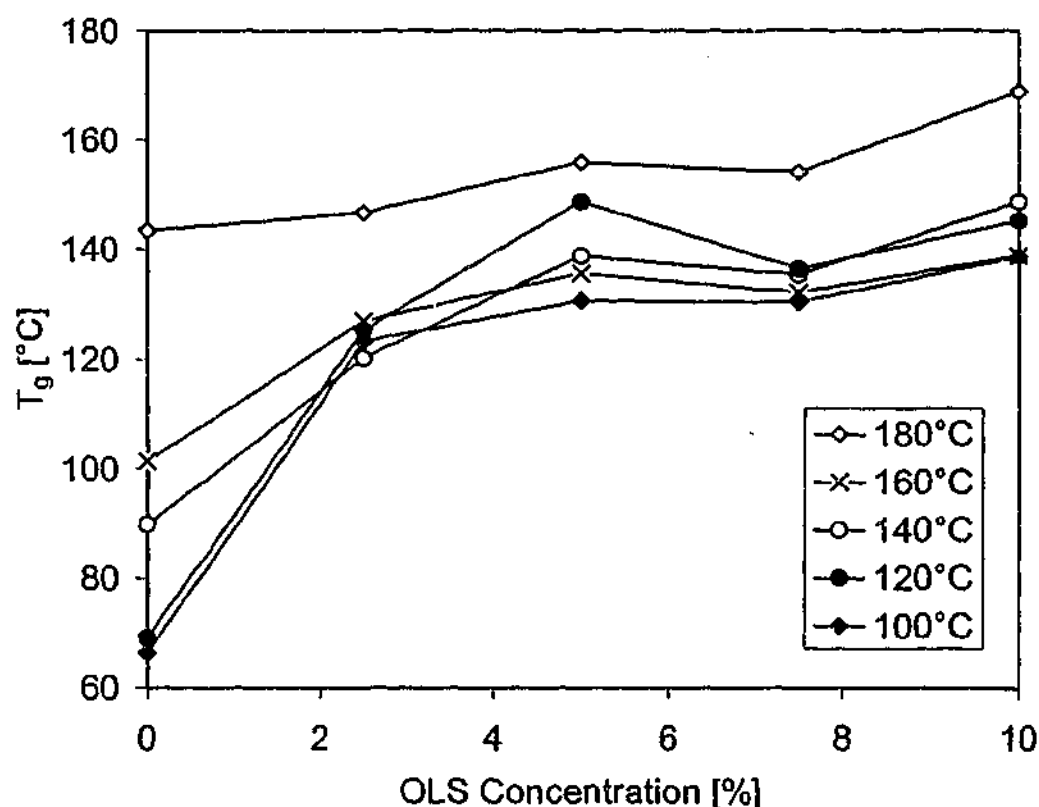
Figure 3.23: Glass transition temperature (T_g) versus cure temperature for DGEBA nanocomposites after isothermal cure at different temperatures. Values are taken from the DMTA temperature rescan at 2 °C per minute and 1 Hz.

Vitrification occurs when the glass transition temperature of the curing polymer approaches the isothermal cure temperature. At the point when the glassy network is formed, a second peak is often observed in the tan δ traces. The vitrification times were determined from the second peak in tan δ traces at 10 Hz as illustrated in the experimental section (Figure 2.8). An example for

vitrification times as a function of organoclay concentration at different cure temperatures is shown for the TGDDM based system in Figure 3.24. It was found that the vitrification times are generally reduced due to the presence of the layered silicate filler. This means that even after gelation, when the molecular mobility is strongly reduced, the rate of reaction remains affected (accelerated) by the catalytic effect of the alkylamine ions as discussed above.
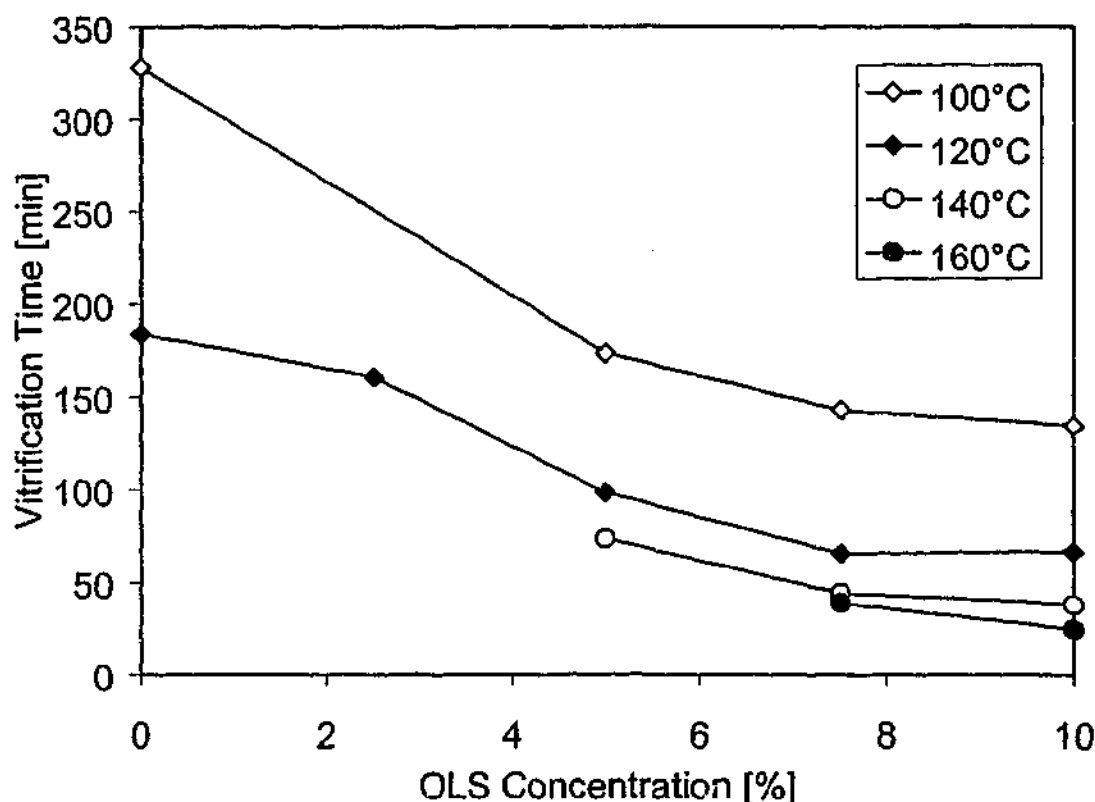
Figure 3.24: Vitrification times of TGDDM/DETDA containing 0 - 10 % OLS as determined from the torsion braid test (10 Hz).

The DGEBA based systems and some of the TGDDM based nanocomposites did not show vitrification peaks at higher isothermal cure temperatures. In the case of the DGEBA systems, this can simply be explained by the fact that the T_g is below the isothermal cure temperature and therefore vitrification does not occur. In the case of the TGDDM systems it may apply that the vitrification peak is so broad and weak that it could not be determined accurately. In fact, it has been reported previously [129] that vitrification is a gradual process that takes place over a significant period of cure, and thus is more diffuse than gelation.

This is enhanced by the entrapment, in the glassy state of a range of molecular environments that cause the peak to be broad.

3.5   Intercalation during Mixing and Cure

To further investigate the formation of the morphology during cure, the relationship between cure time and degree of exfoliation was examined in the DGEBA and TGDDM nanocomposite containing 7.5 % organoclay. The reactive nanocomposite mixtures were made up, as described in the experimental section, and cured for 1 to 10 minutes at 140 °C in order to follow the silicate layer delamination process during cure. After one-minute intervals, samples were taken from the oven and stored at -20 °C to avoid further reaction. XRD measurements were taken from each sample in a range of $2\theta = 1 - 10°$. Figure 3.25 illustrates the increase in d-spacing of the organoclay for the DGEBA and TGDDM nanocomposites during the first 10 minutes of cure. In both cases significant changes in the interlayer distance of the clay occurred during the first few minutes. Due to the increasing intensity in the XRD signal at low angles the (001)-peaks are difficult to detect. However it is observed that this peak soon loses intensity, becoming almost completely absent after 7 minutes. At the same time, the (002)-peak broadens and shifts towards lower angles and thus higher interlayer distances. Due to the resolution of the wide angle XRD measurement and the fact that exfoliation appears not to be a sudden, but rather a gradual process, it is not possible to say that exfoliation takes place after a precise amount of time, however, both systems show a high degree of intercalation after 8 - 10 minutes. The degree of conversion at the stage of cure at which the greater degree of intercalation occurs is of significance, since this determines the time frame available to mechanically manipulate exfoliation during cure. The residual exothermic enthalpy of reaction of samples at the given cure time was determined using differential scanning calorimetry and compared to the energy of cure of unreacted, catalysed monomer, allowing the degree of conversion to be determined.
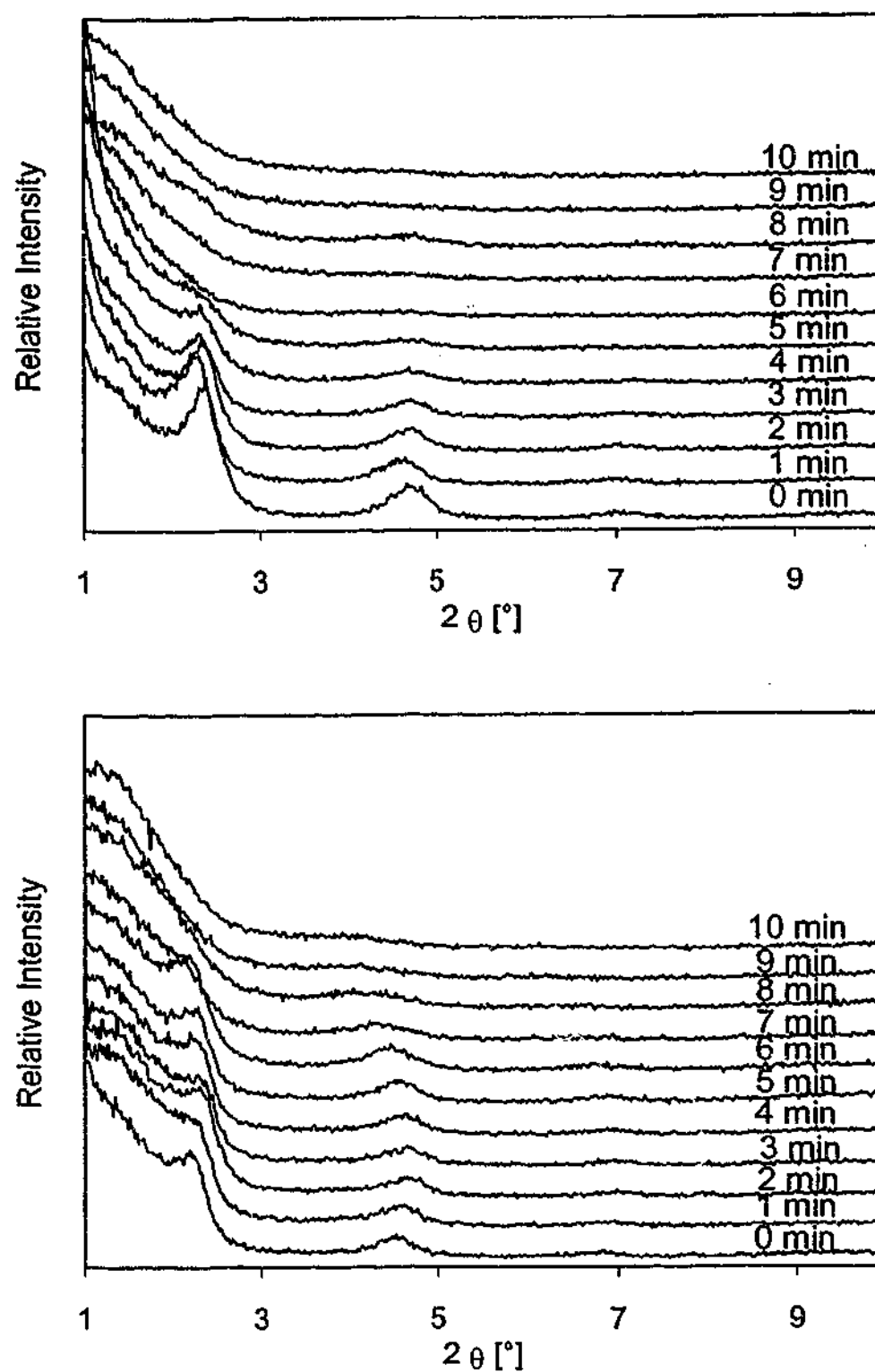
Figure 3.25: XRD series of the DGEBA (top) and TGDDM (bottom) based nanocomposite containing 7.5 % organoclay. Traces from the top to the bottom show the development of the d-spacing during the first minutes of cure at 140 °C.

The degree of reaction was found to be 22 ± 3 % (8 minutes) or 26 ± 3 % (10 minutes) for the DGEBA based system and 13 ± 3 % or 18 ± 3 % (8 and 10 minutes respectively) for the TGDDM based system. Earlier in this chapter, it was demonstrated that the DGEBA-based nanocomposite had a conversion at gelation of about 75 % and for the TGDDM 60 %. It is thus clear that major changes in the interlayer distances of these systems occur during the early state of cure, significantly earlier than gelation.

Chapter 4
Morphology and Physical Properties

The aim of the following chapter is to investigate the effect of cure temperature and layered silicate concentration on the morphology of the nanocomposites. Two different series of experiments are discussed. Initially, a range of epoxy nanocomposites was prepared using different cure temperatures at a constant organoclay concentration of 7.5 %. The morphology of these materials was analysed using WAXS. In a further step, a series of nanocomposites with different organoclay concentrations were synthesised following the 100 °C and 160 °C cure profile. The morphology of each material was probed using WAXS. Furthermore, the structures of selected systems were analysed in more detail using different microscopy techniques as well as gas displaced pycnometry and positron annihilation lifetime spectroscopy. An attempt to improve the organoclay separation through induced shear forces during cure will also be discussed.

4.1   Morphology Studies - XRD

4.1.1   Nanocomposite Formation at Different Cure Temperatures

The influence of the cure temperature on the morphology of the different epoxy nanocomposite systems was investigated. A range of DETDA-cured epoxy nanocomposites based on the three different resins (DGEBA, TGAP, and TGDDM) containing 7.5 % organoclay were prepared following different cure cycles, as illustrated in Table 2.1 in the experimental section. The average distance between two silicate layers, the d-spacing, was determined after cure using wide angle XRD. Wide angle x-ray traces as a function of the initial cure

temperature are shown in Figure 4.1 to Figure 4.3 for all three epoxy resin systems. Identifications of the (001) and (002) diffraction peaks are summarized in Table 4.1 (in section 4.2). The (00l) peaks represent the reflections of stacks of clay layers. Shift of those peaks in the XRD spectrum relate to changes in the distance between the silicate platelets. The initial d-spacing of the dried organoclay was determined to be 23 Å.

XRD traces of the DGEBA-based systems did not show any peaks in the low-angle range, indicating that highly intercalated or exfoliated nanocomposite structure results at cure temperatures between 80 °C and 160 °C. It should be noted that the lowest angle able to be measured with this technique was $2\theta = 1°$, which correlates with a d-spacing of 88 Å for the given wavelength of 1.540598 Å. In addition, the intensity of the XRD signal increases towards lower diffraction angles due to the higher background radiation of the main beam that occurs. This may overlap or interfere with peaks in that region and sometimes obscure signals related to d-spacings greater than 50 Å. This may be particularly true if the platelets show a greater distribution in layer distances, rather than repeating distances of the same length. The traces of the TGAP sample, cured at 80 °C, show a clear (001) peak at $2\theta = 2°$, signifying a d-spacing of 45 Å and indicating a high level of intercalation. With increasing cure temperature the (001) peak in TGAP disappears from the range that can be examined using WAXS, although the (002) peak and a small signal of the (003) peak can still be observed. Peaks in the range of 20 - 25 Å are related to the (002) reflection, representing the half-length of the actual average distance (40-50 Å) between two silicate layers. The (002) peak itself shifts slightly towards lower angles (higher d-spacings) with increasing cure temperature and decreases in intensity. XRD results of the TGAP sample cured at 100 °C show slightly higher values of the d-spacing than were expected from the general trend of the temperature series. As shown in Figure 4.3, the TGDDM based nanocomposites show a slight monotonic increase in the average d-spacing with increasing cure temperature. No peaks are apparent in the low angle range for the TGDDM-based nanocomposite cured at a temperature of 160 °C. Comparison between the two higher functionality epoxy resin systems shows

that, in spite of its significantly higher viscosity, the TGDDM system produces a nanocomposite with more improved d-spacing compared with the less-viscous TGAP system. However, both systems exhibit improved layer separation at increased cure temperatures.

For both DGEBA and the high-functionality systems investigated, it was found that increased cure temperature yielded better exfoliation. Whilst this was not the case for a 4,4'-diaminodiphenyl sulfone (DDS) cured TGDDM nanocomposite [77], similar results have recently been reported for various DGEBA based systems [75, 78]. In fact, recent in-situ small angle XRD studies by Tolle and Anderson [78] have shown, that higher cure temperatures resulted in both earlier initiation of exfoliation, as well as greater silicate spacing in the final material for a m-phenylene diamine cured DGEBA nanocomposite system using the same commercially-available organoclay as in this work. However, the authors did not directly comment on a possible mechanism justifying the improved layer separation.

As outlined in the literature review, the mechanism of organoclay exfoliation in epoxy-layered silicate nanocomposites has been the focus of various studies and it was pointed out that control of intra- and extra-gallery reaction is the key to overcome the attractive forces between the silicate layers and achieve exfoliation. The improved organoclay delamination at increased temperatures may be related to a number of aspects, one being that the lower viscosity or enhanced molecular mobility improves mass transfer into the clay galleries. Increased cure temperatures are also known to favour homopolymerization [69]. The catalytic effect of the organoclay on both resin-amine cure and homopolymerization as discussed in more detail in Chapter 3, may shift the equilibrium between inter- and extra-gallery reaction towards a higher reaction rate within the clay galleries. The structure and chemistry of the epoxy resin is clearly a significant factor in determining the equilibrium between inter- and extra-gallery reactions, and hence the morphology of the nanocomposite.
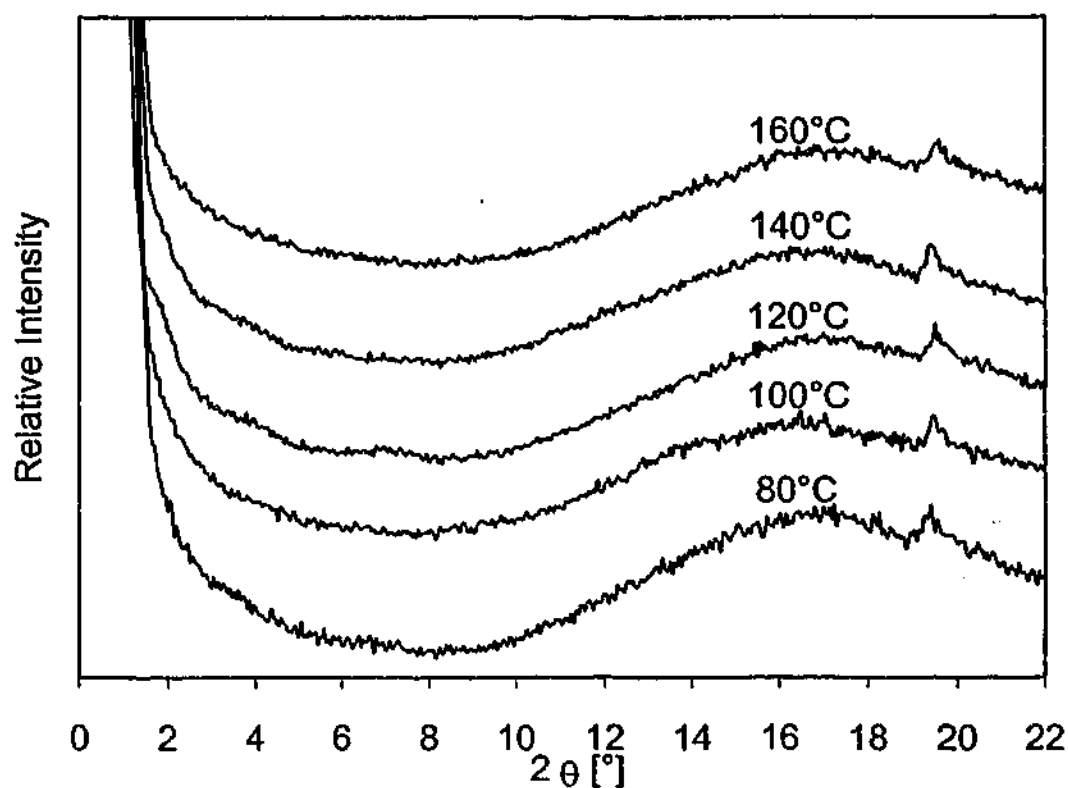
Figure 4.1: WAXS of DGEBA nanocomposites containing 7.5 % OLS, cured at different temperature profiles.
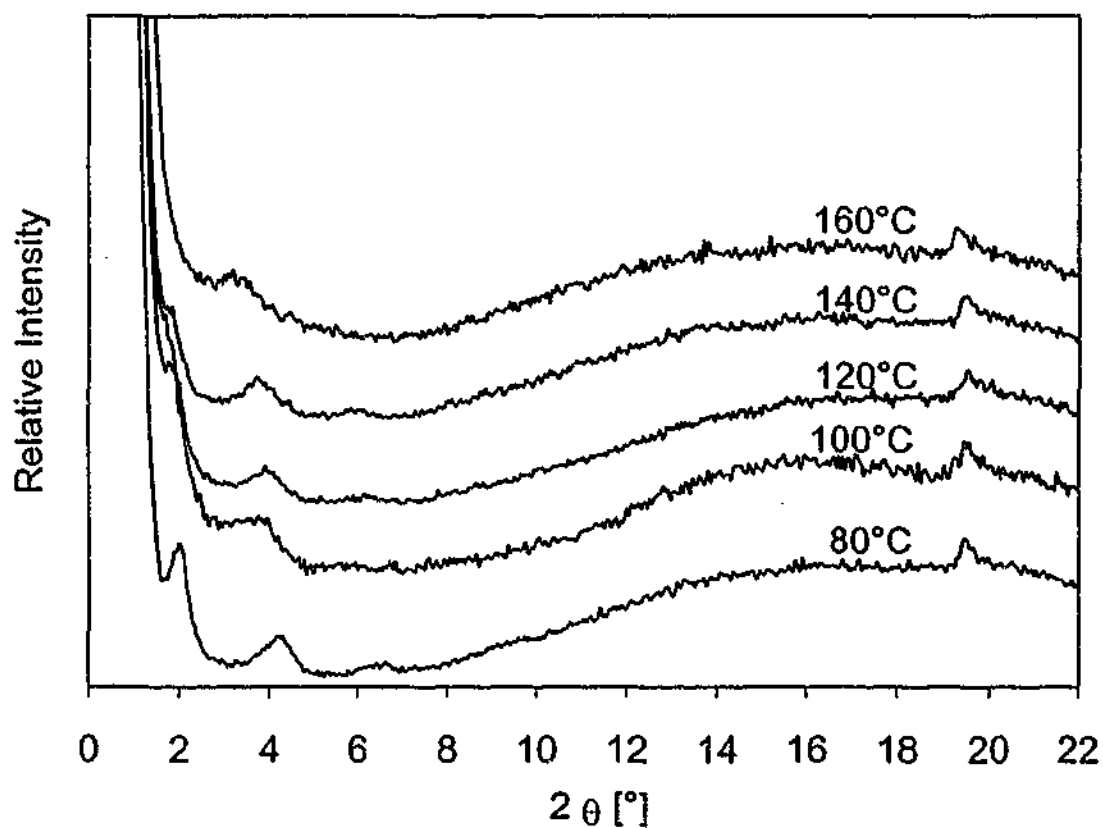
Figure 4.2: WAXS of TGAP nanocomposites containing 7.5 % OLS, cured at different temperature profiles.
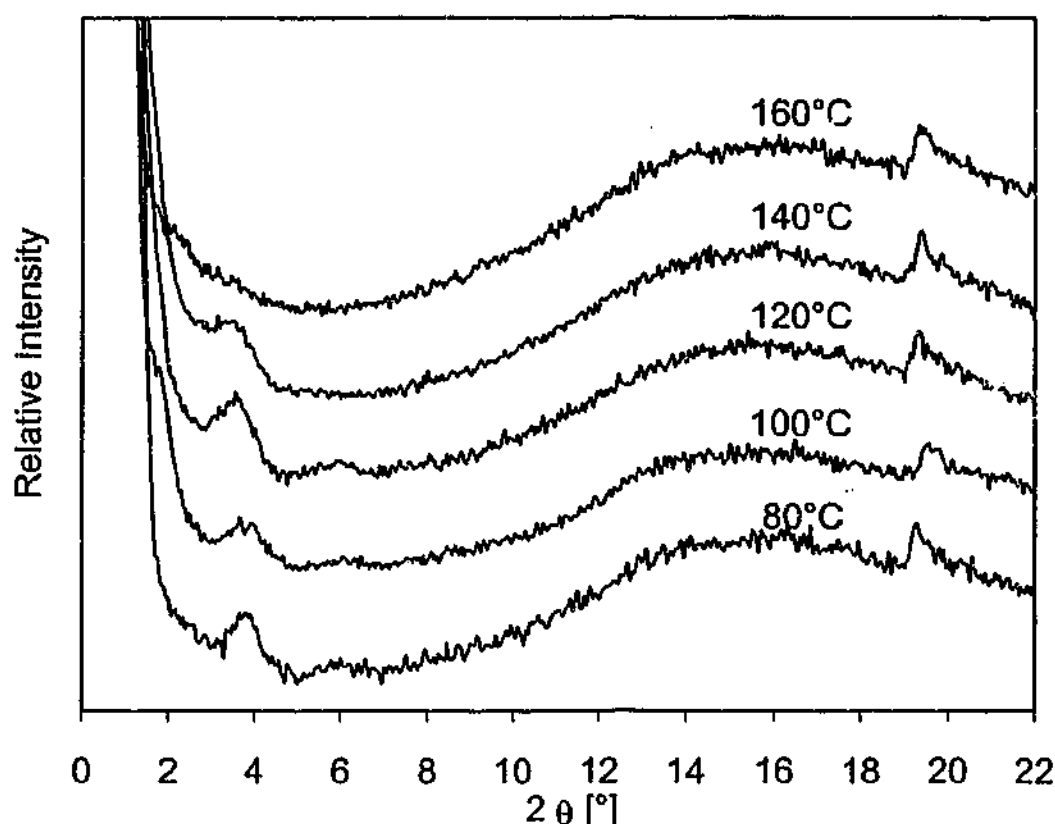
Figure 4.3: WAXS of TGDDM nanocomposites containing 7.5 % OLS, cured at different temperature profiles.

To further understand the variation in the different resin systems and their ability to exfoliate the silicate platelets, some of the earlier reported results should be recalled. The effect of the organoclay on polymerization reaction has been investigated using differential scanning calorimetry (DSC). Figure 4.4 shows DSC traces of the neat resin hardener reaction as well as of the reaction of the organoclay-catalysed resins (blended with 7.5 % organoclay), scanned at 10 °C/min. It can be seen that the two resins with the most improvement in d-spacing, DGEBA and TGDDM show significantly reduced reaction peaks, indication a strong catalytic effect of the organically modified layered silicate on the cure reactions. The layered silicate-containing DGEBA system shows a broad shoulder or even a second peak at lower temperatures, which is likely to be related to the clay-catalysed polymerization or homopolymerization respectively. The TGDDM/organoclay/hardener blend shows a broadened peak with the peak maximum shifted by about 30 °C towards lower temperatures. In

contrast, the TGAP system, which did show the least improvement in the d-spacing, appears to be less significantly affected by the organoclay addition.
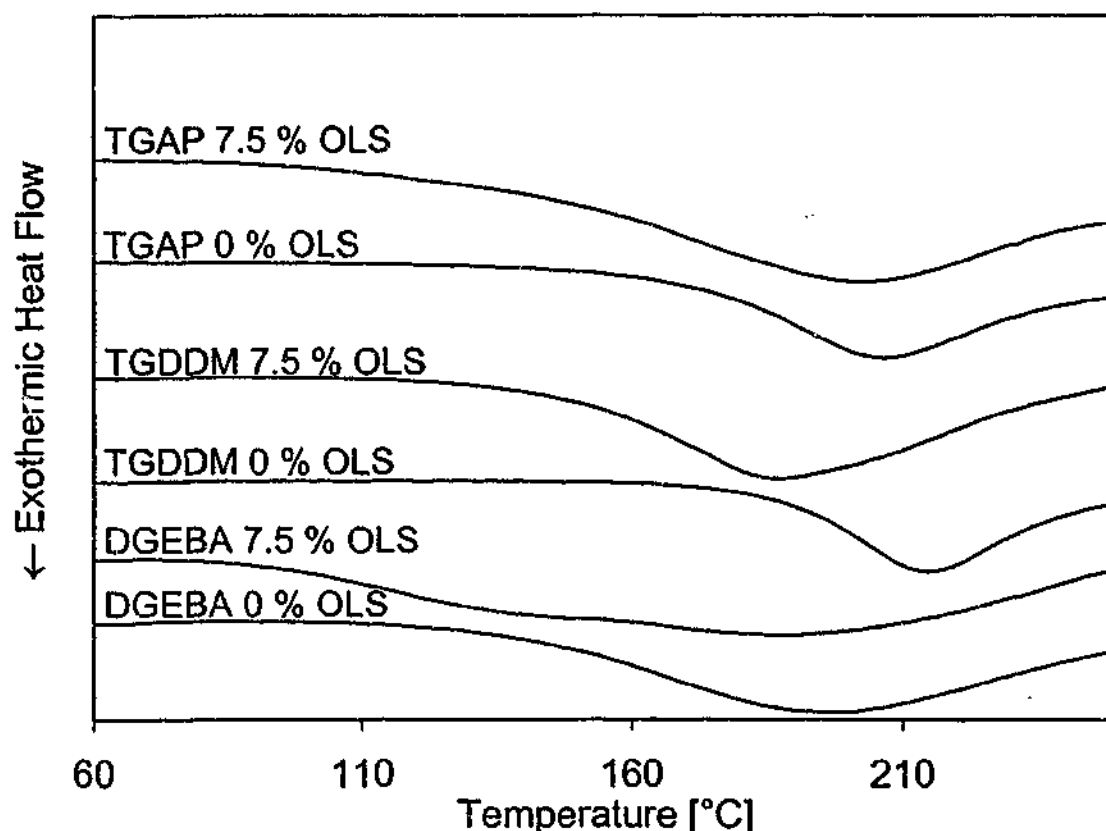
Figure 4.4: DSC analysis of neat and layered silicate catalysed cure reaction, determined at a scanning rate of 10 °C/minute.

To verify the ability of the epoxy resins to move into the organoclay galleries the viscosities of the different epoxy resins should also be recalled. Comparison of the η values (here at 60 °C at 1 rad/s), shows that the TGAP resin has the lowest viscosity of 0.04 Pa· s, compared with 0.17 Pa· s for DGEBA and 1.30 Pa· s for TGDDM. Since the higher viscosity TGDDM resin has shown better layer separation than the low-viscous TGAP resin, it becomes clear that at the given reaction temperatures, the initial viscosity of the resin is not the determining factor for the exfoliation process. Hence, the ability of the organoclay to act as a catalyst for the different epoxy resins systems and the affinity of the resin towards the clay compatibilizer, may be more significant parameters for improved in exfoliation. Brown et al. [64] pointed out the critical

balance of the miscibility of the resin with the organically modified layered silicate. If the miscibility between the modified layered silicate and the epoxy resin is high, an unacceptable increase in viscosity up to the formation of a physical gel will occur and disable further processing. However, insufficient affinity between resin and layered silicate will reduce the reaction within the galleries that leads to the layer separation. Indicators for the affinity between both components are the change in viscosity and the increase in the layer d-spacing during the initial mixing before cure has commenced.

4.1.2   Nanocomposite Formation at Different Concentrations

A series of nanocomposites with the organoclay concentrations varying from 0 - 10 % were synthesised using two different cure profiles, namely the 100 °C and 160 °C cure cycle. WAXS traces of the clay concentration series cured at the 100 °C profile show that the organoclay with an initial d-spacing of 23 Å is either highly intercalated or (ordered) exfoliated in the DGEBA based system (Figure 4.5) as indicated by the lack of any peaks in the low-angle region. Only the DGEBA nanocomposite of the highest organoclay concentration (10 % OLS) shows a distinct peak correlating to a d-spacing of 48 Å. In contrast to the DGEBA based systems, resins of higher functionality show distinctive peaks, even at lower organoclay concentrations, indicating that these samples have a higher degree of intercalated rather than fully exfoliated layered silicate. WAXS traces are shown for the 100 °C series of TGAP in Figure 4.6 and of TGDDM in Figure 4.7. In any event, the peak observed around 25 Å or $2\theta = 4°$ correlates to the (002) plane and therefore represents half the distance of the d-spacing.

Relative Intensity

d(001) = 48Å

2.5 % OLS

5 % OLS

7.5 % OLS
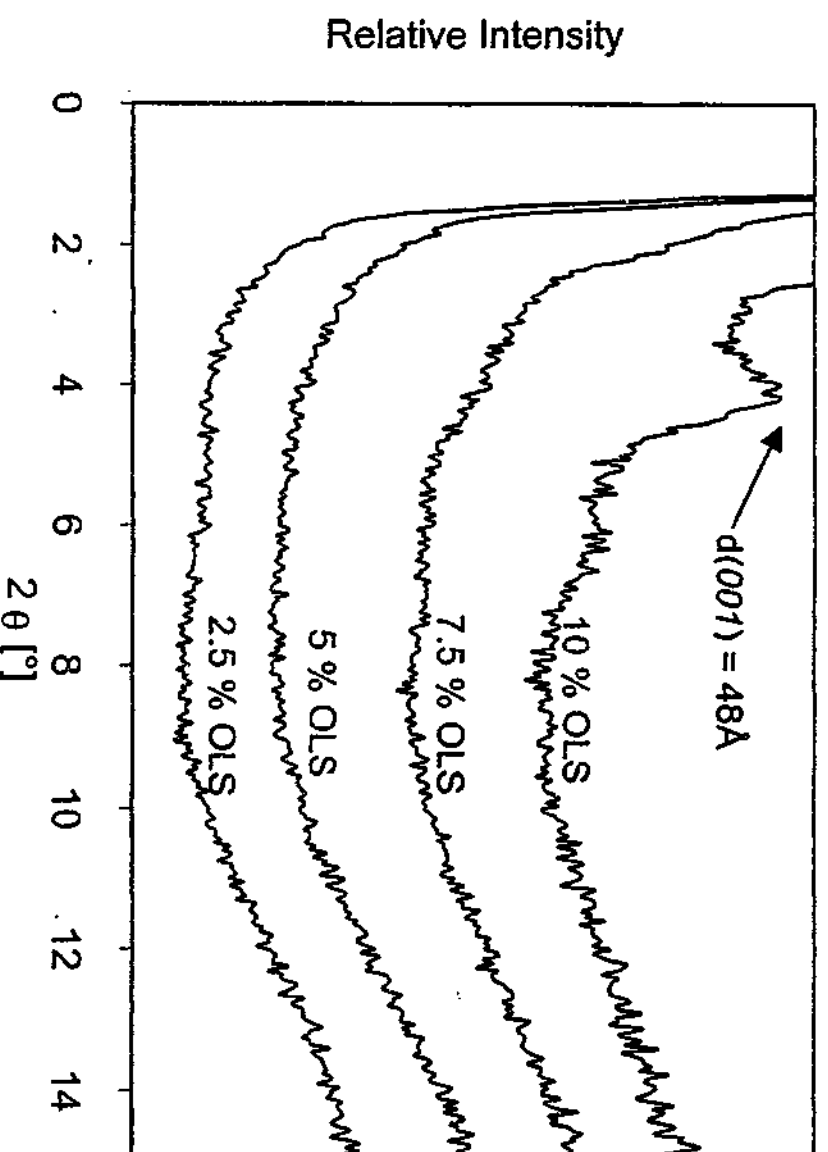
10 % OLS

Figure 4.5: WAXS patterns of DGEBA nanocomposites containing 2.5 - 10 % OLS, cured at 100 °C.

Relative Intensity

d(001) = 40.2Å

d(002) = 20.5Å

d(002) = 21.8Å

10 % OLS

7.5 % OLS

5 % OLS

2.5 % OLS
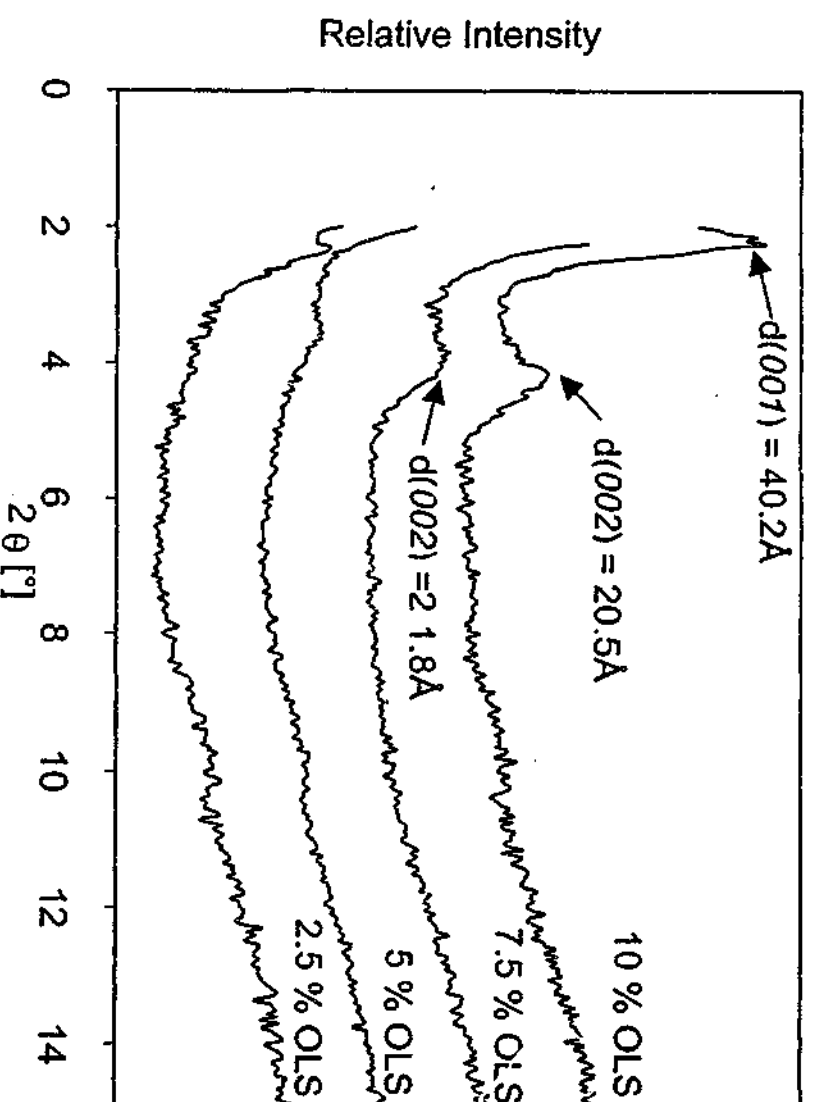
Figure 4.6: WAXS patterns of TGAP nanocomposites containing 2.5 - 10 % OLS, cured at 100 °C.
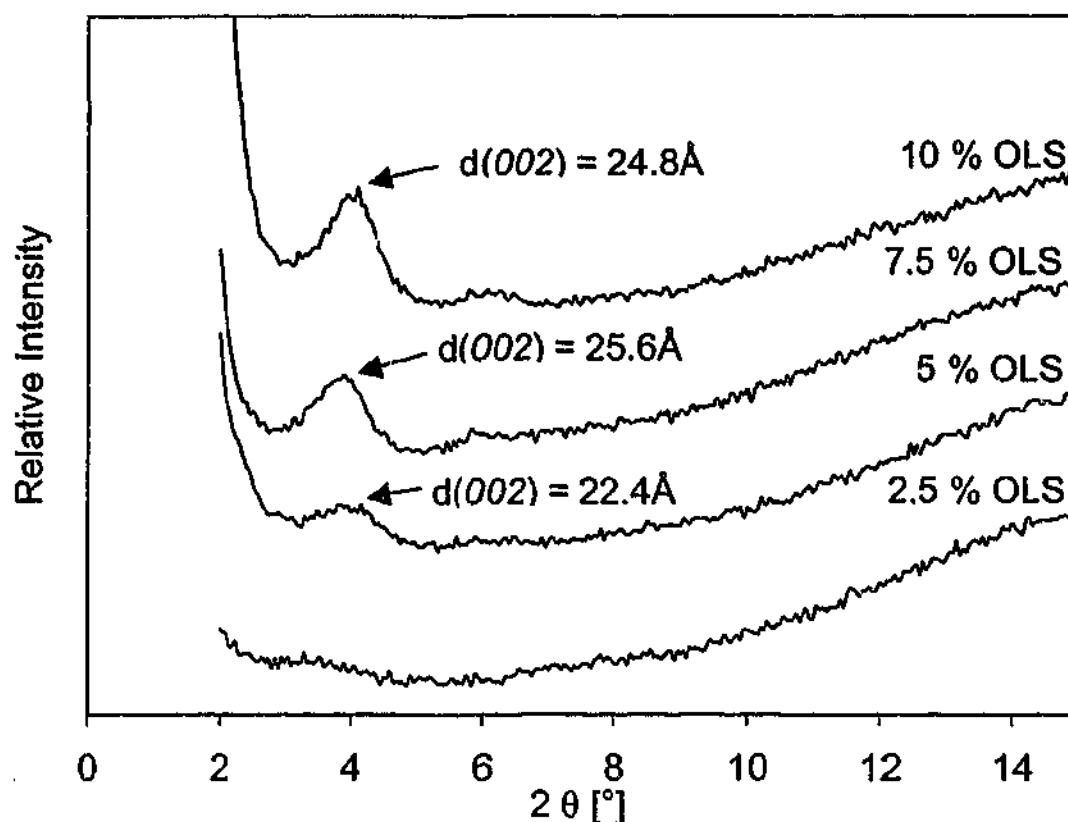
Figure 4.7: WAXS patterns of TGDDM containing 2.5 - 10 % OLS cured at 100 °C.

4.2   *Morphology Studies - Microscopy*

Before further investigating the nanostructure of the composites, optical microscopy was used to image the bulk surface. Optical micrographs as illustrated in Figure 4.8 for the DGEBA- and Figure 4.9 for the TGDDM-composite systems containing 5 % organoclay, show large particulate phases, indicating that aggregates of silicate layers exist even for the DGEBA-based system (which is well exfoliated according to XRD measurements). Kornmann et al. [77] have recently shown similar results for the μm-scale morphology of different TGDDM based nanocomposites in low-magnification SEM images. In their work, good agreement between the dispersion of aggregates on the μm-scale image and the dispersion on the nm-scale was observed. It was reported that the nanocomposite systems with more homogeneously dispersed aggregates on the μm-level have shown improved exfoliation compared to those composites that showed lower microscale dispersion.
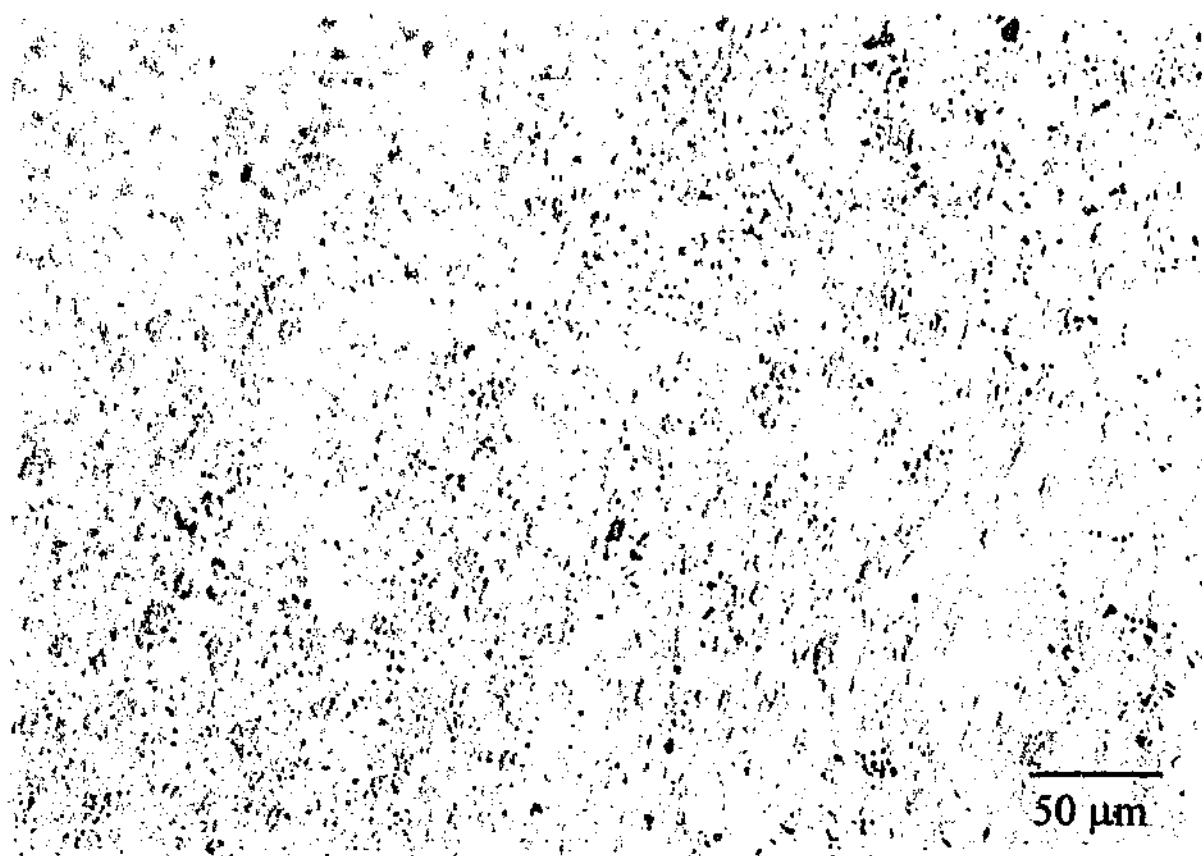
Figure 4.8: Optical micrograph of a TGAP nanocomposite containing 5 % OLS.
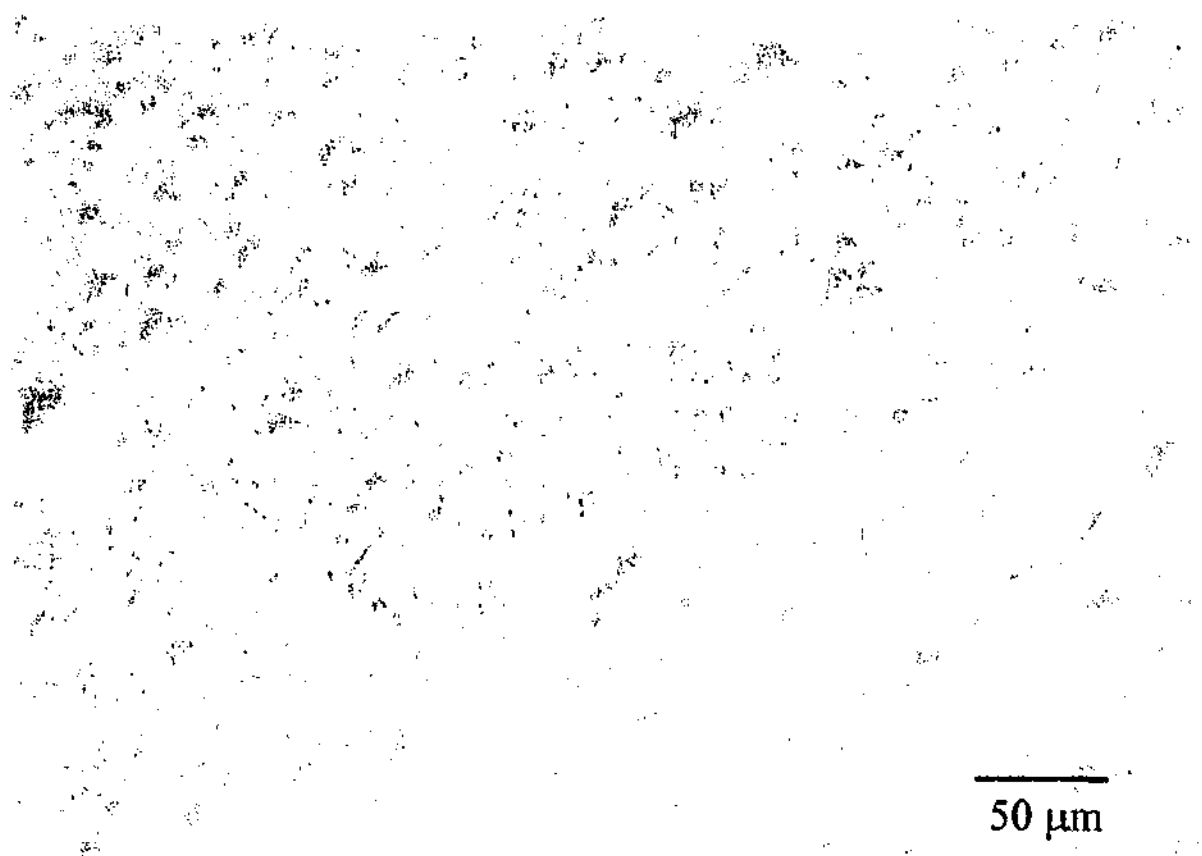
*Figure 4.9: Optical micrograph of a TGDDM nanocomposite containing
5 % OLS.*

Figure 4.10 and Figure 4.11 show atomic force microscopy (AFM) phase contrast images of the DGEBA nanocomposite containing 5 % layered silicate. Figure 4.11 represents a higher magnification of the selected area shown in Figure 4.10. Clearly a striated structure can be seen with increasing phase intervals at the top of the picture. Both optical microscopy and AFM images show that at least part of the silicate content is still arranged in tactoids or stacks of layers rather than forming a homogenous morphology through the whole material. The use of AFM to investigate the surface of nanocomposites has been reported previously [31, 140]. Zilg et al. [31] also examined intercalated epoxy layered silicate nanocomposites in the phase contrast mode. This work even determined the distance between silicate layers from AFM images. Furthermore, it was noted in this work that the AFM tip was able to strain and deplete individual silicate platelets, indicating that the layered silicates are rather flexible compared to the glassy epoxy matrix, in spite of the fact that layered silicates are often believed to be glassy and rigid.

Reichert et al. [140] investigated etched samples of poly(propylene)/OLS nanocomposites using AFM in both the height and phase contrast mode. The images allowed detecting both large silicate platelets and fine dispersed silicate platelets in skeleton-like superstructures.

Due to limitations in the range of diffraction angles available from the XRD method and hence d-spacings that can be determined, transmission electron microscopy (TEM) was applied to capture visual images of the nanocomposite morphology at high magnifications. TEM images were taken of nanocomposites containing 7.5 % OLS, which had been cured at 100 °C and 160 °C, respectively. Micrographs are illustrated in Figure 4.12 for DGEBA, Figure 4.13 for TGAP and Figure 4.14 for TGDDM nanocomposites. The thin dark lines in the pictures represent the edges of single silicate platelets. The clay platelets in the TGAP and TGDDM nanocomposites cured at 100 °C show a parallel orientation, as commonly reported for most thermoset-layered silicate nanocomposites synthesized via in-situ polymerization [77].

0   3.31 μM
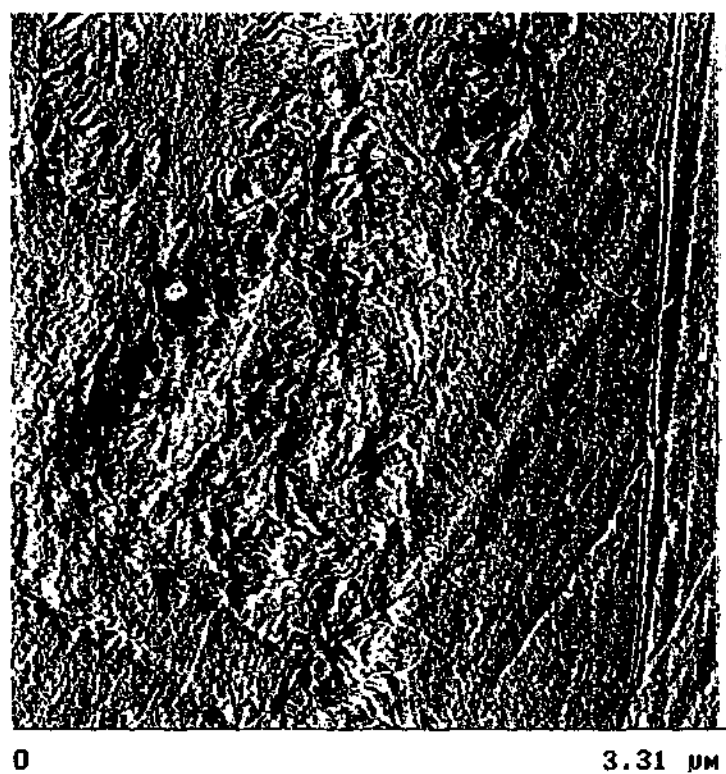
Figure 4.10: Phase contrast AFM image of a DGEBA nanocomposite containing
5 % OLS.
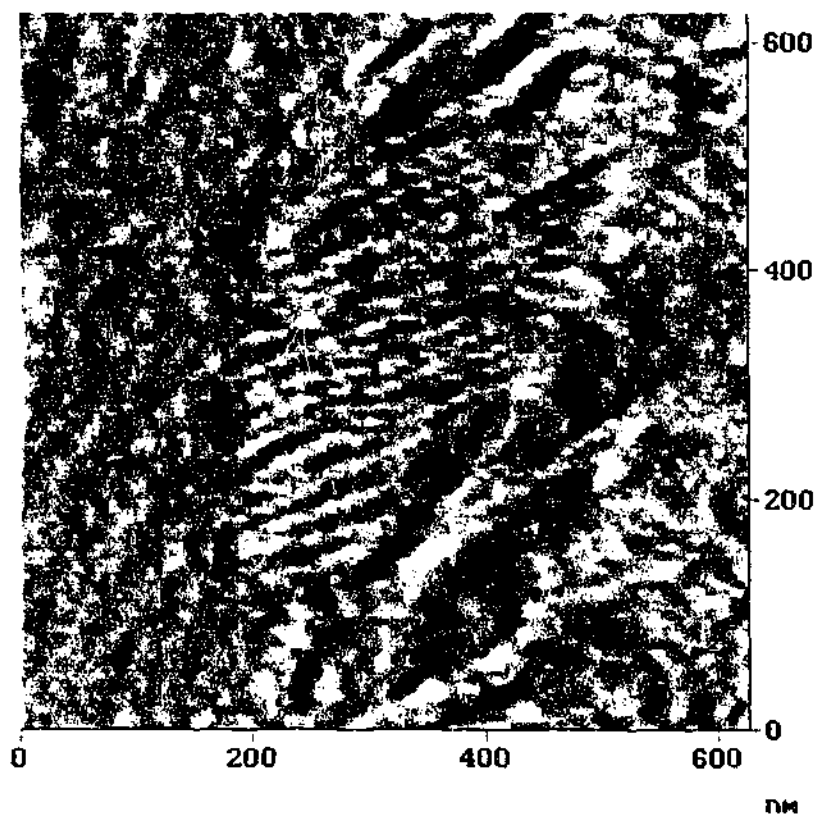
Figure 4.11: Phase contrast AFM image of a DGEBA nanocomposite containing
5 % organoclay - close up of the section indicated with a white square in
Figure 4.10.

The DGEBA nanocomposites and the high-functionality nanocomposites cured at 160 °C also show this parallel structure with an increased d-spacing. However, single platelets and stacks of just a few platelets can also be observed, having been delaminated from the parent tactoids. This coexistence of both individual platelets and layers reminiscent of the original layered silicate aggregate is often observed in TEM micrographs of thermoset systems or melt processed thermoplastics in the absence of high shear forces [45, 70, 73, 76, 90].

Recently, Brown et al. [64] investigated the morphology of different DGEBA based layered silicate nanocomposites. It was interesting to see, that in spite of a transparent appearance and the absence of any peaks in the low-angle range of XRD traces, a structure of intercalated and exfoliated layered silicates was reported according to TEM micrographs.

TEM and XRD are the most powerful techniques used to determine absolute values of the state of organoclay exfoliation and the distance in the interlaminar spacing. Previous work by Zilg et al. [31] has pointed out that different techniques such as TEM, AFM and WAXS may give a different picture of the state of morphology. In their work, TEM images showed some large interlayer distance for a Jeffamine based nanocomposite, whilst WAXS measurements of the same material indicated a poor interlayer. Also in their work, a comparison between AFM and WAXS results for a particular nanocomposite showed a discrepancy of the interlayer distance of 40 Å. Since any of these methods investigates only a limited microscopic area of the bulk material, conclusions on the overall morphology must be made with care.

The average d-spacing of the organoclay was estimated for each system from various measurements of the interlayer distance in different TEM images. Results are summarized in Table 4.1, together with values determined from the XRD data and both sets are in good agreement. TEM images of the DGEBA systems in Figure 4.12 show a mixture of highly intercalated and partially ordered exfoliated organoclay platelets. Only those platelets that showed a parallel arrangement were considered for measurements of the interlayer

distance, determination of the degree of exfoliation being much more difficult. Although the ratio of fully exfoliated clay layers compared to highly intercalated parallel oriented platelets has likely changed with cure temperature, this is not readily quantifiable. Morgan et al. [141] recently pointed out the necessity to consider both the microscale and the nanoscale morphology when describing a layered silicate nanocomposite system. In their work it was highly recommended to apply both techniques, TEM and XRD, to evaluate the material structure. In his review on structural characterization, Vaia [45] discussed the complexity of polymer-layered silicate nanocomposite morphologies. In this work it was pointed out that uniform interlayer expansion is not the general case and nanocomposite structures often consist of regions of smaller expansion (in the interior of crystallites) and larger expansion of full separation (at the exterior of a crystallite). A more systematic nomenclature to describe the various stages of layered silicate dispersion is also suggested in this work.

Table 4.1: (001) and (002) diffraction peaks of the silicates and correlating d-spacing in the nanocomposites containing 7.5 % organoclay as determined from WAXS measurements and TEM, (*) not determined.

Resin system	Cure Temperature [°C]	(001) plane peak	(002) plane peak	d-spacing of (001) plane [Å]	d-spacing (TEM) [Å]
TGAP	80	42.0	20.5	42 ± 2	*
TGAP	100	no peak	25.0	50 ± 2	46
TGAP	120	46.5	22.8	46 ± 2	*
TGAP	140	49.0	22.9	47 ± 2	*
TGAP	160	no peak	26.0	52 ± 2	50
TGDDM	80	no peak	22.6	45 ± 2	*
TGDDM	100	no peak	22.9	46 ± 2	45
TGDDM	120	no peak	24.2	48 ± 2	*
TGDDM	140	no peak	24.9	50 ± 2	*
TGDDM	160	no peak	no peak	exfoliated	60
DGEBA	100	no peak	no peak	exfoliated	85
DGEBA	160	no peak	no peak	exfoliated	95
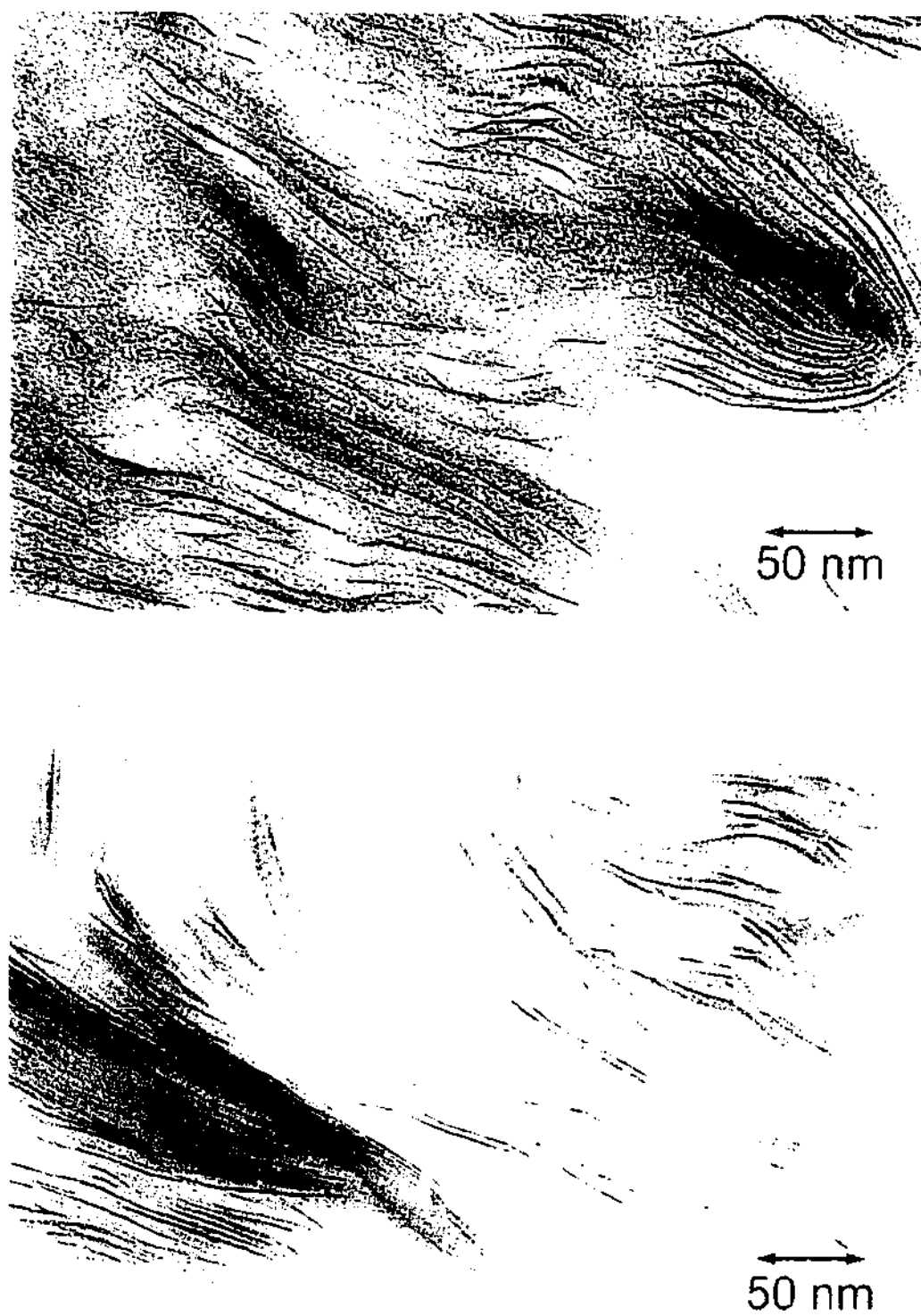
Figure 4.12: TEM micrograph of DGEBA nanocomposite cured at 100 °C (top)
and cured at 160 °C (bottom).
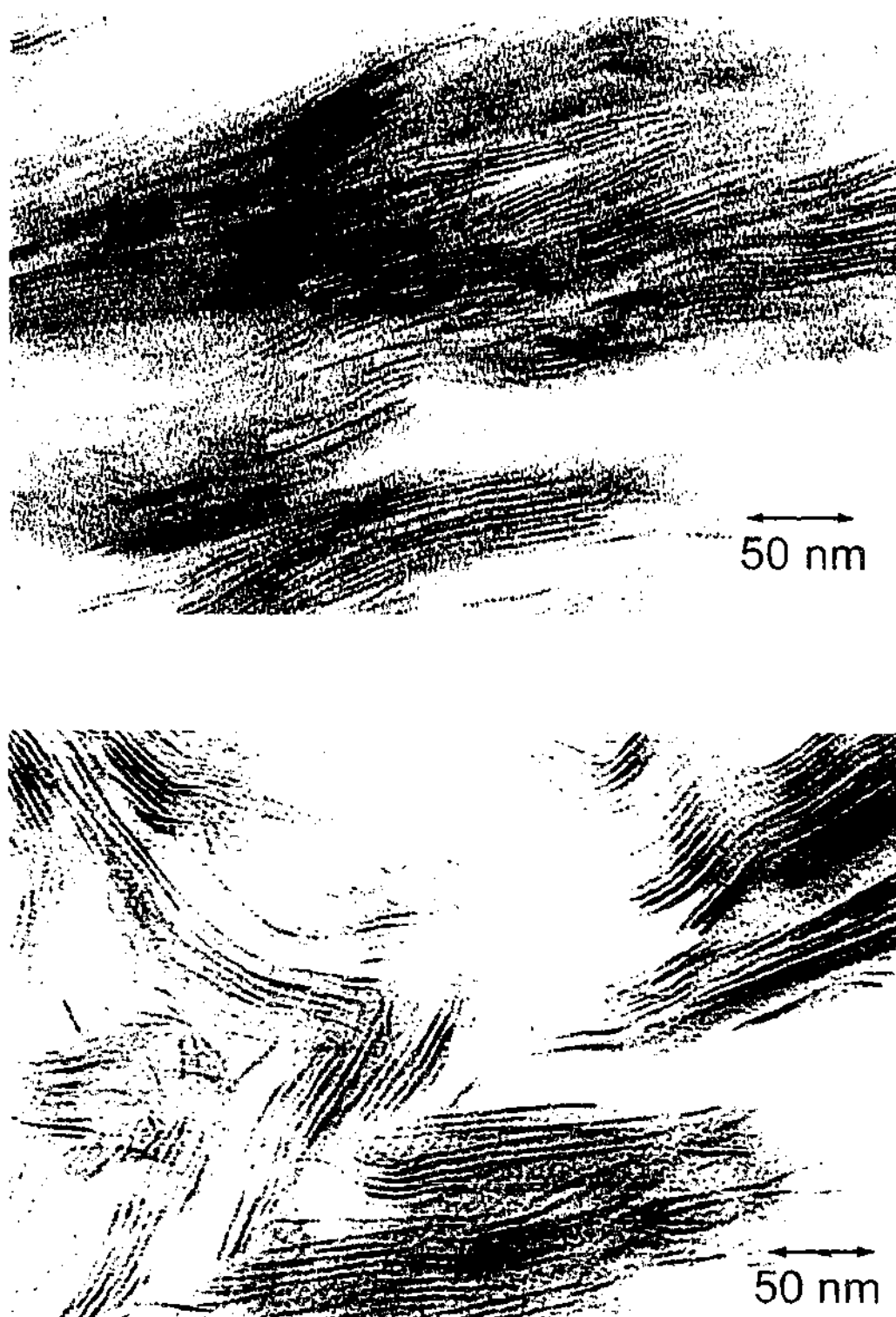
Figure 4.13: TEM micrograph of TGAP nanocomposite cured at 100 °C (top) cured at 160 °C (bottom).

50 nm

50 nm

Figure 4.14: TEM micrograph of TGDDM nanocomposite cured at 100 °C (top)
cured at 160 °C (bottom).

4.2.1 An Attempt to improve Exfoliation

It was found that initial mixing (prior to cure) of the organoclay and resin/hardener material leads to a limited degree of intercalation. This is dependant on the surface energy and polarity of the modified layered silicate, and the nature of the resin and hardener. It has been shown that the cure reaction itself may change polarity in the galleries and allow further material to diffuse into the galleries, thereby forcing the platelets further apart [62]. However, TEM images revealed that even in highly intercalated systems, which do not show any remnant (001) XRD peaks, the majority of the silicate platelets remained in a parallel tactoid structure. Based on the outcome of the experiments above it was decided to investigate whether shear stress imposed during the early stage of cure when clay platelets begin to delaminate, could lead to better exfoliation and thus to the formation of a truly exfoliated nanocomposite. DGEBA was mixed with 7.5 % organoclay at 140 °C, adding the DETDA hardener after 30 minutes, with an amine to epoxy ratio of 0.9. The blend was further mixed at 500 rpm with a PTFE anchor stirrer whilst curing. After 10 minutes the blend was transferred into aluminium trays and further cured at 160 °C for 12 h followed by a postcure at 200 °C for 2 h. TEM images were than taken from microtomed sections of 60 nm thickness and compared with the same system with no shear forces applied during cure as shown in Figure 4.15. The images show that the majority of silicate still remains in tactoids of parallel oriented platelets, with interlayer distances of 80 Å and above. However, it can be seen that some individual platelets are fully separated from their hosting tactoids when such mechanical forces are applied during the exfoliation process. Overall it was unclear whether the induced shear forces gave significant improvement in exfoliation of the layered silicate.
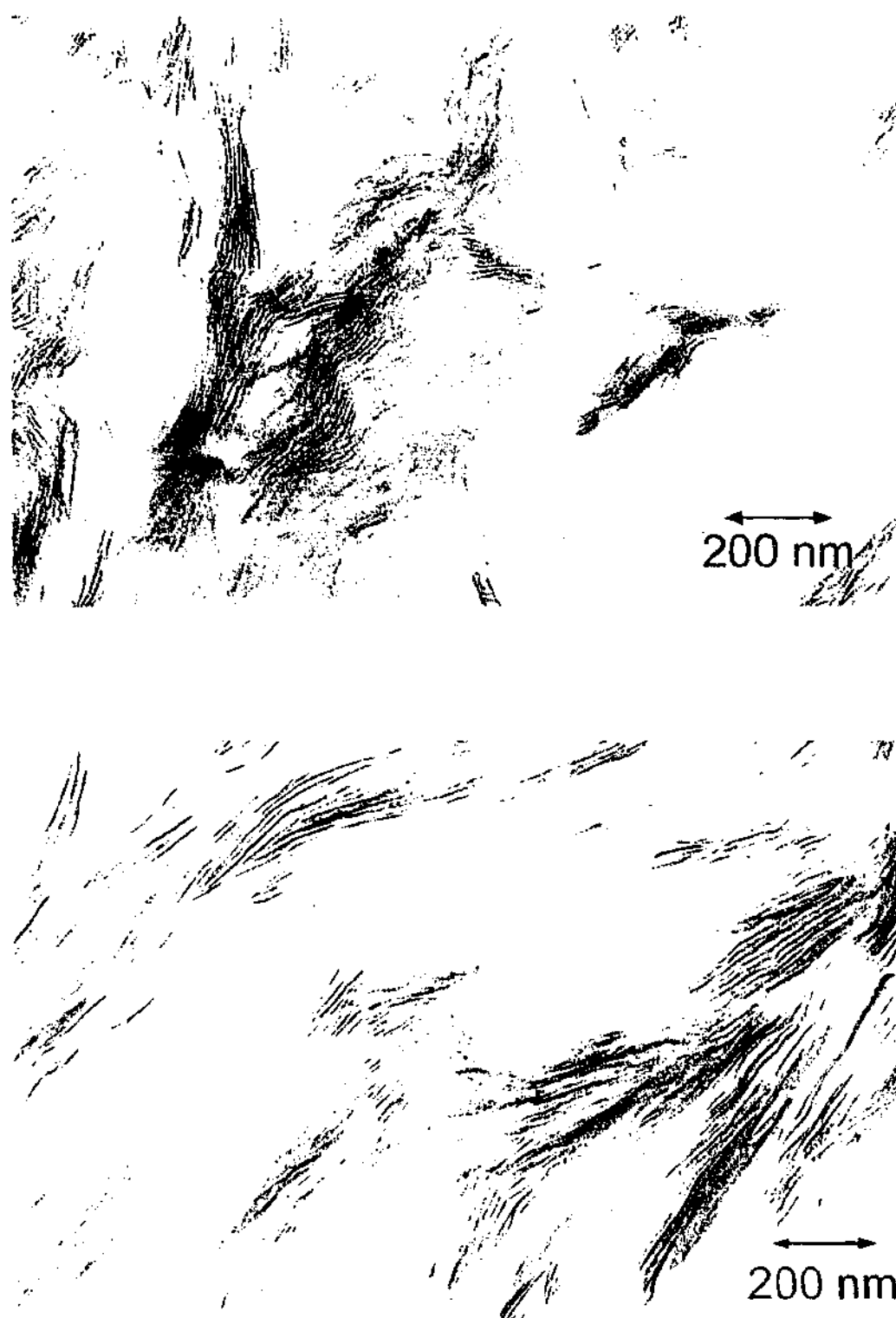
Figure 4.15: TEM micrographs of DGEBA nanocomposites cured under shear forces until close to gelation (top) and the same system cured without shear forces applied during cure (bottom).

4.3   Density

One of the key benefits of epoxy materials is their low density. Hence it was of interest to know how the epoxy nanocomposite density changed with filler addition. Density results of the various nanocomposites after postcure as determined by gas-displacement pycnometry are shown in Figure 4.16. Theoretical densities according to the rule of mixtures were calculated based on an organoclay bulk density of 1.6748 g/cm^3 (as determined with the same method). The rule-of-mixture data is represented in the straight lines in Figure 4.16. All density values are within a range of 1.1925 g/cm^3 - 1.2307 g/cm^3. The increase in specific weight of the resin systems due to the filler content occurs within a small range and is hence not a limiting factor for technical applications, which require low weight material. It is interesting to see that densities are generally slightly below predicted values from the rule of mixtures. The lower density is indicative of poorer packing of the polymer molecules near the silicate layers.

Only a few studies of the effect of layered silicate on polymer density are reported in the literature. Krook et al. [142] investigated the density of nanocomposites synthesized from polyesteramide and the octadecylamine-treated montmorillonite (Nanomer I.30E) as used in our work. The density of the intercalated and partially exfoliated thermoplastic nanocomposite was found to be independent of the processing temperature and extruder screw speed. However, nanocomposite densities were found to be lower than the theoretical values, which was ascribed to induced voids. According to transmission electron microscopy images the voids were almost exclusively located between neighbouring silicate layers. Furthermore, it was theorized that the voids significantly reduced barrier properties, whilst the strength and stiffness showed no effect due to the voids.
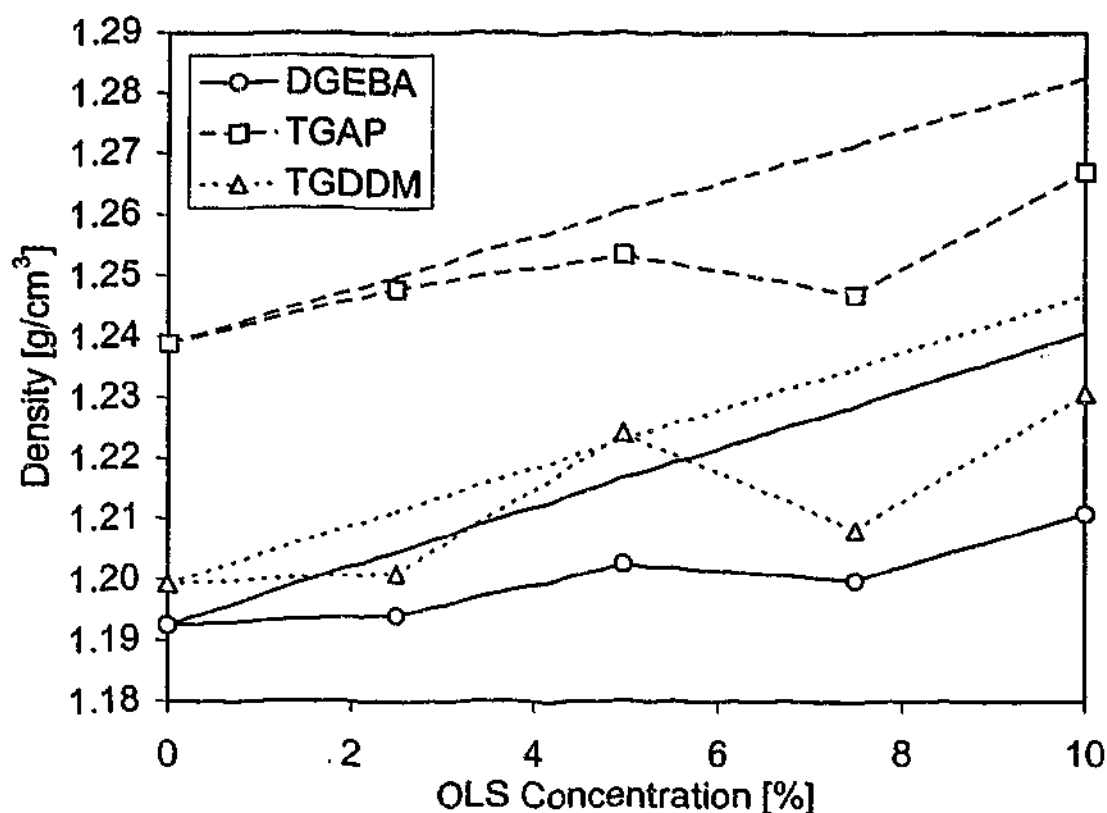
Figure 4.16: Density of postcured epoxy nanocomposites determined by gas displacement pycnometry. The straight lines represent theoretical values determined by the rule of mixtures.

4.4 Free Volume Properties

To date, there have been few studies on free volume properties of polymer layered silicate nanocomposites reported in the literature. The main work reported was a short paper by Olson et al. [143] regarding free volume in highly filled polystyrene nanocomposites as a function of temperature, investigated using positron annihilation lifetime spectroscopy (PALS). In brief, it was found that τ_3 of the organically modified layered silicate showed an increase with increasing temperature, with τ_3 versus temperature traces showing a plateau at 90 °C. The I_3 values remained relatively constant over the temperature range. Both values, τ_3 and I_3, in the nanocomposite formed by 75 % layered silicate and 25 % polystyrene were found to be very close to those of the neat silicate, which was the majority component.

This work investigates the effect of the organoclay on free volume and molecular packing of unfilled epoxy resins and nanocomposites containing 7.5 % organoclay cured at 100 °C and 160 °C, respectively. Figure 4.17 and Figure 4.18 show τ_3, the o-positronium lifetime - an indication for the average free volume size, and I_3, a measure of the number concentration of free volume sites of the neat resins and the nanocomposite systems cured at 100 °C and 160 °C. Only a small difference in the lifetime data of the various resins systems of different structures and functionalities was observed. The τ_3 values were greatest (representing greatest average free volume size) for DGEBA, followed by TGDDM and TGAP with only slightly lower values. This variation is likely due to variations in molecular weight between crosslinks (low for TGAP) and functionality (high for TGDDM). However, of all the three systems, only the DGEBA τ_3 values are noticeably affected by the cure temperature, with a slight increase for higher temperatures. In contrast, the number of free volume sites varied more strongly with cure temperature for all systems, with all I_3 values being greater for the neat systems cured at 160 °C. The fact that the average free volume size does not change significantly between the two different curing temperatures is in good agreement with the PALS studies on various unfilled resin systems (including DGEBA, TGAP and TGDDM) reported by Jeffrey and Pethrick [144]. In their free volume studies on chemically different cured resin systems, it was found for a DDS-cured DGEBA resin that changes in the cure temperature did not lead to significant variation of the mean volume size. In contrast to the work presented here, they found that the number of free volume sites was reduced with increasing initial cure temperature, proposed to be related to densification of the resin, consistent with an increased T_g and reduced free volume for higher cure temperatures. In the same work, comparison between DGEBA, TGAP and TGDDM systems cured with DDM or DDS, respectively, has shown a significantly lower number of free volume sites for TGAP compared to DGEBA and TGDDM, which is also not the case in this thesis. However, the work by Jeffery and Pethrick did show a strong effect of the nature of the hardener on free volume properties.
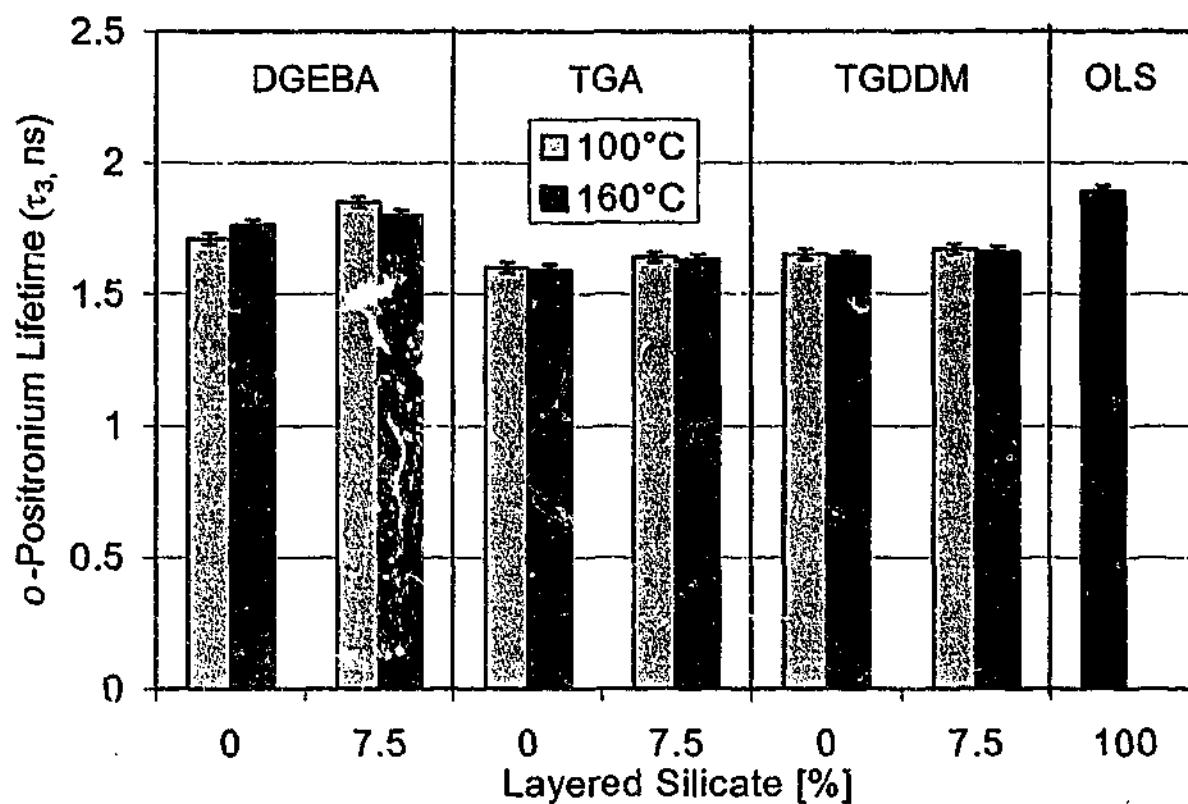
Figure 4.17: o-Positronium lifetime, τ_3 (ns) related to the average free volume size of various epoxy and epoxy nanocomposite systems.
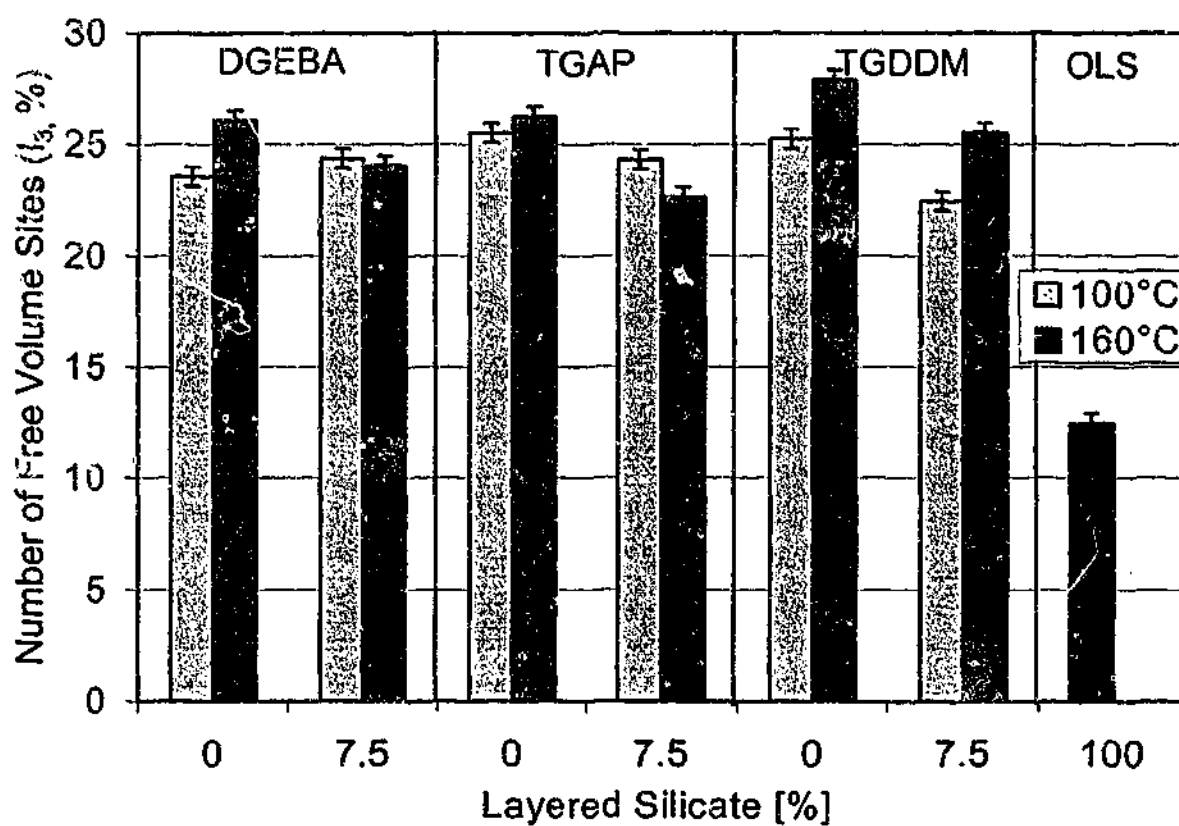
Figure 4.18: Number concentration of free volume sites (I_3) of various epoxy and epoxy layered silicate systems.

Hence it is reasonable that the different structure of the diethyltoluene diamine curing agent used here may show different molecular packing than the materials used by Jeffery and Pethrick, both in an absolute and comparative sense.

Assuming that the free volume sites are of a spherical shape, it is possible to estimate the magnitude of the free volume radius from the semi-empirical equation [145]:

$$\tau_3 = \left[1 - \frac{R}{R_0} + \frac{1}{2\pi}\sin\left(\frac{2\pi R}{R_0}\right)\right]^{-1} \qquad \textit{Equation 21}$$

with τ_3 being the o-Positronium lifetime (ns), R the radius (Å) and $R_0 = R + \Delta R$ where ΔR is the fitted empirical electron layer and equals 1.66 Å. Based on this equation the free volume diameter in the layered silicate has been calculated as 5.5 Å, to be compared with an average distance of 14.2 Å between the surfaces of the two clay platelets (d-spacing minus the layer thickness of 9.6 Å). Although the PALS free volume radius is of the order of the space between layers, its difference may be due to the fact that the free volume is confined in layers, rather than spherical holes. It has been found in zeolites and other inorganic molecular solids that the size as determined by Equation 21 and by other more direct methods, is quite close [145]. The neat organoclay on its own has a larger average free volume size than the resin systems, and thus according to the rule-of-mixtures, all materials containing organoclay may be expected to have a larger free volume size than the corresponding neat systems, which was found to be the case. By contrast, the DGEBA nanocomposite, particularly that cured at 100 °C, showed a greater value of average free volume size than expected by addition. The number of free volume sites (I_3) of the organoclay alone is much lower than the values of cured epoxy resins and most combined epoxy-clay systems showed a concentration slightly above the rule of mixtures with addition of clay. However, once again in opposition to this trend, the DGEBA

nanocomposite cured at 100 °C was the only material that actually showed an increase in free volume site concentration with filler addition. In every other system, I_3 decreases with the filler addition as would be expected from the rule of mixtures.

The combination of τ_3 and I_3 behaviour combines to yield a synergistically greater total free volume fraction of DGEBA 7.5 % at 100 °C, than neat DGEBA, as seen by total free volume fraction data, indicated by $\tau_3{}^3 \cdot I_3$ in Figure 4.19.
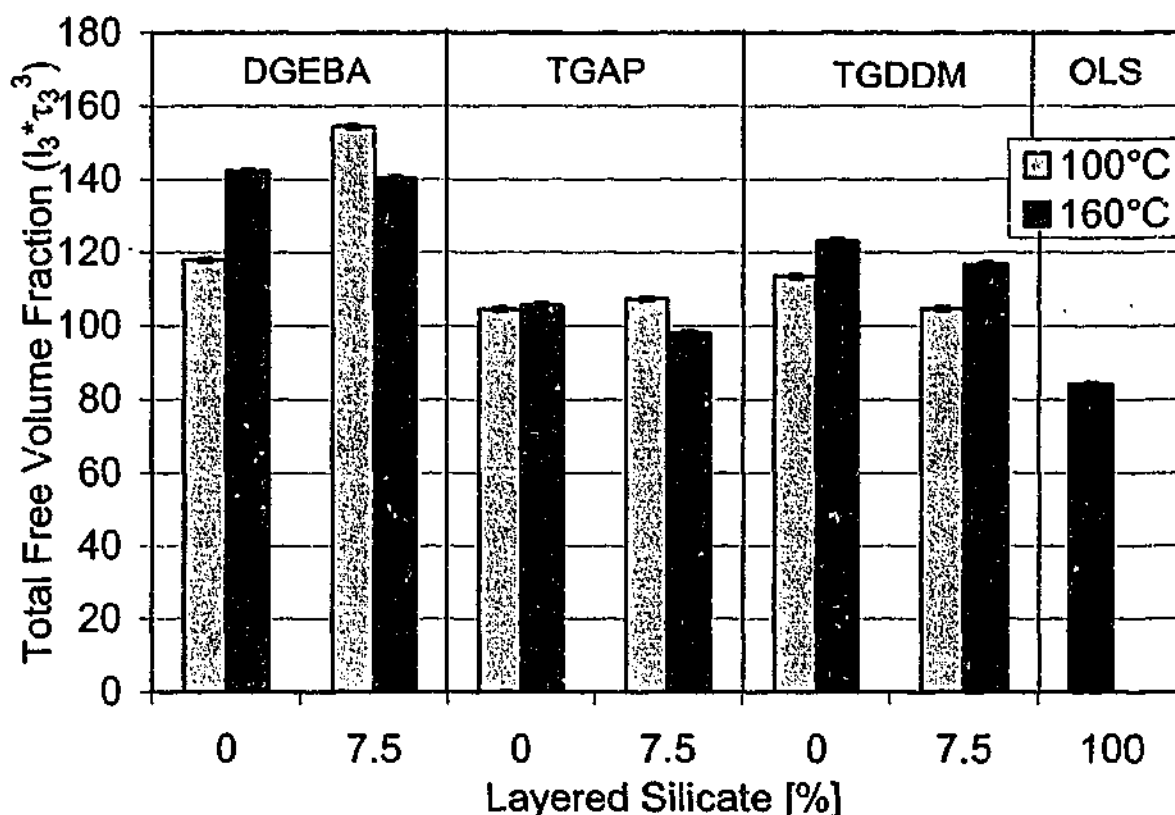
Figure 4.19: $\tau_3{}^3 I_3$, indicative of total free volume fraction of various epoxy- and epoxy-layered silicate systems.

This is consistent with the observed lower T_g and reduced degree of crosslink density postulated for epoxy-clay systems by Chen et al. [65]. DGEBA would be expected to show such effects due to the presence of interface and disruption to crosslink density given it contains the best dispersed layers (although, as discussed above, tactoids still remain alongside delaminated layers).

However, this is confounded by the fact that DGEBA at 160 °C, seemingly slightly better dispersed according to TEM, shows the opposite trend - a

decrease in total free volume with clay addition. TGAP shows little change at either cure temperature and TGDDM at both cure temperatures shows an increase with clay, as for DGEBA 100 °C. It is thus likely that changes in molecular architecture due to the temperature of cure and degree of exfoliation make a simple interpretation of the PALS results difficult. Even considering the difference between neat epoxy and in a binary mixture with clay, the results seem very system dependent. Although all nanocomposites show a lower glass transition with clay addition cured at 100 °C, for example, there is differing behaviour in total free volume fraction as judged by $\tau_3{}^3 \cdot I_3$, with DGEBA decreasing, TGAP remains the same and TGDDM increasing with addition of clay, with the densities showing a negative deviation from the rule of mixtures in almost all cases.

Chapter 5
Thermal Relaxations and Stability

In this chapter, the effect of the organoclay concentration on the thermal relaxations, such as the glass transition temperature and the β-transition, is investigated using dynamic mechanical thermal analysis.

The environmental stability, such as water uptake properties and thermal stability is also investigated. A comparison of DMTA measurements before and after water sorption gives some indication of the effect of the sorbed water on the viscoelastic properties of the nanocomposite materials.

5.1   Dynamic Mechanical Thermal Analysis

Dynamic mechanical thermal analysis was applied in two steps from -100 to 50 °C and from 50 to 300 °C to investigate the influence of the organoclay on the α- and β-relaxation peak temperature. It is likely that these motions can be affected through the organoclay by being influenced by the high surface area of the silicate and its attached octadecyl amine ions. Indeed, Beall [146] claims that in thermoplastic materials, for a concentration of 5 % exfoliated layered silicate, some 50 % of the polymer chains are affected by the organoclay surface.

The α-relaxation is related to the Brownian motion of the main-chains at the transition from the glassy to the rubbery state and the relaxation of dipoles associated with it. The β-transition occurs at significantly lower temperatures and has been widely reported to be related to the crankshaft rotation of the hydroxy ether segments ($-CH_2-CH(OH)-CH_2-O-$) of the crosslinked epoxy network in the glassy state [147, 148]. When a polymer goes through one of

these relaxations, tan δ, the ratio lost to energy stored, shows a maximum and provides a very sensitive means of analysing the α- and β-relaxations.

5.1.1 Glass Transition Temperature

Typical DMTA traces of tan δ as a function of temperature are shown for the TGDDM/DETDA/organoclay system for different organoclay concentrations measured at 1 Hz in Figure 5.1. The traces in the range of 100 - 300 °C represent the relaxation peaks associated with the glass transition temperature.
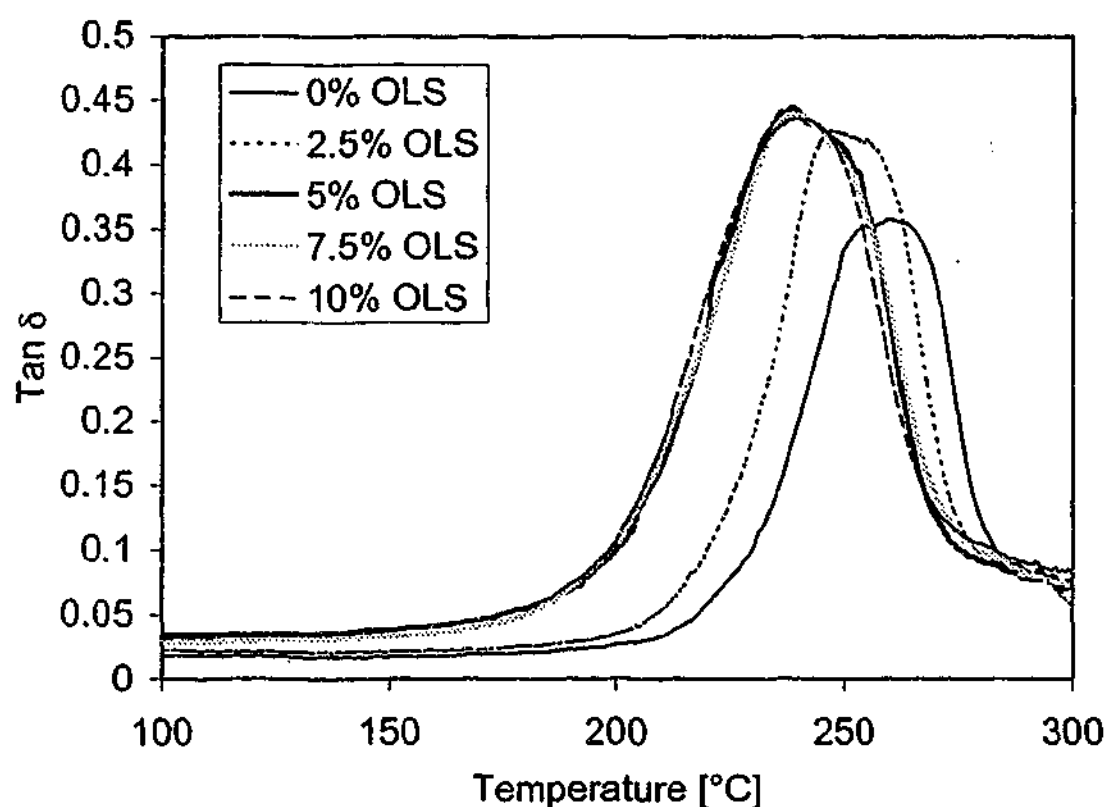
Figure 5.1: Typical DMTA spectrum of TGDDM based nanocomposites cured at 100°C, measurements are taken at 1Hz.

Plots of the glass transition temperature (T_g) as a function of organoclay concentration are shown in Figure 5.2 for the different nanocomposite series cured at 100°C. The value of T_g decreased steadily with increasing organoclay concentrations.
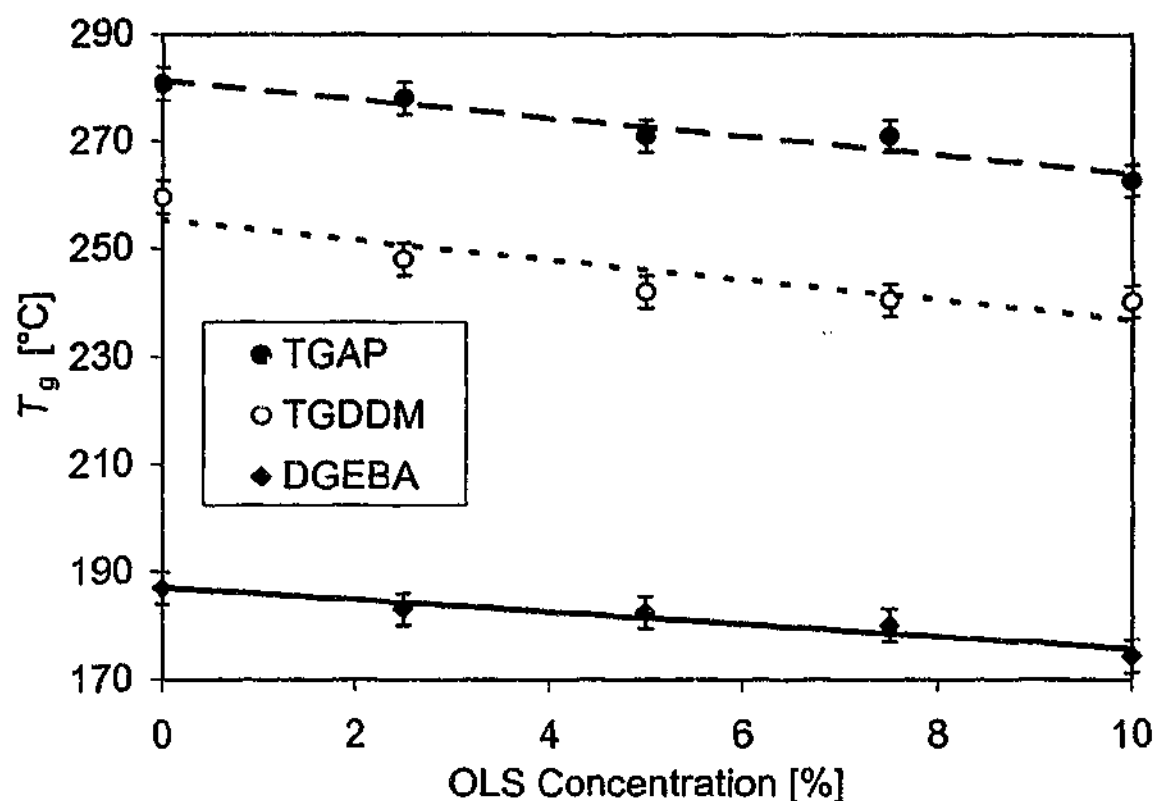
Figure 5.2: Glass transition temperatures as determined from the tan δ peak of DMTA measurements.

The reduction in T_g was found to be in the order of 15 °C for the TGAP and DGEBA based system and 20 °C for the TGDDM based system at an organoclay content of 10 %.

The glass transition temperatures of DGEBA-based epoxy nanocomposites systems have been investigated previously [31, 149, 64, 71, 73, 76, 89, 91, 96]. Whilst increased glass transition temperatures were reported in some cases of intercalated nanocomposite systems [64, 73, 76, 91, 96], others have found a constant [149] or slightly decreased [71] T_g. Zilg et al. [31, 73] have found that effectively intercalated epoxy systems significantly decrease the T_gs of the final resin system. Since it is a decrease this indicates that it is not an 'adsorbed layer' effect, which usually increases the glass transition temperature due to chains being tied down by the surface of the silicate. It was found by Giannelis [150] that the T_g of intercalated polymers as characterized by solid state NMR, show a reduced value of glass transition due to the lack of surrounding entanglements, indicating that molecular mobility is enhanced. However, since

this system is rather more complex, with a range of chemistries possible, it is much more difficult to identify reasons for the decrease in T_g. The organoclay may change the chemistry of the reaction, as has been shown earlier and indeed the organo-ions themselves may catalyse homopolymerization. This is unlikely to lead to the high crosslink densities due to the epoxy-amine reaction. In addition plasticising due to unreacted resin and a general lower crosslink density are reasons that could explain a decrease in T_g. It was assumed that the T_g was reduced due to a combination of factors such as changes in reaction chemistry (epoxy homopolymerization and reduced crosslink density), thermal degradation of the surface modifier (Hoffmann elimination of the ammonium ion) or a plasticising effect of unreacted resin-, hardener- or modifier- monomers. The complexity of the systems does not allow a precise determination of the governing factors that cause the decreased glass transition temperature.

The broadness of the α-relaxation peak of 100 °C series was determined at the half height of the peak and is shown in Figure 5.3.
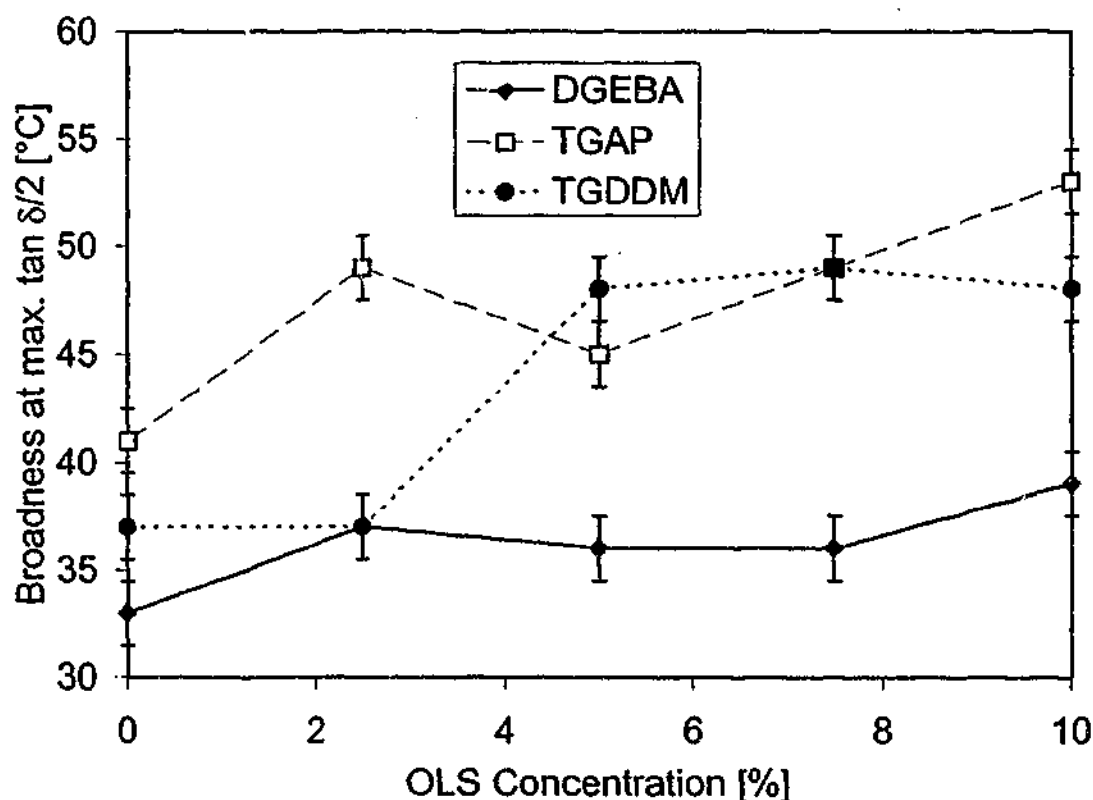
Figure 5.3: Tan δ broadness at half peak height as a function of nanocomposite composition for various composites cured at 100 °C.

Traces of the unfilled systems are generally less broad than those of the organoclay containing epoxy resins. Although the results show some scatter, traces follow a general trend of increasing tan δ peak broadness with increasing clay concentration. The broadening of the α-relaxation might be related to restrained chain mobility that usually occurs in compatible blends, making some chain mobility more difficult and some less, leading to a wider range of different environments and thus spanning a wider temperature range [151]. It can be assumed that molecules that are located close to or even tethered to the silicate show a different mobility than those molecules that are fully embedded in an epoxy environment, and that the concentration of epoxy molecules associated with the clay layers is actually quite high.

5.1.2　β-Relaxation

Figure 5.4 to Figure 5.6 show subambient DMTA traces of the DGEBA, TGAP and TGDDM nanocomposite series determined at a frequency of 1 Hz. Values of the β-relaxation peak temperatures as a function of organoclay concentration are illustrated in Figure 5.7. Similar to the glass transition temperature, the location of the β-relaxation peak for each nanocomposite system decreases steadily with increasing organoclay content. The decrease in the β–transition temperature is consistent although less significant than the reduction in the glass transition peak. The β-relaxation peaks are decreased by some 5 - 7 °C through the addition of 10 % organoclay. Since the peaks are generally very broad and weak with regards to intensity, variations in the peak broadness are more difficult to determine.

The TGDDM- and TGAP-based systems do not exhibit significant changes in the β-relaxation broadening over the different organoclay concentrations. The DGEBA based nanocomposites however show notable broadening at organoclay concentrations of 7.5 % and 10 %, as illustrated Figure 5.4.
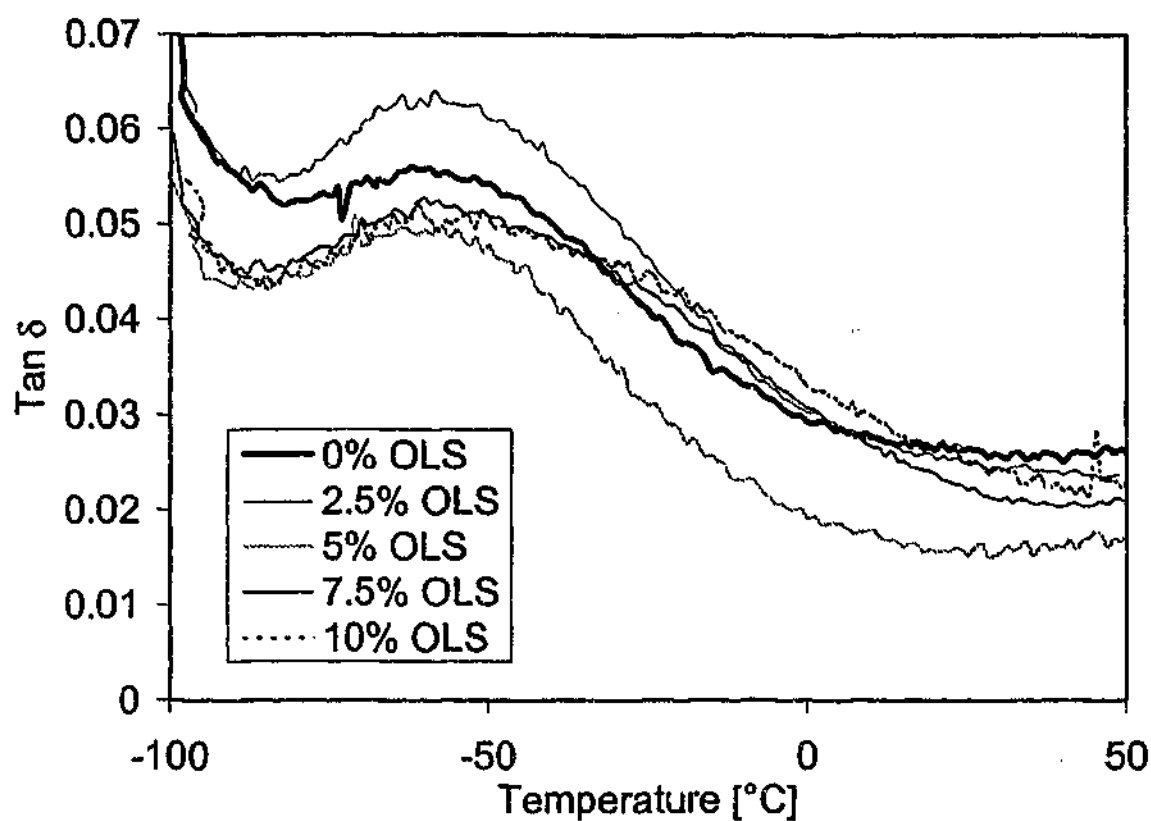
Figure 5.4: Subambient DMTA spectra of DGEBA nanocomposites of different OLS concentrations, determined at a frequency of 1 Hz.
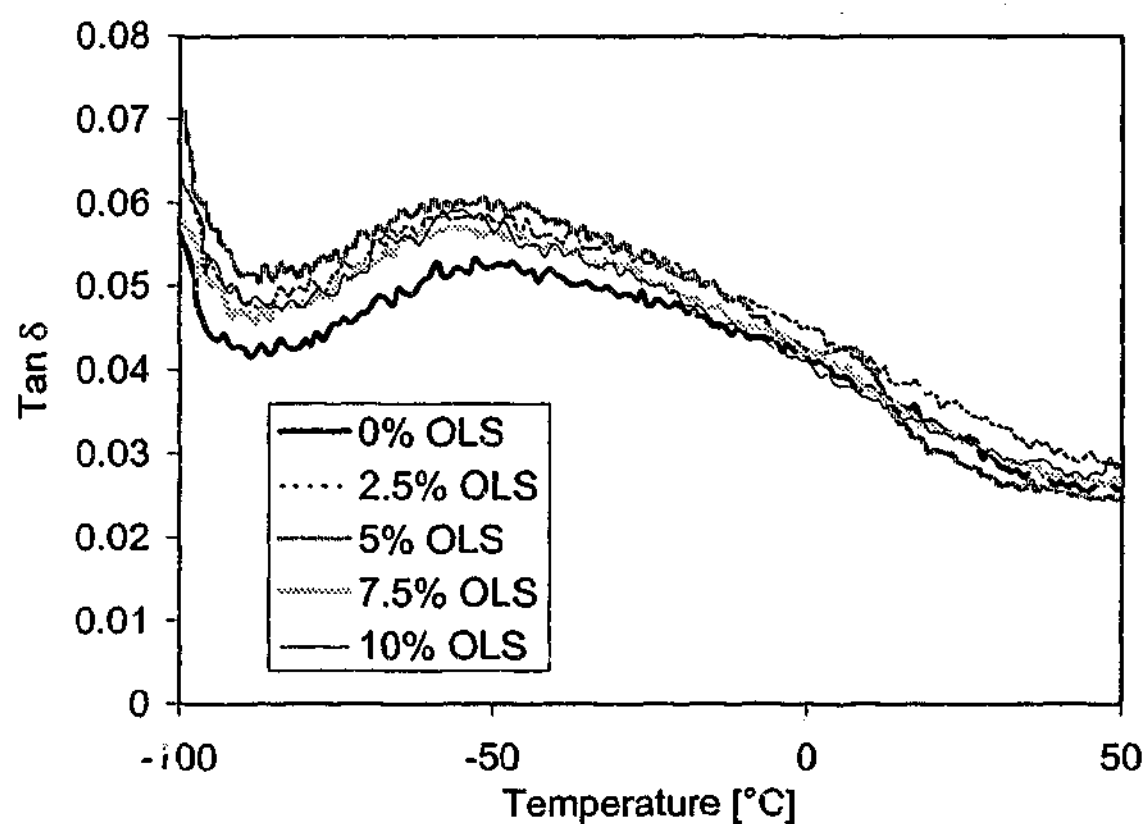
Figure 5.5: Subambient DMTA spectra of TGAP nanocomposites of different organoclay concentrations, determined at a frequency of 1 Hz.
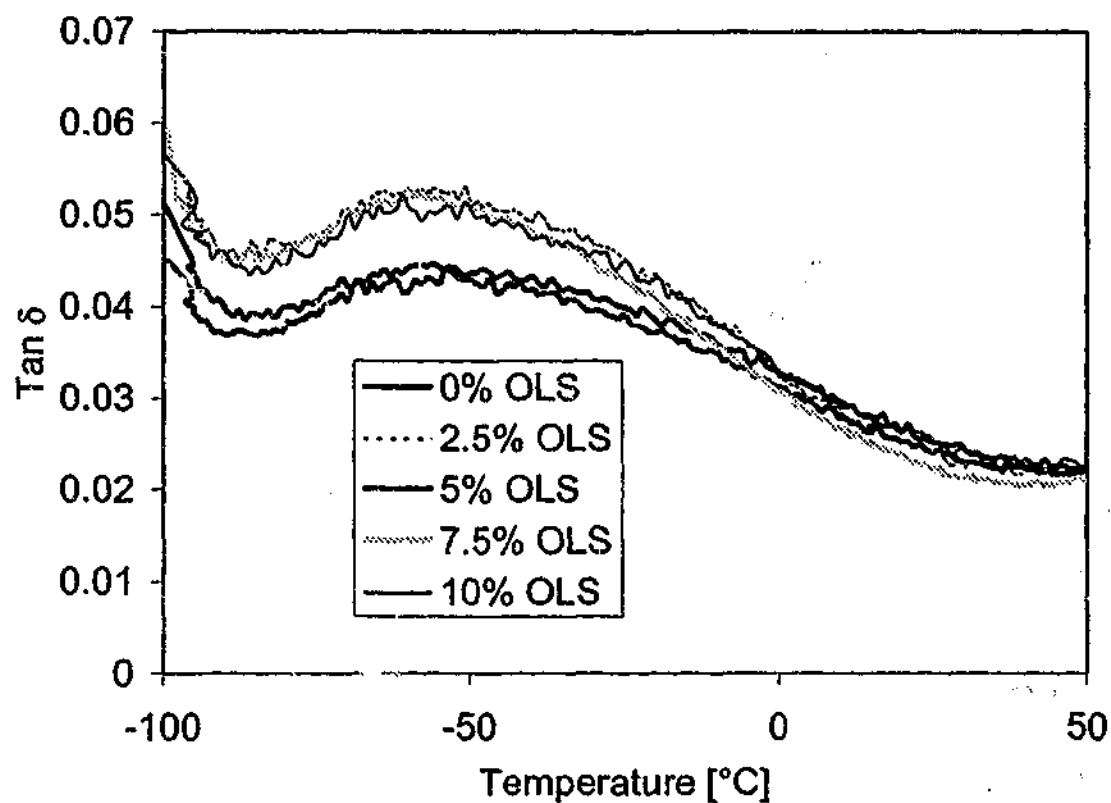
Figure 5.6: Subambient DMTA spectra of TGDDM nanocomposites of different organoclay concentrations, determined at a frequency of 1 Hz.
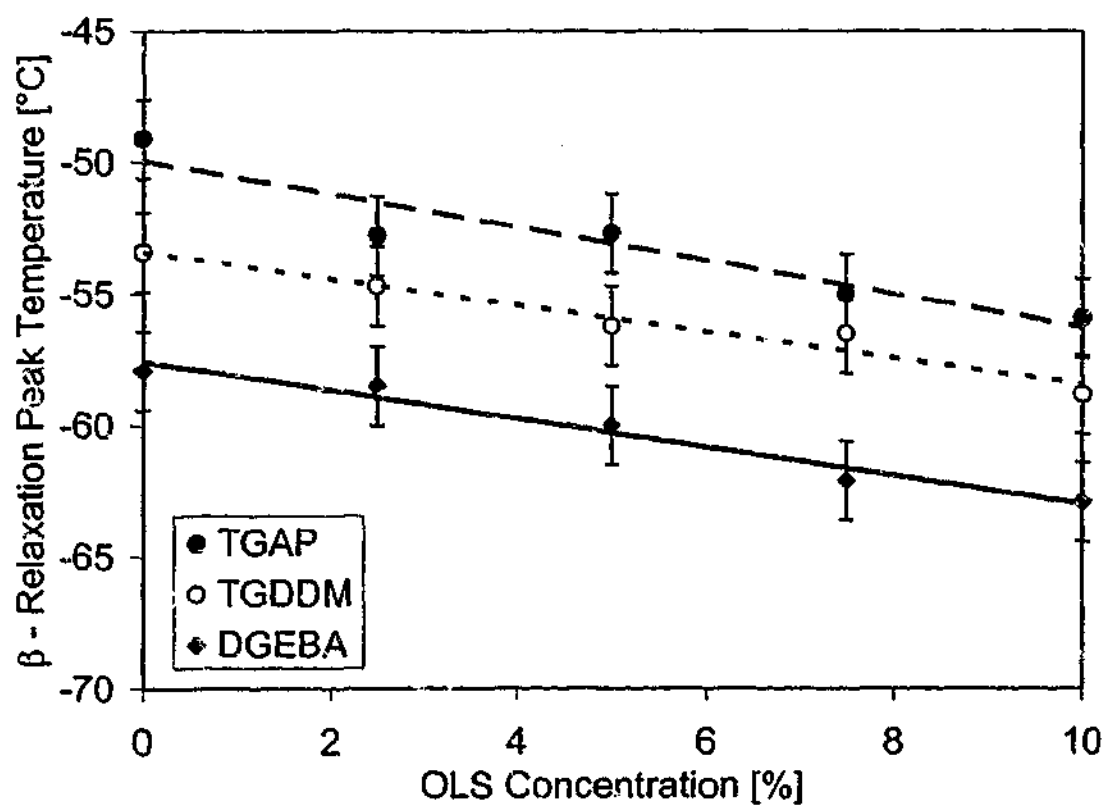
Figure 5.7: β-relaxation peak temperatures as determined from subambient DMTA measurements.

Previous work by the group of Monnerie and Halary [148, 152-155] has focused on the secondary relaxation of epoxy resin systems. It was reported that an increase in crosslink density (as varied by combining with different hardeners of different functionalities) increases the peak height and broadening of the secondary relaxation whilst changes in chain flexibility showed little effect on the viscoelastic response [152]. Imaz et al. [156] have studied the β-transition of a TGDDM based system as a function of crosslink density. In contrast to the work of Monnerie and Halary, an increase in the peak temperature was found with increasing crosslink density. In our systems it appears that incorporation of clay leads to a decrease in both the glass transition- and the secondary relaxation temperature, possibly due to a decrease in effective crosslink density. The fact that the presence of organoclay influences the β-relaxation which involves mobility in the glassy state may indicate the change is significant and that - as previous studies quoted above have shown - the β-relaxation does involve a degree of cooperative motion, rather than only very localized mobility.

5.2　　　Water Sorption Properties

The water uptake of neat epoxy resin systems [157-163] or epoxy-based fibre composites [164, 165] has been widely discussed and is known to have significant effects on the overall properties of the epoxy material. The water molecules can generally be found in two different environments in the polymer matrix: the water is either strongly interacting with specific (polar) groups of the epoxy matrix or clustered together in free volume micro-voids as "free water". The water sorption behaviour is thought to depend both on free volume properties and type and concentration of polar groups in the epoxy system.

The diffusion rate and equilibrium water uptake is markedly affected by the nature of the thermosetting network. Grave et al. [157] showed that the stoichiometric ratio between epoxy resin and hardener significantly determines the water sorption behaviour. In this work it was found that increased amine ratios led to both increased diffusion coefficients and increased equilibrium

water uptake. Early work by Moy and Karasz [166] examined the diffusion of water and the equilibrium water uptake of a high T_g (TGDDM/DDS) resin system. This work reported a plasticising effect by the water due to strong interactions between the water molecules and specific segments of the polymer.

Whilst the effect of water sorption is reversible to a certain extent, the combination of elevated temperatures and absorbed water may also lead to irreversible degradation, which is a particular concern in high performance applications. The major draw back of water sorption that is often reported [158-160, 163] is its plasticising effect, leading to a reduced glass transition temperature, decreased modulus and compressive strengths, chain scission and hardener degradation, as well as possible detachment of the resin from the fibre in composite materials [164, 165].

In the series of experiments presented here, the water uptake properties of nanocomposite materials synthesised on the 100 °C cure cycle were investigated at a water temperature of 80 °C. Figure 5.8 shows an example of the water sorption curve as a function of time, for the series of TGAP based nanocomposites. Equilibrium water sorption values for all systems are shown in Table 5.1. It can be seen that the DGEBA-based systems generally absorb less water than the two resin systems of higher functionality, with values for the TGDDM based materials being below those of TGAP. The equilibrium values show that the neat epoxy systems generally absorb more water than the layered silicate composite materials. A monotonic decrease in equilibrium water sorption with increasing clay concentration, however, was not observed. This could be due to the fact that the water uptake depends on the total surface area exposed to the water molecules [95], where the degree of layer separation or the ratio intercalated/delaminated silicate layers is determined by the organoclay concentration.

Water sorption behaviour is often related to the free volume of a material [157, 159]. The free volume properties of selected materials of this range of nanocomposites have been investigated by PALS in section 4.4. It was found that the DGEBA based materials showed the highest overall free volume.
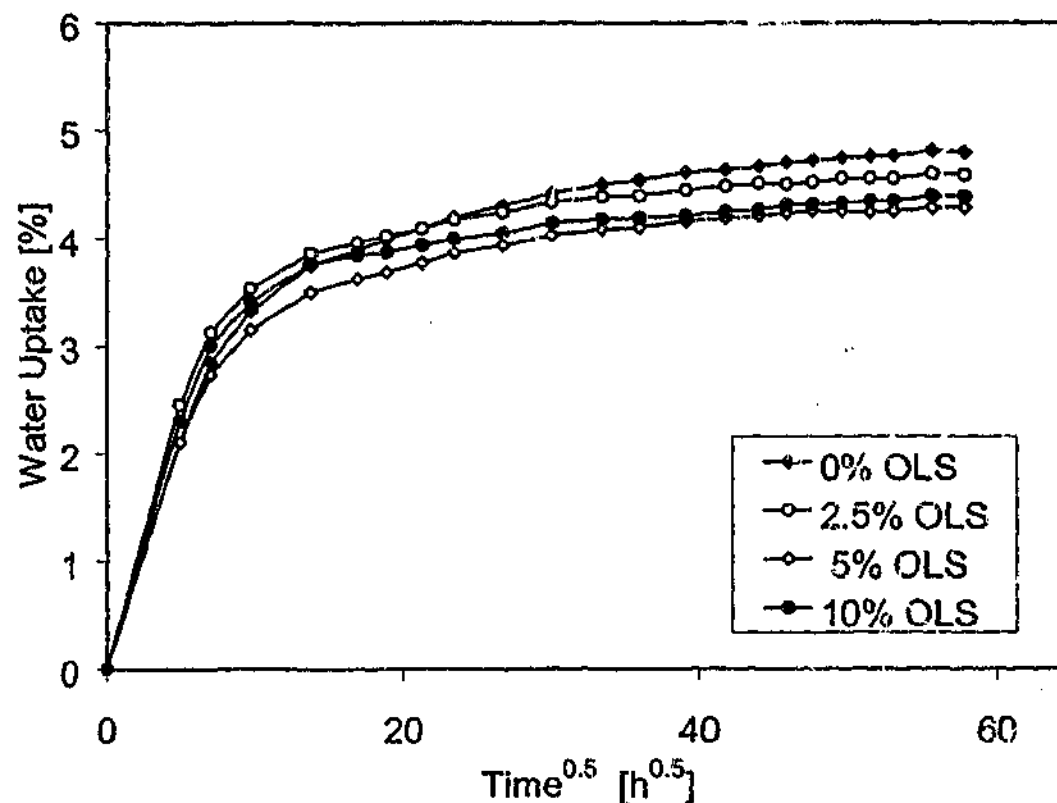
Figure 5.8: Water sorption curve of a series of TGAP based nanocomposites containing different concentrations of OLS.

Furthermore, the differences in free volume properties between the resin systems were not significant. Therefore, it is assumed that the variation in equilibrium water uptake is to a greater extent related to either the differences in polarity of the polymers or to the free volume that is of a scale (greater than angstrom-size) that is not detected using the technique of PALS. Hence, differences in the amount of bond water or free water trapped in voids of the micron sized order would cause the differences in equilibrium water uptake.

The effect of nano-sized free volume as determined by PALS on water sorption of epoxy resins has been investigated previously. Johncock and Tudgey [159] showed an interesting correlation between free volume, glass transition temperature and equilibrium water uptake. In their work a linear relationship between the equilibrium water uptake and T_g was reported. Furthermore, the free volume was considered to be a function of the glass transition temperature. Soles et al. [167] also reported a correlation between equilibrium water uptake and absolute zero hole volume fraction of epoxy resins. The group of Pethrick et

al. [161] showed that a higher concentration of micro-voids (as a result of higher cure temperatures) led to higher concentrations of free water and hence a higher equilibrium water uptake.

In general, the diffusion behaviour of water into epoxy systems has shown to be in good agreement with Fick's second law of diffusion [157, 158]. For the one-dimensional diffusion through an infinite plate Fick's second law of diffusion is commonly expressed as:

$$\frac{\partial C}{\partial t} = D \frac{\partial^2 C}{\partial x^2} \qquad \text{Equation 22}$$

with C being the concentration of the diffusing substance (water), t the time, D the diffusion coefficient and x the length. It was further shown by Crank [168] that this correlation can be simplified for the initial stage of water absorption with $\frac{M_t}{M_\infty} \leq 0.6$ as shown in equation 23:

$$\frac{M_t}{M_\infty} = \frac{4}{L\sqrt{\pi}} \sqrt{D\,t} \qquad \text{Equation 23}$$

with M_t being the amount of water diffused into the polymeric material and M_∞ the amount of water absorbed at equilibrium or infinite time. Data from the first few measurements of experimental series have been fitted to this equation and the diffusion coefficient determined. Results for the diffusion coefficient, D, are also listed in Table 5.1. The order of magnitude of the diffusion coefficients are in good agreement with values reported for other epoxy resin systems [157, 159]. However, a general trend of increasing or decreasing diffusivity with increasing organoclay concentration cannot be found (Table 5.1).

The plasticising effect of the absorbed water was investigated by comparison of the α- and β-relaxation peak before and after water sorption. Dynamic Mechanical Thermal Analysis (DMTA) measurements were performed on each sample after 3670 h storage in distilled water at 80 °C. Measurements were taken in two steps from -100 °C to 50 °C and from 50 °C to 300 °C and compared with the initial dry materials as investigated in section Chapter 5.

Figure 5.9 shows the tan δ traces of dry and wet TGAP resin system as well as the TGAP nanocomposite containing 10 % organoclay as an example. Table 5.1 summarizes the α- and β-relaxation peak temperatures for the wet and dry nanocomposites as well as the width of the α-relaxation peak at half peak height. The effect of the layered silicate on the thermal relaxation of the dry specimens has been the subject of previous discussions in this chapter and will not be further considered. Comparison of the α-relaxation traces between wet and dry samples show that the absorbed water decreases the T_g significantly, along with increased broadening of the peak width due to the range of states of water that exists in the glassy state. It can be found that the amount of water absorbed is not in direct correlation with the decrease in T_g. As shown in Figure 5.9, the wet samples of higher functionality epoxy resins show a shoulder or even a second peak towards lower temperatures. The occurrence of this additional relaxation is indicative of the coexistence of different environments within the sample, such as an additional plasticised phase that contains the sorbed water.

Grave et al. [157] previously reported a similar occurrence of double glass transition peaks after water sorption. In their studies on water sorption of DGEBA cured with stoichiometric variations of triethylenetetramine, it was found that no significant change in the main T_g peak occurred due to water sorbed. However, after water sorption, formation of a second T_g peak at lower temperatures could be observed, with increased peak intensity for higher hardener ratios. It was theorized that no gross plasticisation occurred, whilst network inhomogenities, probably containing higher concentrations of hydroxyl groups, may plasticise particular regions of the material.

Figure 5.10 shows the broad β-relaxation peaks of cured TGDDM and the TGDDM nanocomposite containing 10 % OLS as an example. Values of all systems can be found in Table 5.1. A reduced β-relaxation peak temperature can be found for the wet specimens, similar to the changes in T_g.

Table 5.1: Equilibrium water uptake, diffusion coefficient and α and β-transition peak temperatures of various epoxy nanocomposites as determined from DMTA measurements before and after water sorption.

Sample	Equilibrium Water Uptake [%]	Diffusion Coefficient D [10^{-8} cm^2·s^{-1}]	Relaxation Peak Temperature [°C] / Width at half Peak Height					
			Dry Specimen			Wet Specimen		
			α–Peak	α–Width	β-Peak	α-Peak	α-Width	β-Peak
DGEBA 0% OLS	2.810	4.3	187.0	33	-57.9	161.7	48.5	-65.5
DGEBA 2.5% OLS	2.425	4.7	183.1	37	-58.5	166.3	41.2	-64.4
DGEBA 5% OLS	2.405	4.9	182.5	36	-60.0	162.8	40.9	-65.4
DGEBA 10% OLS	2.659	3.8	174.3	39	-62.9	155.3	45.5	-63.8
TGAP 0% OLS	4.797	2.3	280.8	41	-49.1	236.7	45.1	-59.0
TGAP 2.5% OLS	4.597	3.7	278.1	49	-52.8	236.2	63.2	-58.5
TGAP 5% OLS	4.274	3.1	271.0	45	-52.7	244.6	52.1	-58.5
TGAP 10% OLS	4.330	3.6	262.7	53	-55.9	244.5	70.4	-54.0
TGDDM 0% OLS	3.967	2.3	259.6	37	-53.4	248.6	65.3	-62.4
TGDDM 2.5% OLS	3.746	3.0	248.1	37	-54.7	229.8	43.1	-64.5
TGDDM 5% OLS	3.732	4.1	242.0	48	-56.2	236.2	61.7	-64.4
TGDDM 10% OLS	3.778	3.1	240.2	48	-58.8	228.1	60.9	-63.5
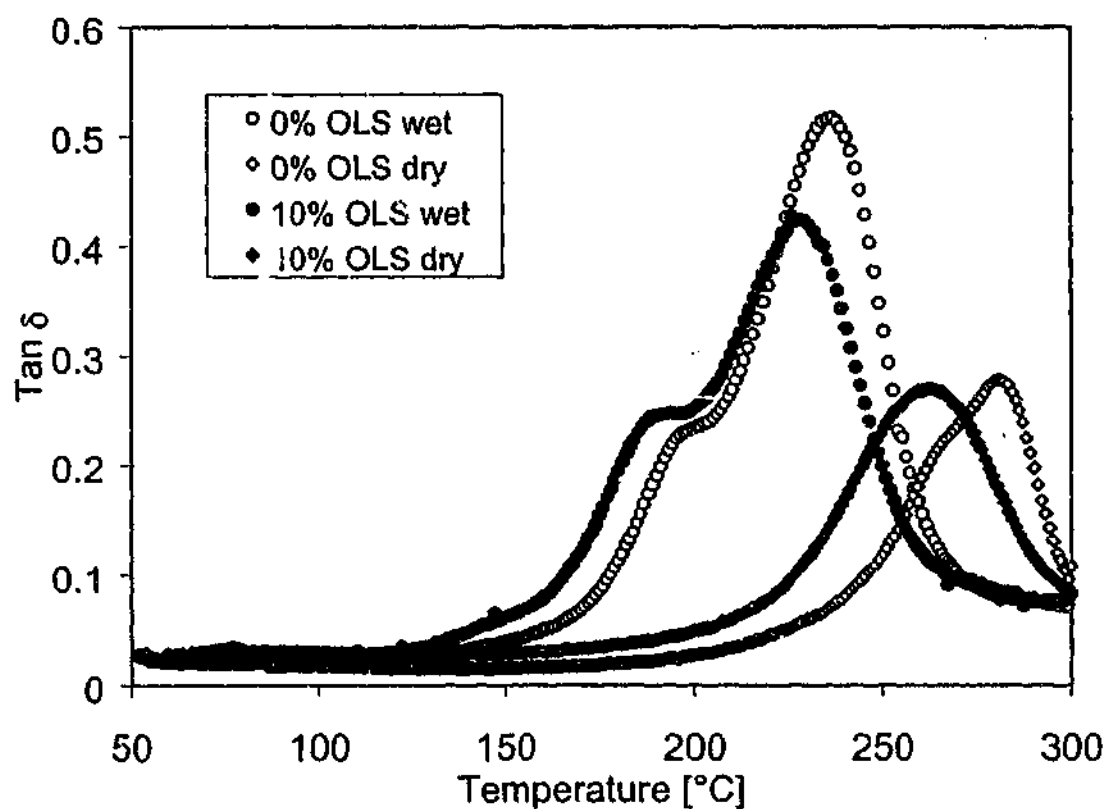
Figure 5.9: Tan δ traces of dry and wet TGAP and TGAP nanocomposites as determined from DMTA measurements at a frequency of 1 Hz.
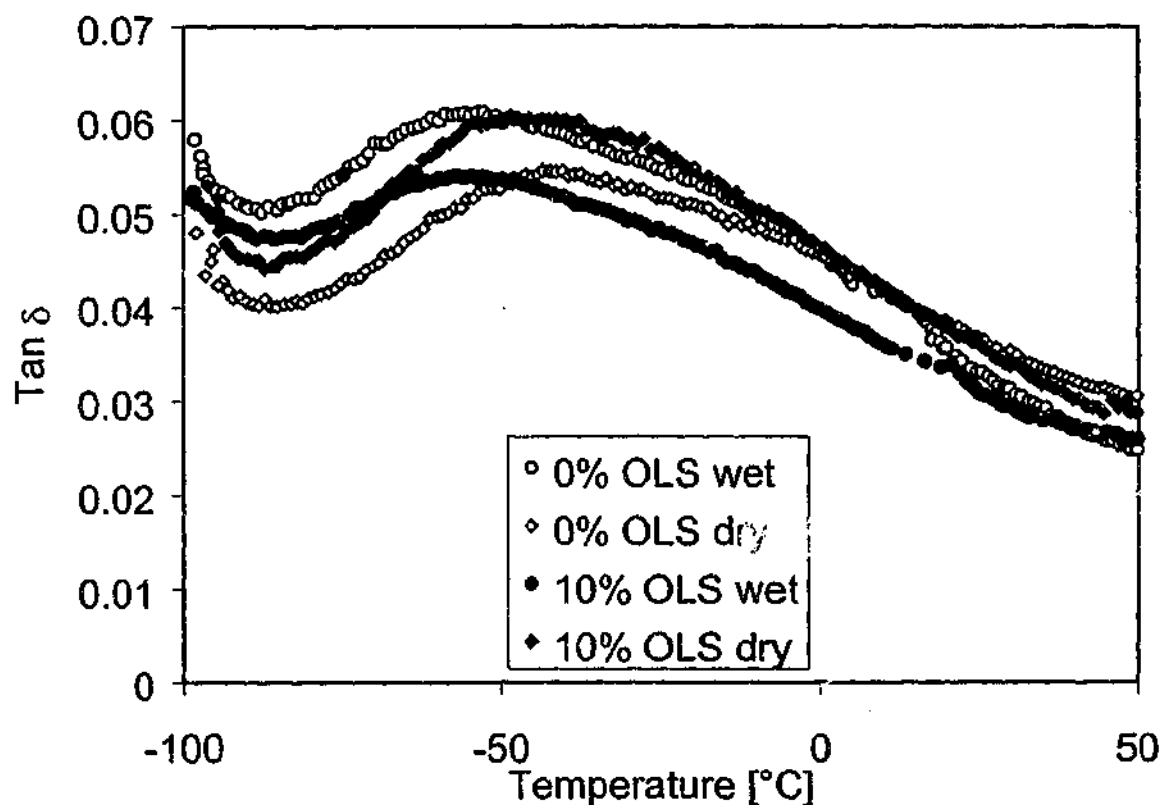
Figure 5.10: Tan δ traces of dry and wet cured TGDDM resins containing 0 and 10 % OLS as determined from DMTA in the subambient state at a frequency of 1 Hz.

5.3   *Thermal Stability*

The thermal stability of epoxy nanocomposite series cured at the 100 °C cycle was determined using thermo gravimetric analysis, TGA under a nitrogen atmosphere. Figure 5.11 shows an example of a TGA trace obtained from the neat TGDDM system and the TGDDM nanocomposite containing 10 % organically modified layered silicate. As illustrated in the figure, the onset and the end set temperature were determined from the intersection of the two tangents. Furthermore, the peak degradation temperature was determined from the first derivative of the TGA curve using the Mettler Toledo STAR[e] software. Table 5.2 shows values for the onset, the end set, the temperature interval between onset and end set (ΔTemp) as well as the degradation peak temperature (degradation peak), determined as the peak of the first derivative and the total weight loss at 700 °C.
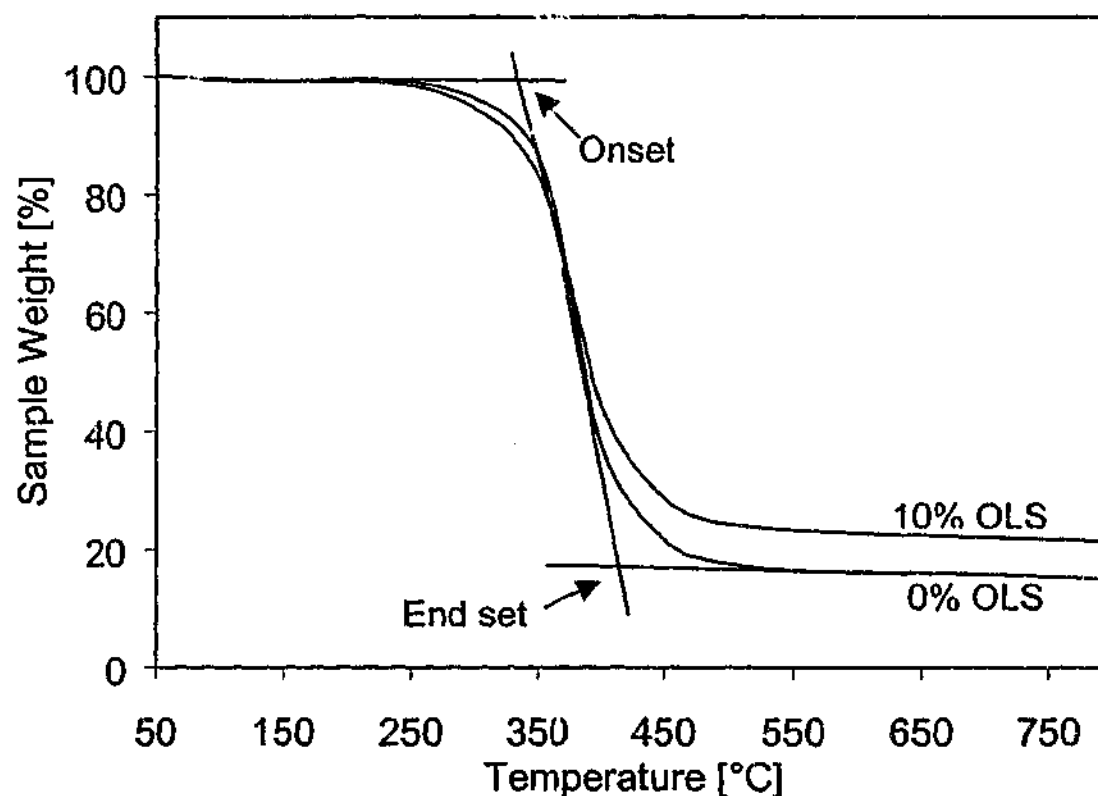
Figure 5.11: TGA of TGDDM and TGDDM nanocomposite containing 10 % OLS.

In general, a slightly decreased onset temperature can be observed with increasing organoclay concentration for the TGDDM nanocomposites. A similar trend is shown for the peak degradation temperature of the DGEBA and TGAP nanocomposite series. Values for TGDDM however only show some scatter around a value of about 378 °C rather than a constant trend of decreasing temperatures. The interval between degradation onset and end set shows a slight trend of broadening for the DGEBA and TGAP series. However, this cannot be observed for the TGDDM series and is not consistent with the reduced onset and peak degradation temperatures.

It is important to note that TGA curves of resin systems with and without organoclay generally show the same behaviour in the lower temperature regime before the onset of degradation. A separate degradation of the interlayer exchanged ions is not observed. It is assumed that the interlayer exchanged ions are well embedded or incorporated into the polymer matrix. TGA traces of the neat organoclay are shown in Figure 2.14 in the materials section, with the degradation of the compatibilizer starting at about 200 °C. This is in good agreement with the degradation behaviour observed for other exfoliated epoxy organoclay nanocomposites by Wang and Pinnavaia [74].

Xie et al. [169] recently reported a detailed investigation of the non-oxidative thermal degradation chemistry of quaternary alkylammonium modified montmorillonite. The onset of true c...anic decomposition (rather than water desorption which could be observed at lower temperatures) was found to be 180°C and the decomposition process divided into four stages: the desorption of water and other low molecular weight species (below 180 °C), the decomposition of organic substances (200 - 500 °C) the dehydroxylation of the aluminosilicate (500 - 700 °C) and the residual organic carbonaceous evolution at 700 - 1000 °C. Furthermore, the work suggested a Hoffmann elimination reaction as the mechanism of the initial thermal degradation.

Table 5.2: Thermal stability parameters of various nanocomposite systems as determined from TGA.

System	Onset [°C]	End set [°C]	Δ Temp [°C]	Degradation peak [°C]	Total wt. loss at 700°C [%]
DGEBA 0% OLS	358.3	405.5	47.2	371.6	88.0
DGEBA 2.5% OLS	357.4	403.9	46.5	369.7	88.6
DGEBA 5% OLS	351.9	402.2	50.3	368.7	85.0
DGEBA 7.5% OLS	351.4	400.7	49.3	367.7	83.4
DGEBA 10% OLS	346.7	401.5	54.8	366.7	80.7
TGAP 0% OLS	342.5	385.5	43.0	360.0	78.5
TGAP 2.5% OLS	344.7	386.9	42.2	357.4	69.0
TGAP 5% OLS	341.0	388.7	47.7	353.3	79.6
TGAP 7.5% OLS	339.0	389.0	50.0	354.3	74.0
TGAP 10% OLS	338.9	389.7	50.8	355.3	72.9
TGDDM 0% OLS	345.4	417.4	72.0	374.9	84.3
TGDDM 2.5% OLS	340.0	423.2	83.2	378.2	81.2
TGDDM 5% OLS	348.5	415.1	66.6	377.6	80.1
TGDDM 7.5% OLS	343.2	420	76.8	379.9	79.1
TGDDM 10% OLS	344.5	419.4	74.9	380.7	77.5

Chapter 6
Mechanical Properties

This chapter discusses the mechanical properties of a series of nanocomposites synthesized via two different cure cycles. The discussion centres upon the measurement of modulus and toughness, and how increasing cure temperature affects the overall cure chemistry. Near infrared measurements indicate the amount of residual cure and changes in network formation as a function of cure temperature. Variations in network formation are discussed and correlated with the mechanical properties.

Some initial work on the application of nano-structured layered silicates to supplementary toughen advanced carbon fibre composites as a ternary system is also given in this chapter.

6.1   Flexural Modulus

The typical flexural stress-strain behaviour in three point bending of a neat resin and of an epoxy nanocomposite containing 5 % layered silicate is shown in Figure 6.1 (for the TGDDM system cured at 100 °C). Traces of the other resin systems and other layered silicate concentrations look similar. The Young's moduli as determined from the three point bend test for the 100°C series of nanocomposites containing 0 - 10 % organoclay are shown in Figure 6.2. All resin systems exhibited a steady increase in modulus with increasing organoclay concentration. In order to compare the relative improvement, the normalized modulus was calculated by dividing nanocomposite modulus values by the value of the neat resin. Figure 6.3 shows the relative increase in modulus for all resin systems is in the order of 20 % for an organoclay concentration of 10 %.
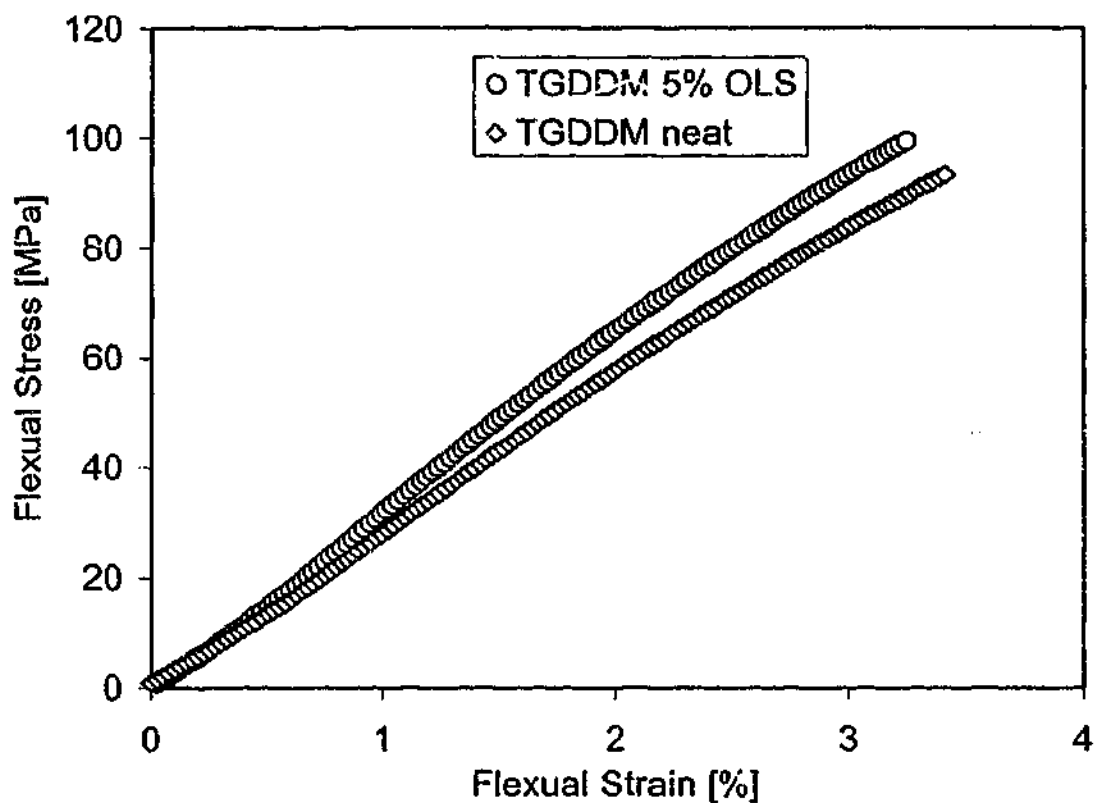
Figure 6.1: Typical stress-strain curve of neat TGDDM and a TGDDM nanocomposite containing 5 % OLS in 3 point bend.
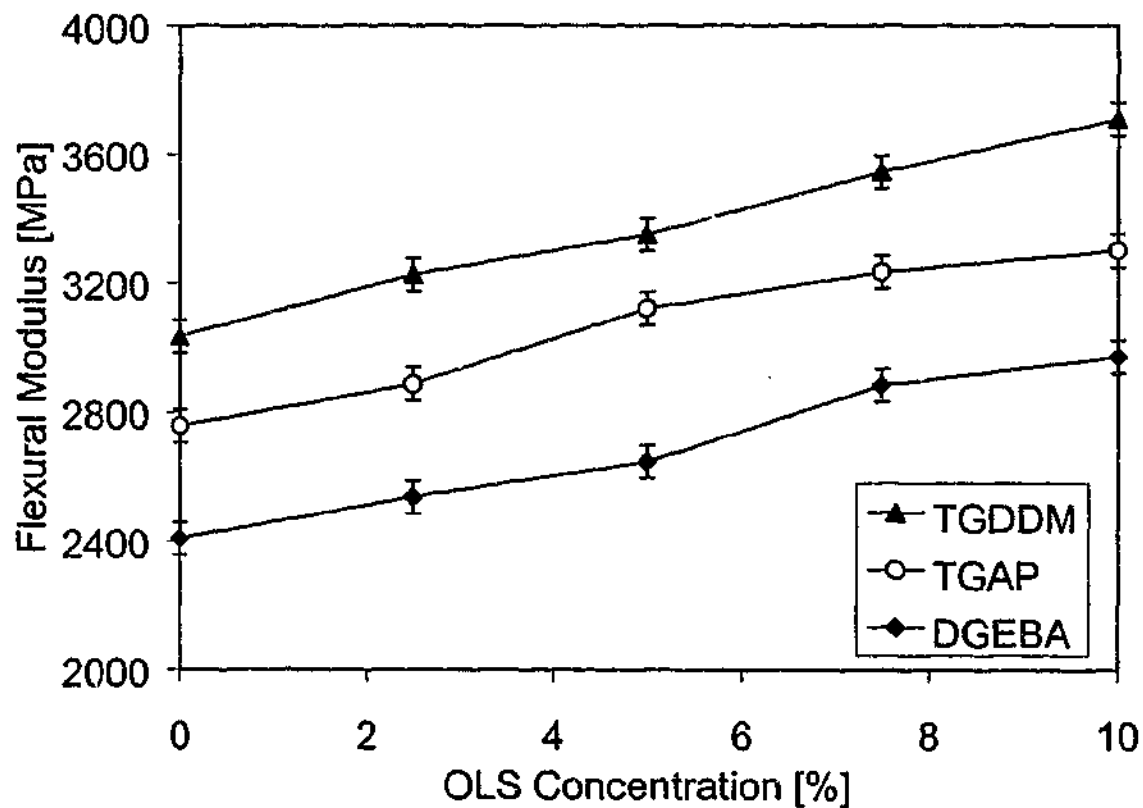
Figure 6.2: Modulus of 100 °C cure cycle series of resin systems containing 0 - 10 % OLS, determined by three point bending.
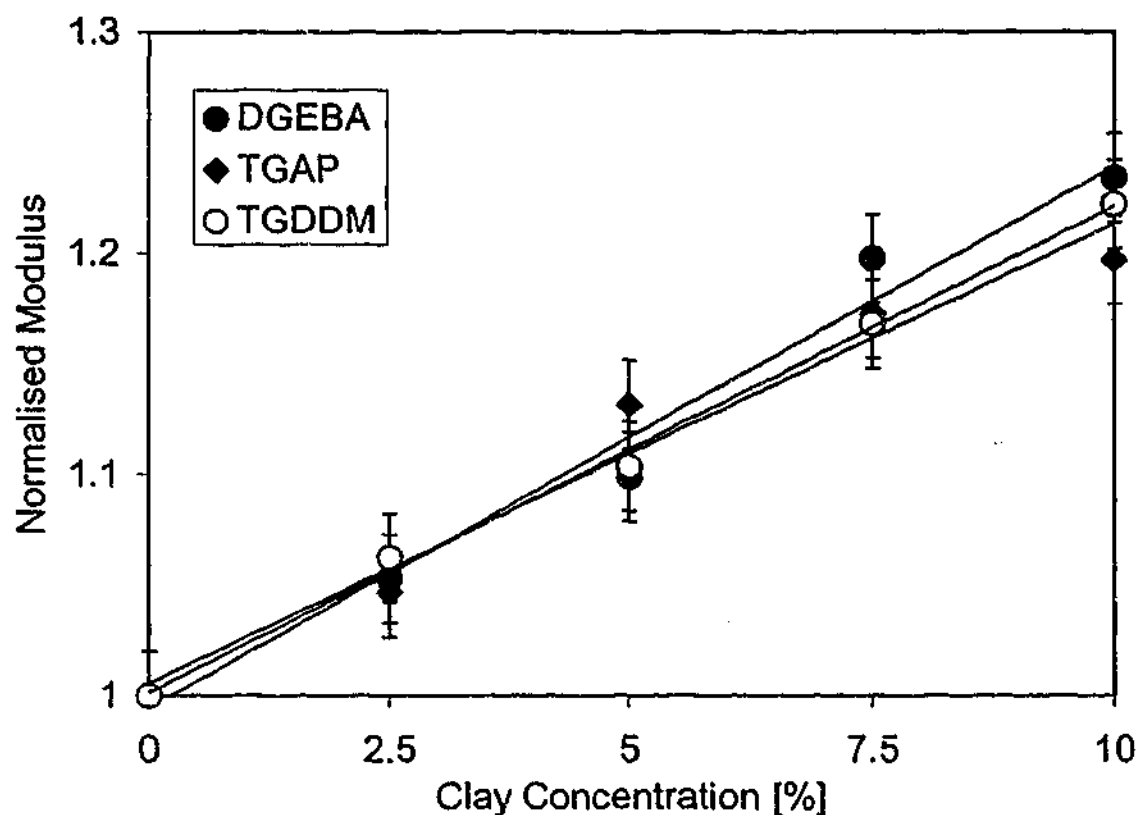
Figure 6.3: Normalised modulus of 100 °C cure cycle series of resin systems containing 0 - 10 % OLS, determined by three point bend test.

Highly flexible, rubbery epoxy systems with low glass transition temperatures have previously been reported to achieve markedly better improvements in modulus in comparison to rigid, highly crosslinked resins. For example Zilg et al. [31] reported an increase in modulus by 10 - 35 % for glassy DGEBA based (anhydride cured) nanocomposites containing 10 % OLS, compared to a more than 10-fold increase in modulus for a rubbery DGEBA/Jeffamine 2000 nanocomposite containing 15 % OLS [70].

The less crosslinked DGEBA system reported here shows only a slightly greater improvement in modulus than the more highly crosslinked TGAP or TGDDM resins. It has to be pointed out that all systems are deep into the glassy state during measurements (at room temperature).

A comparison of the modulus values of a series of nanocomposites cured at the 100 °C and 160 °C cure profile is shown in Figure 6.4 (recalling that the higher cure temperature led to improved intercalation, as shown in Table 4.1). It can be

seen that the modulus values for both temperature series follow a similar trend, i.e. improved modulus with increased organosilicate concentration. Only the DGEBA nanocomposite system containing 7.5 % layered silicate, which was cured at 160 °C did not show a further increase (within the experimental error). Whilst all systems have shown improved organoclay separation with increasing cure temperature (compare Chapter 4), there is no evidence of a direct correlation in improvement in mechanical properties with increasing basal spacing of the clay. Both, neat and nanocomposite systems based on the DGEBA and TGAP resin showed improved stiffness after cure at the higher temperature profile compared to the 100 °C series. The fact that even the neat system increases stiffness indicates that the increased cure temperature also changes network formation. The TGDDM based nanocomposites in contrast, only showed some scatter between increased and decreased modulus with increasing cure temperature, in spite of an increased d-spacing. This indicates that increased cure temperatures not only change the arrangement of the silicate platelets in the polymer matrix, but also have a significant effect on the cure reaction chemistry, as will be discussed later in this chapter.
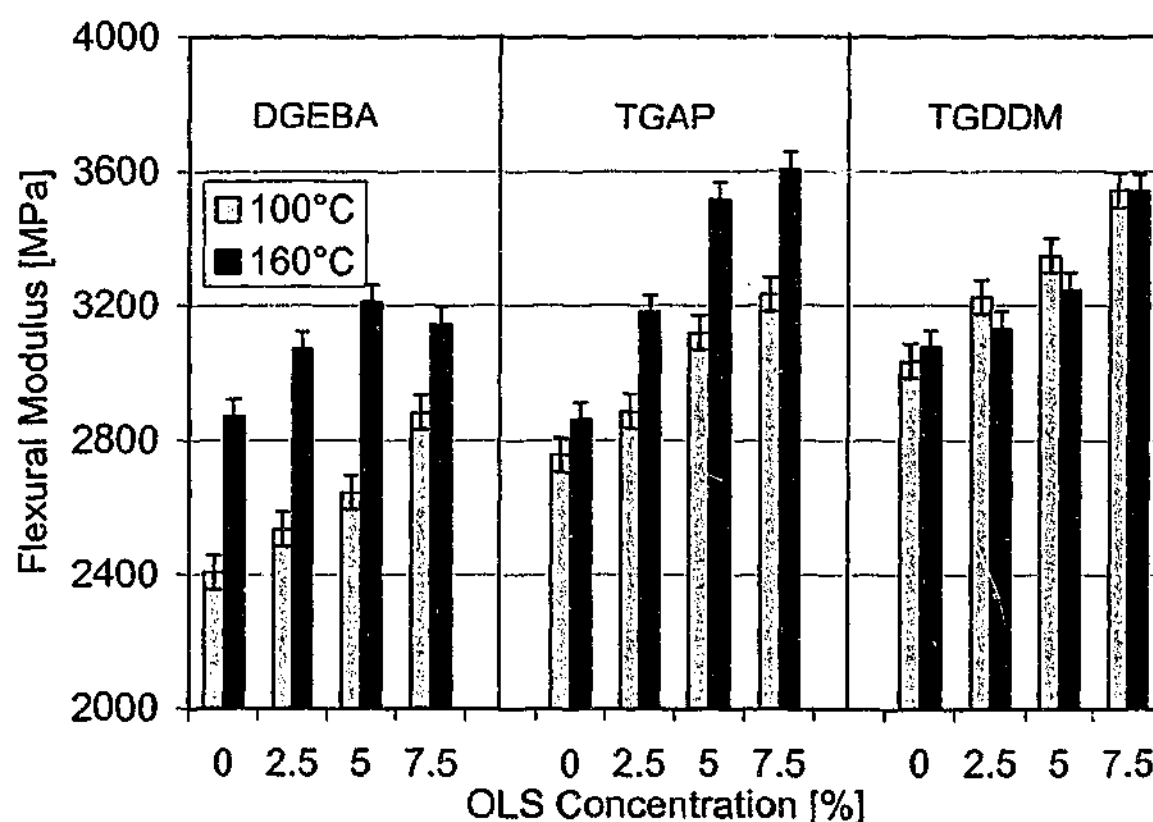
Figure 6.4: Flexural modulus of various epoxy nanocomposite systems cured at different temperature profiles.

In contrast to this, Lan and Pinnavaia [70] previously reported improved flexural properties (tensile strength and modulus) of a rubbery DGEBA/Jeffamine 2000 system with improved exfoliation as controlled by the carbon number of the interlayer exchanged ion. At a given concentration of 10 % organically modified layered silicate the improvement in tensile modulus varied between approximately 300 % (for $CH_3(CH_2)_7NH_3^+$ modified montmorillonite), where the layered silicate was predominantly intercalated in the polymer matrix, and 500 % (for $CH_3(CH_2)17NH_3^+$ modified montmorillonite) for a system which appeared primarily exfoliated.

6.2   Fracture Toughness

The fracture toughness of a series of nanocomposites synthesized at 100 °C and 160 °C, respectively was determined based on the compact tension test (ASTM D 5045 – 96 [112]). The critical stress intensity factor, K_{IC}, was determined from the maximum load at fracture of the crack-initiated samples, as outlined in the experimental section in 2.6.2. Results of the stress intensity factor values of the 100 °C series are illustrated in Figure 6.5, with values normalized by the neat resin shown in Figure 6.6. In either case, an increase in toughness can be observed with increasing organoclay concentration. Whilst most toughening techniques exhibit a loss in stiffness (such as rubber toughened epoxy resins, as illustrated in the literature review in Table 1.1), both toughness and stiffness have been improved through the organoclay incorporation in this work.

The normalized stress intensity factor shows that DGEBA and TGDDM exhibit a relative toughness increase of the same magnitude, whilst TGAP shows only little improvement. The lesser improvement in the TGAP resin system is likely due to be due to its very rigid structure. Generally, the high crosslink density of epoxy resins allows only very little plastic flow.
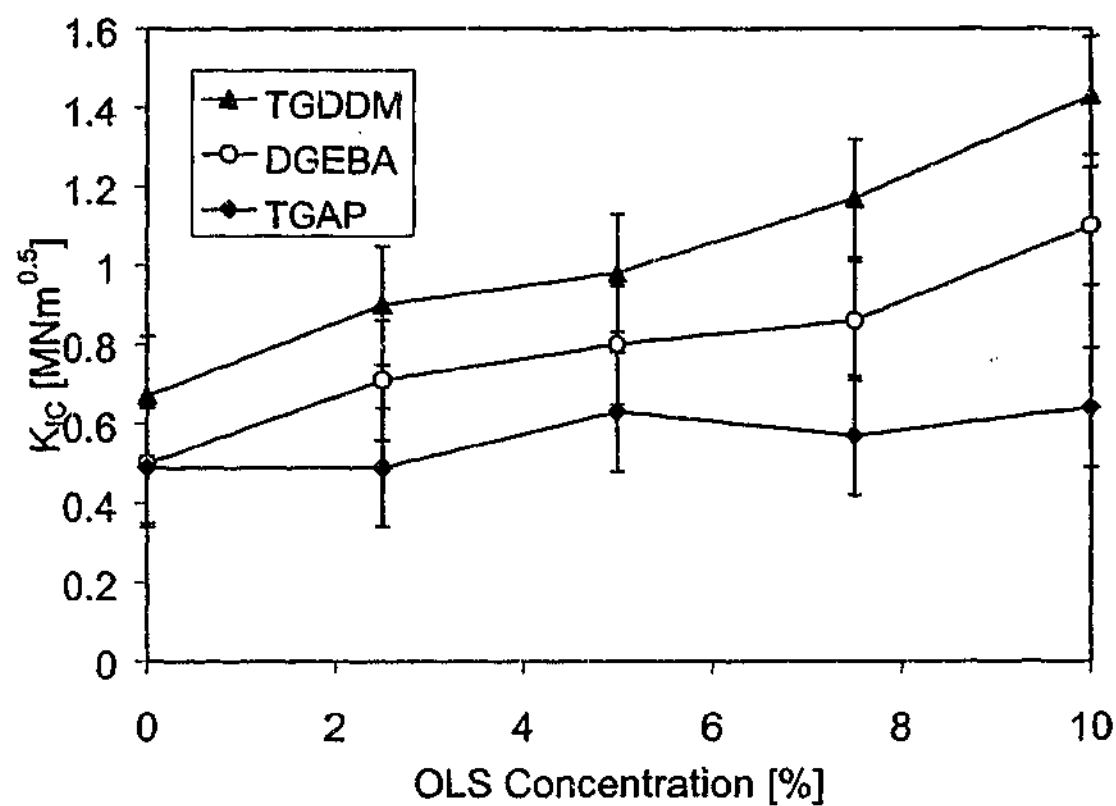
Figure 6.5: Stress intensity factor, K_{IC}, as a function of OLS concentration of epoxy nanocomposites cured at 100 °C.
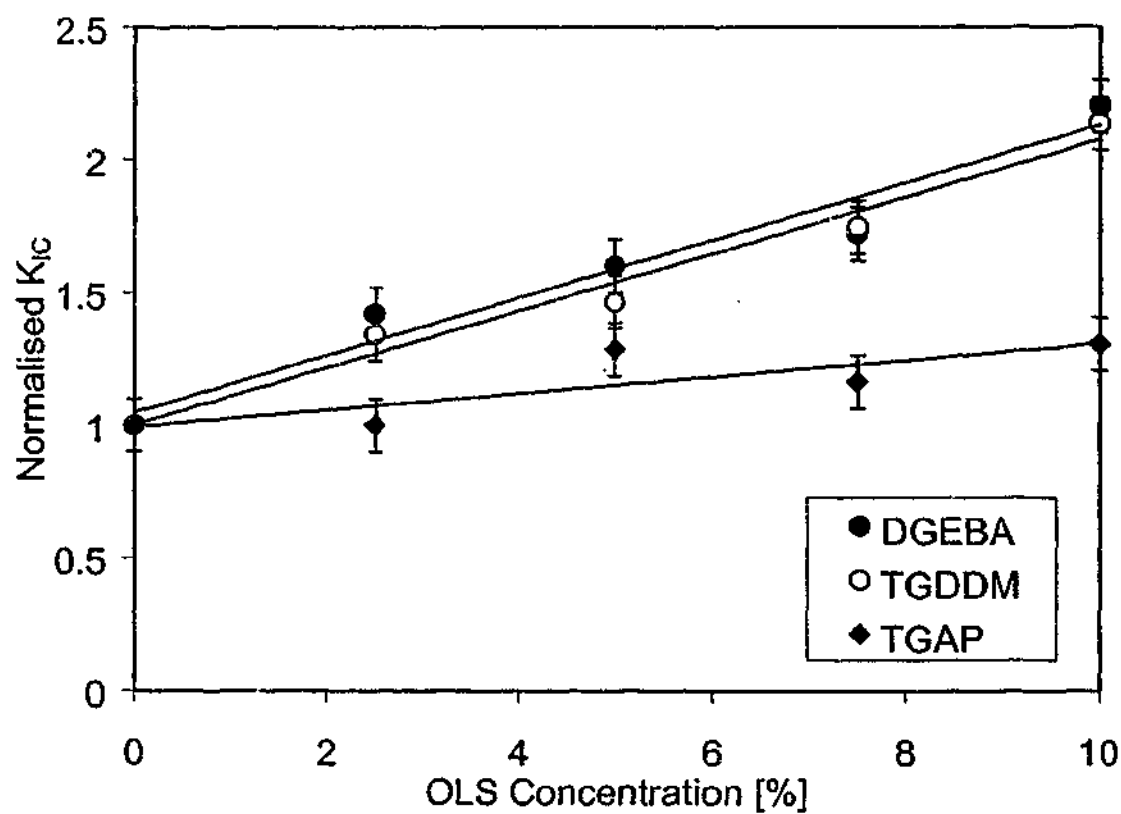
Figure 6.6: Normalized K_{IC} as a function of OLS concentration of epoxy nanocomposites cured at 100 °C.

In comparison with other epoxy systems, the TGAP resin is characterized by an even lower molecular weight between crosslinks with short, rigid bonds, which makes this resin system more difficult to improve in fracture toughness than DGEBA or TGDDM.

Fracture surfaces of the compact tension test specimens were investigated using scanning electron microscopy. Figure 6.7 to Figure 6.9 show the fracture surfaces of the neat TGDDM material as well as the TGDDM and DGEBA nanocomposite containing 7.5 % layered silicate. The surface of the fractured TGAP nanocomposite showed a similar appearance as the nanocomposites based upon the two other epoxy resins.

The fracture surface of the neat TGDDM material shows a very smooth and shiny surface with hackles, typical of brittle fracture. This was similar to the appearance of fracture surfaces of the neat DGEBA and TGAP materials. The fracture surfaces of these nanocomposites, in contrast, show significantly increased roughness and therefore increased fracture surface area with increasing organoclay concentration. The increased fracture surface area would imply improved energy disruption. Similar fracture behaviour was reported previously for other glassy epoxy- [93] and unsaturated polyester [170] layered silicate nanocomposites. Zerda and Lesser [93] investigated the fracture behaviour of intercalated Jeffamine 230 cured DGEBA nanocomposites based upon an alkylammonium-modified montmorillonite. The fracture surfaces images of their nanocomposite looked similar to the micrographs of fractured nanocomposites presented here, i.e. significantly increased textured surface in the nanocomposite was observed. As images of higher magnification revealed that the surface roughness extended into the submicron regime, indicative of the operation of the toughening mechanism on a nanoscale dimension. Their work showed that the intercalated layered silicate makes the crack path extremely tortuous. Crack branching along the path length was visualised on thin sections using polarized light. Also in their work, a concentration of 1.5 % OLS showed only low fracture surface improvement, however, dispersion of the layered silicate at this concentration was low. The work on unsaturated polyester nanocomposites reported by Kornmann et al. [170] also reported

increasing fracture roughness with increasing concentration of unmodified montmorillonite filler. SEM images of their fractured nanocomposite showed a similar rough and textured appearance as micrographs shown by Zerda and Lesser and the images presented here.

Figure 6.8 and Figure 6.9 show areas of greater roughness next to relatively smooth areas. It appears that the aggregates of intercalated silicate platelets (which are also seen in the optical micrographs in Figure 4.8 and Figure 4.9) with their lateral, micron-sized structures contribute to the increased fracture surface, by making the path for the crack propagation more tortuous. This in is good agreement with fracture results found by Zilg et al. [31]. This work reported the mechanism of an improved toughness/stiffness balance through the incorporation of organoclay in the epoxy matrix. It was theorized that the exfoliated structure mainly improves the modulus whereas the remaining tactoids of intercalated organoclay act as a toughening phase, possibly through the shearing of intercalated organoclay layers, being able to absorb energy of the propagating crack.
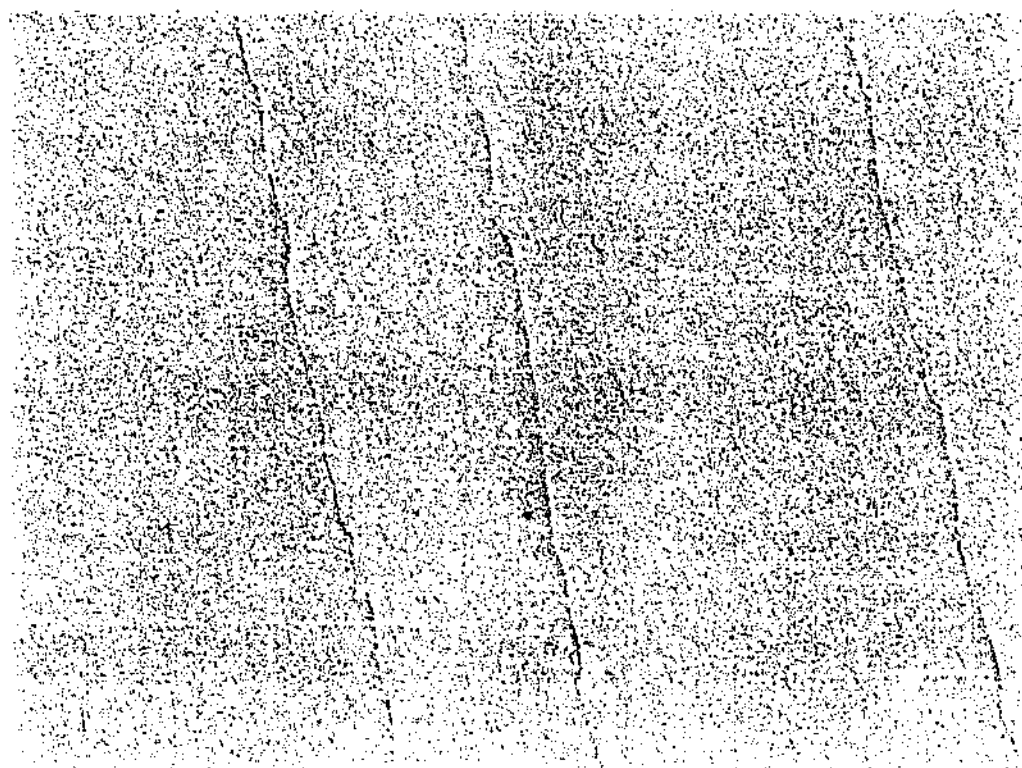
Figure 6.7: Fracture surface of the neat TGDDM resin system.

Figure 6.8: Fracture surface of TGDDM nanocomposite containing 7.5 % OLS.
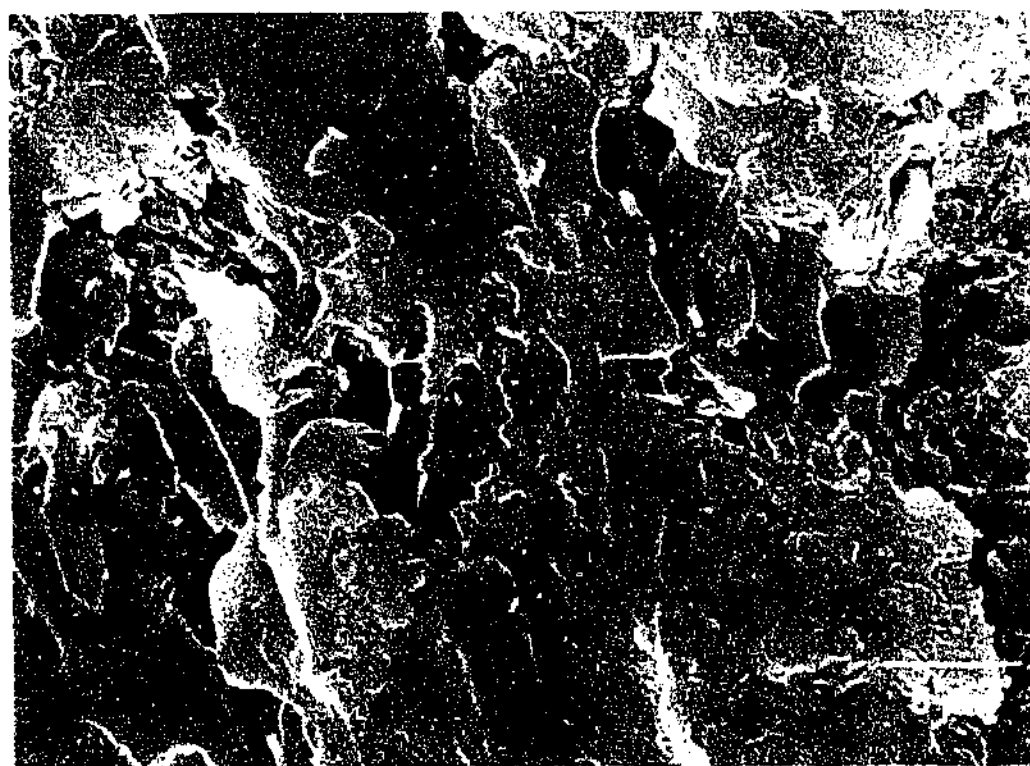
Figure 6.9: Fracture surface of DGEBA nanocomposite containing 7.5 % OLS.

The improvement in toughness and stiffness for the hexahydrophtalic anhydride cured DGEBA nanocomposites at a concentration of 10 % layered silicate varied between 10 – 35 % in modulus and 35 – 85 % in fracture toughness (K_{IC}), depending on the layered silicate modification. These values are in the same order of magnitude as the normalized mechanical properties found in this work, as shown in Figure 6.3 (modulus) and Figure 6.6 (fracture toughness).

A comparison with other high performance epoxy nanocomposites is provided by the recent work by Kornmann et al. [77]. In this work a tetrafunctional TGDDM resin based nanocomposites is synthesized using different layered silicate modifications and the curing agent 4,4'-diaminodiphenyl sulfone (DDS). Results also showed a simultaneous increase in toughness and stiffness in the order of 30 - 40 % in modulus and 40 - 80 % in fracture toughness at a true layered silicate content (i.e. mass fraction of the montmorillonite without the organic modifier) of 4 - 5 %, which is in excellent agreement with the results presented in this thesis. A potential toughening mechanism was only discussed briefly in this work. The authors suggested that an apparent lower crosslink density in the nanocomposite, which may favor yielding in the matrix may cause the improved toughness. However, it was mentioned that further experimental work would be required to identify the fracture mechanism of the high performance nanocomposite materials.

6.3   Temperature Effect on Toughness-Stiffness Balance

All materials show simultaneous improvement in fracture toughness and modulus compared to the neat materials. A summary of the toughness and stiffness data is given in Table 6.1. Within the experimental error, there is a monotonic improvement in both properties with increasing organoclay content.

Recent work by Chen et al. [65] investigated the effect of the cure cycle on the interlayer spacing, the glass transition temperature and the modulus of an anhydride (hexahydro-4-methylphtalic anhydride) cured epoxy (3,4-epoxycyclohexylmethyl-3,4-epoxycyclohexane) layered silicate nanocomposite.

The organoclay used was a bis-2-hydroxyethyl methyl tallow ammonium cation modified montmorillonite. In their work a decrease in T_g and rubbery modulus was reported and proposed to be related to the formation of an interphase consisting of the epoxy resin that is plasticised by the surfactant chains, whilst epoxy network formation itself was thought not to be affected by varying the initial cure temperature. The authors refer to a different epoxy system (DGEBA cured with 3DCM), studied by Franco et al [171], that did not show any effect of the initial cure temperature on T_g, flexural modulus, fracture toughness and height of tan δ. However, the resin system investigated by Chen et al. is based on different resin and hardener monomers.

All organoclay-containing DGEBA systems cured at 160 °C show higher values of toughness and stiffness compared to the nanocomposites cured at 100 °C. The TGAP nanocomposites show significant improvement in modulus along with a modest increase in fracture toughness at the higher cure temperature, whilst both toughness and stiffness results for the TGDDM based nanocomposites remained of the same order and appeared not to be affected by the cure temperature.

The XRD and TEM work described earlier has shown that increased cure temperature improved exfoliation for all series of nanocomposites. Improved exfoliation is often believed to increase mechanical properties, i.e. modulus and tensile strength [70]. However, it is clear from the unfilled resin results in this work that the changes in the initial cure temperature may also affect network formation and molecular architecture.

Comparison between mechanical properties of neat samples shows that an increase in initial cure temperature increases modulus and toughness (except for TGDDM where the toughness and modulus changed little with cure temperature). There are few studies of the effect of cure temperature on epoxy network formation in the literature: Lewis et al. [172] showed that for a high temperature curing diglycidyl ethers based resin system cured with 2,4 tolylene 1,1'bis (3,3 dimethyl urea), the thermal history of a fully-cured system can significantly affect the glass transition temperature by a variation of up to 30 °C

for resin systems cured at different temperatures, but all fully postcured at the same temperature. The highest T_g for this system was achieved for the slowest cure rate (at the lowest cure temperature).

Table 6.1: Mechanical properties of various epoxy nanocomposites.

Resin system	Organoclay [%]	Modulus [MPa]	K_{IC} [MNm$^{0.5}$]
DGEBA 100°C	0	2410 ± 180	0.50 ± 0.05
DGEBA 100°C	2.5	2540 ± 90	0.71 ± 0.16
DGEBA 100°C	5	2650 ± 170	0.80 ± 0.11
DGEBA 100°C	7.5	2880 ± 100	0.86 ± 0.25
DGEBA 160°C	0	2870 ± 70	0.91 ± 0.26
DGEBA 160°C	2.5	3070± 120	1.19 ± 0.24
DGEBA 160°C	5	3210 ± 50	1.32 ± 0.17
DGEBA 160 °C	7.5	3140 ± 40	1.13 ± 0.23
TGAP 100 °C	0	2760 ± 140	0.49 ± 0.10
TGAP 100 °C	2.5	2890 ± 210	0.49 ± 0.10
TGAP 100 °C	5	3120 ± 80	0.63 ± 0.09
TGAP 100 °C	7.5	3230 ± 80	0.57 ± 0.07
TGAP 160 °C	0	2860 ± 120	0.52 ± 0.08
TGAP 160 °C	2.5	3180 ± 270	0.56 ± 0.11
TGAP 160 °C	5	3520 ± 180	0.65 ± 0.08
TGAP 160 °C	7.5	3610 ± 80	0.64 ± 0.09
TGDDM 100 °C	0	3040 ± 40	0.67 ± 0.15
TGDDM 100 °C	2.5	3230 ± 50	0.90 ± 0.11
TGDDM 100 °C	5	3350 ± 70	0.98 ± 0.29
TGDDM 100 °C	7.5	3540 ± 30	1.17 ± 0.04
TGDDM 160 °C	0	3080 ± 150	0.60 ± 0.21
TGDDM 160 °C	2.5	3130 ± 50	1.02 ± 0.25
TGDDM 160 °C	5	3250 ± 70	1.01 ± 0.26
TGDDM 160 °C	7.5	3540 ± 70	1.19 ± 0.27

It was theorized that faster cure led to a less highly crosslinked network due to competing network reactions that form different networks. However, the

different reactions associated with the different networks were not further specified in this work. The cure temperature has also been reported to affect etherification and the molecular weight between crosslinks, M_C. Varley et al. [173] demonstrated for a highly crosslinked resin system (DDS cured TGAP) that etherification occurred in significant amounts at a cure temperature of 160 °C and above. However, it appears that changes in the cure schedule affect different epoxy systems in different ways.

In their studies on dicyandiamide (DDA) cured, benzyldimethylamine catalysed DGEBA, Sautereau, Pascault et al. [174-176] found a strong effect of the cure temperature and accelerator on the reaction mechanism. It was reported that the formation of ether linkages was favored at lower cure temperatures, i.e. more etherification occurred at a cure temperature of 100 °C compared to cure temperatures of 140 °C and 160 °C. Further, the reaction of the DDA at 100 °C was found to be a substitution of the hydrogen atoms by ring-opening of the epoxy groups, whereas at 140 °C and 160 °C the DDA reaction involved transformation of nitrile groups to imine groups.

Since the organically modified layered silicate in this work has a complex catalytic effect on homopolymerization and resin cure with a competition between two or more reactions involving different mechanisms and activation energies, it is likely that the formation of the network structure and therefore thermal and mechanical properties are dependant on the thermal history before postcure. Hence, it is difficult to relate changes in properties of nanocomposites strictly to either issue, i.e. the network structure or the silicate dispersion. Comparison of mechanical properties of the neat resins cured at different temperatures give an indication how strongly the change in structure in each system is affected by changes in the cure temperature. The neat DGEBA systems cured at 100 °C and 160 °C show largely improved toughness and stiffness with increased cure temperature, whilst the two more highly crosslinked resins TGAP and TGDDM show only a modest change in modulus.

According to the dramatic changes in the neat DGEBA system with increased cure temperature, it is likely that the enhancement is to a large extent related to

variation in the epoxy cure chemistry and hence the polymer architecture, rather than significant change in delamination of the organoclay platelets within the epoxy phase. This is further confirmed by the fact that the TGDDM based nanocomposites showed significantly improved intercalation with increased cure temperature; yet show modest changes in mechanical properties (recalling that the DGEBA system increased the average d-spacing from 85 Å to 95 Å and the TGDDM system from 45 to 60 Å with the increased cure temperature as shown by TEM results in Table 4.1).

In order to determine whether there are any differences in conversion as a function of cure cycle the degree of unreacted epoxy groups remaining after cure was investigated using NIR spectroscopy. The area under the 4530 cm^{-1} absorption peak in the FTIR spectra derived from the epoxy moiety [110] was determined and compared with its peak intensity of the unreacted prepolymer blend to calculate the percentage of residual epoxy groups. An example of the NIR traces is shown in Figure 6.10 for the TGAP based nanocomposites and the uncured resin/hardener mix.
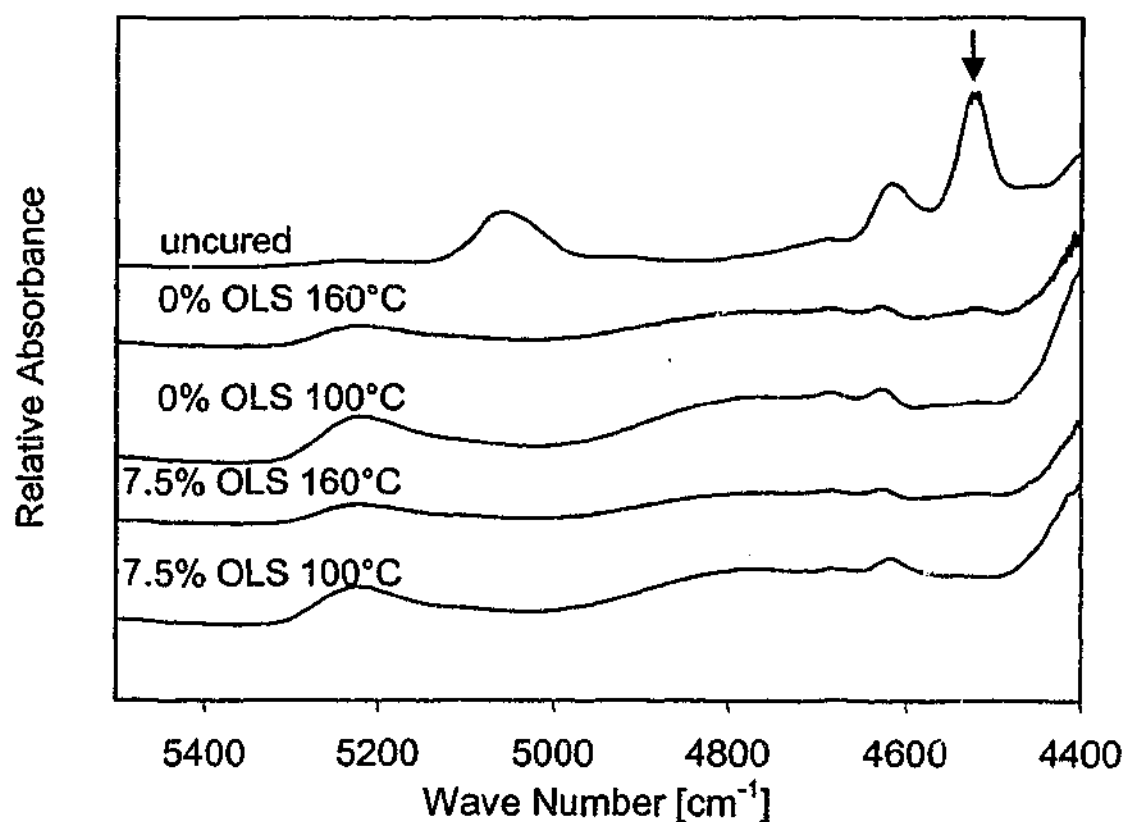
Figure 6.10: Comparison of TGAP based NIR spectra - the 4530 cm^{-1} absorption peak indicates the amount of residual epoxy groups.

Furthermore, the measured glass transition temperatures of these systems should also be recalled. Table 6.2 shows the T_g and percentage residual epoxy groups for neat resins and nanocomposites containing 7.5 % organoclay cured at 100 °C and 160 °C. Comparison of the T_g as an indicator for the degree of cure can only be applied for the neat systems, since the T_g is likely affected not just by the degree of cure, but also by the presence of clay, with the mechanism being not fully understood. For the neat systems it was observed that a higher initial cure temperature resulted in a slightly greater level of residual epoxy groups (remembering that all samples being postcured at the same temperature). This is in good agreement with a slightly decreased glass transition temperature. Organoclay-containing resin systems generally show a higher degree of conversion compared to the neat systems. It can also be observed, that these systems further reduce their T_g with increased, initial cure temperature and improved exfoliation.

Table 6.2: Comparison of the glass transition temperature and % residual epoxy groups of neat and layered silicate filled nanocomposites cured at 100 °C or 160 °C.

Resin system	Organoclay [%]	T_g [°C]	Residual epoxy groups [%]
DGEBA 100°C	0	187 ± 1.5	1.2 ± 0.5
DGEBA 100°C	7.5	180 ± 1.5	0.1 ± 0.5
DGEBA 160°C	0	185 ± 1.5	1.2 ± 0.5
DGEBA 160°C	7.5	173 ± 1.5	0.2 ± 0.5
TGAP 100°C	0	281 ± 1.5	2.0 ± 0.5
TGAP 100°C	7.5	271 ± 1.5	1.6 ± 0.5
TGAP 160°C	0	282 ± 1.5	4.0 ± 0.5
TGAP 160°C	7.5	269 ± 1.5	1.7 ± 0.5
TGDDM 100°C	0	260 ± 1.5	1.4 ± 0.5
TGDDM 100°C	7.5	241 ± 1.5	0.8 ± 0.5
TGDDM 160°C	0	257 ± 1.5	3.9 ± 0.5
TGDDM 160°C	7.5	228 ± 1.5	3.5 ± 0.5

Manipulating the cure temperature may lead to both improved intercalation and modification of the epoxy network. Clearly, variation of the cure profile alone in these systems does not lead to a true, fully exfoliated nanocomposite. Therefore a combination of both improved cure temperature and processing conditions, including much higher shear forces during cure than used here, or the use of swelling agents, which may be more effective at entering clay layers than the epoxy monomer, may be the key to the formation of true, individually-dispersed epoxy nanocomposites. It has to be noted that such homogenous, individual delaminations have not been demonstrated in any reported TEM images of epoxy nanocomposites yet. Even those systems that were optically clear and deemed exfoliated according to XRD analysis consisted of a blend of partially intercalated and exfoliated silicate layers.

6.4   *Z-Directional Toughening of Fibre Composites*

This section investigates the ability to supplementary toughen epoxy fibre composites through the nanocomposite strategy. Series of DGEBA and TGDDM epoxy/unidirectional carbon fibre nanocomposites are synthesised in a range of 0 - 7.5 % layered silicate as outlined in section 2.3.

The carbon fibre content of each system was determined to confirm that all fibre panels are within a fibre concentration range that allows comparison between the different materials. Measurements were conducted according to the ASTM D 3171-76 standard [117] and results listed in Table 6.3.

The fibre volume in the series of DGEBA composites showed excellent consistency at a value of 49 %, whilst the series of TGDDM composites showed some scatter around a value of approximately 55 %. As the mechanical properties of composites change with the fibre volume fraction, conclusions can only be made carefully for the TGDDM series.

Table 6.3: Carbon fibre content in unidirectional epoxy/carbon fibre nanocomposites.

Resin System	OLS Weight [%]	Fibre Weight [%]	Composite Density [g/cm^3]	Fibre Volume [%]
DGEBA	0	59 ± 1	1.457 ± 0.001	48 ± 1
DGEBA	2.5	60 ± 1	1.469 ± 0.001	49 ± 1
DGEBA	5	60 ± 1	1.480 ± 0.001	49 ± 1
DGEBA	7.5	59 ± 1	1.493 ± 0.001	49 ± 1
TGDDM	0	69 ± 1	1.531 ± 0.001	59 ± 1
TGDDM	2.5	65 ± 1	1.504 ± 0.001	54 ± 1
TGDDM	5	58 ± 1	1.480 ± 0.001	48 ± 1
TGDDM	7.5	59 ± 1	1.495 ± 0.001	49 ± 1

6.4.1 Mode I Fracture Toughness

Mode I fracture toughness tests are conducted as outlined in the experimental section. Stable crack growth along the crack initiator plane could be observed for most DGEBA fibre composite samples. However, at some stages fracture displayed slip/stick behaviour, rather than steady crack propagation. This might have occurred due to the influence of the few twill weaves in the fracture plane that could not be removed during prepreg synthesis without damaging the unidirectional fibre.

Difficulties occurred when determining values of $G_{IC\text{-}prop}$ from the plateau in the crack propagation resistance curve as many traces showed major scattering. In some cases a plateau could not be identified. A greater variation in $G_{IC\text{-}prop}$ can be expected due to the dependence of this value on the fibre/matrix interfacial adhesion. Therefore, only $G_{IC\ initial}$, as determined from the first point of deviation from linearity in the load/displacement curves are considered.

Mode I fracture toughness samples of the TGDDM based fibre composites did not break along the crack initiator plane rather than through different planes with the crack initiator sheet remaining partially stuck between the fibre sheets. This occurred in all the samples and can thus not be ascribed to manufacturing

defects in a particular panel. Therefore no mode I fracture data could be obtained for the TGDDM system.

Results for the mode I fracture toughness of the ternary DGEBA composites are shown in Figure 6.11. Both, the maximum load and the initial fracture energy, $G_{IC\ initial}$, show improved in-plane fracture resistance. The maximum load shows an increase by about 25 % along with an increase in $G_{IC\ initial}$ by 50 % at an organoclay concentration of 7.5 %.
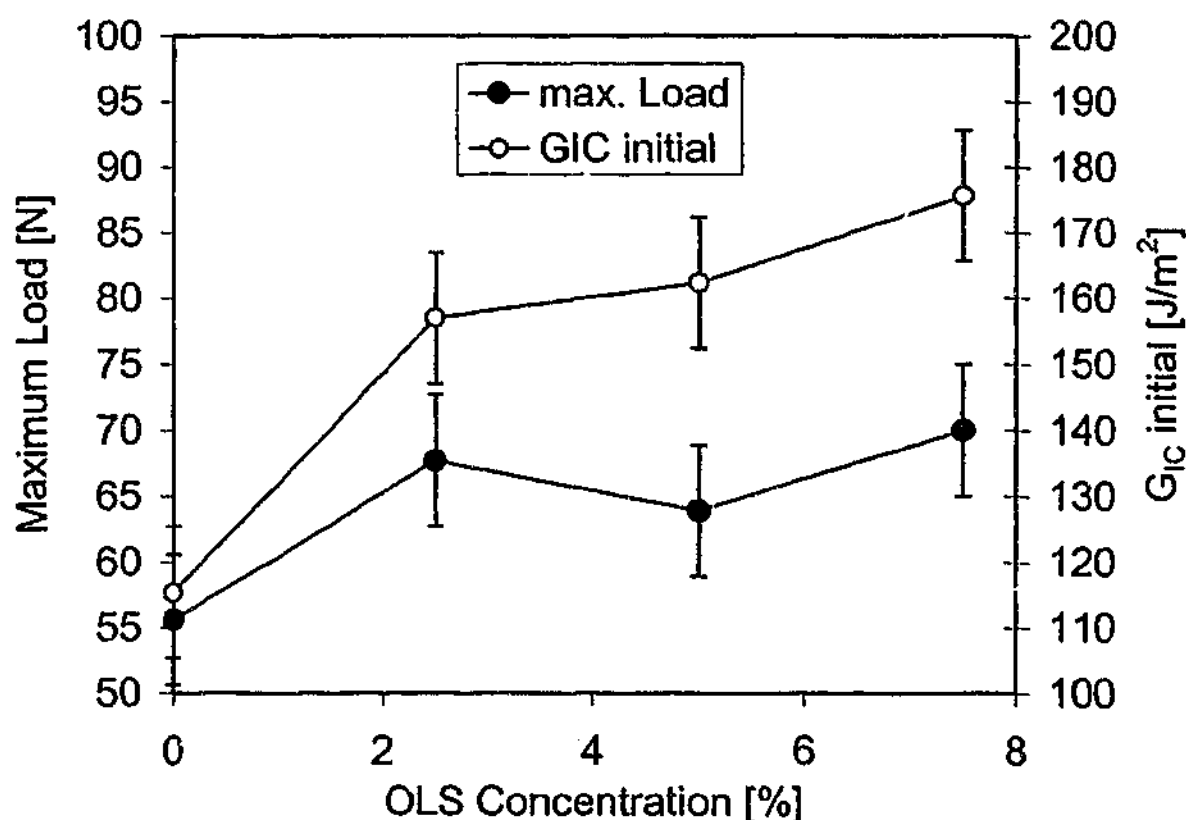
Figure 6.11: In-plane resistance and maximum load of DGEBA carbon fibre
nanocomposite (mode I fracture toughness).

For comparison, the fracture energy of the DGEBA nanocomposites, $G_{IC(N)}$, was calculated from toughness and modulus values of the DGEBA 160 °C series (as shown in Table 6.1), using equation 24:

$$G_{IC(N)} = \frac{K_{IC}^2 \cdot (1 - v^2)}{E} \qquad \textit{Equation 24}$$

where K_{IC} is the stress intensity factor, E the Young's modulus and ν the Poisson's ratio of the material (assumed that $\nu = 0.33$) [177].

A comparison of fracture energies of the neat nanocomposites and the ternary fiber nanocomposite systems is shown in Figure 6.12 (the increased error bars for the epoxy nanocomposites are a result of the error calculation, i.e. the addition of errors for the toughness and modulus).
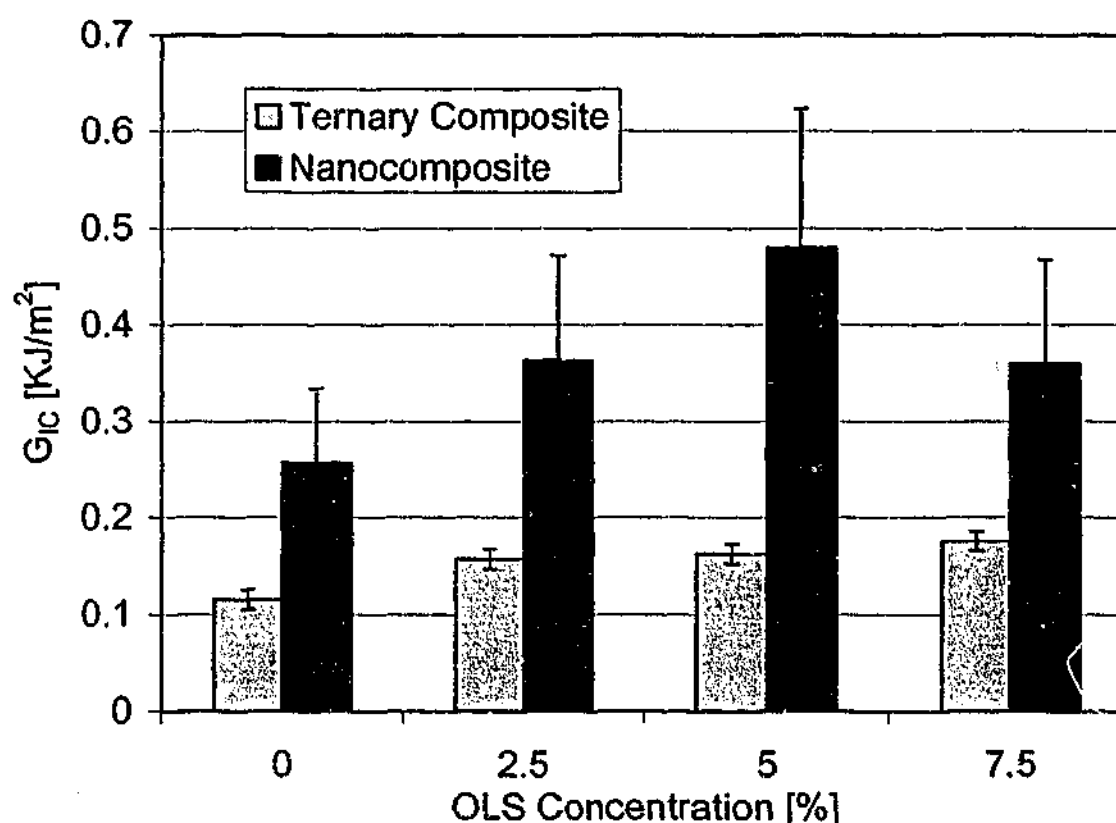
Figure 6.12: Comparison of the fracture energy, G_{IC}, of DGEBA in the neat nanocomposite and the ternary fibre nanocomposite system.

It can be seen that both series of fracture energy values show improvement compared to the systems containing no layered silicate. Furthermore, G_{IC} values increase with increasing organoclay concentration. The nanocomposite containing 7.5 % layered silicate deviates from this series, which may be ascribed to the high error related to the nature of this test. Significantly higher fracture energy values can be found in the neat nanocomposite compared to the fibre nanocomposite system. This is in good agreement with the general

finding for the interlaminar fracture toughness of fiber composites based upon toughened epoxy resins. As previously reported by Hunston et al. [178] and Bradley [179] and more recently reviewed by Kim and Mai [14] improvement in the composite is rather moderate when compared to the fracture toughness of the neat resin matrix. A rubber toughened epoxy, for example, that showed 20 - fold improvement in fracture toughness, gave only an 8 - fold improvement in mode I fracture toughness of the composite, as indicated by the G_{IC} values. An established explanation for the poor translation of the matrix fracture energy into G_{IC} of the composite is that the long rigid reinforcing fibres, sandwiching the thin epoxy film, constrain plastic deformation and limit microcracking at the crack tip respectively [14, 180].

Micro-images were taken from selected mode I fracture surfaces of neat and organoclay containing fibre composites to further understand the fracture mechanism of the layered silicate in the ternary system. Figure 6.13 and Figure 6.14 show typical images of the fracture surfaces of neat fibre composites. Similar to the neat resin system (compare Figure 6.7), a smooth and shiny fracture surface can be observed with few bands (predominately under a 60° angle to the fibre direction, which was also shown by others [181, 182]). The smooth fracture surface is indicative of fracture of brittle unmodified resin as previously shown by others [179, 183].

Fracture surface images of the composite systems containing 2.5 % and 7.5 % organoclay are shown in Figure 6.15 to Figure 6.17. As indicated by the crack within a single plane good fiber/matrix adhesion is maintained in the ternary system. Similar to the neat resin nanocomposites, increased fracture surface forms due to the presence of the organoclay. This implies that the path of the crack tip is distorted, making crack propagation more difficult.
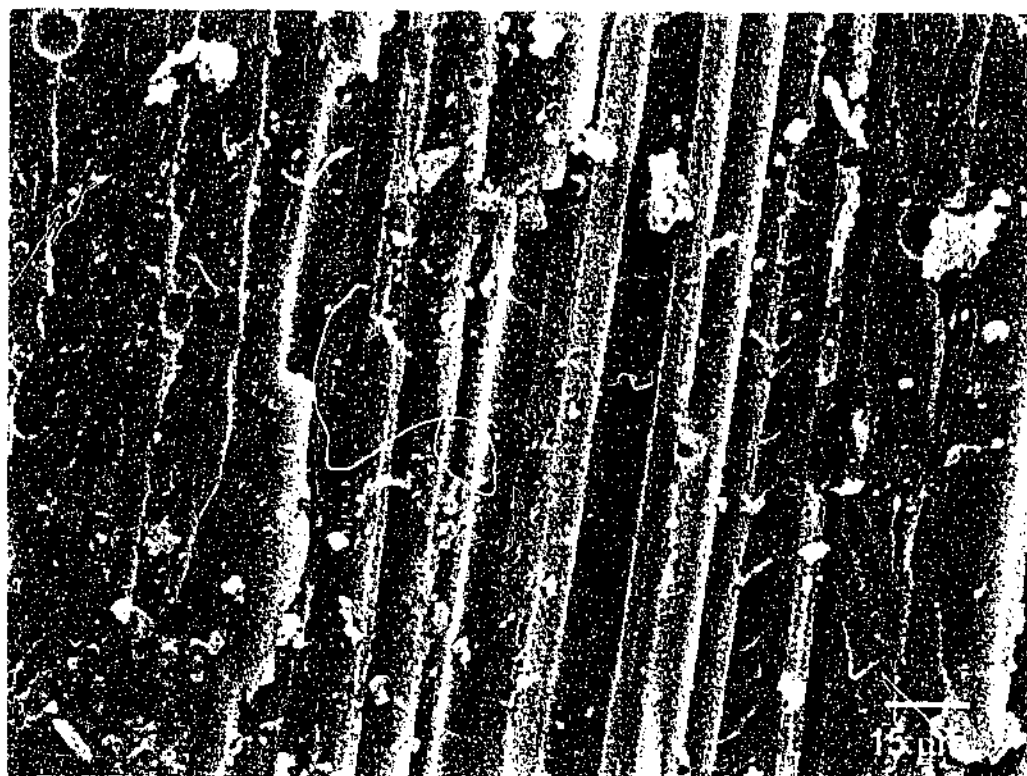
Figure 6.13: SEM image of the mode I fracture test surface of a DGEBA-carbon fibre composite containing 0 % OLS.

Figure 6.14: Close up SEM image of the mode I fracture test surface of a DGEBA-carbon fibre composite containing 0 % OLS.

Figure 6.15: SEM image of the mode I fracture test surface of a DGEBA-carbon
fibre composite containing 2.5 % OLS.
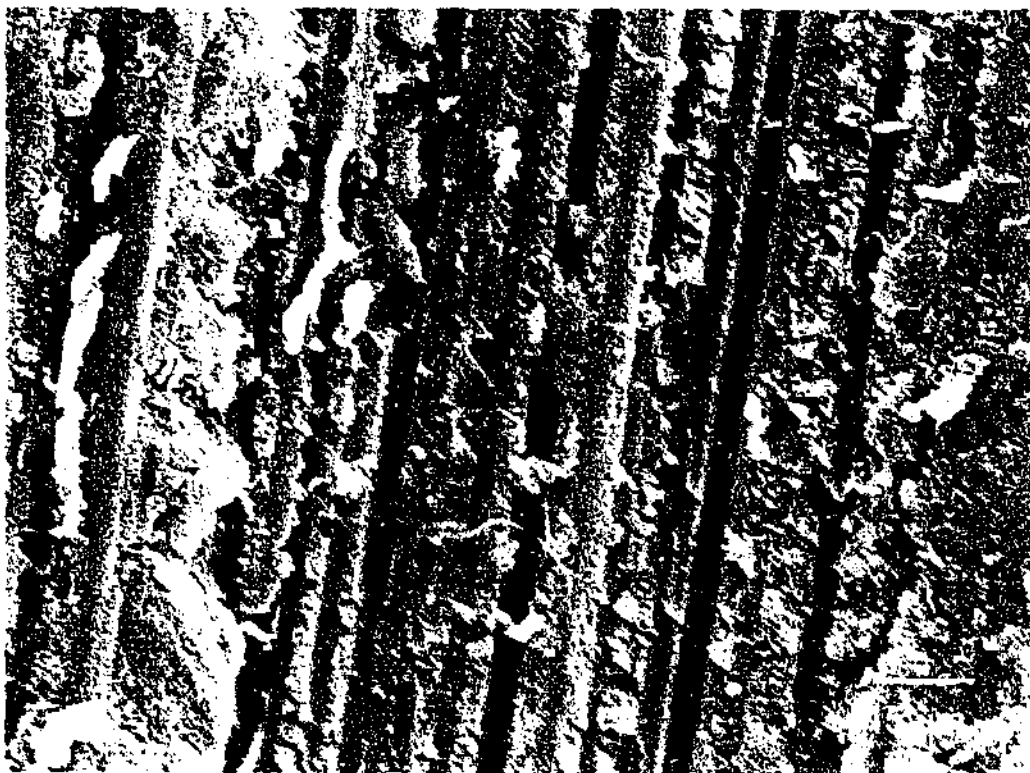
Figure 6.16: SEM image of the mode I fracture test surface of a DGEBA-carbon
fibre composite containing 7.5 % OLS.
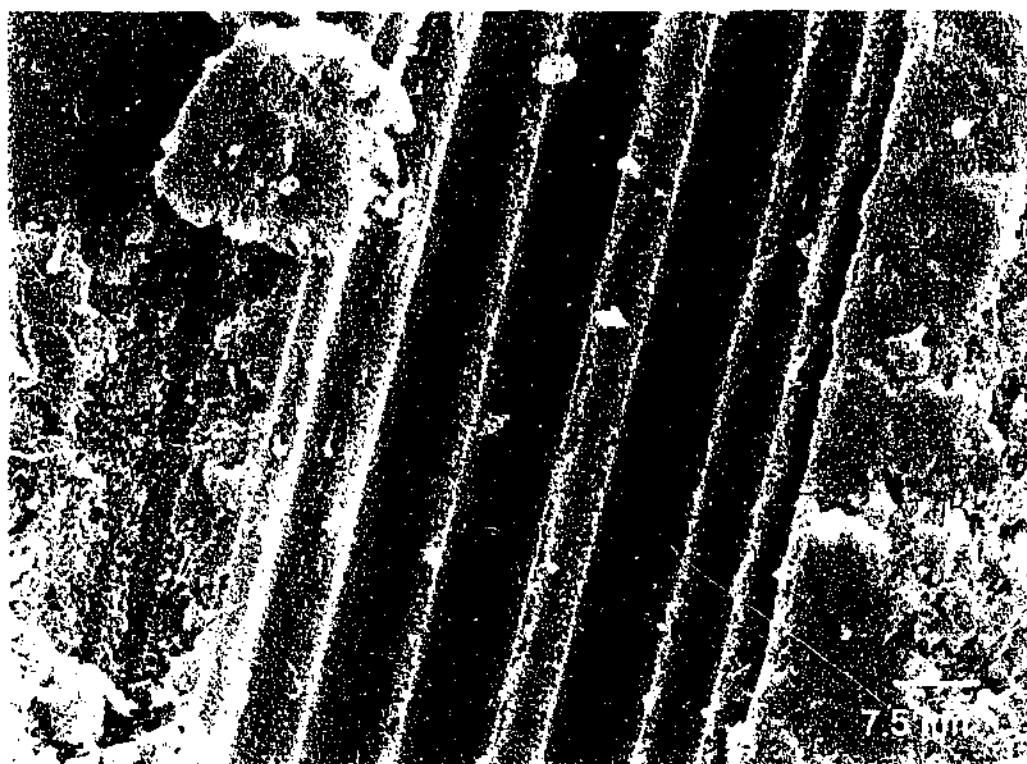
Figure 6.17: Close up SEM image of the mode I fracture test surface of a DGEBA carbon fibre composite containing 7.5 % OLS.

6.4.2 Interlaminar Shear Strength

Values determined for the interlaminar shear strength (ILSS) are shown in Figure 6.18. The values determined are within the same order of magnitude as other epoxy carbon fiber composites reported in the literature (40 – 90 MPa) [14, 184].

The interlaminar shear data did not show any improvement with increasing organoclay concentration. Results for the DGEBA based composite systems scatter around a constant shear strength of about 7100 N/cm^2 (71 MPa) whilst the TGDDM composites, even showing a slight tendency for decreased interlaminar shear strength.
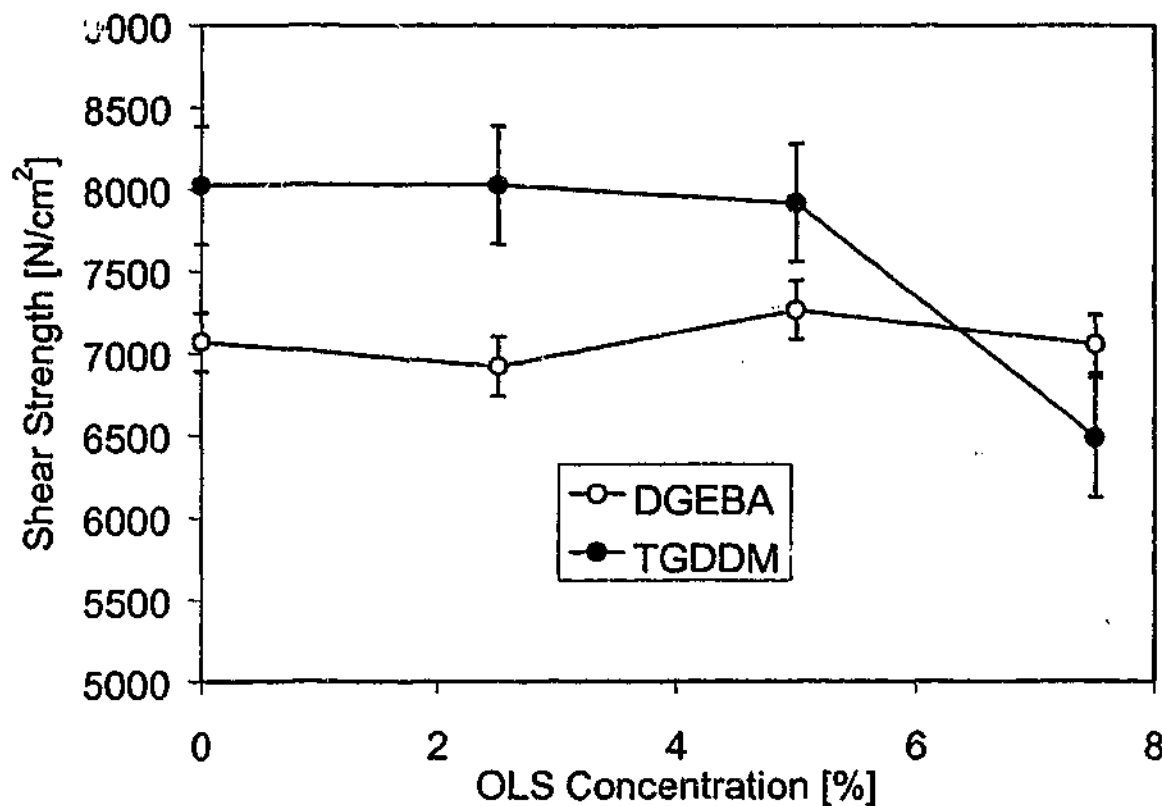
Figure 6.18: Interlaminar shear strength of DGEBA and TGDDM carbon fibre nanocomposites.

Incorporation of the nanofiller into carbon fibre epoxy nanocomposites has shown improved delamination resistance for the DGEBA system according to mode I fracture toughness measurements. However, interlaminar shear measurements did not show any improvement for any of the two systems (DGEBA, TGDDM) investigated.

Recently, Rice et al. [185] have investigated the matrix-dominant properties of a bisphenol F/epichlorohydrin epoxy resin layered silicate fibre composites through four-point flexure measurements. No significant increase in z-axis properties was reported in this work. Little improvement in the order of the variation was found for a fibre composite with low organoclay concentration. Composite systems of higher organoclay concentrations even showed a decreased flexural strength, which was however ascribed to an increased void content in the matrix. Further work is required to verify the potential of layered silicate as a complementary toughener in a ternary, epoxy-fibre nanocomposite systems.

Chapter 7
Conclusions and Further Work

7.1 Conclusions

A systematic study on the effect of an octadecyl amine ion modified layered silicate on three different high performance epoxy resin systems was conducted. The following conclusions presented here summarize the major findings and significance of this project. The conclusions and further work are discussed in terms of the processing conditions and correlating morphology, environmental stability and the mechanical properties of these materials, areas which are of fundamental importance in understanding nanocomposites and vital to unlocking their future potential.

7.1.1 Viscosity and Cure Monitoring Studies

The effect of the organophilic rendered layered silicate on the rheology of different epoxy resin monomers was investigated. It was found that the viscosity of layered silicate containing resins changed little compared to the addition of a micron-sized filler. Both steady and dynamic shear tests showed minor deviation from Newtonian flow behaviour, as seen by the relative invariant magnitude of the Power Law parameters. Fitting the data to the Herschel-Buckley (yield-stress) model showed that only the highly viscous, highest molecular weight resin, TGDDM, possessed any significant yield stress. Comparison between dynamic and steady shear experiments showed good agreement for low layered silicate concentrations (below 7.5 wt%), i.e. the Cox-Merz rule can be applied. Deviations from the Cox-Merz rule appeared at and above 10wt%, although such deviations were only slightly above experimental error. It was found that the activation energies of flow of the uncured prepolymer

mixtures were not markedly affected through the organoclay addition. During mixing of the resin monomer with the OLS (prior to cure), the monomers intercalate the organoclay galleries, increasing the gallery spacing. XRD measurements showed an increase of the interlayer distance of the layered silicate from initially 2.3 nm to 3.9 nm. However, the platelets remain in a stacked formation and do not show the dramatic changes in rheological behaviour that is observed for delaminated layered silicates. Although the individual layered silicate platelets are nanometer-sized with a very high surface area, in the slightly intercalated state after swelling and prior to cure, the lateral micron-sized properties of the layered silicate tactoids are dominating.

The effect of the octadecyl amine ion exchanged organoclay on the cure of the different high-performance epoxy resins was investigated. Dynamic differential scanning calorimetry (DSC) measurements were taken from series of resin/layered silicate and resin/layered silicate/hardener blends, varying from 0 – 10 % in layered silicate concentration. In any case, the addition of the organically modified layered silicate showed a catalytic effect on the homopolymerization and the resin/hardener cure reaction, as indicated by a decrease of the reaction peak temperature in the DSC traces. It was shown that the reaction kinetics of the DGEBA resin system is more strongly catalysed through the addition of organoclay than the two resins of higher functionality. This is likely due to the fact that the organoclay exfoliates to a greater degree in the DGEBA system (as found by TEM and XRD measurements), thus increasing the surface area of the silicate, facilitating the further catalysis of crosslinking reactions.

Isothermal parallel plate rheology measurements were conducted on series of nanocomposite pre-mixes (resin/hardener/layered silicate blends), varying in layered silicate concentration. Gelation could be observed, as judged by the crossover in tan δ traces of different frequencies (tan δ decreases with increasing frequency in the liquid state and increases with increasing frequency in the rubbery state). In some cases, the crossover of tan δ method was not found to show a precise intersection. This occurred for both organoclay-filled

systems, as well as the neat resin and can therefore not be considered as a result of the filler addition. Nonetheless, results were consistent and in good agreement with the gelation times determined from the rapid increase in storage modulus upon gelling. With increasing filler concentration the gelation time was steadily decreased.

The conversion at gelation was determined for selected nanocomposite systems by comparing the residual energy of cure with the complete energy of cure as determined from DSC measurements. Since the conversion at gelation did not decrease with filler addition, the decreased gelation time is assumed to be a result of an improved reaction rate caused by the organically modified layered silicate, and not due to the formation of a physical gel (at lower levels of conversion).

Wide-angle x-ray analysis (XRD) was carried out at different stages of cure to monitor organoclay exfoliation kinetics. It was found that only some (small) degree of conversion (significantly before gelation) was required to obtain significant intercalation. Although blends of liquids with layered silicates are known to form physical gels, the rheological measurements during cure did not show any significant increase in viscosity due to an increase in the interlayer distance or (in case of DGEBA) the exfoliation of layered silicates.

Flexural braid tests, a method where the uncured epoxy blend is painted on an inert glass braid and clamped in a dual cantilever frame to follow the viscoelastic behaviour from the liquid to the rigid thermoset stage during cure, was applied for comparison. Isothermal flexural braid tests confirmed the gelation data from rheology measurements and were further used to determine vitrification times. Gelation values from the flexural braid test showed a similar position in time as values from rheology measurements. The time to vitrification also showed a monotonic decrease with increasing layered silicate concentration.

7.1.2 Morphology and Physical Properties

Investigations of the nanocomposite morphology in the cured polymer matrix using WAXS and different microscopy techniques showed that any given nanocomposite morphology does not fall neatly into the commonly used terms of *intercalated* or *exfoliated* structures with a mixture of both being seen. Care has to be taken when interpreting the overall morphology of a material from micrographs or WAXS results.

The comparison of the nanocomposite formation based on three different epoxy resins with different structures and functionalities has shown that the structure and chemistry of the epoxy resin, its mobility and reactivity, are key factors controlling the increase in layer distances and therefore the morphology of the cured nanocomposite. Two different effects have to be considered when the properties of nanocomposites cured at different temperatures are compared: improved dispersion and better exfoliation of the silicate platelets in the polymer matrix, as well as changes in the nature of the reaction and thus the network formation. Generally, the bifunctional DGEBA resin has shown better exfoliation of the organoclay than the resins of higher functionalities, with individual platelets being separated from the layered silicate aggregates. It was found for all resins that higher cure temperatures led to improved organoclay layer separation, although tactoids were observed in all systems including even DGEBA. At a cure temperature of 100 °C, DGEBA exhibited an average d-spacing of 8.5 nm compared to approximately 4.5 nm for the TGAP and TGDDM nanocomposites. Increasing the cure temperature led to improved layer separation, all resin systems showed an increase in d-spacing by 1 - 1.5 nm when initially cured at 160 °C. The improved intercalation was ascribed to a higher reaction rate within the clay galleries due to the catalytic effect of the interlayer exchanged ions on homopolymerization and resin/hardener cure, as well as improved molecular mobility at higher temperature, enabling further resin and hardener monomers to diffuse into the galleries. However, exfoliation during the in-situ polymerization may not be sufficient to form a true fully homogeneous exfoliated nanocomposite.

Positron annihilation lifetime spectroscopy (PALS) was applied to determine free volume properties of the cured nanocomposites. Briefly, the antiparticle of an electron evolving from the decay of a ^{22}Na source, the positron, is used to investigate the free volume between polymer chains. By appropriate curve fitting of the decay spectra, the lifetimes of *ortho*-positroniums and their intensity can be determined. The lifetime of *ortho*-positronium (τ_3) and its intensity (I_3) are indicative of the free volume in the polymer system.

Free volume measurements were conducted on neat epoxies and nanocomposites containing 7.5 % organically modified layered silicate, cured at 100 °C and 160 °C respectively. The free volume properties did not vary significantly between resins or with cure temperature. Results for the nanocomposites generally follow the rule of mixtures, although there was some suggestion that the presence of clay could lead to increased free volume – with greater free volume in systems where the clay is best dispersed. This was consistent with decreased glass transition temperatures with addition of layered silicate due to disruption and of decreased crosslink density of interfacial regions of clay and epoxy matrix. The average free volume size was greatest for DGEBA, followed by TGDDM and TGAP, and was related to variations in structure and chemistry of the crosslinked thermosets. However the PALS showed complex behaviour with some results being conflicting.

7.1.3 Thermal Relaxations and Stability

Dynamic mechanical thermal analysis (DMTA) of temperature location of the α and β-relaxation showed a steady decrease in both relaxations with increasing organoclay content. A number of possible reasons for this reduction in T_g were discussed. The reduced relaxation temperatures indicate a possible lower crosslink density around the clay particle, perhaps due to the perturbing effects of the clay, even though the layered silicate doesn't noticeably affect conversion. Since the T_g measured is a bulk process, it appears that the fine dispersion of the nanometer-thick clay platelets influences much of the volume

of the epoxy matrix. Further reasons for the decrease in glass transition temperature might be a plasticising effect of the organoclay compatibilizing ions or the thermal degradation of these ions during post cure at high temperatures.

The relaxation peak broadens with increasing organoclay concentration in case of the primary relaxation, with higher organoclay concentrations. Broadening of the α-relaxation was ascribed to a greater distribution of chain mobilities due to different environments, such as molecules embedded in a purely epoxy environment or molecules tethered to the silicate.

The thermal stability of series of nanocomposites was investigated by means of thermogravimetric analysis (TGA) in an inert nitrogen atmosphere. Nanocomposites showed slight indications of reduced thermal stability, as indicated by a decreased onset in thermal degradation in the order of 5 - 10°C at a clay concentration of 10 %. The final char concentration was increased with increasing organoclay concentrations. The changes in thermal stability are of very low significance and it is unlikely that they would be considered as a drawback to any possible industrial application.

Furthermore, the water uptake behaviour, a major concern in glassy high performance epoxy resin systems, was investigated. Measurements of the water sorption at a temperature of 80 °C showed that the equilibrium water uptake of all nanocomposites was reduced compared to the neat epoxy system. The concentration of layered silicate did not correlate proportionally with the reduction in equilibrium water uptake. Values of the equilibrium water uptake for the neat resin systems are 2.8 % for DGEBA, 4.8 for TGAP and 4.0 for the TGDDM system. The absolute reduction varied between 0.4 % - 0.5 % for DGEBA and TGAP and 0.2 % for the TGDDM nanocomposites. The rate of water diffusion remained unaffected.

7.1.4 Mechanical Properties

Although improvement in modulus due to addition of micron-sized fillers often reduces toughness of the material, in this work both toughness and stiffness were simultaneously improved through the incorporation of organoclay. This has been reported previously for various bifunctional DGEBA nanocomposite systems and it was shown here that it also applies to the epoxy systems of higher functionalities, TGAP and TGDDM. For the series of nanocomposites initially cured at 100 °C, all systems exhibit an increase in Young's modulus by approximately 20 % at an organoclay concentration of 10 %. DGEBA and TGDDM have shown a similar increase in toughness with increased layered silicate concentration (approximately 120 % at a clay concentration of 10 %). In contrast, the TGAP nanocomposite systems showed only an increase of approximately 30 %, due to the rigid chemical structure of this resin (very low molecular weight between bonds and very short bonds).

The increased cure temperatures have shown improved modulus and fracture toughness for the DGEBA and, to a lesser degree, for the TGAP nanocomposites. In spite of the increased d-spacing in TGDDM nanocomposites, the mechanical properties remained relatively unaffected by the cure temperature. It is assumed that the effect of the cure temperature on the reaction chemistry and crosslink density has a major impact on mechanical properties along with the changes in organoclay dispersion. More dramatic changes in the nanocc   ⸜ morphology may be required to significantly change the mech⸍   ⸍perties. However, the window of processing temperatures is li⸍   ⸍ide reactions and thermal degradation. Variation of cure temperatu⸍   ⸍ is not sufficient to form a fully dispersed 'true' nanocomposite.

Incorporation of layered silicates into a DGEBA based high performance unidirectional fibre composite showed improvement in mode I fracture toughness in the order of 50 % at a correlating organoclay concentration of 7.5 %. Interlaminar shear tests on fibre nanocomposites based upon all three resins did not show any improvement. However, the work on supplementary

toughened fibre composites through the nanocomposite strategy only presented some initial results and further work is required to evaluate the potential of the application of layered silicates as a supplementary toughener.

7.2   *Proposals for Further Work*

The research presented in this work was conducted in order to assess the potential of organically modified layered silicates as a filler to improve high performance epoxy resin systems. There are a number of criteria an additive has to fulfil to qualify for the use as high performance epoxy reinforcement. In this work, it is shown that the highly dispersed layered silicate can simultaneously improve toughness and stiffness of the resin system. In addition, a number of experiments were conducted to study the environmental stability of this new group of composite materials. High performance epoxy resins such as used in aerospace applications are exposed to an aggressive environment, including heat, moisture and rapid temperature changes. Studies of the effect of the layered silicate on the glass transition temperature, the water uptake and the thermal stability in this work have shown that no significant drawbacks occur in these areas. In fact, some of these properties such as the equilibrium water uptake are also improved through the filler addition. However, not all aspects of environmental stability could be covered in this study and it would be interesting to see how the nanocomposite materials perform under long-term exposure to these aggressive conditions. Further experiments could include the effect of long-term exposure in changing environments (varying temperature and humidity) on mechanical properties.

As outlined previously in the literature review, layered silicates have shown reduced flammability in a number of polymer materials and it is likely that layered silicates could reduce the amount of traditionally used flame retardants in polymers. Therefore, it would be interesting to study the effect of the layered silicate on the flame retardation of the composite by means of cone calorimetry. This is of particular interest since it is the combination of improved properties

that makes the layered silicate strategy an attractive alternative to the more commonly used additives.

There are also a number of aspects that could be investigated in order to improve nanometer-scale dispersion of the layered silicate in the polymer matrix. Recent work by Chin et al [81] has shown that the stoichiometric resin/hardener ration can improve exfoliation for a *m*PDA/DGEBA resin nanocomposite system, which may also occur in the more highly crosslinked systems. The work presented here is centred on one particular (octadecyl ammonium ion) layered silicate modification, as well as one amine, the use of different modifiers and/or hardeners may significantly vary the ratio between intergallery and extragallery reaction and could also lead to better dispersion.

Furthermore, the use of the layered silicate as a supplementary toughener in ternary system is of interest. The potential of high performance carbon fibre composites was only investigated to a small extent in this work. The synthesis and characterisation of fibre composites is very labour intensive and the nature of the mechanical tests involves high errors. Important further investigations in that area would be to vary processing conditions and the resin concentrations in the composite, or the attempt to attach the layered silicate to the fibre surface. Application of layered silicates in other ternary epoxy systems such as rubber toughened epoxy resins to compensate for the loss in modulus has already been undertaken by our research group.

References

1. Ellis, B., *Chemistry and Technology of Epoxy resins*, 1993, Blackie Academic & Professional, London.

2. Kirk-Othmer, *Encyclopedia of Chemical Technology*, 3. ed. Vol. 9, 1980, Wiley, New York, 267.

3. Chiao, L., *Mechanistic Reaction Kinetics of 4,4'-Diaminodiphenyl Sulfone Cured Tetraglycidyl-4,4'-diaminodiphenylmethane Epoxy Resin*, Macromolecules, 1990, **23**, 1286.

4. Min, B. G., Stachurski, Z. H., Hodgkin, J. H., Heath, G. R., *Quantitative analysis of cure reaction of DGEBA/DDS epoxy resins without and with thermoplastic polysulfone modifier using near infra-red spectroscopy*, Polymer, 1993, **34**, 3620.

5. Varley, R., Heath, G., Hawthorne, D. Hodgkin, J. H., Simon, G. P., *Toughening of a trifunctional epoxy system: 1. Near infra-red spectroscopy study of homopolymer cure*, Polymer, 1995, **36**, 1347.

6. Gillham, J. K., *Award Address Formation and Properties of Network Polymeric Materials*, Polymer Engineering & Science, 1979, **19**, 676.

7. Enns, J. B., Gillham, J. K., *Time-temperature-Transformation (TTT) Cure Diagram: Modelling the Cure Behaviour of Thermosets*, Journal of Applied Polymer Science, 1983, **28**, 2567.

8. Sankaran, S., *Chemical Toughening of Epoxies. I:. Mechanical, Thermal, and Microscopic Studies of Epoxies Toughened with Hydroxyl-Terminated Poly(butadiene-co-Acrylonitril)*, Journal of Applied Polymer Science, 1990, **39**, 1635.

9. Bucknall, C. B., Partridge, I. K., *Phase separation in epoxy resins containing polyethersulphone*, Polymer, 1983, **24**, 639.

10. Varley, R., PhD Thesis: *Thermoplastic Modification of a Trifunctional Epoxy Resin System*, 1998, Monash University, Melbourne, Australia.

11. Kinloch, A. J., Shaw, S. J., Hundston, D. L., *Deformation and fracture behaviour of a rubber-toughened epoxy: 2. Failure criteria*, Polymer, 1983, **24**, 1355.

12. Pearson, R. A., Yee, F. A., *The Effect of Crosslink Density on the Toughening Mechanism of Elastomer Modified Epoxies*, Polymer Materials Science and Engineering, 1983, **49**, 316.

13. Pearson, R. A., Yee, F. A., *Toughening mechanisms in thermoplastic-modified epoxies: 1. Modification using poly(phenylene oxide)*, Polymer, 1993, **34**, 3658.

14. Kim, J.-K., Mai, Y.-W., *Engineered Interfaces in Fiber Reinforced Composites*, 1. ed. 1998, Elsevier, Amsterdam.

15. Chung, W. C., Jang, B. C., Chang, T. C., Hwang, L. R., Wilcox, R. C., *Fracture Behaviour in Stitched Multidirectional Composites*, Materials Science and Engineering, 1989, **112**, 157.

16. Ivens, J., Debaere, P., McGoldrick, C., Verpoest, I., Van Der Vleuten, P., *2.5 D fabrics for delamination resistant composite structures*, Composites, 1994, **25**, 139.

17. Zhong, W., Jang, B. Z., *Material Design Approaches for Improved Impact Resistance of Composites*, Key Engineering Materials, 1998, **141-143**, 169.

18. Garcia, R. E., Palmer, R. J., *Structural Property Improvements Through Hybridized Composites*, Toughened Composites, Editor: Johnston, N. J., 1987, American Society for Testing Materials, Philadelphia, 397.

19. Yamashita, S., Hatta, H., Takei, T., Sugano, T., *Interlaminar Reinforcement of Laminar Composites by Addition of Oriented Whiskers in the Matrix*, Journal of Composite Materials, 1992, **26**, 1254.

20. Jang, B. Z., *Fracture Behaviour of Fibre-Resin Composites Containing a Controlled Interlaminar Phase (CIP)*, Science and Engineering of Composite Materials, 1991, **2**, 29.

21. Sohn, M. S., Hu, X. Z., *Unidirectional Carbon Fibre/Epoxy Laminates Interleaved by Film Adhesives and Chopped Kevlar Fibres*, Key Engineering Materials, 1998, **145-149**, 727.

22. Solomon, D. H., Hawthorne, D. G., *Chemistry of Pigments and Fillers*, 1983, Wiley, New York.

23. Hoffmann, U., Endell, K., Wilm, D., *Kristallstruktur und Quellung von Montmorillonit*, Zeitschrift für Kristallographie, 1933, **86**, 340.

24. Alexandre, M., Dubois, P., *Polymer-layered silicate nanocomposites: preparation, properties and use of a new class of materials*, Materials Science and Engineering, 2000, **28**, 1.

25. Wang, Z., Massam, J., Pinnavaia, T. J., *Epoxy-Clay Nanocomposites*, *Polymer-Clay Nanocomposites*, Editor: Pinnavaia, T. J., Beall, G. W., 2000, Wiley, Chichester, 127.

26. Kornmann, X., PhD Thesis: *Synthesis and Characterisation of Thermoset-Layered Silicate Nanocomposites*, 2001, University of Technology, Lulea, Sweden.

27. Theng, B. K. G., *The Chemistry of Clay-Organic Reactions*, 1974, Adam Hilger, London.

28. Bailey, S. W., Brindley, G. W., Johns, W. D., Martin, R. T., Ross, M., *Summary of national and international recommendations on clay mineral*

nomenclature 1969-70 CMS Nomenclature Committee, Clays and Clay Minerals, 1971, **19**, 129.

29. Theng, B. K. G., *Formation and Properties of Clay-Polymer Complexes*, Development in Soil Science, 1979, Elsevier, New York.

30. Akelah, A., Kelly, P., Qutubuddin, S., Moet, A., *Synthesis and Characterization of Epoxyphilic Montmorillonites*, Clay Minerals, 1994, **29**, 169.

31. Zilg, C., Mülhaupt, R., Finter, J., *Morphology and toughness/stiffness balance of nanocomposites based upon anhydride-cured epoxy resins and layered silicates*, Macromolecular Chemistry and Physics, 1999, **200**, 661.

32. Zilg, C., Reichert, P., Dietsche, F., Engelhardt, T., Mülhaupt, R., *Nanocomposites auf Schichtsilikatbasis*, Kunststoffe, 1998, **88**, 1812.

33. Blumstein, A., *Etude des polymérisations en coucher adsorbée*, Bulletin de la Societe Chimique de France, 1961, 899.

34. Hawley, G. C., *Handbook of Reinforcements for Plastics*, Editor: Milewski, J. V., Katz, H. S., 1987, Van Nostrand Reinhold Company, New York.

35. Yano, K., Usuki, A., Okada, A., Kurauchi, T., Kamigaito, O., *Synthesis and Properties of Polyimide-Clay Hybrid*, Journal of Polymer Science: Part A: Polymer Chemistry, 1993, **31**, 2493.

36. Usuki, A., Kojima, Y., Kawasumi, M., Okada, A., Fukushima, Y., Kurauchi, T., Kamigaito, O., *Synthesis of Nylon 6-Clay Hybrid*, Journal of Materials Research, 1993, **8**, 1179.

37. Usuki, A., Kojima, Y., Kawasumi, M., Okada, A., Fukushima, Y., Kurauchi, T., Kamigaito, O., *Mechanical Properties of Nylon 6-clay Hybrid*, Journal of Materials Research, 1993, **8**, 1185.

38. Fukushima, Y., Inagaki, S., *Synthesis of an Intercalated Compound of Montmorillonite and 6-Polyamide*, Journal of Inclusion Phenomena, 1987, **5**, 473.

39. Yano, K., Usuki, A., Okada, A., *Synthesis and Properties of Polyimide-Clay Hybrid Films*, Journal of Polymer Science A: Polymer Chemistry, 1997, **35**, 2289.

40. Lan, T., Kaviratna, P., Pinnavaia, T., *On the Nature of Polyimide-Clay Hybrid Composites*, Chemistry of Materials, 1994, **6**, 573.

41. Yang, Y., Zhu, Z., Yin, J., Wang, X., Qi, Z., *Preparation and properties of hybrids of organo-soluble polyimide and montmorillonite with various chemical surface modification methods*, Polymer, 1999, **40**, 4407.

42. Porter, D., Metcalfe, E., Thomas, M. J. K., *Nanocomposite Fire Retardants - A Review*, Fire and Materials, 2000, **24**, 45.

43. Gilman, J. W., Kashiwagi, T., Lichtenhan, J. D., *Nanocomposites: A Revolutionary New Flame Retardant Approach*, SAMPE Journal, 1997, **33**, 40.

44. Gilman, J., Kashiwagi, T., Brown, J., Lomakin, S., Giannelis, E. *Flammability Studies of Polymer Layered Silicate Nanocomposites, 43rd International SAMPE Symposium*,1998.

45. Vaia, R. A., *Structural Characterization of Polymer-Layered Silicate Nanocomposites*, in *Polymer-clay nanocomposites*, Editor: Pinnavaia, J. T., Beall, G. W., 2000, Wiley, Chichester, 229.

46. Jeon, H. G., Jung, H. T., Hudson, S. D., *Morphology of polymer silicate nanocomposites*, Polymer Bulletin, 1998, **41**, 107.

47. Vaia, R. K., Jandt, K. D., Kramer, E. J., Giannelis, E. P., *Kinetics of Polymer Melt Intercalation*, Macromolecules, 1995, **28**, 8080.

48.   Vaia, R. A., PhD Thesis: *Polymer Melt Intercalation in Mica-Type Silicates*, 1995, Cornell University, Ithaca, NY.

49.   Vaia, R. A., Giannelis, E. P., *Polymer Melt Intercalation in Organically-Modified Layered Silicates: Model Predictions and Experiments*, Macromolecules, 1997, **30**, 8000.

50.   Vaia, R. A., Giannelis, E. P., *Lattice Model of Polymer Melt Intercalation in Organically-Modified Layered Silicates*, Macromolecules, 1997, **30**, 7990.

51.   Liu, L., Qi, Z., Zhu, X., *Studies on nylon 6/clay nanocomposites by melt intercalation process*, Journal of Applied Polymer Science, 1999, **71**, 1133.

52.   Vaia, R. A., Jandt, K. D., Kramer, E. J., Giannelis, E. P., *Microstructural evolution of melt intercalated polymer-organically modified layered silicate nanocomposites*, Chemistry of Materials, 1996, **8**, 2628.

53.   Shen, Z., PhD Thesis: *Nanocomposites of Polymers and Layered Silicates*, 2000, Monash University, Melbourne, Australia.

54.   Kojima, Y., Fukumori, K., Usuki, A., Okada, A., Kurauchi, T., *Gas permeabilities in rubber-clay hybrid*, Journal of Materials Science Letters, 1993, **12**, 889.

55.   Kresge, E., Lohse, D., *Composite tire innerliners and inner tubs*, in *US Patent 5,576,372*, 1996, USA.

56.   Zhang, L., Wang, Y., Wang, Y., Sui, Y., Yu, D., *Morphology and Mechanical Properties of Clay/Styrene-Butadiene Rubber Nanocomposites*, Journal of Applied Polymer Science, 2000, **78**, 1873.

57.   Wang, Y., Zhang, L., Tang, C., Yu, D., *Preparation and Characterization of Rubber-Clay Nanocomposites*, Journal of Applied Polymer Science, 2000, **78**, 1879.

58. Reichert, P., Kressler, J., Thomann, R., Mülhaupt, R., Stöppelmann, G., *Nanocomposites based on a synthetic layer silicate and polyamide-12*, Acta Polymerica, 1998, **49**, 116.

59. LeBaron, P. C., Wang, Z., Pinnavaia, T. J., *Polymer-layered silicate nanocomposites; An Overview*, Applied Clay Science, 1999, **15**, 11.

60. Pinnavaia, T. J., Beall, G. B. (editors.), *Polymer-Clay Nanocomposites.* 1. ed. Wiley Series in Polymer Science, 2000, Wiley, Chichester.

61. Lan, T., Kaviratna, P. D., Pinnavaia, T. J., *Mechanism of Clay Tactoid Exfoliation in Epoxy-Clay Nanocomposites*, Chemistry of Materials, 1995, **7**, 2144.

62. Kornmann, X., Lindberg, H., Berglund, L. A., *Synthesis of epoxy-clay nanocomposites: Influence of the nature of clay on structure*, Polymer, 2001, **42**, 1303.

63. Jiankun, L., Yucai, K., Zongneng, Q., Xiao-Su, Y., *Study on Intercalation and Exfoliation Behaviour of Organoclays in Epoxy Resins*, Journal of Polymer Science: Part B: Polymer Physics, 2001, **39**, 115.

64. Brown, J. M., Curliss, D., Vaia, R. A., *Thermoset-Layered Silicate Nanocomposites, Quaternary Ammonium Montmorillonite with Primary Diamine Cured Epoxies*, Chemistry of Materials, 2000, **12**, 3376.

65. Chen, J.-S., Poliks, M. D., Ober, C. K., Zhang, Y., Wiesner, U., Giannelis, E., *Study of the interlayer expansion mechanism and thermal-mechanical properties of surface-initiated epoxy nanocomposites*, Polymer, 2002, **43**, 4895.

66. Ke, Y., Lü, J., Yi, X., Zhao, J., Qi, Z., *The Effect of Promoter and Curing Process on Exfoliation Behaviour of Epoxy/Clay Nanocomposites*, Journal of Applied Polymer Science, 2000, **78**, 808.

67. Pinnavaia, T. J., Lan, T., Kaviratna, P. D., Wang, Z., Shi, H. *Clay-Reinforced Epoxy Nanocomposites: Synthesis, Properties and Mechanism of Formation*, Polymeric Materials Science and Engineering, American Chemical Society, Chicago, Illinois, 1995, 117.

68. Shi, H., Lan, T., Pinnavaia, T. J., *Interfacial Effects on the Reinforcement Properties of Polymer - Organoclay Nanocomposites*, Chemistry of Materials, 1996, **8**, 1584.

69. Lan, T., Kaviratna, P. D., Pinnavaia, T. J., *Epoxy Self-Polymerization in Smectite Clays*, Journal of Physics and Chemistry of Solids, 1996, **57**, 1005.

70. Lan, T., Pinnavaia, T. J., *Clay-Reinforced Epoxy Nanocomposites*, Chemistry of Materials, 1994, **6**, 2216.

71. Massam, J., Pinnavaia, T. J. *Clay Nanolayer Reinforcement of a Glassy Epoxy Polymer*, Materials Research Society Symposium Proceedings, 1998, **520**, 223.

72. Lan, T., Kaviratna, P. D., Pinnavaia, T. J., *Synthesis, characterization and mechanical properties of epoxy-clay nanocomposites*, Polymer Materials Science and Engineering, 1994, **71**, 527.

73. Zilg, C., Thomann, R., Finter, J., Mülhaupt, R., *The influence of silicate modification and compatibilizers on mechanical properties and morphology of anhydride-cured epoxy nanocomposites*, Macromolecular Materials Engineering, 2000, **280/281**, 41.

74. Wang, Z., Pinnavaia, J. T., *Hybrid Organic-Inorganic Nanocomposites: Exfoliation of Magadiite Nanolayers in an Elastomeric Epoxy Polymer*, Chemistry of Materials, 1998, **10**, 1820.

75. Kornmann, X., Lindberg H., Berglund, L. A., *Synthesis of epoxy-clay nanocomposites. Influence of the nature of the curing agent on structure*, Polymer, 2001, **42**, 4493.

76. Messersmith, P. D., Giannelis, E. P., *Synthesis and Characterization of Layered Silicate-Epoxy Nanocomposites*, Chemistry of Materials, 1994, **6**, 1719.

77. Kornmann, X., Thomann, R., Mülhaupt, R., Finter, J., Berglund, L. A., *High performance epoxy-layered silicate nanocomposites*, Polymer Engineering and Science, 2002, **42**, 1815.

78. Tolle, T. B., Anderson, D. P., *Morphology development in layered silicate thermoset nanocomposites*, Composites Science and Technology, 2002, **62**, 1033.

79. Lan, T., Wang, Z., Shi, H., Pinnavaia, T. J. *Clay-epoxy nanocomposites: relationships between reinforcement properties and the extend of clay layer exfoliation*, Polymeric Materials - Science and Engineering, 1995, Proceedings of the ACS Division of Polymeric Materials, 296.

80. Kaviratna, P. D., Lan, T., Pinnavaia, T. J., *Synthesis of Polyether-Clay Nanocomposites: Kinetics of Epoxide Self-Polymerization in Acidic Smectite Clays*, Polymer Preprints, 1994, **35**, 788.

81. Chin, I.-J., Thurn-Albrecht, T., Kim, C.-H., Russell, T. P., Wang, J., *On exfoliation of montmorillonite in epoxy*, Polymer, 2001, **42**, 5947.

82. Salahuddin, N., Moet, A., Hiltner, A., Baer, E., *Nanoscale highly filled epoxy nanocomposites*, European Polymer Journal, 2002, **38**, 1477.

83. Triantafillidis, C. S., LeBaron, P., Pinnavaia, T. J., *Homostructured Mixed Inorganic - Organic Ion Clays: A New Approach to Epoxy Polymer - Exfoliated Clay Nanocomposites with a Reduced Organic Modifier Content*, Chemistry of Materials, 2002, 14, 4088.

84. Triantafillidis, C. S., LeBaron, P., Pinnavaia, T. J., *Thermoset Epoxy-Clay Nanocomposites: The Dual Role of α,ω-Diamines as Clay Surface Modifiers and Polymer Curing Agents*, Journal of Solid State Chemistry, 2002, **167**, 354.

85. Winter, H., *Can the Gel Point of a Cross-linking Polymer Be Detected by the G' - G" Crossover?*, Polymer Engineering and Science, 1987, **27**, 1698.

86. Halley, P. J., Mackay, M. E., *Chemorheology of Thermosets-An Overview*, Polymer Engineering and Science, 1996, **36**, 593.

87. Halley, P. J., Mackey, M. E., George, G. A., *Determining the gel point of an epoxy resin by various rheological methods*, High Performance Polymers, 1994, **6**, 405.

88. Gillham, J. K., *Formation and Properties of Thermosetting and High Tg Polymeric Materials*, Polymer Engineering and Science, 1986, **26**,1429.

89. Bajaj, P., Jha, N. K., Ananda Kumar, R., *Effect of Mica on the Curing Behaviour of an Amine-Cured Epoxy System: Differential Scanning Calorimetric Studies*, Journal of Applied Polymer Science, 1990, **40**, 203.

90. Butzloff, P., D'Souza, N. A., Golden, T. D., Garrett, D., *Epoxy + Montmorillonite Nanocomposites: Effect of Composition on Reaction Kinetics*, Polymer Engineering and Science, 2001, **41**, 1794.

91. Kelly, P., Akelah, A., Qutubuddin, S., Moet, A., *Reduction of residual stress in montmorillonite/epoxy compounds*, Journal of Materials Science, 1994, **29**, 2274.

92. Wang, Z., Lan, T., Pinnavaia, J. T., *Hybrid Organic-Inorganic Nanocomposites Formed from an Epoxy Polymer and a Layered Silicic Acid (Magadiite)*, Chemistry of Materials, 1996, **8**, 2200.

93. Zerda, A. S., Lesser, A. J., *Intercalated Clay Nanocomposites: Morphology, Mechanics, and Fracture Behaviour,* Journal of Polymer Science: Part B: Polymer Physics, 2001, **39**, 1137.

94. Zerda, A. S., Lesser, A. J. *Intercalated clay nanocomposites: Morphology, mechanics and fracture behaviour,* Materials Research Society Symposium, 2001, **661**, KK7.2.1.

95. Shah, A. P., Gupta, R. K., Gangarao, H. V. S., Powell, C. E., *Moisture diffusion through clay/vinyl ester nanocomposites,* Polymer Nanocomposites, 2001, Montreal, Canada.

96. Lee, D. C., Jang, L. W., *Characterization of Epoxy-Clay Hybrid Composite Prepared by Emulsion Polimerization,* Journal of Applied Polymer Science, 1997, **68**, 1997.

97. Gilman, J. W., Kashiwagi, T., *Polymer-Layered Silicate Nanocomposites with Conventional Flame Retardants,* Polymer-Clay Nanocomposites, Editor: Pinnavaia. J. T. Beall, G. W., 2000, Wiley, Chichester, 193.

98. Gilman, J. W., *Flammability and thermal stability studies of polymer layered-silicate (clay) nanocomposites,* Applied Clay Science, 1999, **15**, 31.

99. Schwarz, O., *Kunststoffkunde,* 4. ed. 1992, Vogel Verlag, Würzburg.

100. Guerrero, P., De la Caba, K., Valea, A., Corcuera, M. A., Mondragon, I, *Influence of cure schedule and stoichiometry on the dynamic mechanical behaviour of tetrafunctional epoxy resin cured with anhydrides,* Polymer, 1996, **37**, 2195.

101. Macosko, C. W., *Rheology Principles, Measurements and application.* 1. ed. 1993, VCH, Weinheim.

102. Laun, H. M., *Rheological properties of aqueous polymer dispersions,* Angewandte Makromolekulare Chemie, 1984, **123/124**, 335.

103. Stutz, H., Mertes, J., *Torsional Braid Analysis and Gelation in Thermoset Resins*, Journal of Applied Polymer Science, 1989, **38**, 781.

104. Aronhime, M. T., Gilham, J. K., *Time-Temperature-Transformation (TTT) Cure Diagram of Thermosetting Polymeric Systems*, Advanced Polymer Science, 1986, **78**, 83.

105. Jiawu, G., Kui, S., Mong, G. Z., *The cure behaviour of tetraglycidyl diaminodiphenyl methane with diaminodiphenyl sulfone*, Thermochimica Acta, 2000, **352-353**, 153.

106. Varley, R., Hodgkin, J. Hawthorne, D., Simon, G., *Toughening of a Trifunctional Epoxy System. IV. Dynamic Mechanical Relaxation Study of the Thermoplastic-Modified Cure Process*, Journal of Polymer Science: Part B: Polymer Physics, 1997, **35**, 153.

107. *Rheometric Scientific*, Hardware Manual 902-50001 Dynamic Mechanical Thermal Analyzer, 1996.

108. Stutz, H., Mertes, J., *Influence of the Structure on Thermoset Curing Kinetics*, Journal of Polymer Science: Part B: Polymer Physics, 1993, **31**, 2031.

109. *JSPDS Powder Diffraction File Database* (CD Rom), 1995.

110. Poisson, N., Lachenal, G., Sautereau, H., *Near- and mid-infrared spectroscopy studies of an epoxy reactive system*, Vibrational Spectroscopy, 1996, **12**, 237.

111. ASTM D 790 M-98, Annual Book of ASTM Standards, 1998. 08.01., 148.

112. ASTM D 5045-96, Annual Book of ASTM Standards, 1999. 08.03., 325.

113. Simon, G. P., *The Use of Positron Annihilation Lifetime Spectroscopy in Probing Free Volume of Multicomponent Polymeric Systems*, Trends in Polymer Science, 1997, **5**, 394.

114. Bigg, D. M., *A Review of Positron Annihilation Lifetime Spectroscopy as Applied to the Physical Aging of Polymers*, Polymer Engineering and Science, 1996, **36**, 737.

115. Pethrick, R. A., *Positron Annihilation - A Probe for Nanoscale Voids and Free Volume?*, Progress in Polymer Science, 1997, **22**, 1.

116. Puff, W., *PFPOSFIT*, Computer Physics Communications, 1983, **30**, 359.

117. ASTM D 3171-76, Annual Book of ASTM Standards. 1990, 15.03., 110.

118. ASTM D 5528-94a, Annual Book of ASTM Standards, 1996, 14.02., 283.

119. ASTM D 2344-84, Annual Book of ASTM Standards, 1995, 15.03.,43.

120. Cox, W. P., Merz, E. H., *Correlation of Dynamic and Steady Flow Viscosities*, Journal of Polymer Science, 1958, **28**, 619.

121. Herschel, W., Bulkley, R., *Measurement of consistency as applied to rubber-benzene solutions*, Kolloid Z, 1926, **39**, 291.

122. Mardis, W. S., *Organoclay Rheology Additives: Past, Present and Future*, Journal of the American Oil Chemists' Society, 1984, **61**, 382.

123. Pignon, F., Magnin, A., Piau, J.-M., *Thixotropic behaviour of clay dispersions: Combinations of scattering and rheometric techniques*, Journal of Rheology, 1998, **42**, 1349.

124. Krishnamoorti, R., Giannelis, E. P., *Rheology of End-Tethered Polymer Layered Silicate Nanocomposites*, Macromolecules, 1997, **30**, 4097.

125. Kemnetz, S. J., Still, A. L., Cody, C. A., Schwindt, R., *Origin of Organoclay Rheological Properties in Coating Systems*, Journal of Coating Technology, 1989, **61**, 47.

126. Krishnamoorti, R., Ren, J., Silva, A. S., *Shear response of layered silicate nanocomposites*, Journal of Chemical Physics, 2001, **114**, 4968.

127. Solomon, M. J., Almusallam, A. S., Seefeld, K. F., Somwangthanaroj, A., Varadan, P., *Rheology of Polypropylene/Clay Hybrid Materials*, Macromolecules, 2001, **34**, 1864.

128. Lange, J., Johansson, M., Kelly, C. T., Halley, P. J., *Gelation behaviour during chainwise crosslinking polymerisation of methacrylate resins*, Polymer, 1999, **40**, 5699.

129. Lange, J., Altmann, N., Kelly, C. T., Halley, P. J., *Understanding vitrification during cure of epoxy resins using dynamic scanning calorimetry and rheological techniques*, Polymer, 2000, **41**, 5949.

130. Mortimer, S., Ryan, A. J., Stanford, J. L., *Rheological Behaviour and Gel-Point Determination for a Model Lewis Acid-Initiated Chain Growth Epoxy Resin*, Macromolecules, 2001, **34**, 2973.

131. Barral, L., Cano, J., Lopez, J., Nogueira, P., Ramirez, C., Abad, M. J., *Isothermal Cure of an Epoxy System Containing Tetraglycidyl-4,4'-diaminodiphenylmethane (TGDDM), a Multifunctional Novolac Glycidyl Ether and 4,4'-Diaminodiphenylsulphone (DDS): Vitrification and Gelation*, Polymer International, 1997, **42**, 301.

132. Bicerano, J. B., Douglas, J. F., Brune, D. A., *Model for the Viscosity of Particle Dispersions*, Journal of Macromolecular Science, Reviews in Macromolecular Chemistry and Physics, 1999, **39**, 561.

133. Krishnamoorti, R., Silva, A. S., *Rheological Properties of Polymer-Layered Silicate Nanocomposites*, Polymer Clay Nanocomposites, Editor: Pinnavaia, J. T., Beall, G. W., 2000, Wiley, Chichester, 315.

134. Flory, P. J., *Principles of Polymer Chemistry*, 1953, Cornell University Press, Ithaca, NY.

135. Harran, D., Grenier-Loustalot, M. F., Monge, Ph., *Avancement de la Reaction Chimique au Point de Gel d'une Resins Epoxide*, European Polymer Journal, 1988, **24**, 225.

136. Bonnaud, L., Pascault, J. P., Sautereau, H., *Kinetic of a thermoplastic-modified epoxy-aromatic diamine formulation: modeling and influence of a trifunctional epoxy prepolymer*, European Polymer Journal, 2000, **36**, 1313.

137. Cadenato, A., Salla, J. M., Ramis, X., Morancho, J. M., Marroyo, L. M., Martin, J. L., *Determination of Gel and Vitrification Times of Thermoset Curing Process by Means of TMA, DMTA and DSC Techniques TTT diagram*, Journal of Thermal Analysis, 1997, **49**, 269.

138. Ramis, X., Salla, J. M., *Time-Temperature Transformation (TTT) Cure Diagram of an Unsaturated Polyester Resin,* Journal of Polymer Science: Part B: Polymer Physics, 1997, **35**, 371.

139. Hagen, R., Salmén, L., *Comparison of Dynamic Mechanical Measurements and T_g with Two Different Instruments*, Polymer Testing, 1994, **13**, 113.

140. Reichert, P., Nitz, H., Klinke, S., Brandsch, R., Thomann, R., Mülhaupt, R., *Poly(propylene)/organoclay nanocomposite formation: Influence of compatibilizer functionality and organoclay modification*, Macromolecular Materials Engineering, 2000, **275**, 8.

141. Morgan, A. B., Gilman, J. W., Jackson, C. L., *Characterization of the Dispersion of Clay in a Polyetherimide Nanocomposite*, Macromolecules, 2001, **34**, 2735.

142. Krook, K., Albertsson, A.-C., Gedde, U. W., Hedenqvist, M. S., *Barrier and Mechanical Properties of Montmorillonite/Polyesteramide Nanocomposites*, Polymer Engineering and Science, 2002, **42**, 1238.

143. Olson, B. G., Peng, Z. L., Sriyhawatpong, R., McGrevey, J. D., Ishida, H., Jamieson, A. M., Manias, E., Giannelis, E. P., *Free Volume in Layered Organoclay-Polystyrene Nanocomposites*, Materials Science Forum, 1997, **255-257**, 336.

144. Jeffrey, K., Pethrick, R. A., *Influence of chemical structure on free volume in epoxy resins: A positron annihilation study*, European Polymer Journal, 1994, **30**, 153.

145. Nakanishi, H., Wang, S. J., Jean, Y. C. *Proceedings of International Conference on Positron Annihilation in Fluids*, 1987, World Scientific Publishing, Singapore.

146. Beall, G. W., *New Conceptual Model for Interpreting Nanocomposite Behaviour*, in *Polymer-Clay Nanocomposites*, Editor: Pinnavaia, T. J., Beall, G. W., 2000, Wiley: Chichester, 267.

147. Pogany, G. A., *Gamma relaxation in epoxy resins and related polymers*, Polymer, 1970, **11**, 66.

148. Lautrêtre, F., Eustache, R.-P., Monnerie, L., *High-resolution solid-state 13C nuclear magnetic resonance investigation of local motions in model epoxy resins*, Polymer, 1995, **36**, 267.

149. Lee, A., Lichtenhan, J. D., *Thermal and viscoelastic property of epoxy-clay and hybrid inorganic epoxy nanocomposites*, Journal of Applied Polymer Science, 1999, **73**, 1993.

150. Zax, D., Yang, D., Santos, R., Hegemann, H., Giannelis, H., Manias, E., *Dynamic heterogeneity in nanoconfined poly(styrene) chains*, Journal of Chemical Physics, 2000, **112**, 2945.

151. Lin, M.-S., Lee, S.-T., *Mechanical behaviour of fully and semi-interpenetrating polymer networks based on epoxy and acrylics*, Polymer, 1997, **38**, 53.

152. Cukierman, S., Halary, J.-L., Monnerie, L., *Dynamic Mechanical Response of Model Epoxy Networks in the Glassy state*, Polymer Engineering and Science, 1991, **31**, 1476.

153. Heux, L., Laupretre, F., Halary, J. L., Monnerie, L., *Dynamic mechanical and ^{13}C N.M.R. analysis of the effects of antiplasticization on the β secondary relaxation of aryl-aliphatic epoxy resins*, Polymer, 1997, **39**, 1269.

154. Heux, L., Halary, J. L., Laupretre, F., Monnerie, L., *Dynamic mechanical and 13C N.M.R. investigations of molecular motions involved in the β relaxation of epoxy networks based on DGEBA and aliphatic amines*, Polymer, 1997, **38**, 1767.

155. Bershtein, V. A., Peschanskaya, N. N., Halary, J. L., Monnerie, L., *The sub-T_g relaxations in pure and plastizised model epoxy networks as studied by high resolution creep rate spectroscopy*, Polymer, 1999, **40**, 6687.

156. Imaz, J. J., Jurado, M. J., Corcuera, M. A., Mondragon, I., *Physical and Mechanical Behaviour of Tetraglycidyl Diaminodiphenyl Methane (TGDDM)/m-Phenylene Diamine (m-PDA) Epoxy Systems*, Journal of Applied Polymer Science, 1992, **46**, 147.

157. Grave, C., McEwan, I., Pethrick, R. A., *Influence of Stoichiometric Ratio on water Absorption in Epoxy Resins*, Journal of Applied Polymer Science, 1998, **69**, 2369.

158. Nogueira, P., Ramirez, C., Torres, A., Abad, M., Cano, J., Lopez, J., Lopez-Bueno, I., Barral, L., *Effect of Water Sorption on the Structure and Mechanical Properties of an Epoxy Resin System*, Journal of Applied Polymer Science, 2001, **80**, 71.

159. Johncock, P., Tudgey, G. F., *Some Effects of Structure, Composition and Cure on the Water Absorption and Glass Transition Temperature of Amine-cured Epoxies*, British Polymer Journal, 1986, **18**, 292.

160. De Neve, B., Shanahan, M. E. R., *Water absorption by an epoxy resin and its effect on the mechanical properties and infra-red spectra*, Polymer, 1993, **34**, 5099.

161. Pethrick, R. A., Hollins, E. A., McEwan, I., Pollock, E. A., Hayward, D., *Effect of Cure Temperature on the Structure and Water Absorption of Epoxy/Amine Thermosets*, Polymer International, 1996, **39**, 275.

162. Mikols, W. J., Seferis, J. C., Apicella, A., Nicolais, L., *Evaluation of Structural Changes in Epoxy Systems by Moisture Sorption-Desorption and Dynamic Mechanical Studies*, Polymer Composites, 1982, **3**, 118.

163. Tcharkhtchi, A., Bronnec, P. Y., Verdu, J., *Water absorption characteristics of diglycidylether of butane diol-3,5-diethyl-diaminotoluene networks*, Polymer, 2000, **41**, 5777.

164. Choi, H. S., Ahn, K. J., Nam, J.-D., Chun, H. J., *Hygroscopic aspects of epoxy/carbon fiber composite laminates in aircraft environments*, Composites: Part A, 2001, **32**, 709.

165. Andreopoulos, A. G., Tarantili, P. A., *Water Sorption Characteristics of Epoxy Resin-UHMPE Fibers Composites*, Journal of Applied Polymer Science, 1998, **70**, 747.

166. Moy, P., Karasz, F. E., *Epoxy-Water Interactions*, Polymer Engineering and Science, 1980, **20**, 315.

167. Soles, C. L., Chang, F. T., Bolan, B. A., Hristov, H. A., Gidley, D. W., Yee, A. F., *Contributions of the Nanovoid Structure to the Moisture Absorption of Epoxy Resins*, Journal of Polymer Science: Part B: Polymer Physics, 1998, **36**, 3035.

168. Crank, J., *The Mathematics of Diffusion*, 1956, Clarendon Press, Oxford.

169. Xie, W., Gao, Z., Pan, W.-P., Hunter, D., Singh, A., Vaia, R., *Thermal Degradation Chemistry of Alkyl Quaternary Ammonium Montmorillonite*, Chemistry of Materials, 2001, **13**, 2979.

170. Kornmann, X., Berglund, L. A., Sterte, J., *Nanocomposites Based on Montmorillonite and Unsaturated Polyester*, Polymer Engineering and Science, 1998, **38**, 1351.

171. Franco, M., Corcuera, M. A., Gavalda, J., Valea, A., Mondragon, I., *Influence of Curing Conditions on the Morphology and Physical Properties of Epoxy Resins Modified with a Liquid Polyamine*, Journal of Polymer Science: Part B: Polymer Physics, 1997, **35**, 233.

172. Lewis, A. F., Doyle, M. J., Gillham, J. K., *Effect of the Cure History on Dynamic Mechanical Properties of an Epoxy Resin*, Polymer Engineering and Science, 1979, **19**, 683.

173. Varley, R., Hodgkin, J. H., Simon, G. P., *Toughening of Trifunctional Epoxy System. V. Structire-Property Relationships of Neat Resin*, Journal of Applied Polymer Science, 2000, **77**, 237.

174. Amdouni, N., Sautereau, H., Gérard, J.-F., Pascault, J.-P., *Epoxy networks based on dicyandiamide: effect of the cure cycle on viscoelastic and mechanical properties*, Polymer, 1990, **31**, 1245.

175. Lin, Y. G., Sautereau, H., Pascault, J. P., *BDMA-Catalyzed DDA-Epoxy Resin System: Temperature and Composition Effects on Cure Mechanism*, Journal of Polymer Science: Part A: Polymer Chemistry, 1986, **24**, 2171.

176. Lin, Y. G., Galy, J., Sautereau, H., Pascault, J. P., *Crosslinked Polymers*, Editor: Sedlacek, B., 1987, W. de Gruyter, Berlin, 148.

177. *Hütte Die Grundlagen der Ingenieurwissenschaften.* 30. ed, Editor: Czichos, H., 1996, Springer, Berlin.

178. Hunston, D. L., Moulton, R. J., Johnston, N. J., Bascom, W. D., *Matrix Resin Effect in Composite Delamination: Mode I Fracture Aspects, Toughened Composites,* Editor: Johnston, N. J., 1987, ASTM STP 937, Philadelphia.

179. Bradley, W. L., *Relationship of matrix toughness to interlaminar fracture toughness, Composite Materials Series - Application of Fracture Mechanics to Composite Materials,* Editor: Friedrich, K., 1989, Elsevier, Amsterdam.

180. Bascom, W. D., Cottingham, R. L., *Effect of Temperature on the Adhesive Fracture Behaviour of an Elastomer-Epoxy Resin,* Journal of Adhesion, 1976, **7**, 333.

181. Park, B. Y., Kim, S. C., Jung, B., *Interlaminar Fracture Toughness of Carbon Fiber/Epoxy Composites using Short Kevlar Fiber and/or Nylon-6 Powder Reinforcement,* Polymers for Advanced Technologies, 1997, **8**, 371.

182. Sohn, M.-S., Hu, X.-Z., *Comparative study of dynamic and static delamination behaviour of carbon fibre/epoxy composite laminates,* Composites Science and Technology, 1995, **26**, 849.

183. Lin, T. L., Jang, B. Z., *Fracture Behaviour of Hybrid Composites Containing Both Short and Continuous Fibers,* Polymer Composites, 1990, **11**, 291.

184. Lin, T. L., Jang, B. Z., *Mechanical Properties of Hybrid Composites Containing Both Short and Continuous Fibers,* Antec'89, 1989, 1552.

185. Rice, B. P., Chen, C., Cloos, L., Curliss, D., *Carbon Fiber Composites: Organoclay-Aerospace Epoxy Nanocomposites, Part I.* SAMPE Journal, 2001, **37**, 7.